

# Towards the Development of Calcium Ion Batteries

by

John Rogosic

B.S., Materials Science and Engineering

B.S., Comparative Media Studies

Massachusetts Institute of Technology, 2008

Submitted to the Department of Materials Science and Engineering  
in partial fulfillment of the requirements for the degree of

**Doctor of Philosophy**

at the

MASSACHUSETTS INSTITUTE OF TECHNOLOGY

June 2014

© 2014 Massachusetts Institute of Technology. All rights reserved.

**Signature redacted**

Signature of Author.....



.....  
Department of Materials Science and Engineering  
May 21<sup>st</sup>, 2014

**Signature redacted**

Certified by.....



.....  
Donald R. Sadoway  
Professor of Materials Chemistry  
Thesis Supervisor

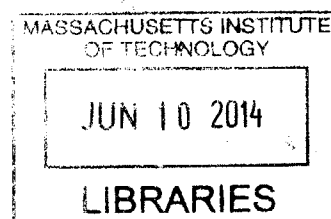
**Signature redacted**

Accepted by.....



.....  
Gerbrand Ceder  
Chair, Departmental Committee on Graduate Students

**ARCHIVES**



# **Towards the Development of Calcium Ion Batteries**

by

John Rogosic

Submitted to the Department of Materials Science and Engineering  
on May 21<sup>st</sup>, 2014, in partial fulfillment of the  
requirements for the degree of  
**Doctor of Philosophy**

## **Abstract**

A novel system for the study of calcium-ion electroactive materials has been developed, characterized, and utilized to screen a number of candidate calcium intercalation compounds. The system is comprised of a dried, pre-electrolyzed calcium perchlorate salt in acetonitrile solvent electrolyte combined with solid-liquid metal slush counter and reference electrodes utilizing inert molybdenum, borosilicate glass, and polytetrafluoroethylene cell components. The counter and reference electrodes consist of saturated calcium amalgam and a calcium mercury intermetallic phase, denoted as  $\text{CaHg}_{11}\text{-Ca}_{(\text{Hg})}^{\text{sat}}$ , with a nominal calcium concentration of 5 mole percent. Reference electrodes were found to be stable for many weeks with no drift and high precision ( $\pm 2$  mV), and lie at a potential value of approximately -2.043 V versus the standard hydrogen electrode or 0.825 V versus the  $\text{Ca/Ca}^{2+}$  couple.

Several transition metal oxide and other chalcogen-based structures were explored as calcium cathode materials. Vanadium oxide ( $\text{V}_2\text{O}_5$ ), iron sulfide ( $\text{FeS}_2$ ) and molybdenum selenide ( $\text{Mo}_3\text{Se}_4$ ) could be reversibly cycled. The behavior of  $\text{Mo}_3\text{Se}_4$  was studied in greater detail, and its electrochemical performance suggested sluggish calcium transport resulted in rate limited capacity. Microscale ( $\sim 2.5$   $\mu\text{m}$  particle diameter) powders demonstrated a reversible capacity less than 3 percent of theoretical for the host compound. Nanoscaling, higher temperature cycling, and chemo-structural alteration of  $\text{Mo}_3\text{Se}_4$  increased capacity utilization fourfold. Calcium content of electroactive samples was confirmed by energy dispersive x-ray spectroscopy. X-ray photoelectron spectroscopy and x-ray diffractometry studies provided supporting evidence of calcium intercalation into the  $\text{Mo}_3\text{Se}_4$  Chevrel phase structure. Furthermore, preliminary results are presented involving beryllium and aluminum electrochemistry in the  $\text{Mo}_3\text{Se}_4$  Chevrel phase.

Thesis Supervisor: Donald R. Sadoway  
Title: Professor of Materials Chemistry

*To my father Ivan, and uncles Ilija and Čiro.*

*Thank you for teaching me the value of patience, debate, and humor in engineering.*

*I will do my best with your lessons.*

## Acknowledgements and Thanks

No man is an island, and I am no exception. Although somewhat cliché, I think this statement captures the fact that each of us, both in our successes and failures, are inextricably linked to those we rely on for help, support, and friendship. I would never have made it as far as I have without a group of extraordinary family, friends, and colleagues. I owe everyone so much that it would be foolish to think I could recount it all in a single page. Below, I give my thanks to those I can recall at this moment, and my apologies to those whose contributions have gone unmentioned, but are no less deserving of my gratitude.

Let me begin by thanking my mother. Without you Mom, I would not be. I have learned more from you than I am willing to admit, but your most valuable lesson has been in the value of keeping my word.

Thank you to my students: all of you. You made the PhD process doubly rewarding for me. I wish you all the brightest futures, and hope that I have given you a fraction of what you have given me.

Thanks to the entire Department of Materials Science and Engineering and MIT. Without the guidance and aid of the exceptional professors, instructors, and support staff over the last decade I would be living a different life today. To name just a few individuals of many: Mike Tarkanian, you've been a source of advice for countless students, both professional and personal. You do so much, and are exceptional at all you do. Professor Schuh, you helped me discover my professional confidence, and that deserves a special note. Keep it up with future generations. Angelita, I can't find the words, but I think you know. Thanks.

Professor Sadoway, you are inspiration incarnate. I recall walking into your freshman chemistry class a decade ago without a clue that you would shape me as much as you have. You've taught me to look at the big picture and relate it to the task at hand, to communicate clearly, that motivation is key, and that knowing how to ask the right questions is priceless. For all this, and so much more, I thank you.

Professors Allen and Ceder, I thank you sincerely for all of your discussions and advice. Interacting with you both over the years, as members of my thesis committee, as educators, and as colleagues has been enlightening on so many levels.

I would like to thank all the members of GroupSadoway, both current and former. Your knowledge and friendship have aided me in innumerable ways. Even in our disagreements, there lay hidden immeasurable value. I thank you all. Rohun, you deserve particular note for your help in study of the Ca-Hg system. I hope your UROP experience in our group was as rewarding for you as it was for me to mentor you.

I owe a special thanks to all the colleagues and professionals who worked with me in training, experimental design, and data collection on various materials spectroscopy techniques. Scott Speakman, John Guske, Don Galler, Matthew Smith, Tim Milakovich, and Elisabeth Shaw, I appreciate your time and energies, and acknowledge your contributions to this work.

And finally, thank you to everyone who has touched my personal life during my PhD years. Without you I am not sure I would have made it through. You were always there when I needed you most. Thanks.



# Contents

List of Figures .....	8
List of Tables .....	11
List of Symbols .....	12
Chapter 1: Motivation, Scope, and Challenges .....	13
1.1 Energy Storage and Abundance .....	14
1.2 Battery Basics .....	15
1.3 Theoretical Considerations Concerning Calcium .....	16
1.3.1 Operating Voltage .....	20
1.3.2 Capacity and Energy Density .....	21
1.3.3 Reactivity and Passivity .....	23
Chapter 2: Background, Inspiration, and Requirements for Ca-Ion Study .....	26
2.1 Requirements for the Study of Calcium-Ion Electrochemistry .....	26
2.1.1 “There is no half-cell” .....	26
2.1.2 Half-cell Workarounds from the Literature .....	27
2.2 Inspiration and Background for the Ca-Hg two-phase Electrode .....	31
2.2.1 Functionality as a reference electrode .....	31
2.2.2 Functionality as a counter electrode .....	33
2.2.3 Literature Review of the Ca-Hg System .....	33
2.3 Literature Review of Calcium and Multivalent Ion Electrochemistry .....	34
2.3.1 Review of $V_2O_5$ .....	35
2.3.2 Review of $WO_3$ .....	35
2.3.3 Review of $CaCrO_4$ .....	36
2.3.4 Review of $K_2FeO_3$ .....	36
2.3.5 Review of $FeS_2$ .....	36
2.3.6 Review of $TiS_2$ .....	37
2.3.7 Review of S .....	37
2.3.8 Review of $Mo_6X_8$ (X = S, Se, Te) .....	37
2.4 Discussion of Multivalent Intercalation Candidates .....	40
2.5 Chapter Summary .....	42

Chapter 3: Procedures and Methods .....	43
3.1 Electrochemical Techniques .....	43
3.1.1 Open Circuit Voltage .....	43
3.1.2 Potentiostatic Hold .....	44
3.1.3 Cyclic Voltammetry .....	44
3.1.4 AC Impedance .....	46
3.1.5 Galvanic Pulse .....	46
3.1.6 Galvanic Titration .....	47
3.1.7 Galvanostatic Intermittent Titration Technique .....	48
3.2 Materials Characterization .....	50
3.2.1 X-Ray Diffraction .....	50
3.2.2 Scanning Electron Microscopy and Energy Dispersive X-ray Spectroscopy .....	52
3.2.3 Transmission Electron Microscopy .....	53
3.2.4 X-ray Photoelectron Spectroscopy .....	53
3.3 Experimental Apparatus .....	54
3.3.1 Vessel Design Challenges .....	54
3.3.2 Three Electrode Vessel Design .....	55
3.3.3 Composite Electrode Preparation Techniques .....	57
3.4 Electrolyte Considerations .....	58
3.4.1 Selection of Electrolyte .....	60
3.4.2 Testing and Characterization of the Calcium Perchlorate/Acetonitrile Electrolyte .....	62
3.4.3 Salt Drying Procedures .....	64
3.5 Preparation of Ca-Hg Electrodes .....	66
3.6 Preparation of Chevrel Phase Powders .....	67
3.6.1 Solid-State Synthesis of $\text{Cu}_2\text{Mo}_6\text{X}_8$ (X = S, Se, Te) .....	67
3.6.2 Acid Leaching Procedures .....	69
3.7 Chapter Summary .....	70
Chapter 4: Experimental Characterization of the Ca-Hg System .....	71
4.1 Calcium amalgam concentration OCV measurements .....	71
4.2 Determination of the $\text{CaHg}_{11}\text{-Ca}_{(\text{Hg})}^{\text{sat}}$ electrode potential .....	72
4.2.1 Calcium Metal Measurements .....	73
4.2.2 Infinite Dilution Measurements .....	74
4.2.2.1 Chemical Amalgam Preparation .....	74
4.2.2.2 Titration-Relaxation Measurements .....	75
4.2.2.3 Cyclic Voltammetry .....	76
4.2.2.4 Residual OCV after AC Impedance Measurement .....	77
4.2.2.5 Summary of Measurements and Discussion .....	78
4.3 Stability of the $\text{CaHg}_{11}\text{-Ca}_{(\text{Hg})}^{\text{sat}}$ two-phase Reference .....	79
4.3.1 Short Term Behavior .....	79
4.3.2 Long Term Behavior .....	80
4.3.3 Variation in Chemical Composition .....	82
4.3.4 Mechanical Perturbation .....	83
4.4 Kinetic Considerations .....	85

4.4.1 Voltammetric Measurements .....	85
4.4.2 Impedance Measurements .....	87
4.4.3 Galvanic Behavior of the the $\text{CaHg}_{11}\text{-Ca}_{(\text{Hg})}^{\text{sat}}$ Electrode .....	92
4.5 Chapter Summary .....	98
Chapter 5: Positive Electrode Material Experimental Results .....	99
5.1 Vanadium oxide as a model multivalent ion intercalation system .....	99
5.2 A qualitative study of transition metal oxides and sulfides .....	102
5.3 Electrochemical Behavior of $\text{Mo}_6\text{Se}_8$ .....	110
5.3.1 Rate effects on the performance of $\text{Mo}_6\text{Se}_8$ .....	112
5.3.2 Temperature effects on the performance of $\text{Mo}_6\text{Se}_8$ .....	115
5.3.3 Particle size effects on the performance of $\text{Mo}_6\text{Se}_8$ .....	120
5.3.4 Compositional effects on the performance of $\text{Mo}_6\text{Se}_8$ .....	125
5.4 Chapter Summary .....	131
Chapter 6: Materials Characterization in Support of Calcium Intercalation .....	132
6.1 SEM/EDS Analysis of $\text{Ca}_x\text{Mo}_6\text{Se}_8$ .....	132
6.2 XRD Analysis of $\text{Ca}_x\text{Mo}_6\text{Se}_8$ .....	135
6.3 TEM Analysis of $\text{Ca}_x\text{Mo}_6\text{Se}_8$ .....	140
6.4 XPS Analysis of $\text{Ca}_x\text{Mo}_6\text{Se}_8$ .....	146
6.5 Chapter Summary .....	153
Chapter 7: Concluding Remarks and Future Directions .....	155
Appendix A. Aluminum and the Chevrel Phase .....	162
Appendix B. Beryllium and the Chevrel Phase .....	171
Appendix C. Particle Size Determination .....	175
Appendix D. Rietveld Refinement Details .....	177
Bibliography .....	182
Epilogue .....	189

# List of Figures

1. Calcium metal electrode in organic electrolyte.....	25
2. Calcium-Mercury phase diagram.....	31
3. Structure of the $\text{Pb}_{11}\text{Mo}_6\text{S}_8$ Chevrel phase .....	38
4. Discharge profile for $\text{Mg}^{2+}$ into $\text{Mo}_6\text{S}_8$ . ....	39
5. Typical waveform for a cyclic voltammogram .....	45
6. Theoretical current and voltage curves for GITT protocol .....	49
7. Custom three-electrode vessel design .....	56
8. Electrochemical window of calcium perchlorate in acetonitrile electrolyte.....	63
9. Acetonitrile decomposition product.....	63
10. OCV as a function of calcium amalgam concentration .....	72
11. Extrapolation of calcium alloying curve during cyclic voltammetry. ....	77
12. Long term stability of the $\text{CaHg}_{11}\text{-Ca}_{(\text{Hg})}^{\text{sat}}$ reference electrode.....	80
13. Variation of the $\text{CaHg}_{11}\text{-Ca}_{(\text{Hg})}^{\text{sat}}$ reference electrode potential with composition.....	83
14. Electrode response to mechanical perturbation .....	84
15. Cyclic voltammograms performed on 0.5 M calcium perchlorate in acetonitrile solutions .....	86
16. AC impedance spectra for mercury electrodes .....	89
17. Charge transfer resistance dependence on calcium concentration.....	91
18. Galvanic behavior of the the $\text{CaHg}_{11}\text{-Ca}_{(\text{Hg})}^{\text{sat}}$ electrode .....	93
19. Linear analysis of the $\text{CaHg}_{11}\text{-Ca}_{(\text{Hg})}^{\text{sat}}$ electrode overpotential .....	95

20. Tafel plot of calcium-mercury electrode.....	96
21. Intermetallic growth on the $\text{CaHg}_{11}$ - $\text{Ca}_{(\text{Hg})}^{\text{sat}}$ electrode.....	97
22. Calcium electrolyte CVs for $\text{V}_2\text{O}_5$ electrode. ....	100
23. First cycle behavior of $\text{V}_2\text{O}_5$ electrode.....	101
24. Calcium electrolyte CVs for $\text{WO}_3$ electrode.....	103
25. Calcium electrolyte CVs for $\text{CaCrO}_4$ electrode .....	104
26. Calcium electrolyte CVs for $\text{K}_2\text{FeO}_4$ electrode .....	105
27. Calcium electrolyte CVs for $\text{FeS}_2$ electrode .....	106
28. Calcium electrolyte CVs for $\text{TiS}_2$ electrode.....	107
29. Calcium electrolyte CVs for $\text{Mo}_6\text{S}_8$ electrode. ....	108
30. Calcium electrolyte CVs for $\text{Mo}_6\text{Se}_8$ electrode.....	109
31. Calcium electrolyte CVs for S electrode.....	110
32. Galvanic cycling profile for $\text{Mo}_6\text{Se}_8$ .....	111
33. Galvanic cycling rate series for $\text{Mo}_6\text{Se}_8$ .....	114
34. Galvanic cycling temperature series .....	116
35. Variation of capacity with temperature.....	117
36. Temperature dependence of normalized discharge capacity and fade rate.....	118
37. Comparison of cycling rate and temperature effects on first cycle profiles. ....	119
38. SEM image of typical “microscale” $\text{Mo}_6\text{Se}_8$ particles.....	120
39. SEM image of typical “nanoscale” $\text{Mo}_6\text{Se}_8$ particles. ....	122
40. Effect of particle size on first cycle behavior of $\text{Mo}_6\text{Se}_8$ .....	123
41. Nanoscale first cycle performance improvements. ....	124
42. Cycling performance of nanoscale $\text{Mo}_6\text{Se}_8$ electrodes. ....	125
43. Cyclic voltammogram of $\text{Cu}_x\text{Mo}_6\text{Se}_8$ . ....	127
44. SEM image of as-synthesized $\text{Cu}_2\text{Mo}_6\text{S}_{0.5}\text{Se}_{6.5}\text{Te}_1$ . ....	129
45. Electrochemical behavior of $\text{Mo}_6\text{S}_{0.5}\text{Se}_{6.5}\text{Te}_1$ .....	130

47. Typical post-mortem SEM image of $\text{Ca}_x\text{Mo}_6\text{Se}_8$ powders. ....	135
48. Intensity comparison of experimental and Rietveld XRD spectra.....	139
49. Typical TEM image of $\text{Ca}_x\text{Mo}_6\text{Se}_8$ particle .....	141
51. Typical dark-field TEM image of “nanoscale” particles .....	144
52. Typical TEM-EDS line scan of $\text{Ca}_x\text{Mo}_6\text{Se}_8$ .....	145
53. XPS spectra for $\text{Ca}2p$ .....	147
54. XPS spectrum for $\text{O}1s$ .....	148
55. XPS spectrum for $\text{Se}3d$ . ....	149
56. XPS spectra for $\text{Mo}3d$ .....	150
57. Cyclic voltammograms of various $\text{AlCl}_3$ -EMIMCl ionic liquids.....	165
58. Calcium-platinum phase diagram.....	166
59. Cyclic voltammogram of Al deposition/dissolution on carbon WE.....	167
60. Cyclic voltammogram of $\text{Mo}_6\text{Se}_8$ on carbon WE.....	168
61. Galvanic cycling behavior of $\text{Mo}_6\text{Se}_8$ .....	170
62. Comparison of beryllium chloride and ionic liquid properties.....	172
63. Cyclic voltammogram of $\text{BeCl}_2$ -BMIMCl electrolyte and SEM micrograph of deposit.....	173
64. Cyclic voltammogram of $\text{Mo}_6\text{Se}_8$ in beryllium electrolyte.....	174
65. TEM micrographs of typical $\text{Mo}_6\text{Se}_8$ particles.....	176
66. Intensity comparison of experimental and Tietveld XRD spectra.....	179
67. Intensity comparison of experimental and Tietveld XRD spectra.....	180

# List of Tables

1. Ion selection criteria . . . . .	18
2. Theoretical energy densities for various ions . . . . .	23
3. Solubility of calcium salts in organic solvents . . . . .	61
4. Equivalent circuit model parameters for amalgam impedance measurements . . . . .	91
5. Rietveld refinement parameters . . . . .	178

# List of Symbols

$F$  : Faraday's constant

$OCV$  : open circuit voltage

$\eta$  : electrode overpotential

$\eta_{ct}$  : charge transfer overpotential

$\eta_{mt}$  : mass transfer overpotential

$\eta_{ohm}$  : ohmic overpotential

$V$  : voltage

$e$  : fundamental electric charge

$j$  : current density

$Q$  : capacity

$E$  : measured cell voltage

$T$  : temperature

$X_s$  : mole fraction of species s

$\gamma_s$  : activity coefficient of species s

$Z$  : valence of charged species

$R$  : resistance



# Chapter 1:

## Motivation, Scope and Challenges

The primary goal of this thesis is to explore calcium as an alternative to lithium intercalant secondary battery chemistries. Historically little work has been undertaken in this area, as until recent years it was believed that lithium would provide the best possible performance metrics for storage technology given its light weight and high voltage. The needs of consumers have evolved to the point where other chemistries have the potential to offer benefits over current state-of-the-art lithium technology, particularly in the areas of cost and volumetric energy density. Given the low historical interest in non-lithium systems however, little data exists quantifying their performance and few studies have attempted to overcome the numerous challenges facing their further development. This thesis aims to address the lack of exploration of alternative chemistries, particularly calcium, which remains one of the most promising underexplored alternative ion candidates to lithium.

One necessary step on the path towards new energy storage technologies is the basic assessment and characterization of candidate electrode materials. However, the study of calcium-based systems involves such numerous difficulties that many potential researchers shy away from the challenge. The result is that while a great deal of research time and effort has been expended on further refinement of lithium-ion technology, relatively little energy has been spent exploring promising, albeit more difficult to achieve alternative chemistries such as calcium. A main motivation of the work conducted in this thesis is

the broadening of the domain of non-lithium secondary storage intercalation battery research. To that end, the scope of this thesis has been divided between the development of systems capable of studying calcium-ion intercalation compounds, and the study of such compounds themselves. Important contributions have been made on both fronts, and although a fully-functioning calcium-ion battery may still be years off, this work has laid important groundwork for its development.

## **1.1 Energy Storage and Abundance**

Energy storage is recognized as a key area for research in the 21<sup>st</sup> century. Storage technologies permeate our lives, from mobile phones and laptops to electric vehicles to the emerging market for grid-scale energy storage, the uses for energy storage devices continues to grow. Although a rapidly growing market, energy storage has encompassed only a very small percentage of the world's overall energy supply. Electrical energy is typically generated and consumed directly off the grid. Much of the energy associated with transportation is derived directly from fossil fuels. In fact, only small-scale mobile applications have been considered in the development of a number of energy storage technologies.<sup>1</sup>

In the limited framework of small, mobile devices with lower power and energy requirements, lithium ion technology has evolved and thrived due to its superior gravimetric energy density. However, as the energy storage markets, both mobile and stationary, continue to grow, lithium ion technology will likely lag behind the market in terms of the required cost metrics, as well as in volumetric energy density. One of the main factors in determining whether storage is a viable option, and one of the main reasons for the storage bottleneck in today's world is the prohibitively expensive cost of lithium ion batteries for a number of energy storage applications. By moving away from a more expensive system, costs associated with materials, design, and safety can be reduced and energy storage technologies can evolve in the direction the market requires. To that end, batteries designed from more earth abundant materials are desired. Calcium is amongst the most abundant elements in the earth's crust, and as such, is an excellent choice as a battery candidate.

## 1.2 Battery Basics

Before discussing the motivation behind the selection of calcium as a promising candidate system for battery design, one must have a reasonable understanding of how a battery operates. The following section is dedicated to an elementary discussion of battery operation, as well as specifics related to ion-insertion batteries. This discussion lays the foundation for the framework used to assess the theoretical considerations of calcium in the next section (Section 1.3).

At its most basic level, a battery is an electrochemical energy storage device. The free energy of a chemical reaction is harnessed in a controlled manner such that it can be stored for extended periods of time and called upon when needed. A battery converts this chemical energy (energy associated with bonds within the material) into electrical energy (a gradient in electrical potential which can set electrons in motion). Batteries are typically classified as primary (single use-energy generation devices) or secondary (multiple use-energy storage devices). Batteries can be similarly divided into conversion batteries (e.g. lead acid) or intercalation batteries (e.g. lithium ion).<sup>2</sup>

Every battery consists of at least two electrodes, one of each polarity, separated by an electrolyte. During charge and discharge of the cell electron transfer reactions occur at each electrode resulting in generation and consumption of mobile electrons. Mass is transferred between the electrodes via diffusion of ionic species through the electrolyte. The electrolyte is designed to have poor electronic conductivity such that electrons are forced to find a different path to complete the circuit. Separate ionic and electronic currents of equal magnitude result, with electrons traveling through an external circuit of the end user's choosing. The maximum theoretical energy able to be extracted is related to the free energy of reaction. One can express this relationship in the following equation<sup>2</sup>;

$$\Delta G = -nFE_{rxn} \quad (1)$$

where  $E_{rxn}$  is defined as the potential difference between the electrodes,  $n$  is the number of electrons passed per unit of reaction, and  $F$  is the Faraday constant. In practice, inefficiencies associated with

various resistance mechanisms (e.g. charge transfer, ohmic, mass transfer denoted as  $\eta_{ct}$ ,  $\eta_{ohm}$ , and  $\eta_{mt}$  respectively) reduce the operating voltage of the battery from the theoretical value of  $E_{rxn}$ .

$$E = E_{rxn} - \eta_{ct} - \eta_{ohm} - \eta_{mt} \quad (2)$$

The magnitude of these various resistances varies between different battery chemistries, a result of the different physical mechanisms involved. Other losses can exist as well, although the three mentioned above are present in all batteries.<sup>2</sup>

While a number of conversion batteries involve multi-electron transfer reactions, common intercalation batteries consist of a single electron transfer step. The industry standard for intercalation batteries is lithium, which is chosen for its high charge-to-mass ratio and high battery operating voltage. Ultimately, the total energy able to be extracted from a battery is the product of its capacity (number of electrons) times the voltage at which these electrons are extracted (operating potential).

Typically these values of capacity and energy are normalized by metrics such as mass, volume, or cost depending on the application of interest and whichever metric produces numbers that make the technology appear most promising. By moving away from a mono-valent intercalant ion to one of higher valence it is possible to realize gravimetric and volumetric capacity gains that scale roughly linearly with the valence of the active species, provided that the host is capable of accepting the same number of intercalating ion species and provides for compensating electrons corresponding to their valence. This multiplicative increase in storage capacity allows (in theory) for a similar increase in energy stored, within the constraints of cell operating voltage. More detailed considerations concerning calcium are discussed in section 1.3.

### 1.3 Theoretical Considerations Concerning Calcium

Secondary storage intercalant batteries rely on a cation which is moved back and forth between two electrodes through the electrolyte. The cation of choice for today's commercialized technologies is

the lithium ion. Lithium was identified as a superior candidate decades ago due to several factors, including its low plating potential (resulting in a high cell voltage) and light weight (providing electrons at 7g/mol). However, if one focuses on performance metrics such as cost, safety, or materials availability then other candidates can surpass lithium in desirability.

In selecting an active ion, one should consider multiple factors such as cell operating voltage, available valence states, ion size, materials rarity and cost, and ion weight. The following is a list of descriptors for criteria to be considered:

1. Ions should have a stable valence state without a redox couple to prevent complications with chemically shorting the cell through the electrolyte.
2. The ions should be of small size when incorporated into solids, such that they are able to occupy sites within the intercalant host as well as diffuse through the host with ease. It should be noted that ion size and valence are not the only two factors that contribute to mobility within the host network, but there is certainly a correlation between these properties.
3. The weight of the ion normalized by its valence should be as low as possible, such as to provide electrons at a low mass penalty to the cell. This weight consideration only applies in cases where gravimetric capacity is of interest.
4. The cost of the ion should be taken into account, as well as its earth abundance and rarity. Were a system to be broadly applied it should be made from readily available or harvestable materials and should not rely on rare species with low natural abundance, and those which are difficult to isolate and process.
5. In order to maximize energy density, the metal deposition potential should be as negative possible for the ion of interest. A more negative plating potential results in a higher overall cell operating voltage.

Based on the above listed criteria, the following elements tabulated below would make reasonable candidates for use as alternatives to lithium chemistries.

Ion	Normalized Mass g/mol e	Ionic Radius <sup>3, 4</sup> Å	Crustal Abundance <sup>5, 6, 7</sup> ppm	Plating Potential vs. SHE V	Intercalant Ion Charge Density e/Å <sup>3</sup>
Li <sup>+</sup>	6.9	0.76	20	-3.04	0.54
K <sup>+</sup>	39	1.38	15,000	-2.93	0.09
Ba <sup>2+</sup>	68.5	1.35	500	-2.91	0.19
Sr <sup>2+</sup>	44	1.12	360	-2.89	0.34
Ca <sup>2+</sup>	20	1.00	50,000	-2.87	0.49
Na <sup>+</sup>	23	1.02	23,000	-2.71	0.23
Mg <sup>2+</sup>	12	0.72	29,000	-2.37	1.28
Y <sup>3+</sup>	29.7	0.9	30	-2.37	0.98
Be <sup>2+</sup>	4.5	0.35	3	-1.85	11.14
Al <sup>3+</sup>	9	0.54	82,000	-1.66	4.55
Ti <sup>2+</sup> -Ti <sup>4+</sup>	12-24*	0.6	6,600	-1.37	2.21-4.42*
V <sup>2+</sup> -V <sup>5+</sup>	12-25*	0.59	190	-1.18	2.33-5.83*

Table 1. **Ion selection criteria.** Highlighted species are of noteable interest.

\* refers to a range calculated based off of a spread of valencies.

Sodium, magnesium, calcium, and aluminum (highlighted in blue) are the most promising candidates from a scalable performance standpoint. Aluminum is considered in spite of its relatively high plating potential due to its light weight and trivalency. Although it has a low plating potential, potassium was eliminated as it is quite heavy and boasts a large ionic radius, however some work does exist looking to commercialize potassium ion Prussian blue batteries.<sup>8,9</sup> Although interesting due to its extremely small size and light weight, beryllium is particularly expensive and boasts a somewhat lower potential. Titanium although abundant, has a much higher plating potential relative to other candidates, and

possesses multiple redox states. Vanadium, yttrium, and barium were eliminated for their rarity and weight.

Another important metric to consider when exploring potential intercalate ions is charge density. Multivalent ions have a greater charge, and hence would be expected to bind more tightly to their surroundings than monovalent ions in a similar environment. Ions that are too tightly bound would be immobile within host structures. The argument however, depends on how the charge is distributed throughout the ion, with small ions having a greater charge density than larger ions of comparable valence. Using lithium as a standard for comparison, ions such as sodium and potassium have a lower charge density and so immobility due to charge density is expected to be less of an issue than other factors, such as steric effects due to ion size. Similarly, small multivalent ions such as magnesium, beryllium, and aluminum have a charge density that is far higher than that of lithium, such that tight binding due to electrostatic forces is much more of a concern than ion steric effects. Calcium, interestingly, has a charge density that is on the order of that of lithium

From the four most promising abundant candidates, calcium is the most underrepresented within the literature. Sodium batteries began their development alongside lithium decades ago. In more recent years, initiatives have been taken to further develop magnesium batteries.

However calcium sits at an interesting intersection between magnesium and sodium. Its divalency allows it to boast comparable volumetric and gravimetric capacities to that of magnesium, although it has the added benefit of having about a 0.5 V lower plating potential. Thus, for a given intercalation potential in a given electrode material, the theoretical energy density (particularly when defined volumetrically), should be higher for that of calcium than of magnesium. Arguments that calcium is too heavy for practical use in batteries are easily countered by the observation that calcium is actually lighter than sodium on a per electron basis – meaning that calcium batteries are expected to boast higher gravimetric capacity than sodium. When considering the convergence of these factors; operating voltage, mass per mole of

electrons, and capacity per intercalated ion, the conclusion is clear: all signs point to calcium as an ideal candidate battery chemistry. The following sections of this introductory chapter will elaborate on these considerations with respect to calcium, as well as postulate why such an attractive battery system has been understudied for so many years.

### **1.3.1 Operating Voltage**

The voltage obtained between the two electrodes within a battery is a primary driver in the energy able to be stored by the cell. Different factors limit the potential at each of the electrodes, the combination of which sets the theoretical window in which a battery can operate.

On the positive electrode side, the state of the material as well as the free energy change upon ion intercalation determines the discharge profile of that material. The literature is in some disagreement as to the manner in which the discharge voltage of a material will vary as the ion is varied. Some authors predict that in general, the intercalation potential will always be lower as we move to multivalent ions from lithium. However, there is experimental evidence to suggest that this theory is not always applicable, with published cases suggest that the positive electrode material's active potential can be comparable to, or even greater than that of lithium, such as in the case of vanadium pentoxide.<sup>10, 11, 12, 13</sup> In reality, the observed intercalation potential is a complex function of the free energy of the system that involves redox shifts, phase equilibria, internal strain energy, and interfacial energies, among other factors. State of the art computational techniques can help explain, and even predict the behavior of particular intercalation compound candidates. The electrolytic window can also limit the upper operating potential of a system. In the realm of lithium ion batteries the electrolytic window is a real limiting factor in the study of high-potential intercalation cathodes. Ultimately, the fundamental upper bound on the operating voltage of a battery is a question of both materials affinity (the potential at which intercalation/deintercalation steps will occur) and materials stability (as is the case with electrolyte decomposition).



The negative electrode has a much clearer ‘floor’ on its potential as set by the plating potential of the ionic species involved. Although the practical plating potential depends on the substrate and electrolyte used as the over potentials vary for kinetic reasons, the thermodynamic limit on the negative electrode can be approximately set by the position of the metal in the electrochemical series. Calcium’s plating potential in the electrochemical series (aqueous) is only 150 mV above that of lithium’s, and is hundreds of millivolts more negative than that of sodium, magnesium, and aluminum.<sup>14</sup> Hence, for a given intercalation compound that would hypothetically intercalate all five of the aforementioned ions at the same potential, calcium would offer the second highest system voltage.

### **1.3.2 Capacity and Energy Density**

The capacity of an electro-active material refers to the amount of charge (number of electrons) that can be stored within the material. This metric is directly related to the number of compensating electrons which can be housed within the material upon an ion’s intercalation. In turn this can be correlated to the maximum amount of work able to be extracted from the electrochemical system. A more correct measurement of secondary battery performance would be the reversible capacity, or the capacity retained by the material after repeated cycling.

As capacity is a ‘counting’ metric of sorts, one can predict the theoretical capacity by use of a phase diagram. For a particular system, by identifying, (or predicting) the end-member phases upon charge and discharge, one can calculate the number of electrons that would need to be passed into the material to compensate for the insertion of the intercalant ions. This calculation must also take into account the valence state of the ions to be inserted into the host material. Lastly capacities are typically normalized by some metric, such as volume or mass, to determine the volumetric or gravimetric capacities respectively.

It should be noted that in the lithium ion literature there is no clear convention for how to report capacity calculations and capacities can be calculated based on the intercalated or un-intercalated electro-

active species. One example of this is that the gravimetric capacity of lithium insertion into silicon is often reported as higher than that of pure lithium metal, which is merely an artifact of the silicon calculation being performed without the weight of the lithium taken into account. Such inconsistency is less important in the context of lithium literature where every mole of electrons costs 7 grams, however when ions of different masses are used it would make the most sense to be sure to include the weight of the active ion of interest in calculations. In the interests of transparency, it makes sense to utilize the intercalated weight as the weight of the active material, and the intercalated volume as the volume of active material, when reporting results. As such, calcium systems will tend to have on average lower gravimetric capacities than their lithium, magnesium, or aluminum counterparts, assuming that the same number of compensating electrons are provided. Alternatively, assuming that the same number of ions are able to be accommodated by a host structure, the gravimetric capacity will in fact scale somewhat less than linearly with the valence of the intercalant ion as compared to lithium.

Energy density refers to the normalized work able to be extracted from a particular system. Common normalizations gravimetric and volumetric energy densities can be presented, as can those for cost. The energy density is simply the integral of voltage discharge profile with respect to capacity. Assuming that capacity is a factor that can scale approximately linearly with the valence of ions involved in some systems, and the possible operating voltage is not too greatly diminished by the plating potential of the electro-active species of interest, then moving to a calcium ion system can provide marked gains in energy density. Furthermore, by moving to a metallic anode, one can observe dramatic increases in energy density and specific energy over the conventional carbon anodes of today's lithium ion technology, as illustrated by table 2 below:

Ion	Metallic Anode Capacity (C/cm <sup>3</sup> )	Hypothetical Cell Specific Energy (MJ/kg)
Li <sup>+</sup>	7400	2.2
Na <sup>+</sup>	4000	1.9
K <sup>+</sup>	2100	1.6
Be <sup>2+</sup>	39500	2.8
Mg <sup>2+</sup>	13800	3.1
Ca <sup>2+</sup>	7400	3.4
Al <sup>3+</sup>	28900	3.5

Table 2. **Theoretical energy densities for various ions.** Metallic anode capacity reflects the charge stored within a pure metallic anode. The specific cell energy assumes a complete cell, with a cathode operating at the theoretical valence shift required for the ion of interest, and assumes a 3.5 V cathode (vs. Li) of  $M_w \sim 150$  g/mol.

The use of metallic anodes, is in fact, one of the major reasons that research has shifted towards multivalent ion systems, particularly in the case of magnesium which is known to plate in a non-dendritic fashion. Without metallic anodes, the volumetric and gravimetric energy density gains over lithium-ion technologies are more muted, however reasons such as scalability of production still provides motivation for the development of non-lithium based systems. Although currently there does not exist a room temperature electrolyte capable of reversible calcium plating and stripping, there is hope that one could be developed in the future. As the focus of this thesis is positive electrode intercalation compounds, the question of metallic calcium plating and stripping is not addressed experimentally, and that work is left to a future generation of researchers.

### 1.3.3 Reactivity and Passivity

While it is often difficult to explain the lack of a substantial body of active research in a particular area, calcium prevents several obvious experimental challenges that could explain why few published sources report on calcium electrochemistry. These challenges relate to its reactivity, and affect every aspect of an electrochemical cell ranging from the electrolyte, to the electrodes, to the inert current collectors and housing components.

In general, calcium forms particularly stable compounds – so stable in fact that nature has chosen calcium compounds (particularly carbonate) as one of its main structural elements (e.g. seashells, eggshells, etc...). Calcium oxide is near the bottom of the Ellingham diagram, meaning that it is so stable that calcium will react with almost all other oxides to displace them. Contrary to the ordering of the metals within the electrochemical series calcium (along with magnesium and aluminum) has an oxide that is far more stable than that of lithium or sodium. Such bonding strength extends to the realm of other ionic solids. This presents a particular issue when it comes to designing a calcium ion conducting electrolyte. Unlike the monovalent cation salts, calcium salts tend to be sparingly soluble in a variety of electrolytes. The binding energy of the ionic solid is so great that it, in general, tends to exceed the enthalpic and entropic gains from breaking up the crystal and entering solution. Similarly, it is likely that any solvent system aggressive enough to break up these stable compounds will possibly form tightly-bound complexes, perhaps rendering the electrolyte ineffective as a calcium-ion conductor even though a quantity of calcium-ion containing salt has been solubilized (see section 3.4 for further electrolyte considerations).

Bare calcium metal is extremely reactive. Any oxygen or water contaminants within a cell will immediately react. The reaction of alkali and alkaline metals with organic solvents is commonplace, however in the case of lithium and sodium metal it is serendipitous that such reactions tend to be non-passivating to the electrode. As such electrochemical characterization can be undertaken with relatively minor difficulty. Furthermore, it can be the case that the surface layers reach a stable thickness and prevent further corrosion, while still being ionically conducting and allowing for metallic plating/stripping and the establishment of a stable electrochemical potential. Calcium, unfortunately, forms surface films which tend to passivate calcium metal. An image of calcium metal immersed in a typical organic electrolyte solvent is shown in figure 1 below.

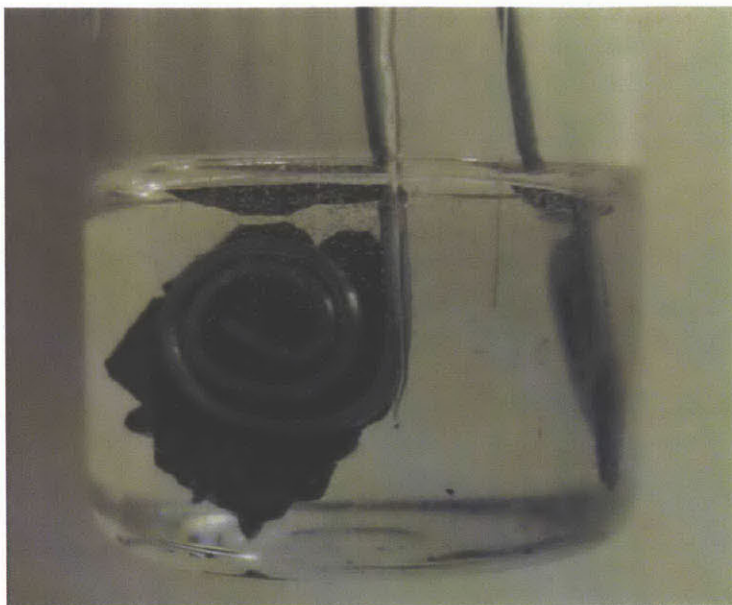


Figure 1. **Calcium metal electrode in organic electrolyte.** Metallic calcium electrode ( $\sim 1 \text{ cm}^2$  area) pressed onto a molybdenum wire current collector immersed in propylene carbonate electrolyte. Bubble evolution is visible in the image, and the originally metallic electrode quickly discolors to dark black.

This surface passivation layer makes studying calcium-ion systems using a metallic calcium half-cell difficult (see section 2.2 for details).

Lastly, intercalation compounds are likely to present some trouble with calcium. Particularly low-potential insertion materials will likely be unstable in the presence of oxygen, water, and other forms of contamination. It is entirely feasible that upon intercalation, calcium from within the compound can escape to react with an external element to the active material, for example oxygen adsorbed onto the surface of the material. The result of this hypothetical interaction would be to coat some segments of particles with a CaO layer, effectively passivating the intercalation electrode.

Although clear challenges exist in the pursuit of calcium batteries, one mustn't be disheartened by the seeming insurmountable task. The potential benefits of calcium-ion technology certainly warrant more focused efforts to tackle the challenges involved.

# **Chapter 2: Background, Inspiration and Requirements for Ca-Ion Study**

Several key requirements for the development and study of calcium ion systems are discussed in this chapter. The absence of a reversible electrochemical half-cell and the challenges it poses are addressed. Several solutions to these issues drawn from the literature are discussed, along with a newly proposed system for the study of calcium-based systems. A literature review of calcium electroactive materials reveals numerous potential candidates for study. An analysis of the prospects for the candidate materials concludes the chapter.

## **2.1 Requirements for the Study of Calcium-Ion Electrochemistry**

### **2.1.1 “There is no half-cell”**

The most common method for the study of lithium-ion intercalation compounds is the lithium half-cell. Metallic lithium is often used as a negative electrode in two electrode studies. For electrochemical measurements requiring greater precision, two separate lithium electrodes can be used in a three-electrode cell configuration, one as a reference and one as a counter electrode. Lithium metal can be reversibly electroplated in a number of electrolyte solutions and provides a stable equilibrium potential. Unlike lithium however, calcium metal is incompatible with most organic and ionic liquid based electrolyte solvents. Solvent decomposition occurs on the surface of the calcium metal, forming a surface layer that tends to be both ionically and electronically insulating, precluding its use as both a

reference and a counter electrode. At elevated temperatures, molten salt electrolytes can be used to reversibly deposit and strip metallic calcium in both the solid and liquid state.<sup>15</sup> However, metallic calcium tends to solubilize in molten salts containing calcium cations at high temperatures, resulting in a typically high self-discharge current.<sup>16</sup> Furthermore, the lowest reported temperature molten salt electrolyte capable of reversible calcium electrochemistry is at 396 degrees C.<sup>16</sup> To this date, a stable calcium metal half cell has not been proposed in the literature, particularly not at room temperature. A recent publication on the calcium-sulfur system (published after much of the research presented in this thesis was conducted) utilizes an acetonitrile-based electrolyte with calcium perchlorate salt.<sup>17</sup> The authors conclude that in such a system, metallic calcium cannot be electrochemically deposited due to the formation of a passivation layer on the metal's surface. It is proposed that the passivation layer breaks down upon anodic bias, allowing for calcium metal to be stripped<sup>17</sup>, a fact not supported by observations in this thesis. Regardless, a stable reference potential cannot be obtained with direct use of calcium metal in an acetonitrile-based electrolyte, thus quantitative electrochemistry in such a half-cell system is impossible.

### **2.1.2 Half-cell workarounds from literature**

Several means exist to perform electrochemical measurements in the absence of a stable half-cell, namely by focusing on and decoupling particular tasks of cell components. A reference electrode must primarily provide a stable value of potential with respect to time, while a counter electrode must be able to act as both an electron source and an electrode sink for the electrochemical cell. In order to effectively study any particular electrode material candidate, these needs must be met.

Reference electrodes separated from the primary electrochemical chamber are the most common means by which electrochemists address the issue of reference electrode stability and compatibility. A separate chamber contains an electrolyte solution in which the reference electrode is immersed, and contact is made with the primary chamber through the use of a salt bridge or frit of some kind. Such

electrodes are typically referred to as reference electrodes of the second kind. Electrodes assembled in this manner suffer from several key drawbacks, namely;

- 1) the electrode potential tends to drift over time as diffusion acts between the separate chambers
- 2) differences in composition result in a junction potential between the electrodes
- 3) such electrodes are very sensitive to human error in assembly and performance

Regardless, of their limitations, these tend to be commonly implemented, and there are a variety of options described in the literature, such as the commonly used Ag-AgCl reference, which are even commercially available.

A second, even simpler reference electrode is referred to as a reference electrode of the third kind, or a quasi-reference electrode, as it does not establish a well-defined thermodynamic potential with the system. Typical quasi-reference electrodes consist of a noble metal wire or foil. A common example of this is the silver quasi-reference, where a piece of silver is inserted directly into the cell. At first the potential fluctuates wildly, but after some time the silver reaches a state of quasi-equilibrium with the electrolyte. Ammatucci and coworkers have utilized such an electrode in a carbonate based electrolyte for the study of calcium electrochemistry involving vanadium oxide and found that it drifts several hundred millivolts over the first few hours, followed by a period of relative stability on the order of tens of millivolts.<sup>18</sup> Work in this thesis supports their claims, and found that the silver quasi-reference randomly fluctuated in a range of roughly 30 mV over a few days. The benefit to such an electrode is its ease of assembly, however its usefulness in quantitative electrochemical measurements is somewhat questionable. For qualitative examinations however, a quasi-reference electrode can be sufficient.

Another possibility extracted from the literature is that of a vibrating electrode. Between the 1920s and 1950s, when experimentalists sought to quantify the potential of metallic calcium electrodes, several developed a technique by which a carefully crafted metallic electrode was rubbed against a rough



surface (such as glass) many times a second.<sup>19</sup> The constant vibration continuously renewed the electrode surface, exposing bare calcium to the electrolyte and establishing an electrode potential that was relatively more stable, and consistently at more negative potentials, than that provided by calcium metal allowed to equilibrate with the electrolyte.<sup>19</sup> Unfortunately, such measurements resulted in inconsistent results for the calcium electrode potential and were prone to experimental error. Using such an electrode would be extremely impractical today, particularly when the electrochemical and thermodynamic properties of a bare metallic electrode in incompatible electrolytes are not of primary interest in this study.

A new reference electrode of the first kind for the study of calcium electrochemistry that avoids many of the issues with current literature standard reference electrodes is proposed and described in section 2.2 of this thesis. In addition to providing a stable reference electrode, the proposed system acts as an acceptable faradaic counter electrode as well. Before presenting such a system however, two alternative counter electrodes from the literature were considered.

One such class of counter electrode involves capacitive charge storage. Rather than creating a system akin to a battery, researchers have sought to create hybrid cells capable of storing charge in the electrolyte double layer on high surface area electrodes.<sup>18</sup> Carbon is a commonly used material for such capacitive charge storage. Such materials tend to have sloping voltage profiles during cycling, and relatively fast electrode kinetics. It is no surprise that small, monoatomic cations can be stored on a double layer. Amatucci and coworkers demonstrated such capacitive charge storage works with complex anions such as  $\text{PF}_6^-$  with acceptable cycling performance.<sup>18</sup> Their work relied on use of a commercially available activated carbon fabric commonly used for filtration systems. Capacitive electrodes have also been constructed using “hard carbon”, by Whitacre and coworkers. These capacity electrodes have been applied to aqueous sodium ion battery technology, currently being commercialized by Aquion Energy.<sup>20</sup>

Another class of counter electrode commonly used in the electrochemistry literature is the inert counter electrode, designed to irreversibly provide/remove electrons to/from the system through

decomposition processes. Such electrodes do not undergo reversible faradaic processes in which a species is oxidized and reduced on, but instead they commonly decompose one of the electrolyte constituents. A common example of this can be found in the molten salt literature where chloride melts will evolve chlorine gas, which escapes from the electrolyte. In the case of organic electrolytes with dissolved salts, decomposition products can be more complex, and either involve breakdown of one of the anionic species in solution or a polymerization/decomposition of the solvent itself. Such counter electrodes typically operate in such a manner that they polarize until the potential of one of the decomposition reactions at the edge of the electrochemical window of the electrolyte is reached. Common candidates for such counter electrodes involve noble metal wires (such as platinum and silver), glassy carbon rods, as well as mercury pools. In many cases of electrolyte decomposition of complex anion salts and organic solvents, the products are at least somewhat soluble in the electrolyte solution, and pose a threat of contamination of the electrochemical signal observed at the working electrode. In order to minimize such contamination, fritted flooded cell designs are commonly used when working with decomposition counter electrodes. The frit acts as a diffusion barrier which prevents decomposition species from traveling to the working electrode on the time scale of the experiment. One cell chamber typically contains a working and reference electrode, with the counter electrode contained in the other chamber. This configuration allows one to ignore overpotentials associated with mass transport due to the frit. Unfortunately, the fact that presence of the frit prevents rapid mass transport between the working and counter electrodes, so the electrolyte contained within the working electrode chamber must be sufficient in quantity so as not to be depleted of active species over the course of an experiment. Such an active species depletion of the electrolyte could result in an appreciable change in concentration, and thus activity and thermodynamic properties of the active species in solution during the course of electrochemical measurements if cells are not carefully scaled to keep the solute concentration approximately constant over the course of a measurement.

## 2.2 Inspiration and Background for the Ca-Hg two-phase Electrode

Each of the reference and counter electrodes used for the study of calcium electrochemistry drawn from the literature has several drawbacks. In the interests of eliminating as many of these issues as possible, a single electrode consisting of a saturated liquid calcium amalgam in equilibrium with a solid intermetallic phase,  $\text{CaHg}_{11}$ , is proposed to satisfy the desired criteria of both a reference and counter electrode. The calcium-mercury phase diagram and the two-phase region of interest are shown below in figure 2.

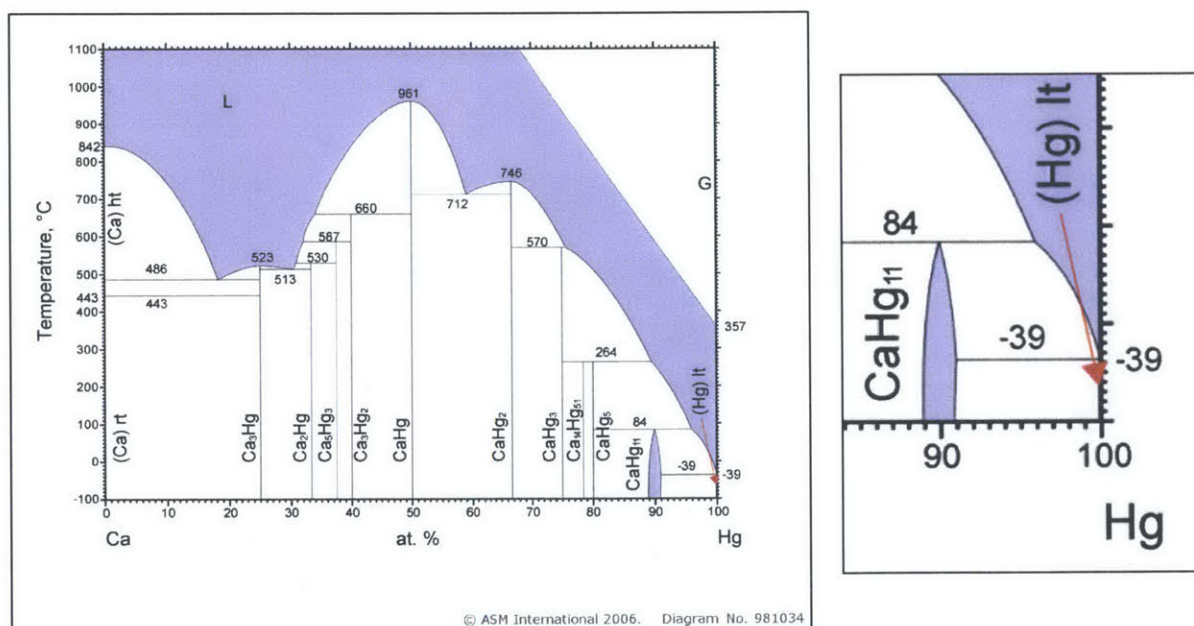


Figure 2. **Calcium-Mercury phase diagram.** The phase diagram is given over the entire composition range (left), with the region of interest for operation as a two-phase electrode given by the expanded region at high mercury content between 90 and 100 atomic percent mercury (right).<sup>21</sup>

Theoretical background concerning the operation of such an electrode, as well as literature evidence supporting its functionality, are described in the remainder of this section.

### 2.2.1 Functionality as a reference electrode

Two-phase reference electrodes take advantage of the fact that the free energies of the end member phases are constant throughout a two phase region, a direct manifestation of the conditions for

equilibrium and Gibbs' phase rule. As the overall system composition varies across a two-phase region, the phase fractions vary but the compositions of the end member components remain fixed. Since the potential of an electrochemical system is related directly to its free energy by the Nernst equation, if the free energies of each phase within the two phase mixture remain constant across the region, then the voltage must remain constant throughout that region as well. Examination of the calcium-mercury phase diagram presented in figure 2 shows limited solubility of calcium in liquid mercury on the order of 1 atomic percent calcium. The intermetallic  $\text{CaHg}_{11}$  compound is centered around 8.3 atomic percent calcium and has a non-negligible tolerance for off stoichiometry of over one percent. These factors suggest a two-phase window of at least 5 atomic percent between these two end members to operate the reference electrode where it is robust to compositional variation due either to preparation technique or corrosion/reaction with the electrolyte solution, current collectors, or containment vessel.

One of the main problems with using calcium metal as a reference electrode is its extreme reactivity – metallic calcium will react with organic solvents and form a surface layer. Lithium, sodium, and other reactive metals experience the same phenomenon, however unlike its monovalent counterparts, divalent calcium ions are unable to pass through the passivating surface layer. The proposed  $\text{CaHg}_{11}$ – $\text{Ca}_{(\text{Hg})}^{\text{sat}}$  electrode circumvents the issue of calcium's reactivity in three ways. Firstly, the potential of the electrode will lie higher, in absolute terms, than the calcium metal electrode potential, therefore decomposition processes are less likely to occur, and those that do occur will happen at a slower rate since there is a reduced thermodynamic driving force as compared to the case of metallic calcium. Secondly, the activity of calcium in an alloyed electrode is lower than the activity of calcium in its metallic state (which by definition has a value of 1). For the case of a dilute electrode containing only a few atomic percent calcium, it is likely that the activity is many orders of magnitude lower, hence calcium's relative reactivity will be far lower than in the metallic state, and the formation of decomposition products is likely to proceed at a drastically slower pace. Finally, and perhaps most interestingly, is the partially liquid nature of the two phase  $\text{CaHg}_{11}$ – $\text{Ca}_{(\text{Hg})}^{\text{sat}}$  electrode, which allows for a

dynamic electrode surface. Any electrolyte decomposition that does occur on the surface of the electrode and create a passivation product is unlikely to completely isolate the electrode from ionic contact with the solution. Flow within the electrolyte and electrode can locally disturb the surface of the electrode, and as such regularly expose fresh surface to the electrolyte. This should provide for a sufficiently robust and stable reference potential. The validity of these assumptions will be explored experimentally in greater detail in Chapter 4.

### 2.2.2 Functionality as a counter electrode

Several of the same features that make the  $\text{CaHg}_{11}\text{--Ca}_{(\text{Hg})}^{\text{sat}}$  electrode a promising reference electrode candidate enable its functionality as a counter electrode as well. The more positive potential of the two-phase electrode with respect to pure calcium increases the likelihood that the electrode will be thermodynamically stable with organic electrolytes. Furthermore, in the event that electrode is not truly stable, the reduced activity of calcium in the amalgam will result in a lower rate of reaction between calcium and the electrolyte, thus decreasing the rate at which undesirable electrolyte decomposition reactions occur. Finally, the presence of a dynamic surface layer enables the possibility that current can be passed through the electrode even in the presence of a passivating film on the electrode surface. Of minor concern to its use as a faradaic electrode, mercury metal is known to generally have very poor charge transfer properties. Still, when functioning as a counter electrode, area can be increased sufficiently such that sluggish kinetics should not prove detrimental, as is shown experimentally in Chapter 4.

### 2.2.3 Literature Review of the Ca-Hg System

Calcium and mercury share a long history together, dating back to 1808, when the first reported production of metallic calcium appears.<sup>22</sup> Calcium chloride was electrolyzed on a mercury electrode to produce a calcium amalgam. Since then, scientists have explored a number of different salt and electrolyte combinations for the production and study of calcium amalgam systems, as well as characterized the thermodynamic properties of those systems in great detail. A good review of earlier

work, by James Butler, summarizes much of the work carried out by previous authors.<sup>19</sup> Originally the calcium amalgam electrode was believed to be irreversible, however later work in fact showed that the electrode was reversible and provided for reasonable electrochemical stability in a variety of non-aqueous electrolytes.<sup>19,23,24,25,26,27</sup> Investigators have determined the diffusion coefficient of calcium in dilute amalgam electrodes, as well as the thermodynamic properties of dilute amalgams.<sup>28</sup> Several studies have been carried out to explore the complete calcium-mercury phase diagram, as well as determine the structural and lattice parameters of various intermetallic compounds.<sup>29</sup> Unfortunately, little literature exists in the way of formation energies of these compounds, or their electrochemical properties.  $\text{CaHg}_{11}$  was found to be a commonly present intermetallic phase during the electrochemical calcium amalgamation process<sup>29</sup>, and provides promising support that the  $\text{CaHg}_{11}\text{-Ca}_{(\text{Hg})}^{\text{sat}}$  region of the phase diagram is appropriate and feasible for use as a counter electrode, even though electrochemical calcium removal was not studied involving the  $\text{CaHg}_{11}$  intermetallic phase. The lack of sufficiently thorough literature on the two-phase region of interest necessitates further electrochemical interrogation of the system, which is presented in Chapter 4.

## 2.3 Literature review of calcium and multivalent ion electrochemistry

This section lays out a literature review of prior art in the area of calcium and multivalent electrochemistry. The survey explores a number of technologies, ranging from high temperature calcium and thermal batteries developed as early as the 1960s, to multivalent transition metal intercalation compounds developed in the 1980s, and ultimately to more recent work in the 2000s focusing on magnesium and calcium intercalation compounds.<sup>30</sup> The section is subdivided by individual chemistries, providing a brief and cross-cutting review of the highlights of each chemistry, with more detail given to Chevrel phase compounds that are the main focus of this thesis. General crosscutting discussion and conclusions pulled from the literature are addressed in section 2.4.

### 2.3.1 Review of $V_2O_5$

Vanadium pentoxide ( $V_2O_5$ ) first found use in the early thermal battery development, fueled by the need for long shelf-life batteries for ballistic missiles necessitated by the cold war. Vanadium oxide cathodes would sit dormant in frozen salt electrolytes until the electrolyte was heated by an external fuse and melted, upon which the battery could be discharged in a primary fashion by reaction with a metallic anode. Calcium was one of several metals to see successful use in this application.<sup>15,31,32,33,34</sup>

In recent years, vanadium oxide has become known as sort of a catch-all intercalant host, and has been shown to intercalate small cations such as lithium, sodium, magnesium, calcium, yttrium, and even aluminum.<sup>11,12,13,18,35</sup> Authors have also demonstrated that the structure is capable of intercalating more complex organic ions within its intercalation pathways. Ultimately, the  $V_2O_5$  structure suffers from extremely slow kinetics involving multivalent ions, due in part to the difficulty of distributing the high charge of multivalent cations. Authors have combatted this problem by proposing shielding methods, by which partially charged or polarizable molecules are incorporated into the  $V_2O_5$  structure to mitigate the effect of the high charge density intercalant ions and lubricate its motion.<sup>10</sup> The extensive body of literature, and explicit work involving calcium intercalation into vanadium oxide makes this an ideal starting point, and will serve as a basis to test the veracity of the electrochemical system proposed for study in this thesis.

### 2.3.2 Review of $WO_3$

Tungsten oxide ( $WO_3$ ) is another compound applied to early thermal batteries, where it found success as a cathode for calcium-based systems. Although metathetical in nature, the thermal battery material vanadium oxide proved successful as a room temperature intercalation candidate, so tungsten oxide may as well. The high valence state of tungsten within the structure offers the possibility to charge compensate calcium with ease as lower redox states are available.<sup>31,32,33</sup>

### 2.3.3 Review of $\text{CaCrO}_4$

Calcium chromate ( $\text{CaCrO}_4$ ) is an unlikely candidate as a possible calcium electro-active material, although it will be reviewed and tested for completeness as it too found success in early thermal batteries. Upon discharge, the electrode would undergo a molten-salt mediated reaction that would form metal-oxide products, namely calcium oxide and lithium oxide, utilizing cations from the molten salt. The involvement of the lithium salt within the reaction, as well as the formation of metal oxides, makes it extremely unlikely that any sort of process involving the material would be reversible at room temperature involving only calcium-containing electrolyte. However, theoretically, chromium is in a sufficiently high oxidation state to allow for some reaction involving calcium.<sup>31,32,33</sup>

### 2.3.4 Review of $\text{K}_2\text{FeO}_3$

Potassium ferrate is an interesting compound in which iron exists in its 6+ oxidation state. The iron center is able to undergo an electrochemical reaction with lithium and reduce its oxidation state to 3+, resulting in an electron transfer of 3 electrons per formula unit. The reaction mechanism however, was observed to be metathetical and not intercalant in nature, and involves the formation of products that are somewhat irreversible. Authors have strived to modify ferrate preparation and cell assembly techniques to improve electrode utilization, however ultimately whatever challenges limit the electrode's usefulness in the context of an alkaline battery are ultimately likely to be exacerbated in the presence of calcium.<sup>36,37,38,39,40</sup>

### 2.3.5 Review of $\text{FeS}_2$

Iron sulfide batteries were explored from the 1970s through the 1980s for use in automotive applications. Discovered accidentally through the unintended corrosion of steel during the study of metal sulfur batteries, iron sulfide batteries proved a robust technology in their own right. Calcium iron sulfide offers a discharge voltage of about 1.8 V vs. the  $\text{Ca}/\text{Ca}^{2+}$  couple, as well as good cycle life. Ultimately, lithium ion sulfide replaced calcium iron sulfide as a candidate of interest due to its lighter weight, and intended use in mobile applications. The technology encountered challenges involving containment and



sulfur solubility issues, as well as sensitivity to air and moisture. No examination of iron sulfide as a possible room temperature cathode material for calcium is known to date.<sup>31,32,33,41</sup>

### 2.3.6 Review of $\text{TiS}_2$

Titanium disulfide ( $\text{TiS}_2$ ) is a common intercalation compound studied electrochemically in the context of lithium intercalation. Interestingly, multivalent ions such as zinc and magnesium have been shown to intercalate into the structure, likely aided by the increased polarizability of the large anions within the structure, which are able to better accommodate the increased local charge density requirements. Although the potential of the  $\text{TiS}_2$  material is impractically positioned in the context of lithium ion batteries, it is poised to serve as a possible proof of concept structure for calcium intercalation.<sup>30</sup>

### 2.3.7 Review of S

Metal sulfide batteries have been studied for decades as high temperature energy storage solutions for both mobile and stationary applications. The most well known and highly developed such systems are based on sodium-sulfur chemistry and make use of solid beta alumina sodium diffusion membranes as electrolytes.<sup>42</sup> Little work exists in the realm of room temperature sulfide batteries, especially in the realm of calcium, however one recent paper presents evidence of primary calcium-sulfide batteries operated at room temperature in organic electrolyte utilizing a carbon-sulfur composite electrode.<sup>17</sup> The authors suggest that calcium deposition is the irreversible step in their system, and that metallic calcium can be electro-stripped within organic electrolyte under appropriate polarization bias, an observation found not to be reproducible in our own experiments. Still, the behavior of the sulfur electrode is of interest, if it is indeed reversible on its own.

### 2.3.8 Review of $\text{Mo}_6\text{X}_8$ ( $\text{X} = \text{S}, \text{Se}, \text{Te}$ )

The Chevrel phase class of molybdenum cluster calcogens were first synthesized in the 1970s, and since then has been extensively studied for both its low-temperature superconducting properties and

its electrochemical behavior as an intercalant host for a range of monovalent and divalent ions including lithium, sodium, magnesium, zinc, and cadmium.<sup>44,45,46,47,48,49,50</sup> An illustration of the  $\text{PbMo}_6\text{S}_8$  Chevrel phase structure is shown in figure 3 below.

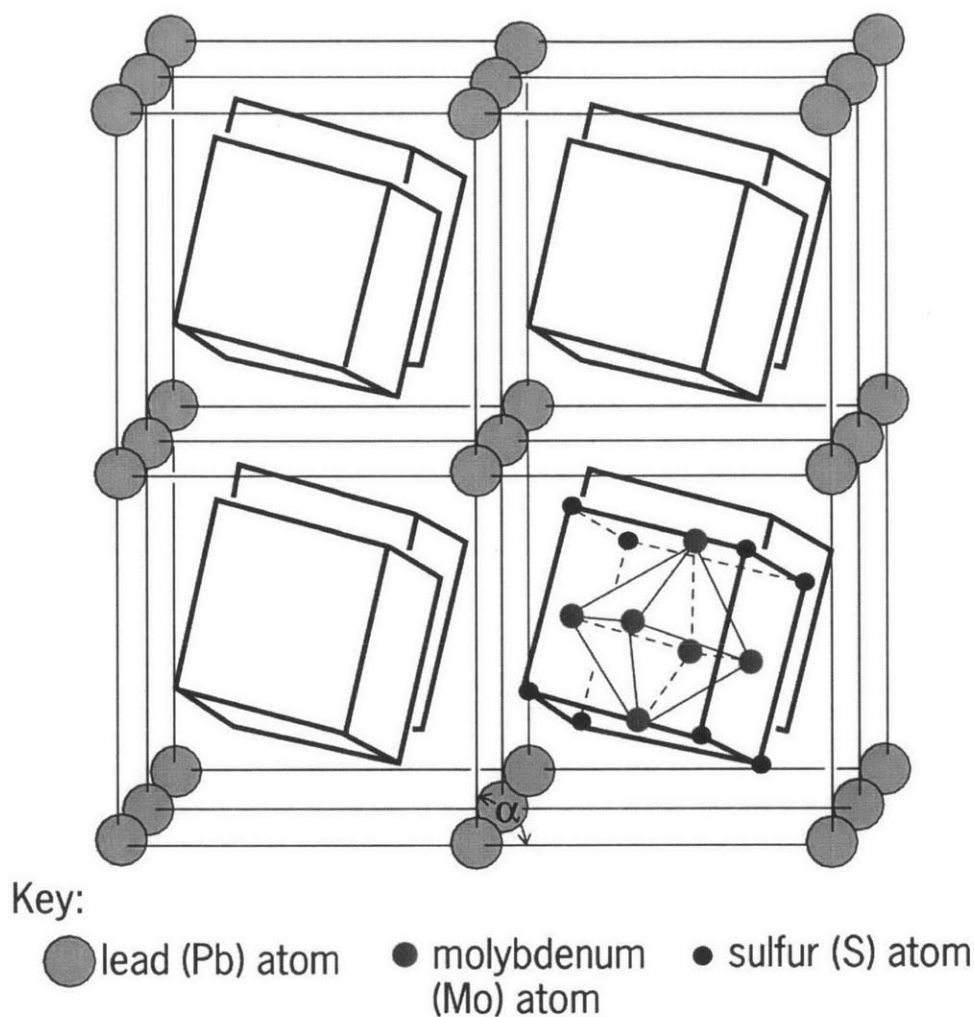


Figure 3. **Structure of the  $\text{Pb}_1\text{Mo}_6\text{S}_8$  Chevrel phase.** Molybdenum “octahedral” clusters are located in the interior of sulfur “cubes”. The lead sits at potential intercalation sites, coordinated within their own “sulfur” cube. Various metal anions rest at different, sometimes delocalized, differently coordinated sub-locations within the lead site.

Professor Aurbach’s group has recently published several papers outlining their steps toward a high energy density magnesium ion battery.<sup>51,52,53,54,55,56,57,58,59,60,61,62,63</sup> They have demonstrated a working electrolyte for direct magnesium plating and stripping (although with a limited electrochemical window) and explored the use of various molybdenum cluster chevrel phase compounds as an intercalant medium for divalent ions. These compounds of the family  $\text{Mo}_6\text{X}_8$  ( $\text{X}=\text{S}, \text{Se}$ ) derive from a family of  $\text{Cu}_2\text{Mo}_6\text{X}_8$

compounds which are metastable in nature. The clustering of the Mo ions allows them to quickly accommodate compensating electrons, demonstrating improved rate performance when compared to other transition metal center oxide hosts. Reversible magnesium capacity near the theoretical value of two atoms per formula unit has been demonstrated, governed by a two step insertion process corresponding to the total net reaction given in equation 3 and reflected by the two-plateau profile in figure 4 below.

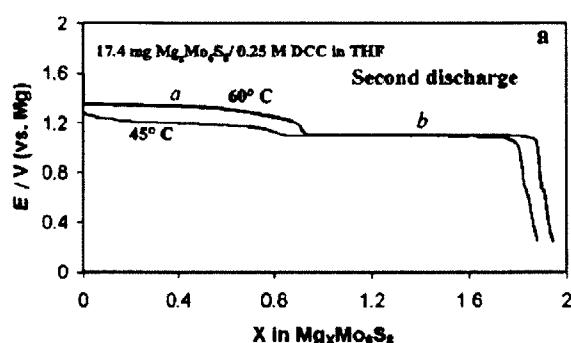
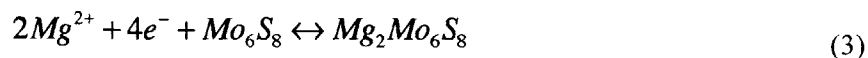


Figure 4. Discharge profile for  $\text{Mg}^{2+}$  into  $\text{Mo}_6\text{S}_8$ . Two different types of coordination exist for Mg intercalation sites, resulting in a two-step discharge profile separated by several hundred millivolts.

Although extremely promising in its rate performance and magnesium utilization, the overall discharge potential is relatively low (on the order of 1V) and the material boasts a theoretical gravimetric capacity of 124.4 mAh/g which is comparable to, but hardly an improvement on current lithium ion systems. The continuation of this vein of research into magnesium ion technology is being further developed in conjunction with Pellion Technologies for commercial applications. As a model system however,  $\text{Mo}_6\text{S}_8$  is extremely promising for the intercalation of multivalent species. Earlier work has documented  $\text{Zn}^{2+}$ ,  $\text{Cd}^{2+}$ , and  $\text{Na}^{+}$  ion mobility in this host, which suggests that the structure could possibly be used to intercalate other divalent, or possibly even higher valency ions.<sup>50</sup> The original classification of the Chevrel structure by Yvon suggested that two types of Chevrel phase behavior exist, “small” cation behavior which consists of mobile delocalized cations within the cavity formed by the calcogen cube, and “large” cation behavior in which a single immobile cation sits at the center of the cavity. Electrochemical

studies have shown however, that “large” cations such as sodium and cadmium are able to electrochemically intercalate into the structure, and the possibility for calcium as a similarly sized ion exists.<sup>64</sup>

## 2.4 Discussion of Multivalent Intercalation Candidates

Calcium electrochemistry is an exciting, yet underdeveloped field, due in no small part to the experimental difficulties of working with calcium outlined in the previous two chapters. Still, several calcium-based technologies have been successfully explored and developed in the literature. The bulk of these technologies have been explored as primary systems, or involve high operating temperatures, which reduces challenges associated with reversibility and kinetics. Room temperature systems have been demonstrated, but have been found to have limited kinetics and poor reversibility. A few classes of compounds have been found to reversibly intercalate multivalent ions successfully at room temperature, namely vanadium oxide, titanium sulfide, and chevrel class cluster compounds. A comparison of the performance of these classes suggests that oxide hosts are unlikely to function well kinetically at room temperature with multivalent ions, due in part to strong interatomic interactions between multivalent ions and the oxygen anionic framework, unless efforts are taken to shield the oxide anionic framework and increase its effective polarizability. Sulfide and selenide containing compounds offer greater anionic polarizability, which one would expect to result in greater multivalent ion mobility. Thus candidates with larger, more polarizable anions, should prove to be more promising from a kinetic point of view. Even though sulfide and selenide containing compounds are promising, structures containing these elements tend to on average offer a lower theoretical operating voltage and lower gravimetric capacities than their oxide counterparts. Still, some promising work has shown that partial anion substitution can allow for improved ion mobility while maintaining a higher operating voltage, offering the best of both worlds.<sup>65</sup> Calcium, fortunately, has a charge to volume ratio that is lower than other multivalent ions such as magnesium, aluminum, and d-block transition metals, although its divalency still offers the possibility of coupling strongly with anions.

In addition to polarizability effects, multivalent ions face two other challenges in the context of intercalation compound design and performance. Intercalation hosts typically consist of transition metals that change valence to charge compensate as ions are inserted into the structure. In order to realize the full capacity potential of multivalent ions, multiple redox shifts are needed per transition metal ion in the host structure. This is not a trivial problem. Some instances of multiple redox state jumps have been shown in the literature, such as  $\text{Ni}^{4+}$  to  $\text{Ni}^{2+}$  in the case appropriately structured metal oxides. The most promising multivalent intercalation compounds however, have been observed to show at best a fractional average redox shift, such as  $2/3$  of an electron per molybdenum atom in Chevrel cluster compounds. Although a challenging design problem, a great deal of effort is being exerted in the magnesium electrochemistry space, particularly in computational studies of new classes of cathode materials, and once promising candidates are found for magnesium such classes of materials, the lessons learned should be adaptable to calcium electrochemistry. One kinetic effect of interest, related to the multiple redox shift problem, is the question of how quickly multiple electrons can jump between transition metal centers within a host material, as ions and electrons need to remain in relative proximity to each other within an insertion host. It may be possible that a “redox drag” effect could be exerted on ions that in principle should have high mobilities due to the efforts of a coupled diffusion phenomenon.

Steric effects are of particular interest in the case of calcium as it is a relatively large ion when compared to lithium, a number of other multivalent ions, and even sodium. Sodium is known to not work in a number of structures that can accommodate lithium with little trouble. Graphite is a classic example of this limitation. Calcium’s size increases the likelihood that it may be too large to sit in particular crystallographic sites without creating additional strain energy. This may have a number of effects, such as limiting the calcium loading of a material, or preventing calcium insertion entirely. Furthermore, intermediate states between energy minima may prove highly unfavorable, resulting in poor calcium mobility.

## 2.5 Chapter Summary

This chapter began by addressing some of the challenges preventing the implementation of a traditional calcium half-cell at room temperature. The key functions of a calcium half-cell were enunciated, and a novel two phase reference and counter electrode for the study of calcium electrochemistry capable of performing these functions was proposed. The system takes advantage of the two phase region formed between the solid  $\text{CaHg}_{11}$  intermetallic compound and saturated liquid calcium amalgam, and is expected to avoid a number of issues with other half-cell substitutes observed in the literature. A general survey of general multivalent ion and calcium-based electrochemistry was performed, and several general conclusions were drawn; (1) multivalent ions tend to show improved performance in more polarizable compounds, (2) the multiple redox shifts required to realize the full potential of multivalent insertion compounds are observed in some, but not all systems, and (3) calcium will potentially suffer from some steric effects.

# Chapter 3: Procedures and Methods

## 3.1 Electrochemical Techniques

Various electrochemical techniques employed throughout this thesis are discussed briefly in this section. A basic description of the technique is given, followed by a description of its utility, as well as any considerations related to the applicability or accuracy of the technique.

### 3.1.1 Open Circuit Voltage

Open circuit voltage (OCV) measurements are a common method to characterize the thermodynamic properties of electrochemical systems. The OCV is effectively the voltage measured between two electrodes at zero current. At its most basic level, a potentiometer measures OCV by passing an exceedingly small amount of current across a large known resistance, and interpolates the voltage drop across the resistor. Assuming the current is small enough, this can be considered to be a “zero” current value of cell potential.

The OCV of a cell can be related to the free energy difference between the electrodes by the Nernst equation, as discussed in Chapter 1 of this thesis. OCV measurements are used to characterize the thermodynamic properties of calcium amalgam electrodes in Chapter 4, as well as look at positive electrode candidates presented in Chapter 5. OCV rests are an integral part of various titration techniques, and can also be used to observe effects related to self-discharge or spontaneous electrode reactions of corrosion.

### **3.1.2 Potentiostatic Hold**

A potentiostatic experiment is one in which a potentiostat is used to fix the potential of a particular electrode relative to a reference electrode. Current is passed as required to maintain the desired potential difference between the electrodes. The method typically results in a current signal that is large at first, to quickly obtain the desired polarization of the electrodes of interest, and then decays slowly over time towards a steady state value. The decayed value of current is characteristic of faradaic processes within the cell, such as alloying or intercalation, and continues to operate until the process operative at the set value of potential is complete. After the desired process is completed, any residual current that continues to pass is typically related to corrosion, self-discharge, or other parasitic reactions within the cell.<sup>2</sup> Potentiostatic holds are a versatile technique used in Chapters 4 and 5, for a number of applications such as cleaning of mercury electrodes, measuring self-discharge or corrosion currents, pre-electrolyzing the electrolytes to remove impurities, and insertion/removal of ions from positive electrode candidates in preparation for analytical techniques such as SEM, TEM, EDS, and XRD.

### **3.1.3 Cyclic Voltammetry**

Cyclic voltammetry is a potential-controlled electrochemical technique in which a potentiostat is used to sweep the potential of the electrode back and forth over time. The current response of the electrode is measured on the various sweeps. Various techniques exist that use different waveforms of potential for the sweeps, such as linear or step-shaped.<sup>2</sup> For this thesis, linear sweep cyclic voltammetry method was used, the waveform of which is shown in the stylized image in figure 5 below.



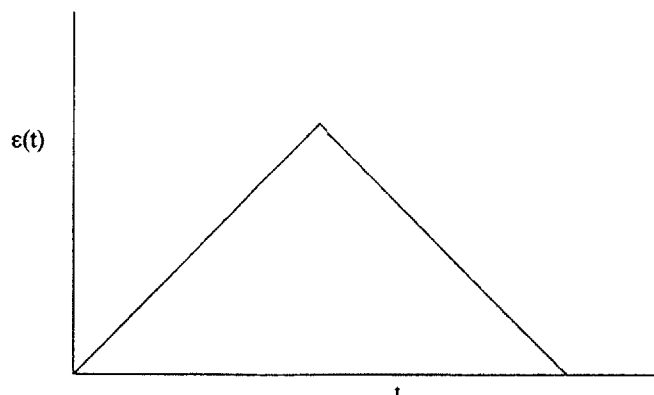


Figure 5. **Typical waveform for a cyclic voltammogram.** The potential is linearly swept with time to a peak value, and then reversed down to the original value. Such sweeps may be repeated in succession for multiple scans.<sup>66</sup>

The current response of the cyclic voltammogram is typically plotted on the dependent variable (y-axis) as a current density normalized by electrode area, however there are cases where it is also useful to plot such voltammograms normalized by electrode mass. This is particularly useful in cases where composite particulate electrodes are used at different effective loadings per unit apparent area, such that the actual surface area loading of the samples can vary greatly from the apparent area. Electrochemical processes tend to appear in peak or wave-like shapes, depending upon the kinetics of the involved processes. Currents corresponding to multiple, overlapping waves tend to be additive. As the potential axis is also effectively a transformation of a time axis, one is able to extract parameters such as material capacity, coulombic efficiency, and pseudo-discharge curves fairly easily. Further integration of the current vs. potential curve can also yield energy information. In all cases of such analysis, it is necessary to know the extent of active material loading on electrodes.<sup>2</sup>

Cyclic voltammetry is the primary means by which the electrochemical window of electrolytes are established, and is applied to that end later in Chapter 3 for preliminary electrolyte screening and characterization. Another common application of cyclic voltammetry is to explore metallic plating and stripping, or alloying and dealloying processes, as will be done in Chapter 4 of this thesis. In Chapter 5, cyclic voltammetry is used to qualitatively screen a variety of potential positive electrode candidates.

### 3.1.4 AC Impedance

Impedance measurements are a common electrochemical technique involving the application of an alternating current or voltage signal to an electrochemical cell. From the applied perturbation, the impedance characteristics of the cell are extrapolated, including real and imaginary components of the resistances as well as phase angle. The frequency of the perturbation is typically varied over many orders of magnitude and the response of the cell is measured. Different resistance mechanisms dominate at different frequency regimes. From such measurements one can postulate an equivalent circuit to describe the interior resistances of the cell. Different internal losses in the cell can be described by quantities such as electrolyte resistance, mass transport, interfacial resistance, and charge transfer resistance.<sup>2</sup> The relative contributions of each of the resistance mechanisms can be compared. Furthermore, the evolution of such resistances can be explored over time. Impedance measurements are used primarily in Chapter 4 to explore the kinetics of the calcium-mercury amalgam electrodes in this thesis.

### 3.1.5 Galvanic Pulse

In galvanostatic measurements, a constant current is passed through the electrochemical system and the potential response is measured as a function of time. Current may be passed for a fixed amount of time, or until a particular potential cutoff or rate of change of potential with time is reached. The sign of the current may be controlled, as well as its magnitude. A common extension of a galvanostatic measurement is galvanic cycling, in which current is passed repeatedly in opposite directions corresponding to the charge-discharge behavior of a battery.<sup>2</sup> Voltage versus capacity profiles are most commonly presented in the literature, where the capacity plotted is a simple transformation of the time access to account for current and electrode mass. Profiles are typically steep in areas corresponding to no faradaic processes, and slopped or level corresponding to areas where faradaic processes such as intercalation, conversion, or corrosion are active. Potential profiles tend to be flat in areas corresponding to two-phase regions within electroactive materials, resulting from the Gibbs phase rule and the conversion of electrode phase fraction between the intercalated and deintercalated phases. The voltage

versus capacity profiles tend to differ on charge and discharge by an overpotential corresponding to the internal resistances of the electrochemical cell. These resistances tend to have a more pronounced effect on potential at higher current rates, as would be expected from dissipative mechanisms. Large electrode polarizations are observed in systems with poor kinetics, while facile systems tend to show small polarizations between charge and discharge curves.<sup>2</sup> Such polarizations affect both the coulombic (through reaching cutoff voltages sooner) and energy (through greater difference in potential between charge and discharge) efficiencies of the cell, which can be easily extracted from galvanic cycling curves, as can fade rates from the comparison of capacities or specific energies over a number of subsequent cycles.

Galvanic measurements will be applied primarily in this thesis to explore the behavior of positive electrode materials as a function of cycling rate and temperature in Chapter 5 of this thesis. Furthermore, the galvanic behavior of calcium amalgam electrodes and the resulting overpotentials will be explored briefly in Chapter 4 to address the application of such systems as faradaic counter electrodes for a pseudo-calcium electrochemical half-cell.

### **3.1.6 Galvanic Titration**

Galvanic titration-relaxation measurements involve the combination of a series of galvanostatic pulses with an open circuit rest between each pulse. Much like other galvanostatic measurements, current is held at a constant value and the voltage response of the system is measured. The duration of such experiments is set either for a particular time, or by a voltage or rate of change of voltage cutoff. After the pulse is completed, an open circuit measurement is taken. The open circuit measurement is followed by another pulse. Such measurements are useful as they allow electrodes to equilibrate and reduce effects associated with transport limitations within the electrode or the electrolyte. Furthermore, they can be used to determine thermodynamic and kinetic parameters from the relaxation values and relaxation times.<sup>2</sup>

Titration measurements are applied in this thesis to the calcium-mercury system in Chapter 4, to explore its thermodynamics. Furthermore, such measurements form the foundation of the galvanostatic intermittent titration technique, used to estimate the diffusivity of calcium in mercury (discussed in greater detail in section 3.1.7). Such titration measurements are also applied in chapter 5 to attempt to fully calcinate electrodes, and determine the OCV values of calcinated and decalcinated electrodes.

### **3.1.7 Galvanostatic Intermittent Titration Technique**

The Galvanostatic Intermittent Titration Technique (GITT) is a pulsed-current electrochemical method commonly used to probe electrode kinetics. The technique, as first described by Weppner and Huggins in 1977, relies on the application of a short current pulse followed by a long relaxation time resulting in an equilibrium charge-discharge profile for the system.<sup>67</sup> Values for the diffusivity of electrode materials can be extracted from the relaxation behavior. Later authors have adapted the technique to probe other materials phenomenon such as determination of nucleation and characterization of phase boundary motion limited processes.<sup>68</sup> The technique has been successfully applied to liquid metal electrodes in addition to solid state electrodes.<sup>69</sup>

The GITT technique is applicable to a number of systems but will be described here in the context of intercalant batteries. During the applied current pulse a small number of ions (typically corresponding to less than 1% of the total capacity of the material) are inserted into the electrode at its surface, establishing a concentration gradient across the active material particles. After the applied current is stopped, the material diffuses into the bulk of the particle. The diffusion coefficient of the ionic species of interest can be determined provided that the current pulse length is sufficiently small that the system follows Fickian diffusion dynamics with a constant diffusion coefficient for the duration of the pulse. Over the course of a single pulse-relaxation couple the potential of the cell will dip and then return as material is first concentrated at the surface and then moves into the bulk of the material, as shown in figure 6 below.

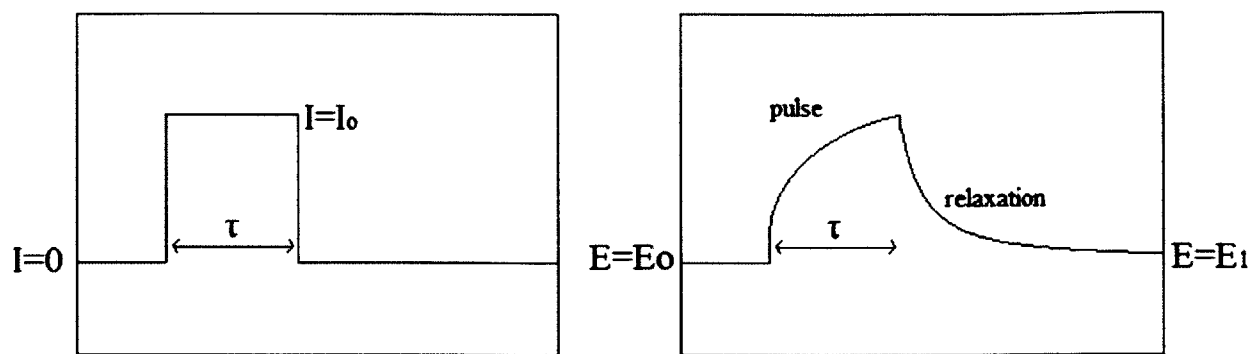


Figure 6. **Theoretical current and voltage curves for GITT protocol.** A current pulse (left) is applied for a time duration  $\tau$  after which the current is discontinued and the cell is allowed to equilibrate. The voltage (right) initially increases in response to the current pulse, and then relaxes to a value slightly different from its initial value.

The characterization of diffusion coefficients within host materials is particularly important in the context of non-lithium battery systems. Several published sources show that one reason for poor performance is the slower ion mobility. Although in some cases it has been shown that kinetic limitations in electrodes correspond not simply to diffusion, but to effects coupled to the redistribution of charge, determining the transport properties of the ions themselves is key in explaining limitations in electrochemical behavior. Although it may seem like a promising technique for the characterization of solid state diffusion in intercalation compounds, the GITT technique is often misapplied in this space. One major assumption related to the GITT technique is the presence of only a single phase domain over the course of the measurement. Authors often meaninglessly apply GITT in the case of two-phase systems where, either at the single particle or composite electrode level, kinetics are not simply governed by diffusion limitations.<sup>70</sup>

In this thesis, GITT is applied to measure the diffusion coefficient of calcium in mercury, in the process of validating the calcium amalgam as an electrochemical system for the study of calcium electrode materials in Chapter 4. The technique will not be applied to solid electrodes, as the veracity of the technique has recently come into question in systems composed of multi-phase electrodes, even in presumably “single phase” regions.<sup>70</sup>

## **3.2 Materials Characterization**

In addition to performing electrochemical experiments, several general analytical techniques are applied in this thesis to characterize materials behavior. Structural transformations in battery compounds are particularly interesting as they play a role in determining the cell voltages and discharge profiles. Two-phase regimes produce broad flat discharge profiles in electrochemical cells. Similarly, chemical composition analysis as well as the determination of valence states of species involved provide evidence of a particular mechanism by which energy storage occurs.

### **3.2.1 X-Ray Diffraction**

X-Ray Diffraction (XRD) is a technique by which X-rays are scattered off a sample of interest and the scattering pattern is measured by a detection device. The pattern is generated as different reflections off of atomic plane orientations within the sample result in constructive – and destructive interference. Information about the atomic-scale ordering of the system can be gleaned. Commonly extracted parameters include crystallographic structure and lattice parameters, degree of crystallinity/amorphy, as well as limited insight into the composition of unknown species.

Numerous classifications of XRD exist with very different system geometries and the sample types. Within the context of battery electrode materials, powder diffraction is the most logical choice as electrodes are typically comprised of a composite of micro or nano-scaled particles with a polymer binding medium and carbon conductive additive. In this case, it can be assumed that the arrangement of electro-active material particles is indeed random as would be necessary for powder diffraction. The effect of the small percentages of binder and carbon additives (typically less than 10% by mass) should not greatly affect the XRD patterns of the material of interest, except to add some slight amorphous scattering to the background. However, in the interests of minimizing these background effects, powder samples devoid of binder or carbon are used for study.

A common practice in the lithium ion literature is to assemble a cell and to discharge it to varying states of discharge corresponding to positions of interest within the discharge profile at which point they are re-opened and the electrodes are extracted for study. For example, cells may be assembled and only partially discharged to the middle of a suspected two-phase plateau before cutting the current and extracting the electrode. The XRD pattern of a biphasic material should contain traces of and provide information on both end-member phases. Typically such diffraction patterns are collected under exposure to air, as the potential at which lithium insertion into these materials occurs is stable with respect to oxygen and moisture. However, the materials of interest in this study are air and moisture sensitive, and as such special sample preparation techniques are required.

In-situ XRD compatible coin cells are one method by which XRD spectra may be collected without exposure to air, however would be impractical in this thesis due to the unique requirements of the counter electrode. The most ubiquitous post-mortem method of handling air sensitive samples is simply to enclose them in Capton film with scotch tape, however this method leaves much to be desired in the way of leakage. Two other cell designs, one involving a rubber o-ring seal and beryllium window, and the other using a glass capillary, were used in this study.

The beryllium windowed sample chamber consists of an aluminum sample holder fitted with a circular beryllium window on one side, and an open hole on the other side. The hole is loaded with a zero background sample holder (ZBH), which is comprised of single crystal silicon cut off-axis to provide no signal to the detector, enclosed in an aluminum ring, and finally wrapped in an o-ring. The specimen is loaded onto the ZBH as one would load typical powder diffractometer samples, and is then pushed into the hole in the aluminum plate forming an o-ring “seal”. Unfortunately this technique does not provide additional active compression of the o-ring, making it less robust than other o-ring seal designs in other applications. The beryllium windowed chamber is useful in that it does not provide any background or amorphous signal due to the substrate or any polymeric or amorphous membranes. The beryllium signal can be accounted for in the analysis of the data to decouple it from the specimen of interest.

Glass capillary sample holders of outer diameter 0.5 mm and wall thickness 0.01 mm supplied by Charles Supper Company were used to study air-sensitive samples. The capillary chamber was loaded with powders in glovebox, and several small pieces of lithium metal foil were placed at the opening of the chamber to act as an oxygen getter. The capillary was then sealed shut with epoxy and allowed to dry in the glovebox.

Slow scan rate XRD scans were performed overnight (11-15 hour data collection time) in order to maximize the obtained signal. Samples were prepared in-glovebox, loaded into the appropriate sample holders, and stored in glovebox until immediately before the collection time. Samples were always prepared such that the electrochemistry of interest was completed during the day, and the XRD samples would be run the same evening, to minimize possible sample degradation over time.

### **3.2.2 Scanning Electron Microscopy and Energy Dispersive X-ray Spectroscopy**

Scanning electron microscopy (SEM) is a technique by which an electron beam is used to generate an image of the surface of a sample. As the electron beam interacts with the sample, secondary and backscattered electrons result, which can be picked up by a detector. SEM provides much greater resolution than an optical microscope, and can provide images on the submicron and nanometer lengthscales. SEM is a common technique for determining the morphology of samples, as well as features such as primary particle size and microstructural features.

A common add-on for the SEM allows for compositional data to be collected through energy dispersive x-ray spectroscopy (EDX). The electron beam of the SEM can liberate electrons from within the atoms of the specimen of interest. Electrons decay to fill those gaps, releasing characteristic wavelengths of radiation that can be interpreted to reveal compositional information about the sample. The spatial accuracy of EDX is determined by the irradiated interaction volume of the SEM as well as the sample of interest. The although the presence of elemental species can be determined with certainty, the



EDX technique is relatively limited when it comes to quantification of samples, with accuracy typically reliable to within no more than a few atomic percent.

### **3.2.3 Transmission Electron Microscopy**

Transmission electron microscopy (TEM) is a common characterization technique by which electrons are passed through a specimen of interest. The electrons interact with the atoms within the specimen and are then captured by a detector, generating an image based on those interactions. In order to gather data, TEM requires thin samples such that they are electron transparent. Typically samples are milled down to the sub-micron to nanometer length scales using a focused ion beam to obtain this transparency. Small individual particles however, can be imaged directly when dispersed appropriately on a grid, without the need for additional milling.

TEM allows for greater magnification than SEM imaging, allowing spatial resolution on the order of atomic length scales. Amorphous and crystalline phases can be distinguished directly through TEM imaging, due to the regularity of stacking in the crystalline case. Furthermore, structural data on the specimen can be directly gathered through electron beam diffraction. Compositional data may also be gathered on the specimens with high spatial accuracy through the use of EDX spectroscopy. EDX in dark field STEM mode was used to collect compositional data in Chapter 5.

### **3.2.4 X-ray Photoelectron Spectroscopy**

X-ray photoelectron spectroscopy (XPS) is a surface-sensitive chemical characterization technique. The specimen of interest is irradiated with high energy x-rays, causing the emission of electrons by the sample. The number and kinetic energies of these electrons are then measured by a detector and related to the elements and orbitals from which they were emitted. The technique is typically sensitive to the parts per thousand concentration range, and in addition to providing chemical identity can also determine the local bonding environment of species. Typically information can be gathered from the first 10 nm of the surface of the specimen, and as such it is not applicable for bulk compositional analysis.

The XPS technique is used to examine the local bonding environment of surface atoms within the Chevrel phase in Chapter 6.

### **3.3 Experimental Apparatus**

This section lays out the considerations leading to the experimental apparatus design used for electrochemical testing in calcium-based systems. Cell and electrode preparation and assembly techniques are described in detail. Subsequent sections in this chapter address electrolyte choice as well as active electrode material synthesis procedures.

#### **3.3.1 Vessel Design Challenges**

Standard batteries operate using only two electrodes, an anode and a cathode. Current is passed between the two electrodes, and work is able to be extracted from the system by passing electrons through an external circuit. The net operating voltage of the cell takes into account reactions at both electrodes. The two electrodes are roughly matched in capacity, as well as for current rates such that kinetics does not pose an issue. Several standard experimental setups exist to mimic the way a battery operates. The most commonly used in the lithium battery industry is the coin cell. Two steel disks are crimped together along with a seam, spacer and spring to keep the two electrodes pressed together. The uniform crimping pressure applied by the crimper tends to ensure a consistent stack pressure between tests. The strength of the spring, as well as the thickness of the spacer can be adjusted to adjust this pressure. Another method involves using screw-top or Swagelok type cells. Both types of two-electrode cell configuration have been historically optimized for compatibility with lithium-ion cell components. Unfortunately, calcium and lithium electrolyte solutions behave remarkably differently. As a result, all commercially available and in-house designed two-electrode compression cells were found to corrode, resulting in poor electrochemical reliability. Additionally, a two-electrode cell is less interesting from an electrochemical characterization standpoint, as the absence of an external reference electrode limits the types of measurements that may be conducted. Furthermore the lack of a reliable metallic anode for the creation of a calcium half-cell precludes the use of a two-electrode compression cell. The success of the two-phase

CaHg<sub>11</sub>-Ca<sub>(Hg)</sub> electrode meant that all experiments would have to be conducted in flooded-flask type cells due to its liquid metal slush nature.

In order to obtain more reliable electrochemical data, a flooded flask-type three electrode cell design was used. Current is still passed between two active electrodes to complete the electrochemical circuit. The same reactions occur as would occur in a two-electrode system. However, by introducing an additional electrode into the cell one can measure the potential between this electrode and another electrode of interest within the cell (typically referred to as a reference electrode). This third electrode has the added benefit that only an exceedingly small amount of current is being passed through it at any given time, so its potential should be very stable and precise (over-potentials due to kinetic effects are drastically minimized). Furthermore, by ‘opening up’ the two electrode system into a three electrode cell, the electroactive area of one of the electrodes can be increased greatly relative to the other. In this manner, the electrochemical reactions at one electrode of interest (typically referred to as the working electrode -WE) can be decoupled from the other electrode (typically referred to as the counter electrode -CE). Typical 3-electrode flask cell designs use an extremely large volume of electrolyte, as well as expose current leads and connectors (typically steel or copper) to the atmosphere of the inner chamber. It was determined that this fact, combined with the volatility of certain electrolyte solutions, resulted in corrosion above the electrolyte line in the cell. In order to circumvent this problem, a custom-built cell was designed, which is discussed in greater detail in the next section.

### **3.3.2 Three electrode vessel design**

A survey of a handbook of phase diagrams, the literature, as well discussions with researchers working with calcium-based systems at high temperatures (typically above 500°C), led to the identification of tungsten and molybdenum as two good candidates for inert current collector materials for the study of calcium electrochemistry. As discussed in the previous section, a number of other metals will undergo extreme corrosion in certain electrolyte solutions. Molybdenum was ultimately chosen, as it is

less brittle than tungsten. The custom-built three-electrode vessel was designed to have only molybdenum, PTFE, and glass in contact with the electrochemical chamber.

The vessel chamber was that of a 20 mL glass vial with a tight-fitting PTFE-lined screw cap (VWR International – Part Number 14231-552). Small holes were machined in the top of the cap, through which molybdenum current leads or composite electrodes were inserted. The vial caps were then sealed with a fast-drying epoxy. For all experiments conducted using pure mercury or two-phase  $\text{CaHg}_{11}\text{-Ca(Hg)}$  electrodes, freshly sanded 1 mm diameter molybdenum metal wire (99.9% purity) was used as a current collector. The wire, which was coiled into a small spiral and bent at the base, was nestled in small glass crucibles into which the mercury solutions were filled. The spiraling of the wire was important to obtain good electrical contact between the liquid electrode and the current collector as mercury does not tend to wet molybdenum metal. A schematic diagram, as well as image of an assembled vessel are shown in figure 7 below.

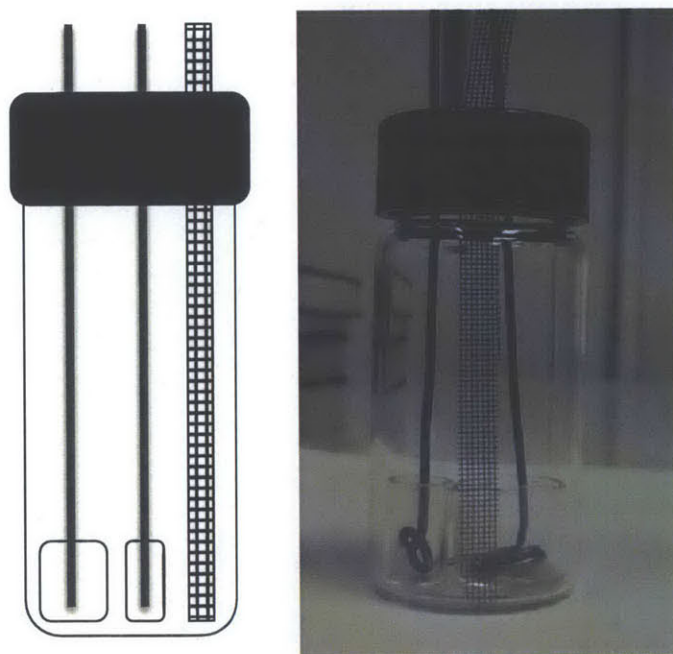


**Figure 7. Custom three-electrode vessel design.** Schematic (left) shows molybdenum positive current collector mesh, molybdenum wire leads, and crucibles to contain  $\text{CaHg}_{11}\text{-Ca(Hg)}$ sat reference and counter electrodes. Photograph of actual cell shown (right). Three-electrode cells utilizing a mercury working electrode were similar, but contained an extra crucible in place of the wire mesh.

Reference electrodes, counter electrodes, and mercury-containing working electrodes were all prepared in the manner described above; however the counter electrode crucibles were always of a larger cross-section. The typical diameter of a working or reference electrode was 6.5 mm, while that of a counter electrode was 13.25 mm, although other sizes were used for some experiments. The depth of the electrode crucibles typically ranged between 0.75 and 1.5 cm, depending on the nature of the experiment conducted.

### **3.3.3 Composite electrode preparation techniques**

Active positive electrode material powders are typically prepared in a composite manner, using a conductive carbon black additive (commonly referred to in the lithium-ion nomenclature as “Super P”), as well as a polymer binder. The purpose of the carbon is to circumvent the poor electronic conductivity of a number of active electrode materials by providing a current path between the current collector and active particles. The binder serves to maintain the mechanical stability of the electrode, particularly in materials that undergo large volume changes upon ion insertion and removal. Binders are chosen to be chemically inert in the system to be investigated. Typically a fluorinated hydrocarbon polymer such as PVDF or PTFE is used. The ratio of binder to carbon additive to active electrode material used in intercalation ion literature varies dramatically, with some authors choosing as little as a few percent binder or carbon, with others including up to as much as 50 weight percent carbon or binder. Composite electrode powders for the work described in this thesis were generally prepared in the following manner:

1. As synthesized or as received active material powders were hand-ground by mortar and pestle for a few minutes.
2. The amorphous carbon additive was added to the powders, and the two were ground by mortar and pestle for between 5 and 15 minutes.
3. The resulting mixture was harvested, placed in a glass vial, and 1 micron diameter PTFE beads were lightly mixed into the powders, and stored until use.

Active electrode material typically accounted for 50 to 65 percent of the electrode by mass. Carbon additive was included in amounts ranging from 10 to 20 percent, and PTFE binder particles were included in quantities ranging from 20 to 40 percent. During all electrochemical analysis, gravimetric quantities are normalized by active electrode mass. Carbon additive and PTFE “blanks” were also prepared in a 50/50 weight ratio for use in background testing. Some data were collected without the use of carbon additives and binder, consisting solely of active material mass, and are noted in the respective data sections. Data presented for the  $\text{Mo}_6\text{Se}_8$  electrodes in this thesis, particularly that used for chemical and structural analysis, was collected without the use of additional binder or carbon additives. No appreciable difference in the electrochemical performance was observed between composite and pure  $\text{Mo}_6\text{Se}_8$  electrodes as the Chevrel phase material is electronically conductive enough.

Unless otherwise noted in a specific section, all positive electrode material experiments presented in this thesis employed a molybdenum mesh current collector. The powder mixture was loaded above and below the current collector, and was then pressed into the collector by manual hydraulic press. Typical active material loading for a single electrode was between 5 mg and 15 mg. Any loose or partially detached segments of pressed powder were detached from the electrode surface before testing by gently caressing the surface and edges of the electrode with a gloved hand.

### **3.4 Electrolyte Considerations**

Which electrolyte solution to apply to a study of calcium electrochemistry is a non-trivial question. Electrolytes must maintain chemical compatibility with their electrodes and cell components, be electrochemically stable over the potential range of interest, be sufficiently pure to prevent undesirable side reactions, and have sufficient ionic conductivity to allow for reasonable rate performance. Furthermore, considerations of cost and operating conditions such as temperature restrict the use of particular electrolytes in particular applications. A variety of electrolytes are commonly used in batteries today, including salts dissolved in aqueous and organic solvents, ionic liquids, molten salts, solid ceramics, and polymers. Solid ceramic electrolytes and molten salts require high operating temperatures

(on the order of hundreds of degrees Celsius) and as such were immediately eliminated as choices since a near room temperature system is desired. Polymer electrolytes are an option, however their conductivities tend to be orders of magnitude lower than that of liquid electrolytes, and interfacial contact issues often necessitate the addition of some liquid lubrication to achieve good performance. As the interest in developing multivalent ion batteries typically focuses on high energy density applications, water was also eliminated as a solvent due to its narrow electrochemical window. Organic and ionic liquid based electrolytes remain as viable options for study, and both were initially explored and will be discussed in the remainder of this chapter.

Since the 1970s, ionic liquids (room-temperature molten salts) have been considered as candidate solutions for electrodeposition of metals and battery electrolytes. Although they have had little success as commercial electrolytes, ionic liquids are unique as they are able to solvate compounds not typically soluble in a number of other solvents at room temperature. Extensive literature exists on a class of ionic liquids used for plating and stripping a number of metals out of their halide complexes. Ionic liquids have also been explored for their performance as electrolytes for lithium ion batteries at both room temperature and elevated temperatures.<sup>71,72</sup> For these reasons, ionic liquids were initially considered as a medium for calcium ion deposition and stripping. However, due to calcium's low potential, many typical ionic liquid constituents are unstable. Attempts to form electrolytes with calcium chloride and imidazolium-based ionic liquids were unsuccessful, although interesting results involving aluminum and beryllium electrochemistry in such systems are explored in Appendices A and B of this thesis.

Two types of organic solvent based electrolyte systems were considered as electrolyte options. The first is the basic lithium analogue of a simple cation paired with a complex anion dissolved in an organic electrolyte. In such a solution, "free lithium ions" exist, although in reality they are in a complex coordinated by a combination of anions and electrolyte molecules. Another class of organic electrolyte uses organometallic complexes, which contain a metal-carbon bond, on the metal center of interest. These organometallic complexes have been shown in the literature to reversibly plate and strip magnesium

metal, however they rely on a very strong Lewis acid which prevents the formation of magnesium oxide on the metal surface.<sup>61,63</sup> Furthermore, such electrolytes do not form a surface film on the surface of magnesium, however given calcium's increased propensity for reaction the development of such an electrolyte is likely even more challenging and could easily be the subject of an entire research program. Given the complexity and challenges of developing an organometallic electrolyte, typical salt and solvent type electrolytes were selected for study in this thesis.

### 3.4.1 Selection of Electrolyte

A number of salt and solvent combinations were screened as potential electrolyte candidates for the study of calcium-ion intercalation systems. Based on a survey of the literature, as well as readily available commercial items, five different salts were tested in five different solvents, for a combination of twenty-five different "traditional organic electrolyte" combinations (in addition to other electrolytes considered in the previous section). Typical battery electrolytes contain about 1.0 M concentration of dissolved salts, however it is common in the literature to see electrochemical testing carried out with more dilute solutions.

<b>Solvent</b>	<b>Propylene Carbonate</b>	<b>Ethylene Carbonate:Dimethyl Carbonate (1:1 by mass)</b>	<b>Acetonitrile</b>	<b>Tetrahydrofuran</b>	<b>Polyethylene Oxide</b>
<b>Salt</b>					
<b>Calcium Chloride</b>	Poor Solubility	Poor Solubility	Poor Solubility	Poor Solubility	Soluble
<b>Calcium Triflate</b>	Soluble, formed a two-phase slush/gel solution	Poor Solubility (two-phase separation, one gel-like and the other liquid)	Partial Solubility	Soluble, formed a two-phase slush/gel solution	Soluble
<b>Calcium Perchlorate</b>	Soluble	Soluble	Soluble	Partial Solubility	Soluble
<b>Calcium Acetate</b>	Poor Solubility	Poor Solubility	Poor Solubility	Poor Solubility, cloudy solution	Poor Solubility
<b>Calcium Hexanoate</b>	Poor Solubility	Poor Solubility	Poor Solubility	Soluble, but cloudy solution	Poor Solubility

Table 3. **Solubility of calcium salts in organic solvents.** Salts were qualitatively classified as "soluble" if a 0.1 M concentration could be obtained in solution. Partial solubility was classified by obvious dissolution of a fraction of the salts, while poor solubility was classified by no discernable difference in the quantity of solid salt remaining.



In order to quickly test the practical applicability of various salt/solvent combinations, solutions were prepared with a nominal concentration of 0.1 M and the qualitative dissolution behavior of the systems was observed over time. A summary of the solubility observations are presented in table 3. In cases where the 0.1 M system was found to be soluble, the concentration of dissolved salts was increased to 0.25 M, 0.5 M, 1.0 M for further testing. Several candidate electrolytes were identified:

1. Calcium perchlorate in carbonate solvents.
2. Calcium perchlorate and calcium triflate in acetonitrile. (Note the triflate was only partially soluble at 0.1 M concentrations).
3. Several salts in low molecular weight PEO solution.

Solvent compatibility tests were carried out with metallic calcium, and in all cases it was visually observed that a layer immediately formed on the surface of the metal. Subsequent electrochemical measurements confirmed that the layer passivated the electrode surface, hence none of the electrolytes would work with metallic calcium. A second round of compatibility measurements was carried out with  $\text{CaHg}_{11}\text{--Ca}_{(\text{Hg})}^{\text{sat}}$ . Vials of amalgam and solvents were observed for several days, and it was determined that the acetonitrile was the most compatible, as there was visually no discoloration of the electrode or electrolyte. Both carbonate solvents quickly reacted with the electrode, forming a flaky black surface layer. THF had a similar reaction, although over a longer time scale. The PEO reaction with the amalgam resulted in the formation of a white, feather-like growth on the surface of the electrode which proceeded to grow into the electrolyte solution.

Electrochemical stability measurements were also carried out on the electrolytes, consisting of OCV measurements of two identical reference electrodes resting in solution, for which no difference in OCV would be expected. Acetonitrile-based electrolytes again performed the best, with carbonate, THF, and PEO electrolytes behaving less reproducibly. The measured OCV varied on the order of tens to hundreds of millivolts in seemingly random fashion for several hours, likely as a result of a reaction

between the electrolyte solvent and the amalgam electrode. Only in the case of acetonitrile was the OCV measured to be stable to within 10 millivolts for the entire duration of the tests. Chapter 4 discusses reference electrode stability in greater detail.

A solution of 0.5 M calcium perchlorate in acetonitrile was selected as an electrolyte. Its conductivity was determined using a Mettler Toledo conductivity probe and found to be 2.3 +/- 0.4 mS/cm. Literature precedent also supports the selection of a perchlorate salt in acetonitrile solution for the study of multivalent ions, as work by Aurbach shows that magnesium perchlorate in acetonitrile allows for reversible insertion of magnesium into Chevrel phase compounds, while the same salt solvated in propylene carbonate does not. The reason postulated for this is the solvation shell energy of the ion in solution.<sup>61</sup> Thus, the behavior of a particular ion in a particular host is coupled to the choice of electrolyte as well. Electrochemical results taken involving a particular electrolyte do not preclude all electrolyte systems, however the choice of calcium perchlorate in acetonitrile is a better place to start than most.

### **3.4.2 Testing and Characterization of the Calcium Perchlorate/Acetonitrile Electrolyte**

The calcium perchlorate in acetonitrile electrolyte was observed to be optically transparent and consisted of a single, non-viscous liquid phase. No observable reaction was noticed between the electrolyte solution and the  $\text{CaHg}_{11}\text{-Ca}_{(\text{Hg})}^{\text{sat}}$  electrodes. Cyclic voltammetry was performed on bare molybdenum wire to explore the electrochemical behavior of the electrolyte. A typical result is shown below in figure 8 below. The correction factor between  $\text{CaHg}_{11}\text{-Ca}_{(\text{Hg})}^{\text{sat}}$  electrodes and calcium plating potential is approximately 0.8 V, as determined by measurement in Chapter 4.

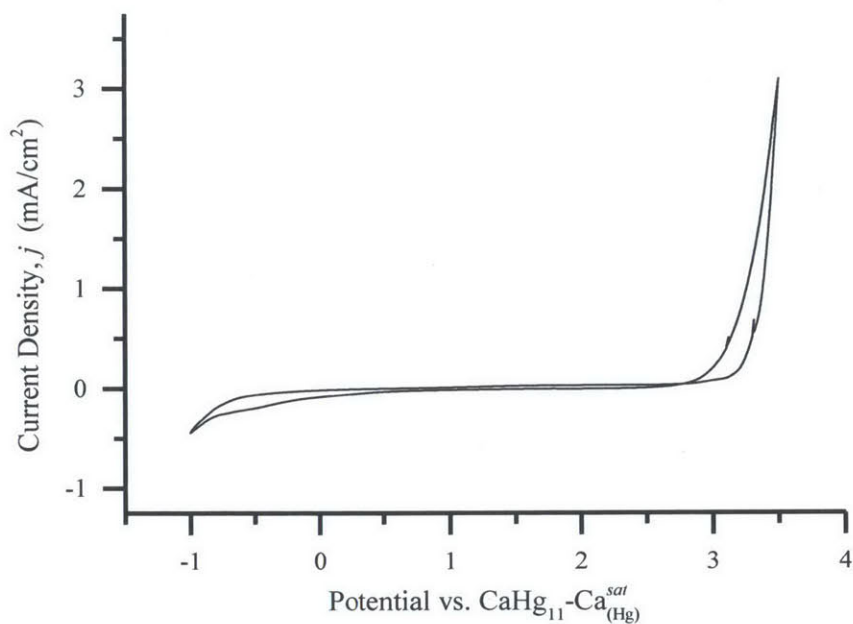


Figure 8. **Electrochemical window of calcium perchlorate in acetonitrile electrolyte.** Electrolyte decomposition occurs at -1 V and 3 V, although a smaller onset of a wave can be seen below 0.5 V corresponding to the breakdown of electrolyte impurities.

Upon first glance, the electrochemical window of the electrolyte spans approximately 4 V, between the onset of appreciable anodic and cathodic currents. A vigorous decomposition reaction is observed above 3.0 V vs.  $\text{CaHg}_{11}\text{-Ca}_{(\text{Hg})}^{\text{sat}}$ , corresponding to the breakdown of the acetonitrile electrolyte solvent.

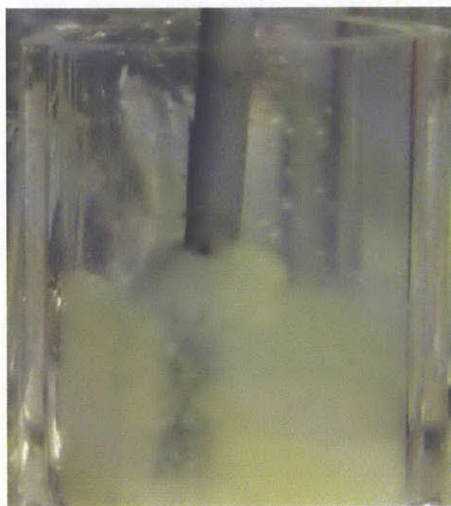


Figure 9. **Acetonitrile decomposition product.** Light green, fluffy, polymeric electrolyte decomposition product is observed on molybdenum wire working electrode.

A potentiostatic hold at 3.5 V revealed the decomposition product macroscopically as a polymeric substance, likely a carbon-nitrogen containing polymerization product. An image of the electrode decomposition product is shown in figure 9.

Although the lower limit of the electrolytic window appears to be at 0.9 V vs.  $\text{CaHg}_{11}\text{-Ca}_{(\text{Hg})}^{\text{sat}}$ , where the voltammogram begins a sharper negative current, a slight onset of gradually increasing negative current can be seen in the area of 0.5 V vs.  $\text{CaHg}_{11}\text{-Ca}_{(\text{Hg})}^{\text{sat}}$  reference. Careful electrochemical interrogation of this region using high surface area carbon/PTFE “blank” electrodes revealed that the current was due to an electrolyte impurity that could be electrolyzed away at low current densities (less than  $5\text{ }\mu\text{A}/\text{cm}^2$  of pressed powder electrode). The presence of the impurity did not appreciably affect higher current density experiments, however in lower current density experiments corresponding to slow discharge rates, large fractions of the current engaged in this parasitic side reaction during the first discharge. For this reason, pre-electrolysis of the electrolyte through the 0.5 V region was carried out in the cell on a sacrificial pressed powder electrode prior to sensitive electrochemical measurements. Ultimately though, a completely “safe” electrochemical window exists in the region of 0.5 V to 2.5 V vs.  $\text{CaHg}_{11}\text{-Ca}_{(\text{Hg})}^{\text{sat}}$ , making this an ideal system for the study of electrode materials in that potential range.

### 3.4.3 Salt Drying Procedures

Several of the salts discussed in the previous section (calcium chloride, calcium triflate, and calcium hexanoate) were commercially available in anhydrous forms were used as received. The remaining salts were obtained as hydrates and dried in house as no distributor or vendor was able or willing to produce the appropriate anhydrous salt of acceptable purity, even though several were contacted. Calcium chlorate tetrahydrate and calcium perchlorate “hydrate” (likely also the tetrahydrate form, although unspecified by the manufacturer) were obtained from Sigma-Aldrich and Alfa Aesar respectively. The literature was consulted to develop an appropriate drying procedure.

Calcium perchlorate is known to form a tetrahydrate form with water. The melting point of the hydrate crystal is below 100°C, although complete expulsion of water from the system is reported at temperatures ranging up to 250°C, at which point the product maintains constant mass. The anhydrous form is reported to be stable up to 270°C, so decomposition as a result of over-drying is of minimal concern.<sup>73</sup> A custom drying protocol was developed, working at high temperature under vacuum without the use of a desiccant.

The drying procedure for calcium perchlorate hydrate salts carried out in this work is as follows:

1. The salt hydrates were opened under atmosphere and placed in a fused-quartz crucible in quantities ranging from 2 grams up to 50 grams, depending on the desired yield.
2. The quartz crucible was quickly placed into a steel crucible sealed by a rubber o-ring and mechanical clamp. The vessel was appropriately insulated was then quickly evacuated, purged with argon, and evacuated again.
3. The vessel, still under an active vacuum (at a pressure of about 10 millitorr), was then placed into a tube furnace and ramped up to 255°C. During the process the vacuum level noticeably degraded, likely due to the evolution of water from the salt hydrate.
4. The system was held at temperature until the vacuum level dropped back down to under 10 millitorr and remained there. The entire process typically took anywhere from 12 hours to 48 hours depending on the quantities of salt being dried. Drying was considered complete when a pressure of under 10 millitorr was reached again.
5. The steel vessel was then ramped down to room temperature, and the vacuum valve closed so as to seal the vessel. While still under vacuum, it was transported to and opened in an argon-filled glovebox ( $\text{H}_2\text{O}/\text{O}_2$  levels below 1 ppm each). A pure white salt was harvested from within the inner quartz crucible in the glovebox and stored in vials until use.

Calcium acetate monohydrate was dried according to a similar procedure, however for different times and temperatures. As the salt was not instrumental to this work, we will not go into details of the drying process, however one may reference the literature for an appropriate drying procedure.<sup>74</sup>

### 3.5 Preparation of Ca-Hg Electrodes

Pure metallic mercury (99.999% - Alfa Aesar) and pure dendritic metallic calcium (99.99% - Sigma Aldrich) were used in the direct chemical preparation of all two-phase and calcium amalgams. Direct dissolution of solid calcium in liquid mercury was carried out in a closed vessel within an inert atmosphere glovebox ( $< 1$  ppm  $O_2$ ). The dissolution of the calcium in the mercury began as a slow process, but accelerated over time, likely due to the fact that the surface of the as-received calcium contained some calcium oxide or other non-metallic product which acted as a barrier to dissolution at the start of the process. This fact is supported by the observation that scraping the surface of the calcium metal and holding it submerged within the mercury pool dramatically speeds up the dissolution process. The process was mildly exothermic. The calcium amalgams were typically allowed to equilibrate for a period ranging from several hours to several days before use, depending on calcium content. The higher the calcium content, the longer the solutions were allowed to equilibrate before testing.

Generic two phase  $CaHg_{11}$ - $Ca_{(Hg)}$  counter and reference electrodes were prepared with a nominal calcium content of 5 atomic percent in large batches containing 100-200 grams of mercury. Upon cell assembly, the calcium-mercury slush was transferred to the appropriate glass crucible of the electrochemical cell using a combination of pipeting and scooping. As such, the true calcium concentration of each reference and counter electrode is unknown. This does not pose a problem for precise electrochemical measurements, as potential and performance were found to be comparable throughout the two-phase region, as demonstrated in Chapter 4.

Two phase electrodes of specific chemical compositions used in thermodynamic and kinetic studies of the calcium-mercury system were prepared directly into small glass crucibles which were

stored in a closed vessel and allowed to equilibrate. This minimized error associated with having to transfer the material between vessels, which almost certainly would result in an arbitrary shift in phase fraction, and by extension the true calcium content in the electrode.

### **3.6 Preparation of Chevrel Phase powders**

Chevrel phase molybdenum cluster compounds are not commercially available, and were synthesized in house. Even though many ternary Chevrel phases have been documented in the superconductor literature, the electrochemical literature suggests that a variety of these phases are electrochemically inert as synthesized. This observation may be due to the formation of a surface passivation layer on the electrode material. Additionally, the  $\text{Mo}_6\text{S}_8$  Chevrel phase is known to be metastable, and cannot be prepared directly without a ternary component. As such, the most common technique by which electrochemically active Chevrel powders are produced is through an indirect synthesis involving acid treatment and chemical deintercalation of a copper-containing Chevrel phase compound. The acid treatment leaches copper out of the material, and the degree of treatment has been documented to affect both the morphology of the powders and their residual copper content.<sup>53</sup>

#### **3.6.1 Solid-State Synthesis of $\text{Cu}_2\text{Mo}_6\text{X}_8$ ( $\text{X} = \text{S}, \text{Se}, \text{Te}$ )**

The preferred method of synthesis of Chevrel phase compounds is a high-temperature solid state process, developed by Chevrel in the 1970s.<sup>43</sup> Several authors studying Chevrel phases since have repeated his procedure.<sup>50,61</sup> This method of synthesis was chosen for this study, although alternative intermediate temperature alternatives that make use of molten salts do exist.<sup>75</sup>

Elemental precursor powders of copper (99.7%, dendritic, Sigma Aldrich), molybdenum (99.9%, 1-2 micron, Sigma Aldrich), sulfur (99.98%, Sigma Aldrich), selenium (99.99%, 100 mesh, Sigma Aldrich), and tellurium (99.8%, 200 mesh, Sigma Aldrich) were weighed out in the appropriate molar ratios in an argon-filled glovebox ( $< 0.1$  ppm  $\text{O}_2$ ,  $< 0.1$  ppm  $\text{H}_2\text{O}$ ) and hand mixed by mortar and pestle for 10 minutes. Typical synthesis batches consisted of 1-2 grams of powder in total. The powders were then

pressed together by a manual screw-press into a small pellet, which was placed into a fused-quartz tube which had been sealed at one end. The tube was removed from the glovebox, quickly connected to a vacuum line, and evacuated. The evacuated tube was then necked and sealed using glass blowing equipment. The sealed ampoules were placed inside a water-cooled cap steel furnace vessel filled halfway with insulating alumina beads. The top half of the vessel was filled with fiberglass insulation and sealed with a rubber o-ring. The vessel was evacuated and backfilled with argon. The steel vessel was then heated to a furnace temperature of between 1150 and 1200°C for periods ranging between 48 hours and 96 hours, depending on the batch synthesis at an approximate ramp rate of 120 degrees per hour.

After heat treatment, the vessels were cooled to room temperature and the fused quartz ampoules of product were recovered. The ampoules were opened in atmosphere and the powder-pellet product was mechanically broken up and lightly ground with mortar and pestle. XRD analysis confirmed that for all but the shortest times the  $\text{Cu}_2\text{Mo}_6\text{X}_8$  yield was quite high, while small quantities of  $\text{MoS}_2$  or elemental precursors could be detected on occasion. Powders were stored under atmosphere in closed vials. EDX analysis confirmed appropriate elemental ratios of components.

A modified synthesis procedure was carried out for particle size reduction experiments to produce “nanoscale” particles, involving reduced heat treatment temperature and duration. Elemental powders were measured as above, loaded into a milling vessel under argon, and ground together using a micronizer (McCrone Micronizing Mill – serial number 130301) for 20 minutes total in 5 minute intervals. The resulting mixture was harvested back in the glovebox and transferred to a steel Swagelok cell for heat treatment. The steel cell was heat treated inside a steel crucible for 16 hours at 900°C. The ramp up rate of the furnace was 2°C/min, and the cell was cooled by shutting off the furnace and removing external insulation such that cooling occurred rapidly. The shortened thermal treatment profile was inspired by similar methods for producing nanoparticles presented in the magnesium ion literature.<sup>76</sup>



### 3.6.2 Acid Leaching Procedures

Several leaching agents have been suggested in the literature as chemical de-intercalation candidates. Aqueous solutions of hydrochloric acid, sulfuric acid, and nitric acid at various pHs have been used, as have solutions of  $I_2$  and  $NO_2BF_4$  in acetonitrile. Studies have been published on the effect of leaching rate and the residual ion content.<sup>53</sup>

The precursor  $Cu_2Mo_6X_8$  ( $X = S, Se, Te$ ) phase was taken as a fine ground powder and poured into a pre-prepared 6 molar hydrochloric acid solution, typically with one to two grams of powder per 20 to 50 mL of acid. Oxygen was bubbled through the solution in order to facilitate the removal of copper.<sup>53</sup> The solution was actively stirred by a magnetic stirrer. The powders were allowed to soak for periods ranging from 6 hours to 12 hours. Upon acid treatment, magnetic stirring was stopped and the solutions were allowed to settle. The particles collected at the bottom of the vessel and the acid was decanted. Deionized water was then added to the vessel and the particles were re-suspended, and then allowed to settle again. Typically 3 to 5 rinsing and decanting steps were used before the final particles were harvested through filtration and dried for several days in air before being stored in closed vials under atmosphere. The copper content and particle morphology was confirmed by SEM-EDS analysis. The phase content of the particles was analyzed by XRD. It was found that acid treatment successfully removed copper from the particles, while leaving the desired Chevrel phases intact. Minimal degradation products (such as  $MoS_2$ ) were detected in some samples, but overall yields tended to be above 90% of the desired phase.

### 3.7 Chapter Summary

Brief technical descriptions of the electrochemical techniques employed in this thesis were described in this chapter. A suite of complementary materials characterization techniques (SEM, TEM, XRD, EDX, and XPS) was chosen to interrogate the chemistry and structure of electro-active materials. The combination of electrochemical and non-electrochemical characterization methods is well suited to relate the electrochemical signal obtained to the specific physical or chemical processes involved. The chapter continues by laying out experimental apparatus design, as well as electrolyte development, and electrode preparation methods. Care was taken at each step of the process to deal with calcium's reactive nature by minimizing oxygen exposure and maintaining an inert environment. Measures taken include; working with strict glovebox protocols, utilizing air-sensitive sample transport vessels and oxygen getters where possible, careful drying of salts, and performing electrolyte pre-electrolysis.

# Chapter 4: Experimental Characterization of the Ca-Hg System

In this chapter the electrochemical behavior of the calcium-mercury system, proposed in Chapter 2 as a venue for the study of calcium electrode material candidates, is characterized. The thermodynamic properties of the system are first explored and the potential of the  $\text{CaHg}_{11} - \text{Ca}_{(\text{Hg})}^{\text{sat}}$  reference electrode is placed within the electrochemical series. The stability of the two-phase reference is examined with respect to variations in composition, time, and mechanical perturbation. The kinetic properties of the calcium-mercury amalgams are then studied with regards to the applicability of the electrode as a calcium-containing faradaic counter electrode.

## 4.1 Calcium amalgam concentration OCV measurements

Calcium amalgams were prepared as outlined in Chapter 3 at varying calcium concentrations ranging from 0 to 8.5 mole percent. OCV measurements of the amalgams were taken against a  $\text{CaHg}_{11} - \text{Ca}_{(\text{Hg})}^{\text{sat}}$  in a standard calcium cell configuration, also outlined in Chapter 3. Excellent agreement was obtained with galvanostatic titration experiments carried out on pure mercury electrodes, the results of which are shown in figure 10 below.

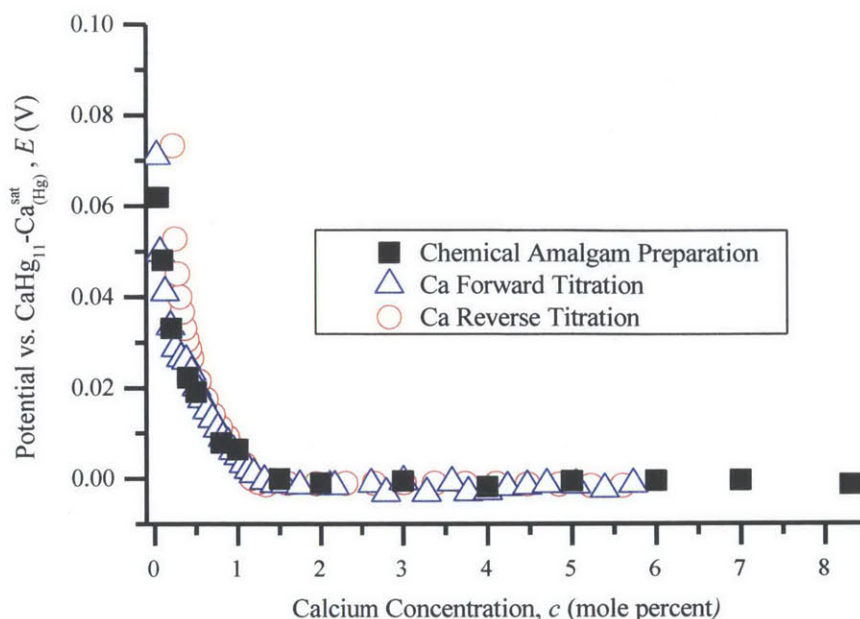


Figure 10. **OCV as a function of calcium amalgam concentration.** The OCV drops sharply from that of pure mercury with the addition of calcium, levels off to the two-phase region at 1.5 atomic percent calcium, and remains stable throughout. Chemical amalgamation, forward titration, and reverse titration curves overlay well.

Good overlap is observed between the calcium insertion and removal titration curves, with over 96 percent coulombic efficiency observed, and both agree well with the OCV curve prepared by direct chemical amalgamation. After an initial drop in voltage, the potential levels off as the mercury electrode enters a two-phase region at about 1.5 at. % calcium, which is consistent with results reported in the literature.<sup>19,25,27,29</sup> The plateau in potential extends through 8 at. % calcium, as would be expected from the calcium-mercury phase diagram. The data presented in the figure are accurate to within  $\pm 2$  mV, which is the accuracy of the reference electrode (determined in section 4.3).

## 4.2 Determination of the $\text{CaHg}_{11}\text{-Ca}_{(\text{Hg})}^{\text{sat}}$ electrode potential

The calcium-mercury system has provided for a means to avoid issues related to calcium's propensity to react and passivate in a wide range of electrolytes. In particular, the  $\text{CaHg}_{11}\text{-Ca}_{(\text{Hg})}^{\text{sat}}$  two-phase electrode has proven to be a robust reference electrode for electrochemical characterization. Boasting a stable potential over a wide range of compositional variation, the electrode is ideal for the

study of calcium-ion intercalation systems. In order to meaningfully compare results with other systems however, the stable potential plateau of the  $\text{CaHg}_{11}\text{-Ca}_{(\text{Hg})}^{\text{sat}}$  electrode potential must be placed within the electrochemical series. This section devotes itself to that endeavor by discussing a variety of techniques by which such measurements may be taken, in series with the results of those particular experiments. A final comparative section is dedicated to the evaluation the various results with relation to one another and assigns a value to the  $\text{CaHg}_{11}\text{-Ca}_{(\text{Hg})}^{\text{sat}}$  electrode potential.

#### 4.2.1 Calcium Metal Measurements

The most obvious and direct means by which one could attempt to place the  $\text{CaHg}_{11}\text{-Ca}_{(\text{Hg})}$  electrode in the electrochemical series is by direct OCV measurement against a metallic calcium electrode in a calcium-ion containing electrolyte. However, were such a measurement to be simple and reproducible, there would be little need to develop a two-phase reference electrode when one could simply use pure metallic calcium as a reference instead. As discussed earlier in this thesis, calcium metal has a strong tendency to react in almost any medium other than vacuum or inert atmospheres. Organic solvents decompose on the surface of metallic calcium, producing a film that prevents the establishment of a consistent electrochemical signal by interfering with ionic transfer. The result is that the measured potential at a metallic calcium electrode will tend to be erratic, and systematically more positive (typically hundreds of millivolts to volts) than the true thermodynamic value of the potential.

One alternative would be to switch from an organic electrolyte at room temperature to an inorganic calcium-ion conductor at higher temperature. Several such electrolytes exist in the literature, including eutectic ternary and quaternary molten salts and solid calcium fluoride.<sup>31</sup> Unfortunately, the high temperature required to exhibit appreciable conductivity in these systems (400-500 C minimum operating temperature) precludes their use as an electrolyte for the characterization of the  $\text{CaHg}_{11}\text{-Ca}_{(\text{Hg})}^{\text{sat}}$  two-phase electrode as the  $\text{CaHg}_{11}$  intermetallic compound undergoes a peritectic reaction at 84 C.<sup>21</sup>

Early attempts to measure the standard potential of the metallic calcium electrode were carried out in a number of organic electrolytes, as reviewed in section 2.2. Calcium's passivity was recognized early during these investigations, and a "vibrating" or "rubbing" electrode was designed in order to obtain a somewhat stable value. The guiding principle is that by continuously mechanically scraping the surface of the calcium metal, fresh calcium is exposed to the electrolyte and able to establish a pseudo-equilibrium potential for a brief time before undergoing corrosion. Unfortunately, few details exist in the literature and the results of these measurements differed substantially between authors, although several suggest reproducible results could be obtained by this method. An attempt was made to obtain a stable value of the calcium potential through scraped calcium electrodes. Unfortunately, the measurements were inconsistent and not reproducible, with the potential ranging by hundreds of millivolts on different measurements. As such, the rubbed calcium calibration method was abandoned and more accurate means of determining the reference potential of the  $\text{CaHg}_{11}\text{-Ca}_{(\text{Hg})}^{\text{sat}}$  was sought.

#### **4.2.2 Infinite Dilution Measurements**

Although a review of the literature did not yield an answer to the question to the standard potential of the  $\text{CaHg}_{11}\text{-Ca}_{(\text{Hg})}^{\text{sat}}$  electrode, a substantial body of literature exists exploring extremely dilute calcium amalgam electrodes. The standard potential of an infinitely dilute solution of calcium in mercury is extrapolated to have a value of -1.996 V vs. SHE.<sup>19</sup> The next most logical way to assess the position of the  $\text{CaHg}_{11}\text{-Ca}_{(\text{Hg})}$  electrode in the electrochemical series would be by comparison to extremely dilute amalgam electrodes, as these would be expected to be stable within the electrolyte and have been very well characterized. Several such methods of obtaining "infinite dilution" data and their results are described in the following sub-sections.

##### **4.2.2.1 Chemical Amalgam Preparation**

Direct chemical dissolution of calcium in mercury to prepare dilute calcium concentration amalgams, although the most obvious method, proved to be an inconsistent and challenging when performed at a small scale. Exposure to minor amounts of oxygen or moisture, as well as the surface

oxide layer on small calcium chunks, likely caused dramatic variations in true calcium content for extremely dilute amalgams. Authors in the literature circumvented these problems by designing complex setups which involved large volumes of amalgam and flowing electrodes.<sup>19</sup> In the interests of minimizing hazardous mercury waste, such an approach was not used in this study, and electrochemical means of amalgamation were instead chosen.

#### 4.2.2.2 Titration-Relaxation Measurements

Electrochemical titration to the desired composition of calcium in mercury was used to produce dilute amalgam concentrations. Pure mercury electrodes were allowed to equilibrate in a standard cell with a pair of  $\text{CaHg}_{11}\text{-Ca}_{(\text{Hg})}^{\text{sat}}$  electrodes, one acting as a reference and the other as a counter. The mercury electrodes were cleaned by a potentiostatic hold at 1.0 V vs. the  $\text{CaHg}_{11}\text{-Ca}_{(\text{Hg})}^{\text{sat}}$  reference, and then current was passed until the desired composition of calcium within the electrode had been reached. Multiple titrations in different cells were performed over the composition range 0.05 to 0.25 mole fraction of calcium. OCV measurements were taken as the electrodes equilibrated. The measured cell potential can be related to the (unknown) reference electrode potential through 4.

$$E = E_{\text{ref}}^{\circ} - E_{\text{Ca(Hg)}}^{\circ} - \frac{RT}{2F} \ln \left( \frac{[\text{Ca}^{2+}][(\text{ClO}_4)^-]^2 \gamma_{\pm}^3}{X_{\text{Ca}} \gamma_{\text{Ca}}} \right) \quad (4)$$

$E_{\text{ref}}^{\circ}$  is the unknown standard potential of the  $\text{CaHg}_{11}\text{-Ca}_{(\text{Hg})}^{\text{sat}}$  electrode,  $E_{\text{Ca(Hg)}}^{\circ}$  is the standard potential of infinitely dilute calcium amalgam,  $[\text{Ca}^{2+}]$  and  $[(\text{ClO}_4)^-]$  are the electrolyte ion concentrations,  $X_{\text{Ca}}$  is the mole fraction of calcium in the amalgam electrode, and  $\gamma_{\text{Ca}}$  is the activity coefficient of calcium in mercury, which was assumed to be 1 in this case as the amalgam is dilute. The activity coefficient of ions in the electrolyte was taken to obey the Davies equation, with assumptions similar to those used by Butler in his analysis of calcium amalgams,<sup>19</sup>

$$\log(\gamma_{\pm}) = -0.5|Z_+Z_-| \left( \frac{\sqrt{I}}{1 + \sqrt{I}} + 0.1|Z_+Z_-|I \right) \quad (5)$$

where,

$$I = 2[Ca^{2+}] + \frac{1}{2}[Ca(ClO_4)^+] + \frac{1}{2}[(ClO_4)^-] \quad (6)$$

and,

$$[Ca(ClO_4)^+] = K_{pair}[Ca^{2+}][Cl^-] \quad (7)$$

The ionic charges are given by  $Z_+$  and  $Z_-$ , and  $K_{pair}$  is the ion pair equilibrium constant. The presence of ionic associates in the electrolyte was assumed for completeness, and in the absence of literature data for ion pairing between calcium and perchlorate ions in acetonitrile, a reasonable value of 0.2 was used as the pairing coefficient. Ultimately a sensitivity analysis was performed with  $K_{pair}$  values ranging from 0 to 1, and the effect on the determined value of potential was less than 3 mV.

In order to determine the standard reference potential of the  $CaHg_{11}-Ca_{(Hg)}^{sat}$  electrode with respect to the standard hydrogen electrode and place it in the electrochemical series, equation 4 was independently solved for eight measured values of potential, yielding -2.043 +/- 0.0016 V vs. SHE as the result (the given error is the standard deviation of the eight measurements). In order to provide a more robust error analysis of the electrode, a voltage error of +/- 2 mV was propagated through the analysis for each respective measurement resulting in a range in potentials from -2.041 V to -2.045 V vs. SHE, with a standard deviation of 2.5 mV. The standard potential of the metallic calcium electrode is -2.868 V vs. SHE in aqueous electrolytes, suggesting that the  $CaHg_{11}-Ca_{(Hg)}^{sat}$  electrode rests at approximately 825 mV above the potential of metallic calcium, according to this method.

#### 4.2.2.3 Cyclic Voltammetry

Another means by which authors commonly determine the potential of electrochemical processes is through the use of linear extrapolation to a zero-current value on cyclic voltammograms. A pure mercury electrode should be relatively inert during a cathodic sweep until a critical potential for calcium alloying is reached. Upon passing this potential, a substantial increase in the current should be measured.



By extrapolating the position of this wave down to the zero-current value, one should be able to assess the value of the calcium amalgam electrode in infinite dilution. While there are some errors inherent in this technique, namely the arbitrary definition of what one would consider to be a “substantial current”, the extrapolated value of potential should serve as good support for data obtained by more accurate methods. Figure 11 below shows a typical alloying sweep on a CV curve.

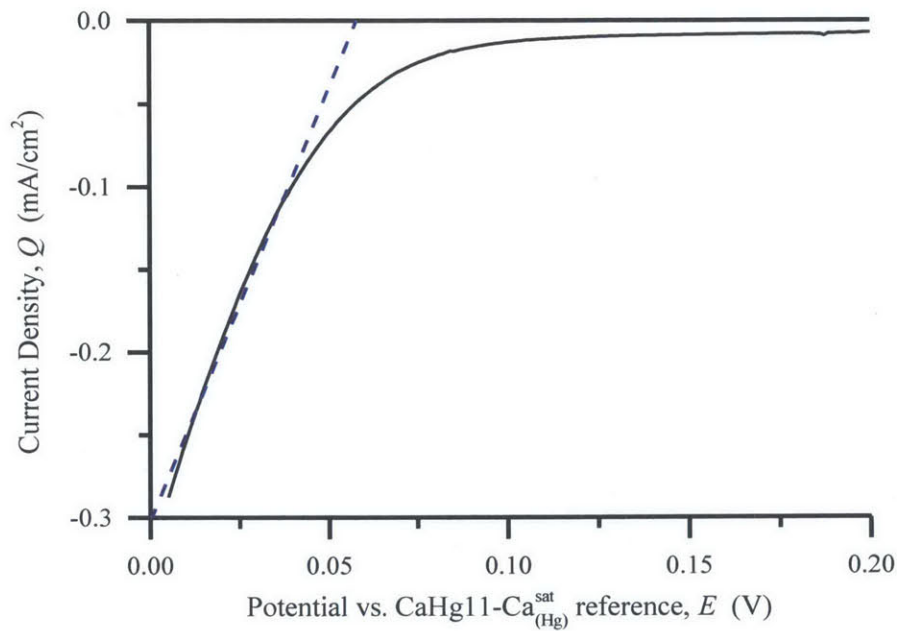


Figure 11. **Extrapolation of calcium alloying curve during cyclic voltammetry.** Typical alloying curve along with linear fit ( $Q = 5.2E - .302$ ,  $R^2 = .991$ ) extrapolated to the zero current limit.

Such extrapolations were carried out on a dozen voltammograms and the average zero-current potential value was found to be 60.8 mV  $\pm$  12.3 mV. Additional variation in the numbers was found as the extrapolation was expanded to include a wide range of values, particularly towards more positive potentials.

#### 4.2.2.4 Residual OCV after AC Impedance Measurement

This technique was conceived of while performing impedance measurements on a pure mercury electrode. Upon application of an AC waveform, whose initial OCV was over a volt, with no applied DC potential, it was observed that the OCV measured before and after the experiment varied dramatically.

The electrode's potential was substantially lower, on the order of 100 mV, and slowly climbed with time. The likely cause of this observation is residual calcium atoms at the surface of the mercury, deposited during the AC impedance measurement. This makes sense, as the exchange current density should be a function of calcium concentration within the electrode, and with a pure mercury electrode the odds of completely extracting all the calcium inserted in a single frequency fluctuation are quite low. This is also consistent with observations discussed in further detail in section 4.4, that calcium removal is in fact the limiting step in dilute amalgam electrodes. Hence, the residual potential measured after the experiment is likely due to a small concentration of calcium remaining at the electrode's surface, which was not quite removed given that substantial overpotentials are required to remove the last bit of calcium from the electrode. The average of five different measurements resulted in a residual OCV measurement of 90 +/- 28 mV. Although hardly rigorous, this residual OCV can be used to help ballpark an approximate value of the  $\text{CaHg}_{11}\text{-Ca}_{(\text{Hg})}$  electrode potential, and confirm the potential as determined by other more accurate methods.

#### 4.2.2.5 *Summary of Measurements and Discussion*

Three different methods for estimating the potential of the  $\text{CaHg}_{11}\text{-Ca}_{(\text{Hg})}^{\text{sat}}$  were presented in this subsection. Ultimately, all of them rely on the known value of the potential of the dilute calcium amalgam electrode. Ultimately, the electrochemical titration method was selected for analysis and the potential of the  $\text{CaHg}_{11}\text{-Ca}_{(\text{Hg})}^{\text{sat}}$  electrode was determined to be approximately -2.043 V vs. SHE, or 0.825 V vs. the  $\text{Ca/Ca}^{2+}$  couple. The observations from cyclic voltammetry and impedance methods were not used as the titration provided for more accurate electrode composition data, however the measured values of potential for "dilute" amalgams by these methods was consistent with the values observed during titration-relaxation measurements. Mathematically, accuracy of the electrode potential was determined to within a spread of 5 mV based on the measurements taken, however a number of assumptions were made about the system including; perfectly known accuracy of the  $\text{Ca/Ca}^{2+}$  couple (which is indeed not the case),

appropriately dilute electrolyte concentrations, and applicability of and assumptions involved in the Davies' model.

### 4.3 Stability of the $\text{CaHg}_{11}\text{-Ca}_{(\text{Hg})}^{\text{sat}}$ two-phase Reference

In this section the stability of the  $\text{CaHg}_{11}\text{-Ca}_{(\text{Hg})}$  with regards to several different parameters is explored. The effects of mechanical perturbation and variation in chemical composition are studied, as is the variation in potential over both short and long time scales. Experimental results in this section demonstrate the robustness of the  $\text{CaHg}_{11}\text{-Ca}_{(\text{Hg})}$  and show excellent regularity in potential over intermediate times with a total absence of systematic drift.

#### 4.3.1 Short Term Behavior

Three-electrode cells were assembled as described in Chapter 3. Each electrode was composed of a calcium-mercury alloy which had been previously prepared by direct dissolution of solid calcium metal into liquid mercury, at a concentration of five atomic percent. Immediately upon immersion in the calcium perchlorate in acetonitrile electrolyte solution, the open circuit voltage was measured between two of the three electrodes. The measurement was carried out for times ranging from between ten minutes and twelve hours. Upon completion of the measurement, the open circuit potential was measured between the dormant electrode in the cell and one of the other electrodes. Measurements were reproduced across several cells. Initial electrode potentials were within 10 mV of each other in all cases, however they drifted randomly in this range for the first several hours of measurement. The variation would subside over time, and the OCV values would level off stably to within 2 mV of each other. Upon measurement against the third electrode in the cell, the potential measured was immediately stable and within 2 mV of the others itself. The behavior suggests that the electrodes undergo some short-term equilibration process with the cell and then ultimately stabilize.

### 4.3.2 Long Term Behavior

Given the reactive nature of calcium metal, one expects some systematic corrosion to occur even though the activity of calcium is effectively lowered through alloying with mercury. Although the electrode has proven to be robust over short times, systematic drift within the electrode was of some concern. Measurement conducted between two identical  $\text{CaHg}_{11}\text{-Ca}_{(\text{Hg})}$  electrodes is unlikely to provide any insight into the occurrence of systematic drift as the two electrodes would likely drift together. In order to quantify the existence of any drift in electrode potential, a long-term stability test was designed. Three electrode cells were assembled (see Chapter 3) consisting of two  $\text{CaHg}_{11}\text{-Ca}_{(\text{Hg})}$  electrodes. These electrodes were immersed in electrolyte and the OCV was measured between the two overnight. On the second day, a third electrode of freshly prepared  $\text{CaHg}_{11}\text{-Ca}_{(\text{Hg})}$  was introduced into the cell and OCV measurements were carried out between the fresh electrode and one of the original  $\text{CaHg}_{11}\text{-Ca}_{(\text{Hg})}$  electrodes. The evolution of potential was measured until equilibration, and each subsequent day thereafter the previous day's electrode was removed and a freshly prepared electrode was inserted.

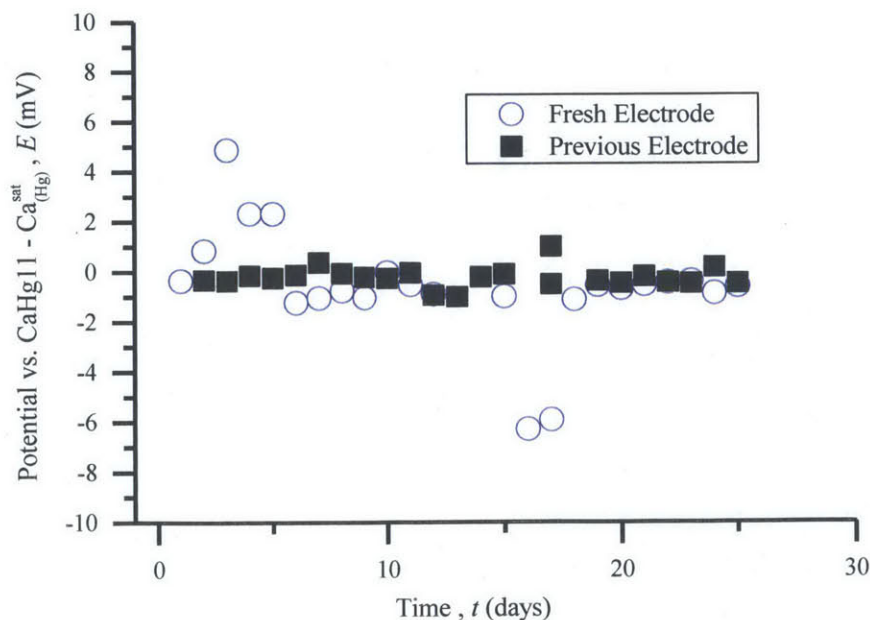


Figure 12. Long term stability of the  $\text{CaHg}_{11}\text{-Ca}_{(\text{Hg})}^{\text{sat}}$  reference electrode. Stability measurements carried out over several weeks show excellent long term stability ( $> 2\text{mV}$  variance, no drift).

Care was taken to avoid cross-contamination of the fresh electrodes, such that the current lead and the glass crucible were replaced each day. The results of the long-term OCV stability measurements are presented in figure 12.

The data support the assertion that there is no systematic drift of the  $\text{CaHg}_{11}\text{-Ca}_{(\text{Hg})}^{\text{sat}}$  electrode over a period of several weeks. This bodes well for its use as a reference electrode, however caution should be taken as although the final equilibrium value ends up within one millivolt of the reference, short-term stability and time to equilibration did vary between the fresh  $\text{CaHg}_{11}\text{-Ca}_{(\text{Hg})}^{\text{sat}}$  electrodes. The  $\text{CaHg}_{11}\text{-Ca}_{(\text{Hg})}^{\text{sat}}$  can experience some variation on the order of several millivolts especially during the initial few minutes of measurement. This is consistent with the results presented in section 4.3.1 concerning the equilibration time of the electrode. The data presented in figure 12 above were taken after 6 hours equilibration time in the cell. The maximum variation in electrode potential never exceeded 10 mV from the reference, and in all cases the  $\text{CaHg}_{11}\text{-Ca}_{(\text{Hg})}^{\text{sat}}$  electrodes equilibrated to within 2 mV of each other by the next day.

One particularly interesting trend is that the freshly prepared  $\text{CaHg}_{11}\text{-Ca}_{(\text{Hg})}^{\text{sat}}$  electrodes tend to systematically increase in potential over the first half hour of measurement, followed by a slow decay and equilibration down to the expected value. This is unlike the observations of OCV behavior between two freshly prepared  $\text{CaHg}_{11}\text{-Ca}_{(\text{Hg})}^{\text{sat}}$  electrodes, which tend to behave more erratically as they come to equilibrium. The behavior observed was consistent across dozens of measurements, and suggests that immediately upon insertion of a freshly prepared  $\text{CaHg}_{11}\text{-Ca}_{(\text{Hg})}^{\text{sat}}$  electrode there is an interaction with the electrolyte. This interaction likely involves the consumption of electrons at the surface of the electrode, as the electrode systematically trends to a more positive value, suggesting electron depletion at the electrode's surface. It is likely that this interaction could involve some minor decomposition of the electrolyte solvent or salt, which forms a stable surface layer, or it could involve the decomposition of some impurities or corrosion of the as-prepared  $\text{CaHg}_{11}\text{-Ca}_{(\text{Hg})}^{\text{sat}}$  electrode. Further effort to identify the source of was not expended, as the resulting perturbation in the potential of the system occurred only over

short times and could be experimentally avoided by allowing the  $\text{CaHg}_{11}\text{-Ca}_{(\text{Hg})}^{\text{sat}}$  reference electrode to pre-equilibrate with its surroundings before conducting electrochemical measurements. The likely reason for such a systematic observation here during the long-term open circuit potential measurements, and the lack of such a systematic observation in the short-medium term measurements described in the previous section, is that in this case one of the  $\text{CaHg}_{11}\text{-Ca}_{(\text{Hg})}^{\text{sat}}$  electrodes has already had a chance to equilibrate with the electrolyte. Thus, the shift in potential that we observe during this process can be attributed entirely to the freshly prepared electrode's equilibration process. In the case of two freshly-prepared electrodes, the potential between the two of them will likely vary more erratically (as is observed), due to differing equilibration behavior for each electrode in the short term.

### 4.3.3 Variation in Chemical Composition

From the calcium-mercury phase diagram, one would expect to observe no variation with potential over a wide range of compositions (see section 2.2). Effectively the liquid-solid phase fraction varies throughout the two-phase region with calcium content while the actual thermodynamic activity of calcium within the electrode remains constant. Two methods were devised to confirm the invariance of electrode potential across the two-phase region.

The primary method of determining the effect of calcium concentration on electrode potential was by chemical amalgam preparation. The details of the measurements conducted are described at the beginning of this chapter, which focuses on the development of a broader open circuit curve for the Ca-Hg system. Shown below in figure 13 is an excerpt from the data collected for figure 10 which focuses on the  $\text{CaHg}_{11}\text{-Ca}_{(\text{Hg})}^{\text{sat}}$  two-phase region.

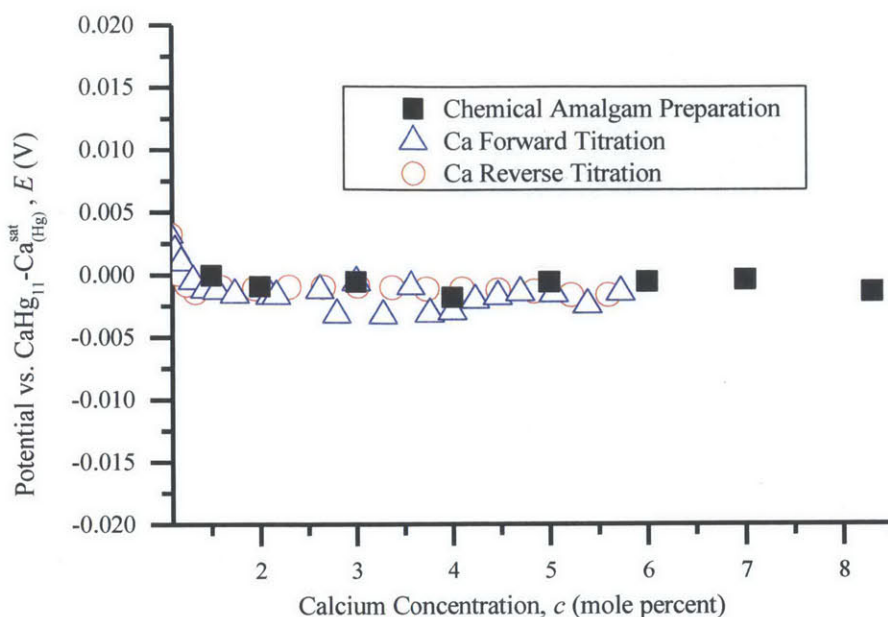


Figure 13. **Variation of the  $\text{CaHg}_{11}\text{-Ca}_{(\text{Hg})}^{\text{sat}}$  reference electrode potential with composition.** Robust stability is observed with respect to variation in electrode calcium content over a range exceeding 6 atomic percent calcium.

As expected, no systematic variation with potential is observed over the course of the measurements. Values for the  $\text{CaHg}_{11}\text{-Ca}_{(\text{Hg})}^{\text{sat}}$  electrode were always found to vary less than 1 mV between fully equilibrated electrodes of different composition over a composition range of 1.5-7 at. % calcium in mercury. The potential of the  $\text{CaHg}_{11}\text{-Ca}_{(\text{Hg})}^{\text{sat}}$  electrode has been found to be invariant with calcium content, as expected based on the theory laid out in Chapter 2. As such, even if some corrosive or parasitic reactions occurred at the electrode surface, resulting in a depletion of calcium, the potential measured will not vary, making the  $\text{CaHg}_{11}\text{-Ca}_{(\text{Hg})}^{\text{sat}}$  electrode ideal for the study of calcium electrochemistry.

#### 4.3.4 Mechanical Perturbation

One additional concern with regards to the stability of the  $\text{CaHg}_{11}\text{-Ca}_{(\text{Hg})}^{\text{sat}}$  liquid-solid two phase electrode is the effect of mechanical perturbation on the measured value of potential. In order to function as a robust reference electrode the value of potential must not vary dramatically as a result of both ambient vibrations (ventilation, construction work, etc..) and regular daily laboratory work (operation of



glovebox, cell preparation, occasionally bumping of testing stand, etc...). While of little concern in the case of a solid electrode, the use of a liquid electrode raises the question of whether or not such a high degree of stability with regards to perturbation can be achieved.

In order to simulate the most violent of mechanical agitations, two experiments were devised. A special two-electrode cell was assembled with a substantial hole was left in the cell top. A molybdenum wire (1 mm diameter) was used to vigorously stir and agitate one  $\text{CaHg}_{11}\text{-Ca}_{(\text{Hg})}^{\text{sat}}$  electrode during an OCV measurement. The electrode was allowed to relax after perturbation and the OCV behavior of the electrode was measured. A second means of agitation was devised to approximate exaggerated regular daily use of the glovebox in which both electrodes would be affected. In this second measurement, the entire glovebox was shaken manually. Again, the system was allowed to relax after the perturbation and the OCV was recorded during equilibration. The OCV response during both forms of mechanical agitation is shown below.

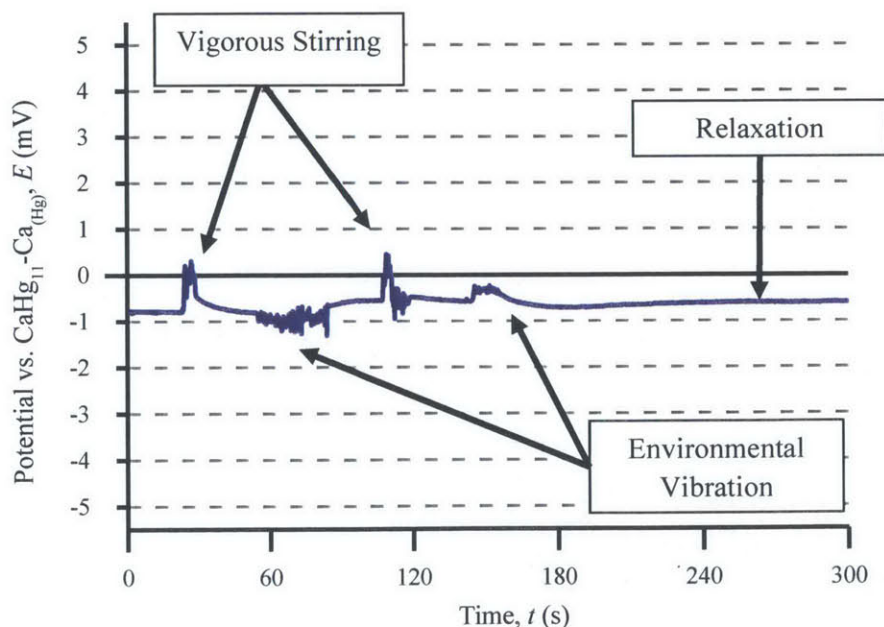


Figure 14. **Electrode response to mechanical perturbation.** Both electrode stirring and mechanical vibration resulted in little deviation from equilibrium electrode values. The electrode potential recovered within minutes.



Application of both forms of mechanical agitation to the system resulted in a deviation of potential on the order of a single millivolt, which is comparable to the uncertainty associated with the assembly of various  $\text{CaHg}_{11}\text{-Ca}_{(\text{Hg})}^{\text{sat}}$  electrodes. Although the magnitude of the perturbation resulted in an extremely small deviation of potential, and the potential quickly relaxed back towards its equilibrium value, for the duration of the perturbation the potential value continued to oscillate randomly. The magnitude of then oscillation itself was on the order of hundreds of microvolts, which is actually somewhat high when considering the stability of the reference in general. However both of these agitations are under extremely exaggerated circumstances and the deviation of the electrode with “regular” mechanical perturbations on a daily basis seems to be much smaller. Such a minor quantity of uncertainty and noise in the reference electrode potential is entirely acceptable during most electrochemical measurements, and should more precise measurements be required, one could always employ the use of an isolation platform to dampen stray mechanical vibrations.

## 4.4 Kinetic Considerations

From a thermodynamic perspective, the calcium-mercury system provides a stable reference potential with regards to a variety of perturbations (e.g. mechanical, temporal, compositional), making it ideal for use as a reference electrode. Mercury systems however, are known to typically have quite sluggish kinetics. As the work proposed in this academic thesis involves the use of a three electrode system, the kinetics of the counter electrode are relevant only in so far as they determine the mismatch in electrode sizes such that the counter electrode is able to undergo faradaic processes of calcium alloying and dealloying without affecting the system appreciably. A counter electrode is of little use in practical testing if it must be unrealistically large or it must be allowed to relax periodically while titrating calcium into or out of the electrode. In this section we briefly explore the kinetics of calcium-mercury amalgams.

### 4.4.1 Voltammetric Measurements

Mercury is known to alloy with calcium and observed to be titratable into amalgams in several electrolytes (water being the most common), however no reports of acetonitrile-based systems were

evident in the literature. Cyclic voltammetry on pure mercury electrodes was used to probe the veracity of the hypothesis that calcium alloying and dealloying can be performed in a continuous fashion in the calcium perchlorate – acetonitrile system and to perform a preliminary examination of achievable current densities. A series of cyclic voltammograms are shown in figure 15 below.

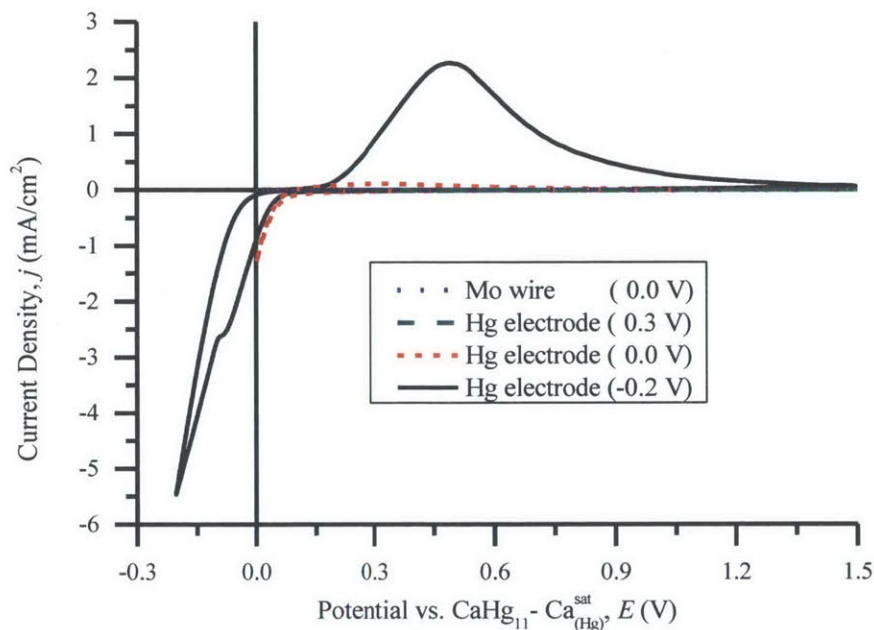


Figure 15. Cyclic voltammograms performed on 0.5 M calcium perchlorate in acetonitrile solutions. Electrochemical calcium alloying and dealloying processes are observed at a sweep rate of 1.0 mV/s.

A bare current collector contained within a glass crucible (used as a baseline) showed no appreciable currents when swept down to the two-phase reference electrode potential. Similarly, pure mercury electrodes drew minimal current when swept in the high potential regime. Upon sweeping down to the reference potential however, appreciable anodic current is drawn, and a cathodic current is observed on the reverse sweep. Polarization to more negative potentials shows a continued alloying process that continues to draw more and more current. Current densities of several milliamps per square centimeter are observed. Although these current densities are low for liquid metals at high temperature (which can be expected to be on the order of hundreds to thousands of milliamps at several hundred degrees)<sup>2</sup>, they are quite acceptable for room temperature electrochemistry in the context of solid state

electrodes. At the greater anodic polarization, a small kink in the alloying curve is observed at around -0.1 V. It is possible that this kink corresponds to the saturation of the calcium amalgamation current, with an additional wave beginning at slightly lower potentials corresponding to the nucleation overpotentials required for the formation of a solid intermetallic phase during the alloying process. This assertion is supported by observations during galvanostatic alloying presented later in this chapter.

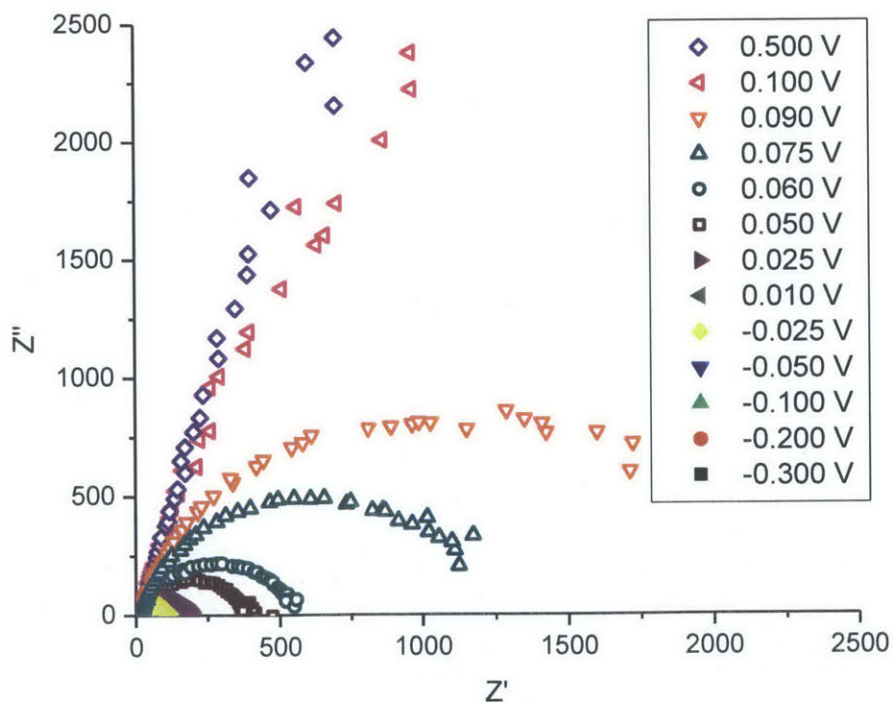
Another feature of note is the nature of the dealloying peak observed during the cathodic sweep. Far greater positive polarizations are needed in order to remove the remaining calcium from the electrode. As opposed to the case of deposition of pure metals on inert electrodes, such as sodium and lithium, the stripping peak does not follow linear behavior upwards from the plating peak and a precipitous drop upon complete metal stripping. Instead it rises slowly with a lesser slope than the plating wave and requires a much greater time for the current signal to drop off. This is consistent with a strained dealloying process in which removing the final bit of calcium from the amalgam takes substantial time and would be expected as the concentration of calcium within the amalgam is quite dilute, as opposed to the case of stripping of a pure metallic electrode.

#### **4.4.2 Impedance Measurements**

Impedance spectroscopy was performed on both pure mercury and two phase calcium-mercury electrodes to probe the primary mechanism of electrochemical resistance in the cell. Potential-controlled measurements were taken at several amplitudes of perturbation and results were found to be consistent. A sinusoidal perturbation amplitude of 5 mV was used to collect the data presented in this chapter. Working electrodes of surface area  $0.33 \text{ cm}^2$  were used and were undersized relative to counter electrodes, and separate  $\text{CaHg}_{11}\text{-Ca}_{(\text{Hg})}^{\text{sat}}$  reference electrodes were used. Electrolyte resistance consistently lay between 12 and 15 ohms for the cell geometry used and was reproducible between measurements. In general, charge transfer resistance was found to be the primary resistance mechanism in the system.

Measurements were carried out on pure mercury electrodes. Resistances were found to be many thousands of ohms on mercury electrodes subjected to an AC voltage signal with no applied DC potential. Furthermore, asymmetry was observed in the calcium alloying/dealloying process as consistently the mercury electrodes were measured to have a lower OCV after impedance measurements (this phenomenon was one method utilized to approximate a dilute calcium amalgam for determination of the  $\text{CaHg}_{11}\text{-Ca}_{(\text{Hg})}^{\text{sat}}$  potential in section 4.1 of this thesis).

Additional measurements were carried out under an applied DC potential in addition to the AC waveform. At high potentials, the resistances remained extremely high, however they drop as the applied DC potential is lowered. Figure 16 below demonstrates the behavior in both the high and low potential regimes.



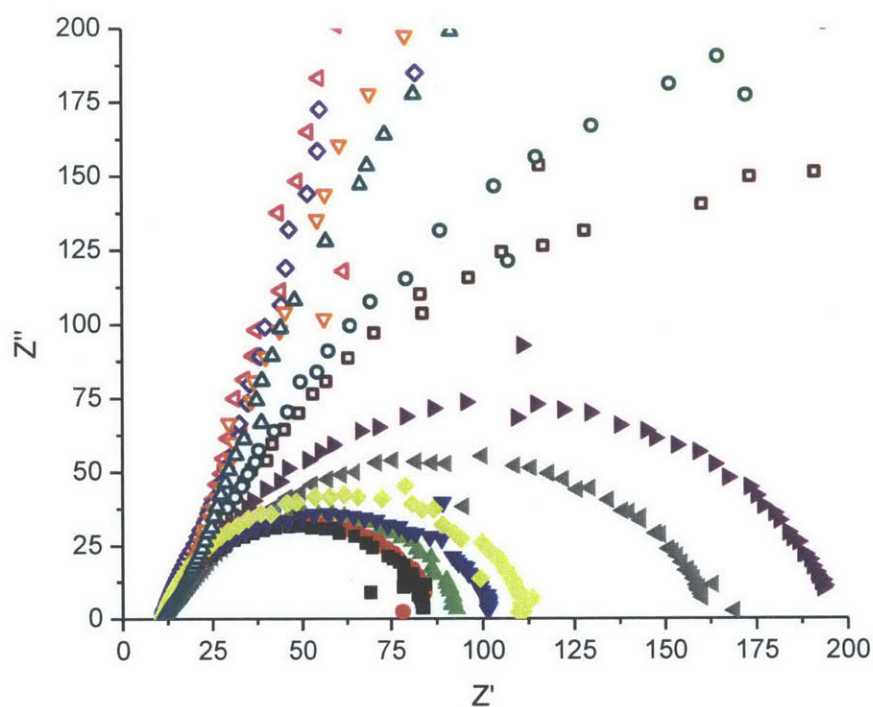


Figure 16. **AC impedance spectra for mercury electrodes.** Spectra were collected at an AC amplitude perturbation of 5 mV with a constant applied DC potential, noted by the legend. Resistances are present in ohms.

The impedance data for various polarizations presented above were fitted with an equivalent circuit model consisting of a resistor in series with a parallel configuration of a resistor and a constant phase element (CPE). Good agreement between experimental data and the equivalent circuit was obtained. Values of the electrolyte and charge transfer resistances, as well as the CPE criterion, are presented in table 4 below.

DC Polarization (V)	Rs	Rp	CPE-T	CPE-P	ChiSqr
-0.3	11.48	71.11	0.00000858	0.91946	0.0049956
-0.2	11.04	74.88	9.01E-06	0.9258	0.000419
-0.1	11.09	81.89	1.12E-05	0.92214	0.0006572
-0.05	11.1	92	2.57E-05	0.8597	0.0026894
0	11.52	145.1	0.00006452	0.77601	0.0040128
0.01	11.5	156.8	7.06E-05	0.74797	0.0027156
0.025	11.6	181.4	2.21E-05	0.87854	0.0034664
0.05	10.89	378.2	2.95E-05	0.82599	0.0029176
0.06	11.52	575.9	5.67E-05	0.79049	0.00601
0.075	12.15	1301	5.27E-05	0.83043	0.010185
0.082	12.27	1858	0.0000601	0.7914	0.0077363
0.09	12.02	2273	5.5876E-05	0.82975	0.0080892

Table 4. Equivalent circuit model parameters for amalgam impedance measurements. Resistances are presented in units of ohms.

One would expect a charge transfer resistance on the order of 100 to 150 ohms to be observed on the  $\text{CaHg}_{11}\text{-Ca}_{(\text{Hg})}^{\text{sat}}$  two-phase electrodes, assuming the primary resistance mechanism is of charge transfer in nature and that the behavior the system is somewhat governed by the observed potential. In order to confirm this, as well as explore any effects due to the phase fraction of solid intermetallic on the behavior of the system, impedance measurements were carried out on a concentration series of chemically amalgamated electrodes. The resulting measurements are tabulated and presented below in figure 17.

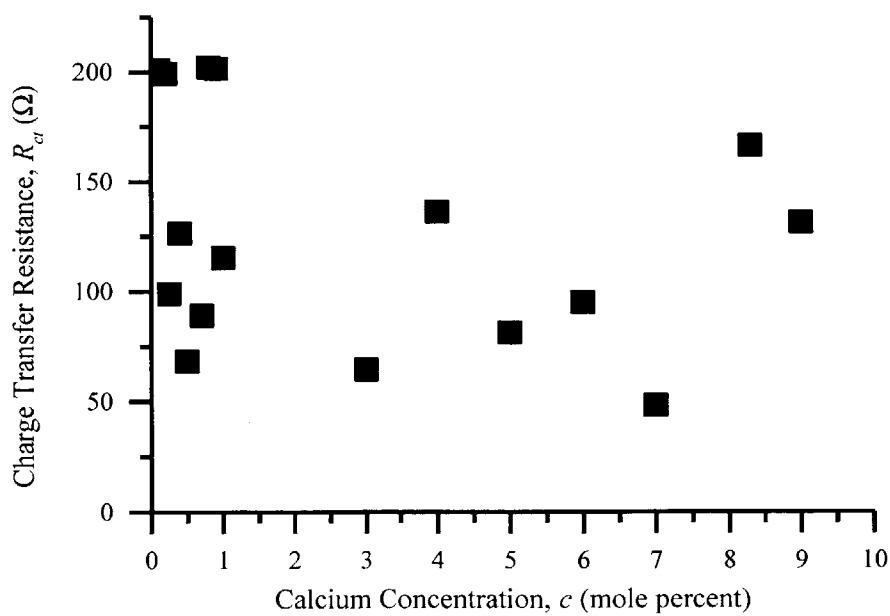
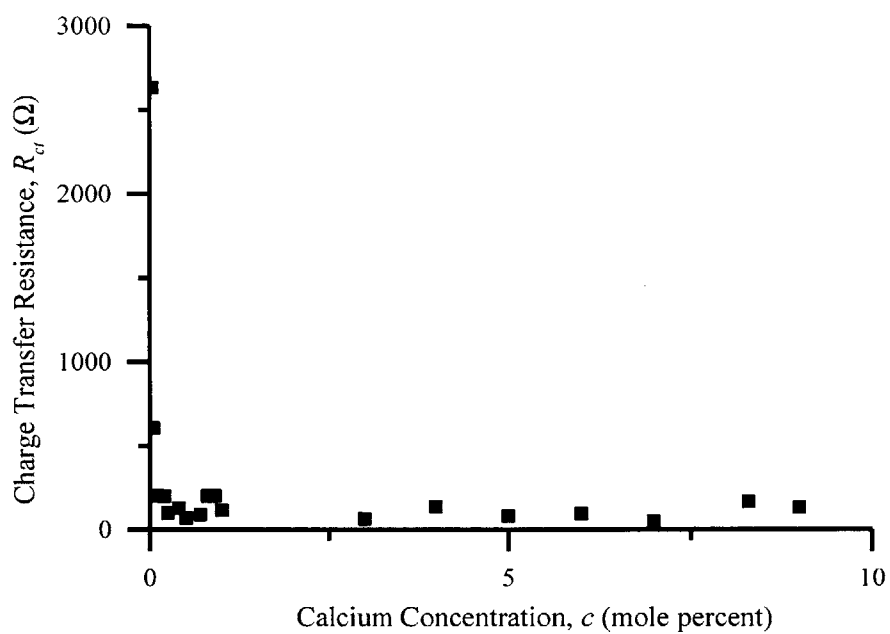


Figure 17. **Charge transfer resistance dependence on calcium concentration.** With the exception of extremely low calcium concentrations, there appeared to be no trend in charge transfer resistance with calcium content.

Very dilute amalgams were observed to have charge transfer resistances on the order of several thousand ohms, however the number was consistently beneath 200 ohms for calcium amalgam concentrations greater than 0.1 percent. Interestingly, no clear trend was observed with calcium concentration within the concentration range of 0.3 to 9 atomic percent calcium. This result could be due to the surface formation of a small quantity of liquid phase between the electrolyte and any solid intermetallic. Any theoretical reaction between the electrode and the electrolyte would consume calcium, slightly depleting the surface locally of calcium, and creating a small amount of liquid at the interface, and thus negating the effect of solid phase fraction. Another possibility to explain this observation is that the charge transfer properties of the liquid and solid amalgam phases are similar enough that any variation in the amount of solid phase at the interface does not appreciably affect the measurement. Regardless, after equilibration of the cell completed, charge transfer resistance could be expected to reside in the range of 50 to 200 ohms, which is acceptable for the operation of the electrode galvanically at reasonable current rates.

#### **4.4.3 Behavior of the $\text{CaHg}_{11}\text{-Ca}_{(\text{Hg})}^{\text{sat}}$ electrode under galvanic conditions**

In the previous section the primary resistances in the cell were determined to be charge transfer in nature, on the order of 50-200 ohms, with an electrolyte resistance contributing an additional 10-15 ohms of resistance. Assuming an overall cell resistance on the high end of this at 200 ohms, and a typical operating current of 100 microamps, an electrode overpotential of roughly 20 millivolts would be expected on an electrode of dimensions used above. This number would scale down as the electrode area increased. In order to confirm this estimation, galvanic alloying/ and dealloying tests were performed at various current densities. For each current, different lengths of time were chosen such that in a total amount of charge passed of 0.25 mAh/g, which for a 4g mercury electrode amounts to 1 mAh of charge. This degree of charging was chosen to approximate the amount to which an electrode would be charged or discharged in a typical positive electrode experiment in this cell configuration, which is the ultimate purpose for the characterization of the  $\text{CaHg}_{11}\text{-Ca}_{(\text{Hg})}^{\text{sat}}$  electrodes. The resulting galvanic charge/discharge profiles are presented below in figure 18.



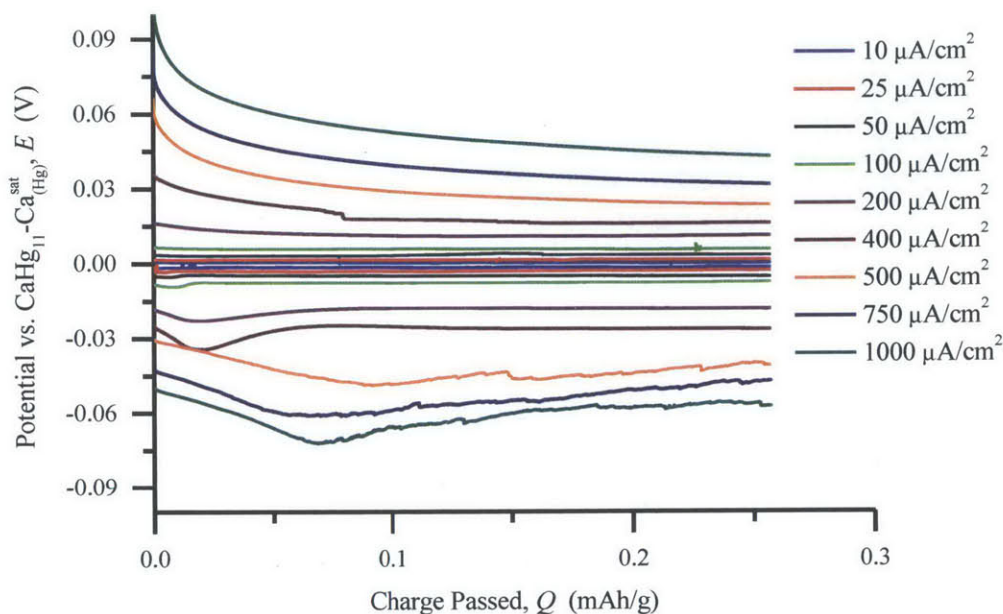


Figure 18. **Galvanic behavior of the the  $\text{CaHg}_{11}\text{-Ca}_{(\text{Hg})}^{\text{sat}}$  electrode.** Different current rates are applied for a fixed charge duration. Electrode overpotentials increase with applied current.

Low overpotentials are observed for both the charge and discharge currents for reasonable current densities (under  $200 \mu\text{A}/\text{cm}^2$ ), with overpotentials being extremely small and current profiles generally flat. However, even when driven at higher currents (up to  $1000 \mu\text{A}/\text{cm}^2$ ), the system exhibits overpotentials under 100 mV. This suggests that the electrode can be cycled galvanically in a faradaic manner under a wide range of current conditions with minimal polarization, and thus a low risk of electrolyte decomposition or activation of other parasitic side reactions.

Several interesting features can be observed in the galvanic profiles, across the entire range of current densities. On calcium insertion, the electrodes polarize as current is passed, and then continue to polarize to more negative values until a local minimum in the potential response is reached. After this the potential shifts to a more positive value, and ultimately levels off to a constant potential as further insertion is reached. Such an overpotential could be considered to be characteristic of nucleation of a new phase, in this case what would be imagined to be a solid intermetallic phase in a liquid electrode.

However, given that the electrode is already within the two-phase region and contained roughly half solid fraction, there would be expected to be enough solid intermetallic phase present that it could simply grow at the expense of the liquid phase without need for further nucleation events. One possibility however, is that the intermetallic phase has a surface layer which must be broken down in order to continue its growth, while another is that a pure solid intermetallic phase does not remain in contact with the liquid electrolyte surface due to some calcium depletion, so in fact the electrode surface is a near saturated liquid and requires a nucleation event to occur to continue calcium enrichment of the electrode. Regardless of the nature of this event, it is unimportant as it does not necessitate substantial overpotentials beyond those due to other mechanisms within the cell, and do not continue for lower current densities. Although similar features are observed at higher current densities, they do not entirely disappear, with the voltage profile oscillating irregularly for the remainder of the titration time after the potential minimum has been reached. These must be due to some mechanism by which the surface of the electrode never achieves equilibrium during the titration time. One plausible explanation is that due to the combined effect of convection acting locally on slightly calcium-enriched intermetallic phases in the metal electrode, bringing them in contact with and carrying them away from the surface, resulting in a mixed potential measurement between intermetallic phases with different calcium activities.

Calcium removal from the two-phase electrode, showed a similar decaying overpotential of a slightly different configuration. Electrode polarization was initially at its highest once current was passed, and slowly decayed down to a constant value of potential. This suggests that the calcium removal process becomes easier with time as a constant current is passed, and might suggest the break down of some surface layer or other barrier to calcium transport. Another possible explanation of the observed phenomenon is if the energetically preferred path for calcium transport out of the electrode is through the liquid, and not the solid intermetallic phase. The local depletion of calcium at the surface would result in the local dissolution of any intermetallic phase, causing it to liquefy, and ultimately increasing the effective surface area for calcium transport and lowering the effective current density. Once again,

regardless of the possible reasons for the behavior of the two-phase electrode in this manner, experimentally observed overpotentials are sufficiently low to allow for its operation as a faradaic counter electrode.

Electrode overpotentials are expected to increase with current density. In the case that such overpotentials are strictly due to a manifestation Ohm's law acting on internal resistances of the system, one would expect a linear response between current density and overpotential. A linear fit of the average electrode overpotentials extracted from the equilibrated electrode potential values in figure 18 above are displayed in figure 19 below.

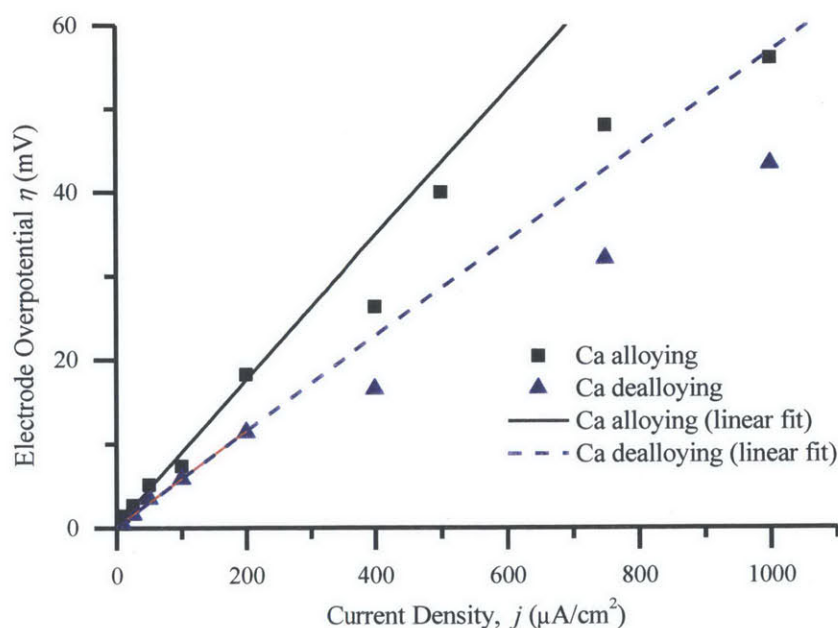


Figure 19. **Linear analysis of the  $\text{CaHg}_{11}\text{-Ca(Hg)}^{\text{sat}}$  electrode overpotential.** Overpotentials obey a linear fit at low polarization, however deviate from linearity at higher current densities.

Although upon cursory examination one might be tempted to imagine that these electrodes follow a linear fit, comparison of the goodness of fit at low and high current densities clearly shows that there is a clear negative deviation from the linear fit at high currents. In the case of large enough polarizations, electrodes

commonly display Tafel behavior, where the overpotential varies log linearly with current density. The same data rescaled onto a Tafel plot are shown in 20 below.

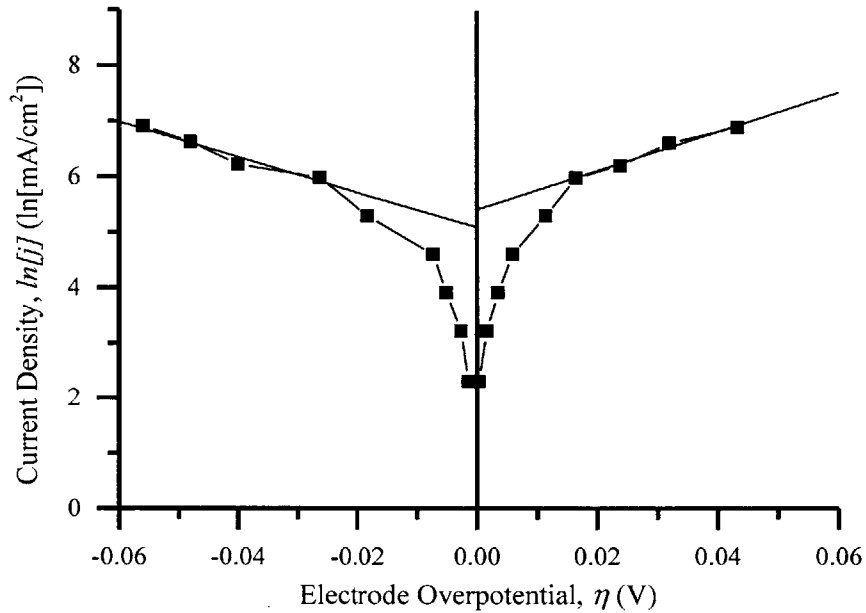


Figure 20. **Tafel plot of calcium-mercury electrode.** Linear fits show good  $R^2=.99$  of respective equations  $-31.5\eta + 5.093$  and  $35.3\eta - 5.413$ .

High values of overpotential display a good linear fit with high  $R^2$  agreement. The Tafel equation can be used to related the electrochemical kinetics of the alloying and dealloying processes to the electrode overpotential, and to extract the exchange current density (corresponding to the rate of reaction corresponding to the electrode's natural dynamic equilibrium, under no electrode polarization).

$$\eta = A \ln\left(\frac{i}{i_0}\right) \quad (8)$$

The electrode overpotential,  $\eta$ , is related to the current density,  $i$ , and the exchange current density,  $i_0$ , by the Tafel slope,  $A$ . The data presented above yield values of 162 and 224  $\mu\text{A}/\text{cm}^2$  respectively. Such current densities, although quite low for liquid metal electrodes at high temperature, make sense for sluggish mercury electrodes at room temperature. Furthermore, such values suggest that currents on the order of 10s to 100s of microamps per square centimeter are indeed appropriate for the

galvanic operation of the calcium mercury electrode as they are well within the natural equilibrium exchange current at the electrode's surface.

Galvanostatic calcium alloying could be carried out continuously for many hours with relatively constant overpotentials, which remained stable and smooth at reasonable current densities, as discussed earlier in this section. The calcium alloying process however, over prolonged times, was observed to result in the formation of a  $\text{CaHg}_{11}$  intermetallic phase which would gradually grow upwards from the working electrode surface and along the current path towards the counter electrode. An image of an alloying growth for a calcium alloying process of several atomic percent calcium is shown in figure 21.

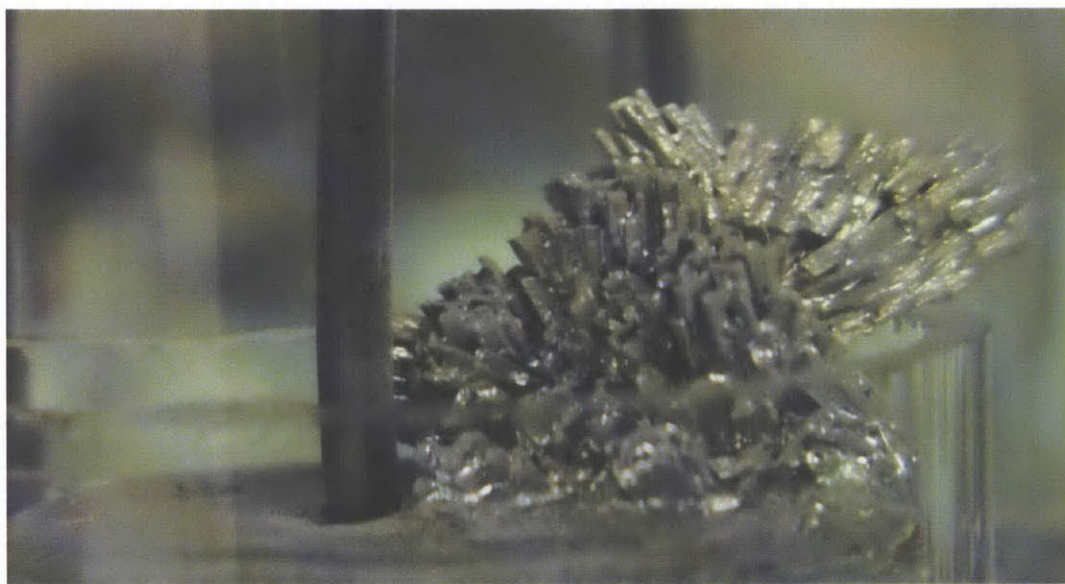


Figure 21. **Intermetallic growth on the  $\text{CaHg}_{11}\text{-Ca}_{(\text{Hg})}^{\text{sat}}$  electrode.** Growth occurs at high current densities for prolonged calcination, and follows expected electric field lines within the electrolyte.

Such growths however, although they appear to be a substantial short circuit threat to the electrochemical cell, require a large amount of calcium alloying to form and extend away from the electrode surface. As long as the  $\text{CaHg}_{11}\text{-Ca}_{(\text{Hg})}^{\text{sat}}$  electrodes used in this thesis are sufficiently large relative to the size of the positive working electrode candidates of interest, only small perturbations in calcium concentration are required, and hence cell shorting is easily avoided. Furthermore, the dendritic growth process is visually obvious in the cell design, and has never proven to be an issue in cell testing.



When appropriately driven with small currents for short times, a root-time linear voltage response could be observed for calcium alloying in dilute amalgam electrodes, which is an indication that the electrode potential varies under diffusion limitations. Under such conditions, GITT can be used to estimate the diffusivity of calcium within liquid mercury. A procedure for the application of GITT to liquid metal electrodes has been enunciated in the literature.<sup>69</sup> When applied in this case, diffusion values for calcium in mercury can be extracted and are found to lie in the range of  $10^{-5}$  to  $10^{-6}$  cm<sup>2</sup>/s, which is consistent with literature value of  $7.43 \times 10^{-6}$  cm<sup>2</sup>/s for calcium diffusivity in room temperature amalgam electrodes.<sup>28</sup>

## 4.5 Chapter Summary

In this chapter we have presented experimental evidence that the calcium-mercury system can act as both a robust reference and counter electrode for the study of calcium-ion active materials candidates. The potential of the  $\text{CaHg}_{11}\text{-Ca}_{(\text{Hg})}^{\text{sat}}$  two phase electrode was determined to be 0.825 V with respect to the  $\text{Ca}/\text{Ca}^{2+}$  couple. Reference electrodes were found to be stable over many weeks with no appreciable drift and minimal sensitivity to mechanical perturbation and compositional variation. Furthermore the primary resistance mechanism of the system was observed to due to charge transfer at the mercury electrode surface. In the potential range corresponding to the operation of the  $\text{CaHg}_{11}\text{-Ca}_{(\text{Hg})}^{\text{sat}}$  electrode as a counter electrode this resistance was acceptably low to result in minimal over potentials at the electrode surface when operating at reasonable current densities. The next chapter will apply the electrodes characterized in this section to the study of calcium-active positive electrode materials.

# Chapter 5: Positive Electrode Material

## Experimental Results

### 5.1 Vanadium oxide as a model multivalent ion intercalation system

A unique system for the study of calcium intercalation compounds was developed and characterized in detail in the previous chapter. Before moving directly onto studying the performance of the Chevrel phase electrodes in calcium-ion conducting electrolytes, steps must be taken to systematically prove that the  $\text{CaHg}_{11}\text{-Ca}_{(\text{Hg})}^{\text{sat}}$  counter and reference electrodes, as well as the  $\text{Ca}(\text{ClO}_4)_2$  in acetonitrile electrolyte, are capable of producing a functioning electrochemical cell with a known calcium electro-active compound as the working electrode. The  $\text{V}_2\text{O}_5$  system has been previously studied by Amattucci and coworkers.<sup>10,11</sup> This section is devoted to studies undertaken on vanadium oxide that confirm the utility of the proposed pseudo-half cell system.

Cyclic voltammetry performed on microelectrodes confirmed the electrochemical activity of vanadium oxide in the system, a typical result of which is shown in figure 22 below.

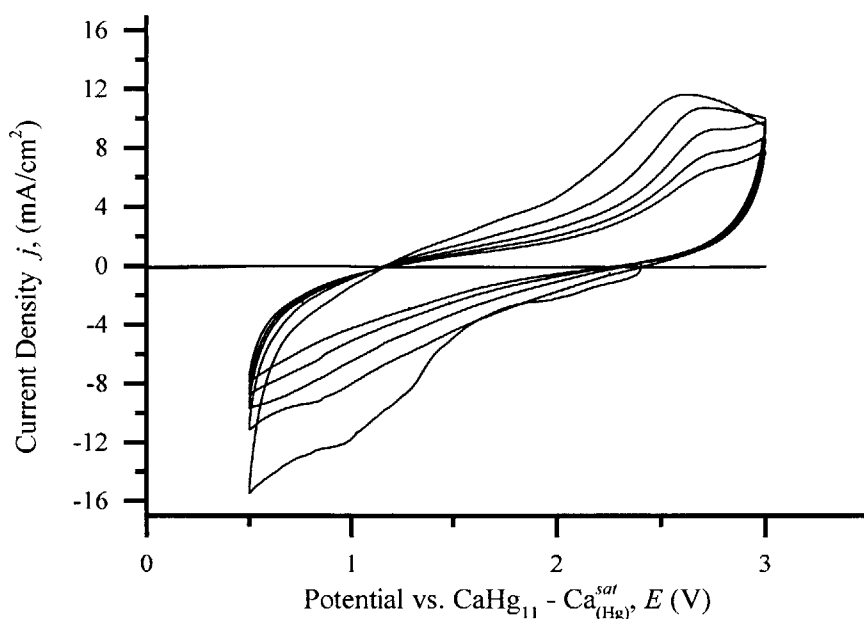


Figure 22. **Calcium electrolyte CVs for  $V_2O_5$  electrode.** Cyclic voltammogram of 5 sweeps on a  $V_2O_5$  working electrode. Comparable currents are observed on the anodic and cathodic sweeps.

A single broad feature is observed with a gradual sloping current increasing with potential. The shape of the curve is consistent with data in the published literature for vanadium oxide tested in calcium perchlorate in propylene carbonate electrolyte.<sup>10,11</sup>

Additional vanadium oxide electrodes pressed onto molybdenum mesh were cycled under constant current charge-discharge conditions. Cycling data reproduced was also found to be consistent with the literature. Fast capacity fade was observed during cycling. In addition, a large polarization was observed between charge and discharge. The first discharge-charge cycle of a typical electrode is shown in figure 23 below.



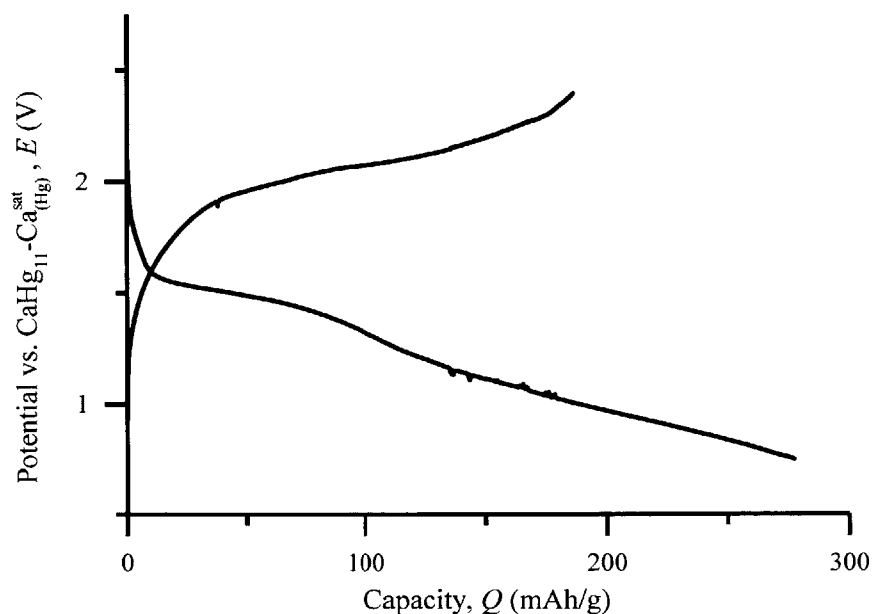


Figure 23. **First cycle behavior of  $V_2O_5$  electrode.** First discharge and charge cycle of  $V_2O_5$  composite electrode, exhibiting near theoretical capacity (94%) on first discharge, with substantially less observed on charge. Further cycles (not shown) resulted in fast capacity loss.

Confirmation of calcium as the electroactive species responsible for the electrochemical signal in the vanadium oxide tests was desired. SEM-EDX measurements were performed on discharged electrodes post-mortem and the calcium to vanadium ratio was found to be 1:2, which is consistent with the formation of the  $CaV_2O_5$  stoichiometry. The reproducible cycling behavior and presence of calcium in post-mortem studies is consistent with the literature and demonstrates the appropriateness of this system as an avenue to study calcium electroactive materials.

This section has demonstrated the validity of the proposed calcium-mercury reference and counter electrode system with the calcium perchlorate in acetonitrile electrolyte for the study of calcium ion compounds. The vanadium oxide system, known to intercalate numerous ions, performs as expected. Further sections of this chapter explore more novel compounds as calcium intercalation candidates.

## 5.2 A qualitative study of transition metal oxides and sulfides

Multivalent ion intercalation poses several challenges relating to ion charge density and mobility, as well as the requirement of multiple electron redox steps (discussed in detail in Chapter 1). A survey of the literature (presented in Chapter 2) identified a number of potential calcium intercalation compound candidates, some inspired by the lithium and magnesium ion literature, with others inspired by prior art in high temperature calcium molten salt systems. Preliminary screening cyclic voltammetry was carried out on microelectrodes pressed with candidate calcium intercalation compound powders to identify which, if any, of these candidates would prove to be electroactive with calcium. All results presented in this section utilized a sweep rate of 1 mV/s and were performed on custom constructed molybdenum disc electrodes loosely pressed with active material powders (see Chapter 3 for preparation technique), and are representative of several repeated trials. Quantitative data cannot be extracted from this technique due to unavoidable difference in active material loading resulting from the powder pressing technique, and thus the current densities presented in this section are normalized by the cross-section of the molybdenum disc electrode and not by the mass or true active particulate density. The remainder of this section presents the results for all candidate compounds beginning with oxides and followed by chalcogen compounds.

Tungsten oxide ( $\text{WO}_3$ ) is an early thermal battery compound for use in calcium molten salt batteries at elevated temperatures. Commercially available tungsten oxide ( $\text{WO}_3$ ) powder (Sigma-Aldrich,  $d < 100$  nm) was used as received from Sigma-Aldrich and pressed onto the microelectrode.

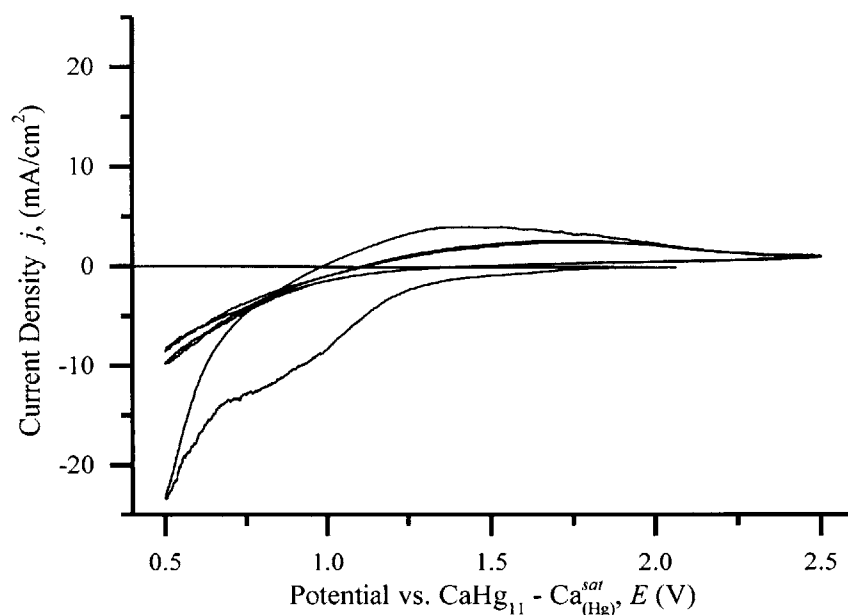


Figure 24. **Calcium electrolyte CVs for WO<sub>3</sub> electrode.** Cyclic voltammogram of 3 sweeps on a tungsten oxide working electrode shown (black), as well as Mo mesh baseline (blue) in calcium perchlorate in acetonitrile.

Electrochemical signal was observed in the case of WO<sub>3</sub> with an appreciable current observed on sweeps to more negative potentials, with a broad feature observed on the reverse peak. The electrochemical response was largest on the first cycle and more muted on subsequent cycles. Attempts to charge and discharge larger WO<sub>3</sub> electrodes galvanostatically were unsuccessful and resulted in simple electrode polarization response.

Another thermal battery compound, calcium chromate (CaCrO<sub>4</sub>) was explored, namely as a curiosity and for completeness, although the mechanism of operation in thermal batteries involved a reaction with a lithium-containing molten salt and it is unlikely that the compound would be a good intercalation candidate for calcium electrochemistry. Calcium chromate (CaCrO<sub>4</sub>) (Sigma-Aldrich) was studied as received.

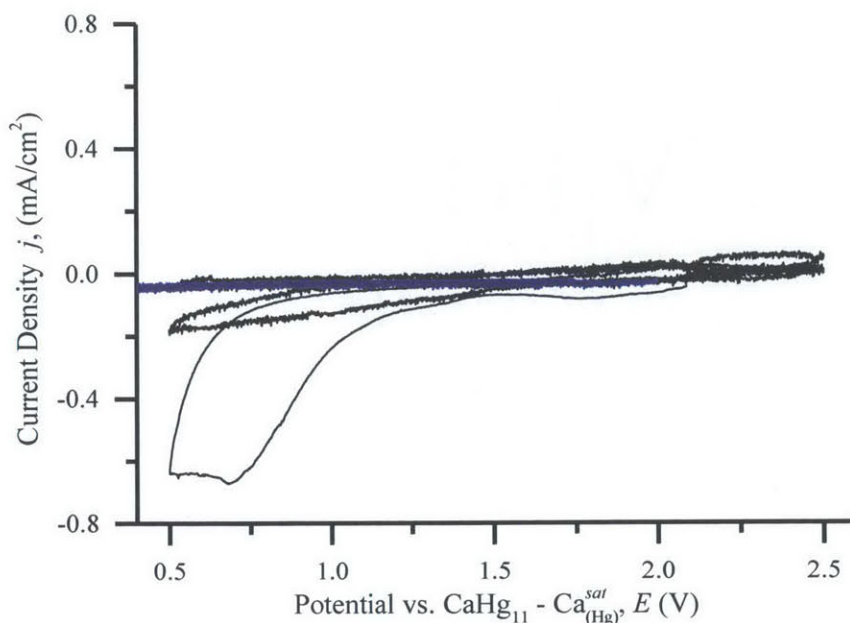


Figure 25. **Calcium electrolyte CVs for  $\text{CaCrO}_4$  electrode.** Cyclic voltammogram of 3 sweeps on a calcium chromate working electrode shown (black), as well as Mo mesh baseline (blue).

As expected, the electrochemical response of the calcium chromate system is poor, with electrochemical signal on the order of baseline. Some small electrochemical response was observed on the first discharge, however there is no charge removed on the subsequent reverse sweep and similarly the magnitude of the current is very close to the baseline current observed. Subsequent sweeps showed effectively a baseline response, with the slightly higher and sloped current response characteristic of a larger true surface area counter electrode than the base metallic current collector.

Potassium ferrate ( $\text{K}_2\text{FeO}_4$ ) was a potentially interesting candidate for study due to the fact that the iron transition metal center in the compound undergoes a multiple electron redox shift during discharge with lithium cations. However, the mechanism of discharge observed was shown to be metathetical, not intercalation, and involved formation of lithium compounds, the calcium analogues of which could be expected to behave differently.<sup>36,37,40</sup> Potassium ferrate powder (Sigma-Aldrich, > 90%) was used as received. No electrochemical response was observed over multiple trials, as can be seen below in figure 26.

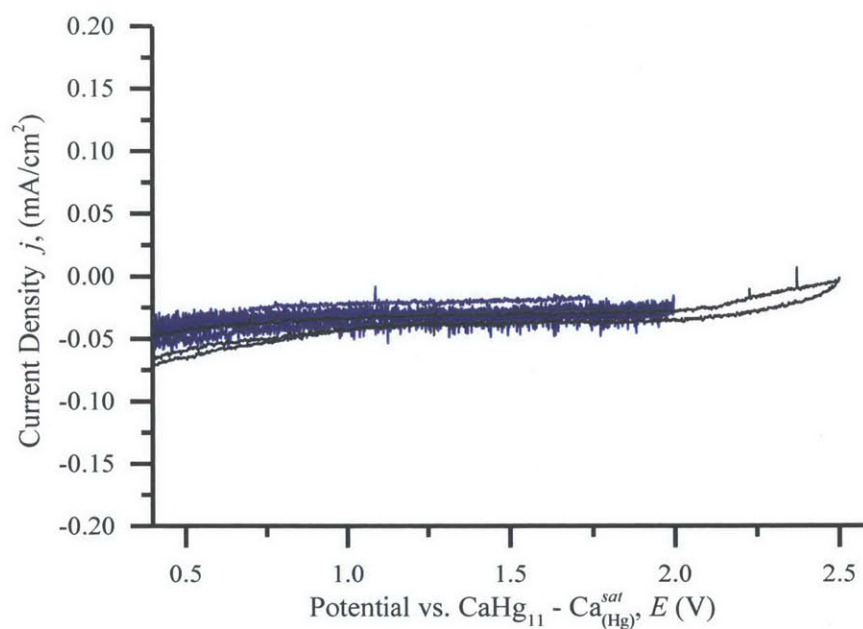


Figure 26. **Calcium electrolyte CVs for  $\text{K}_2\text{FeO}_4$  electrode.** Cyclic voltammogram of 3 sweeps on a potassium ferrate working electrode shown (black), as well as Mo mesh baseline (blue).

High temperature calcium iron sulfide ( $\text{FeS}_2$ ) batteries were developed using molten salt electrolytes, and are discussed in greater detail in Chapter 2. Iron sulfide (Alfa Aesar, >99.9%) was studied as received in the room temperature organic electrolyte system, with the results presented below.

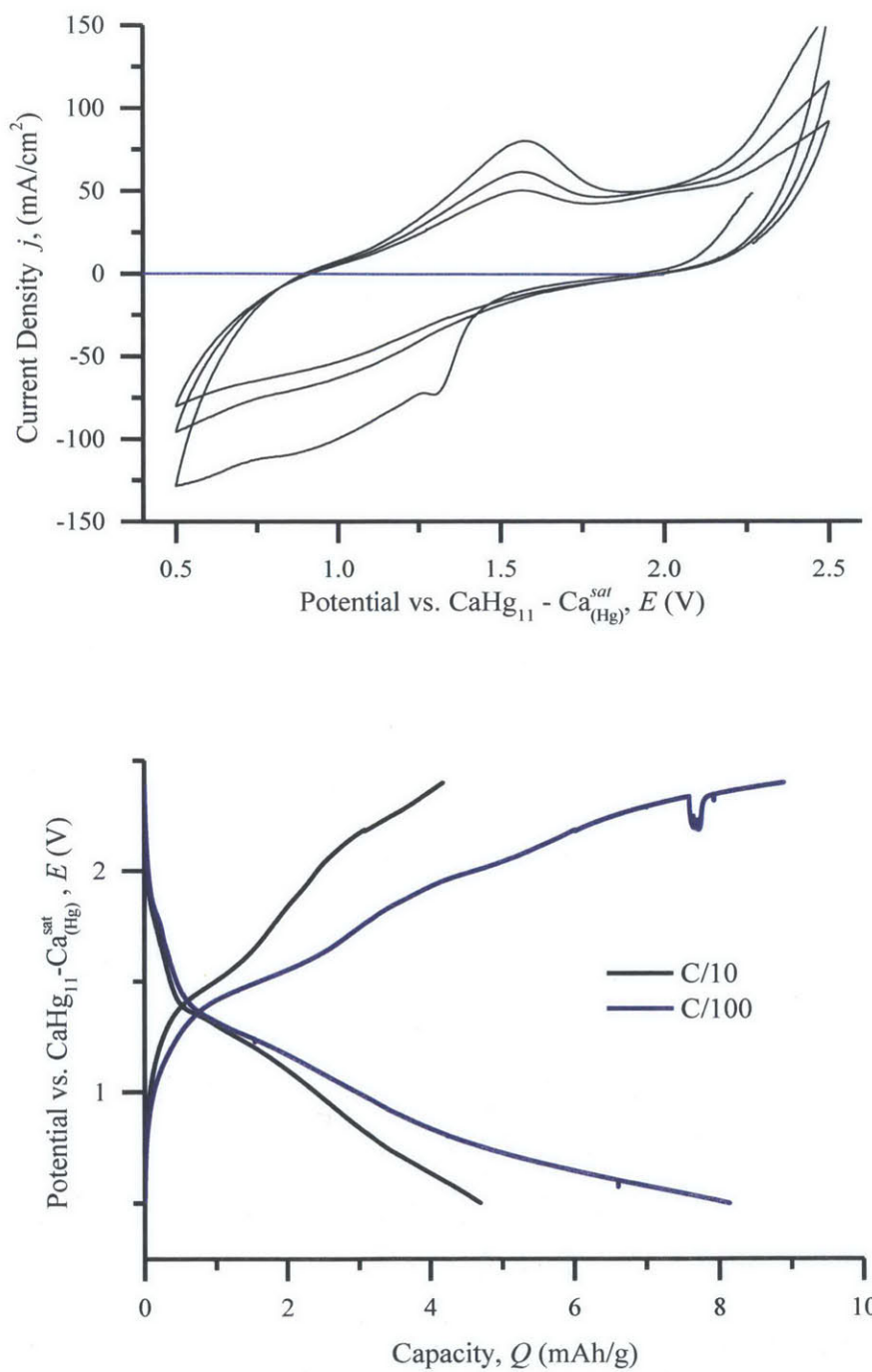


Figure 27. **FeS<sub>2</sub> CVs and cycles.** Cyclic voltammogram (top) of 3 sweeps on an iron sulfide working electrode shown (black), as well as Mo mesh baseline (blue). First galvanic discharge and charge cycles (bottom) shown at two different current rates.

The initial open circuit potential of the iron sulfide compound was found to be around 2.1 V against the reference, and not particularly stable. Upon polarization to more negative potentials a positive current was

initially drawn to the electrode, counter to what would be expected during such a sweep. Appreciable currents were drawn on both the anodic and cathodic sweeps, and remained for several cycles. Galvanic experiments were performed on larger electrodes, which were cycled at somewhat limited capacity for 10 cycles. First cycle utilization was 4% of theoretical at C/10 and 6% of theoretical at C/100 cycling rates. The qualitative features of the first cycle charge and discharge profile mimic those in the cyclic voltammogram, as would be expected. Minimal capacity fade was observed.

Titanium disulfide ( $\text{TiS}_2$ ), an intercalation compound known to intercalate several different types of ions, was used as received (Sigma-Aldrich, > 99.9%). A single sharp peak is observed on the first sweep in the first wave, followed by a second smaller wave at lower potentials. A double peak feature is present at higher potentials on the reverse sweep. These most pronounced features quickly vanish on subsequent cycles, suggesting the process cannot be used in a rechargeable cell.

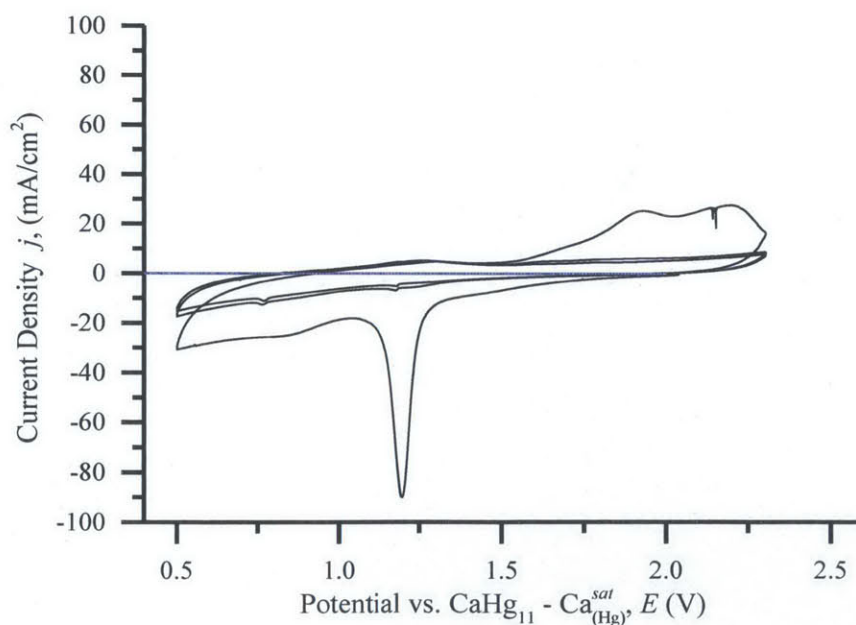


Figure 28. **Calcium electrolyte CVs for  $\text{TiS}_2$  electrode.** Cyclic voltammogram of 3 sweeps on a titanium disulfide working electrode shown (black), as well as Mo mesh baseline (blue).



Molybdenum sulfide ( $\text{Mo}_6\text{S}_8$ ) and molybdenum selenide ( $\text{Mo}_6\text{Se}_8$ ) Chevrel phase compounds were custom synthesized (see Chapter 3 for details). Both phases are known to intercalate numerous monovalent and divalent ions<sup>50,51</sup>, and are discussed in greater detail in Chapter 2. The sulfide phase demonstrated relatively weak electrochemical signal which was somewhat noisy. Furthermore there was a large polarization observed between cathodic and anodic currents. This could likely be due to the size of the calcium ions being too large for the intercalation cavities within the sulfide structure. The selenide phase on the other hand showed a much stronger current response with little noise in the signal. A set of well defined peaks, characteristic of a phase change upon intercalation, were observed on multiple sweeps. A closer examination of the selenide structure follows in the next section.

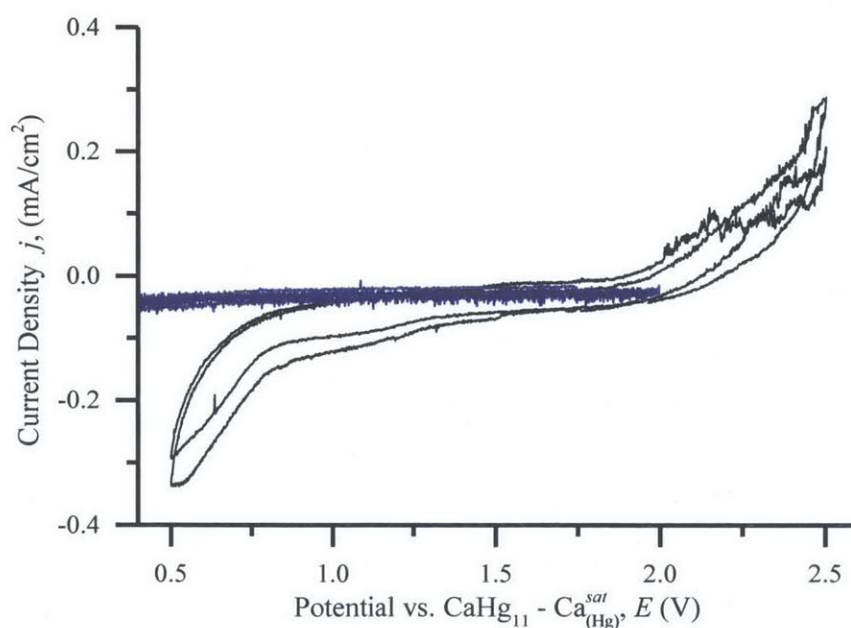


Figure 29. **Calcium electrolyte CVs for  $\text{Mo}_6\text{S}_8$  electrode.** Cyclic voltammogram of 2 sweeps on a molybdenum sulfide working electrode shown (black), as well as Mo mesh baseline (blue).



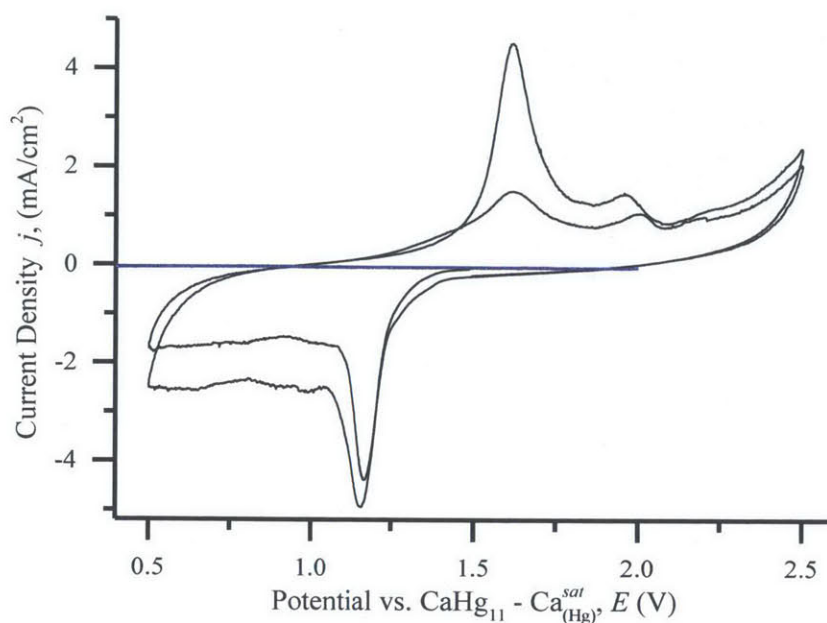


Figure 30. **Calcium electrolyte CVs for Mo<sub>6</sub>Se<sub>8</sub> electrode.** Cyclic voltammogram of 2 sweeps on a molybdenum selenide working electrode shown (black), as well as Mo mesh baseline (blue).

High temperature metal sulfide batteries have been in existence for quite some time, however recently published work explored calcium-sulfide primary cells at room temperature.<sup>17</sup> The work used specialized sulfur-carbon composite electrodes, however attempts were made to reproduce the work using pure as-received sulfur powder (Sigma-Aldrich, > 99.5%). Irreversible capacity was observed on the electrode on the first few sweeps, suggesting that calcium-sulfur could be used as a primary battery system, however the discharge current density was particularly low and not of further interest.

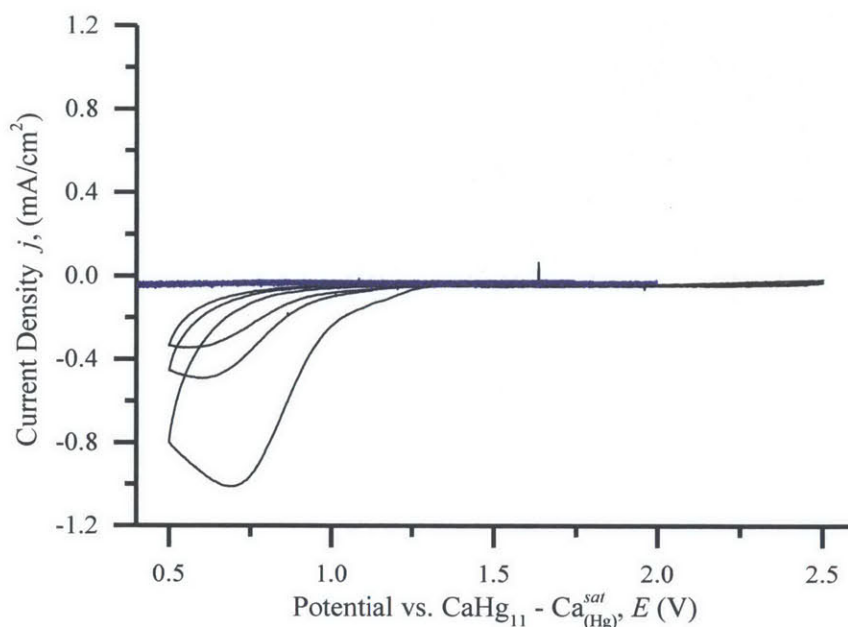


Figure 31. **Calcium electrolyte CVs for S electrode.** Cyclic voltammogram of 3 sweeps on a sulfur working electrode shown (black), as well as Mo mesh baseline (blue).

The preliminary assessment presented in this chapter identified several interesting calcium electrochemistry candidates through voltammetric studies, namely tungsten oxide ( $\text{WO}_3$ ), iron sulfide ( $\text{FeS}_2$ ), and the Chevrel structure of molybdenum selenide ( $\text{Mo}_6\text{Se}_8$ ). Of these three candidates, molybdenum selenide was observed to have the most promising electrochemical response in both cyclic voltammograms as well as preliminary galvanic studies. The remainder of this thesis will aim to evaluate the electrochemical performance of molybdenum selenide as a calcium intercalation compound, and provide analytical support of calcium as the electroactive species.

### 5.3 Electrochemical Behavior of $\text{Mo}_6\text{Se}_8$

This section explores the electrochemical performance of the  $\text{Mo}_6\text{Se}_8$  electrode with regards to permutations in cycling rate, particle size, operating temperature, and compound stoichiometry. The reader should recall from Chapter 2 that the  $\text{Mo}_6\text{Se}_8$  Chevrel phase compound is electronically capable of accommodating up to 4 electrons per cluster of 6 molybdenum atoms, which yields a theoretical maximum capacity of 88.8 mAh/g based solely off of the mass of the pure  $\text{Mo}_6\text{Se}_8$  phase. Assuming this

capacity is achieved, a terminal stoichiometry of  $\text{Ca}_2\text{Mo}_6\text{Se}_8$  is expected. However, if only one calcium ion is able to intercalate per unit cell, due to its fairly large size, then a terminal stoichiometry of  $\text{Ca}_1\text{Mo}_6\text{Se}_8$  would be anticipated representing a theoretical capacity of 44.4 mAh/g. Note that all capacity data presented in this section and subsequent subsections have been calculated using the mass of the compound's non-intercalated stoichiometry.

Molybdenum selenide ( $\text{Mo}_6\text{Se}_8$ ) is able to undergo reversible galvanic cycling, as previously mentioned in section 5.2. Shown below is the 16<sup>th</sup> discharge and charge cycle for a typical  $\text{Mo}_6\text{Se}_8$  electrode cycled at a C/200 rate.

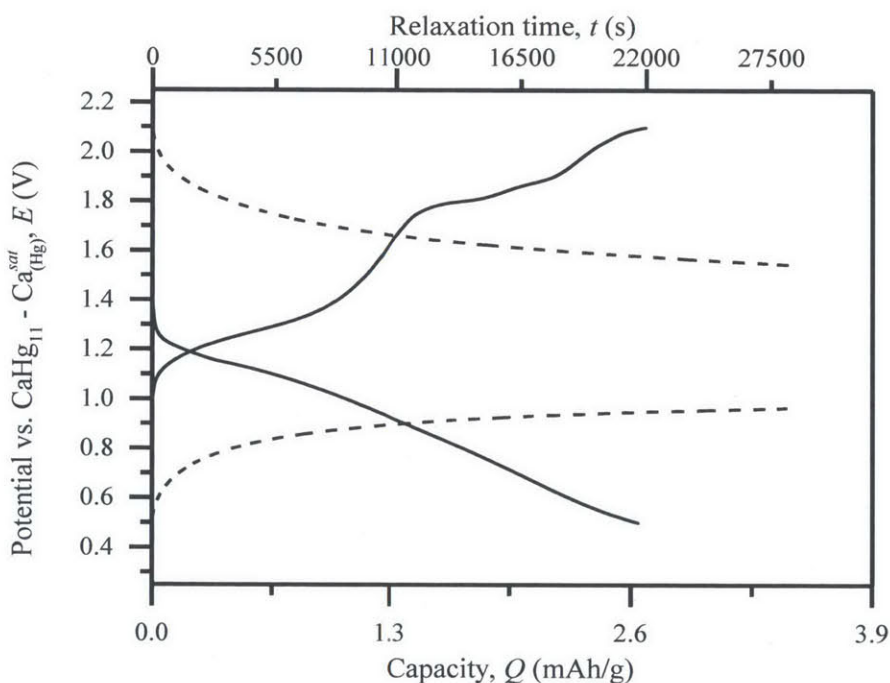


Figure 32. **Galvanic cycling profile for  $\text{Mo}_6\text{Se}_8$ .** The 16<sup>th</sup> discharge and charge cycles are shown (solid) along with subsequent OCV relaxation curves corresponding to rest periods (dashed).

The discharge curve consists of a broadly sloping feature below 1.2 V vs. reference, with a shallower slope at first and then becoming steeper as the discharge deepens. This behavior is uncharacteristic of intercalation in the Chevrel phase in the cases of other ions, which exhibit flat potential profiles on discharge. The charge curve contains more features, with the first capacity removed below the onset of

appreciable capacity on the discharge curve, suggesting that the calcium insertion process is complex and does not involve sites of totally equivalent energy.

The cell was allowed to equilibrate during an OCV measurement on this particular cycle after both discharge and charge, with the two states exhibiting distinct OCV relaxation behavior and values. The capacity of the system remained over this period, and combined with the high columbic efficiency suggests that the observed discharge and charge phenomena are related and not simply corrosive currents. Furthermore, the distinct features of the charge/discharge profile and the large polarization between the end of discharge and the onset of charge suggest that this is not a capacitive process, but likely involves intercalation or some other faradaic reaction between the  $\text{Mo}_6\text{Se}_8$  compound and the electrolyte, presumably in which calcium plays a key role (see Chapter 6 for further discussion).

Interestingly, the observed reversible capacity is well below the theoretical capacity for the  $\text{Mo}_6\text{Se}_8$  compound, less than 3% if  $\text{Ca}_2\text{Mo}_6\text{Se}_8$  is considered as the terminal stoichiometry in the electron transfer limited case. First cycle capacities were observed to be somewhat higher, but never exceeded 5% of the theoretical value. Capacity faded quickly upon cycling, although columbic efficiency remained high between cycles. Several factors could contribute to this low capacity including corrosion of the electrode material, formation of an inhibitive surface layer, or generally poor kinetic and transport properties within the electrode. The remainder of this section will address methods by which the reversible capacity of  $\text{Mo}_6\text{Se}_8$  was investigated and improved.

### **5.3.1 Rate effects on the performance of $\text{Mo}_6\text{Se}_8$**

Achievable electrode material capacity in the case of intercalation compounds sometimes obeys a strong cycling rate dependence, owing to poor transport properties. Different  $\text{Mo}_6\text{Se}_8$  electrodes were prepared and cycled at three different current rates,  $C/10$ ,  $C/20$ , and  $C/200$ . The first and third discharge and charge cycles are shown figure 33 and exhibit a trend with capacity as would be expected of rate limiting performance. The capacity for the  $C/10$  rate is less than half that observed at  $C/200$ , with  $C/20$

lying between them. The onset of discharge occurs at higher potential for lower cycling rates, with the discharge curve displaying a flattening discharge slope at lower rates as well. The changes observed in the charging curves are more pronounced, with the flat discharge feature observed at around 1.5 V shrinking and disappearing at higher cycling rates.

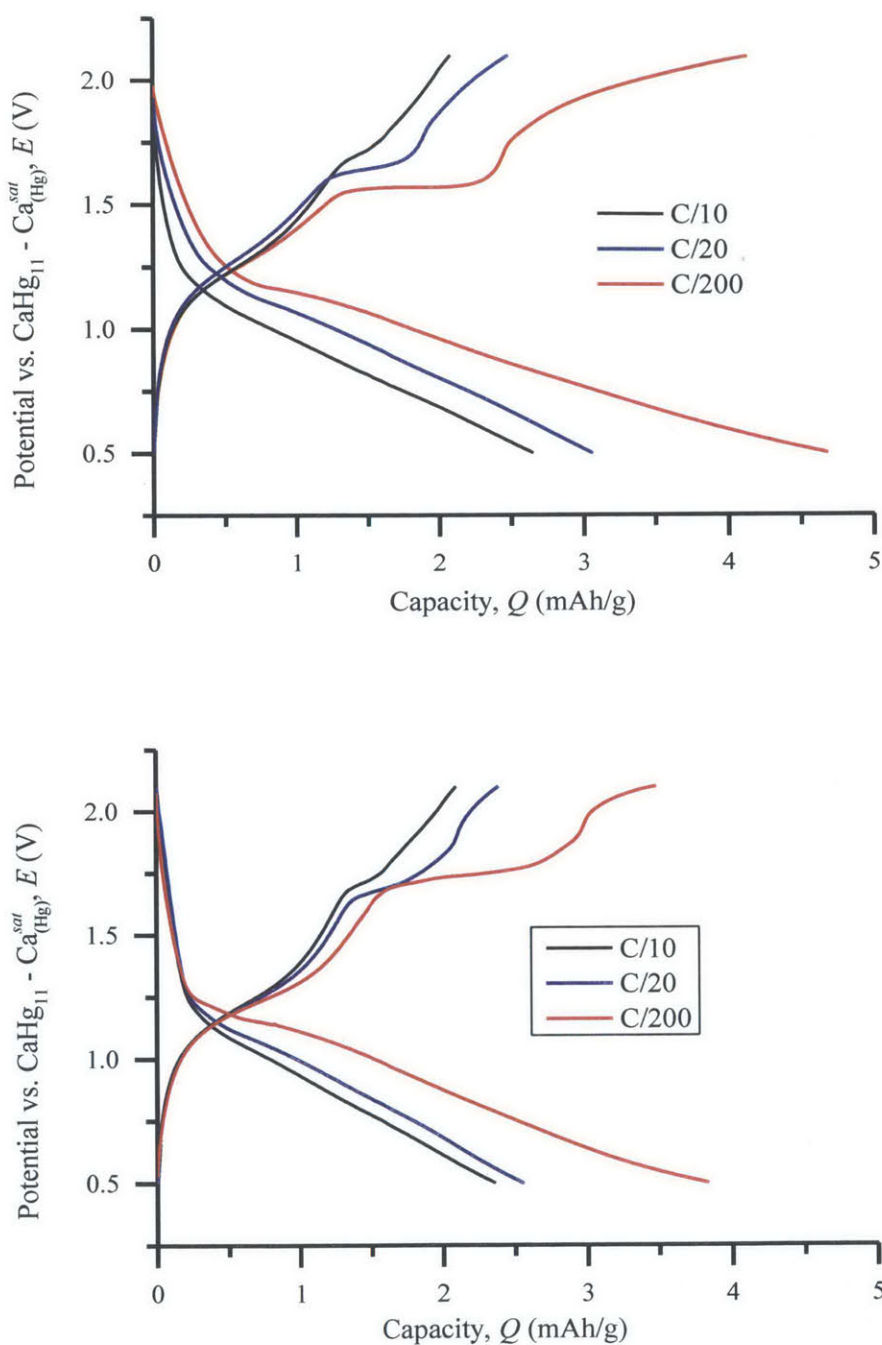


Figure 33. **Galvanic cycling rate series for  $\text{Mo}_6\text{Se}_8$ .** First cycle (top) and third cycle (bottom) are shown. Electrode utilization increases as cycling rate decreases.

The discharge and charge curves also show different characteristics between cycles. In general, as cycle number increases so does the polarization of the electrode, with the onset of discharge occurring at a lower potential and the onset of charge at a higher potential. Furthermore, the slopes of the profile tend to

steepen on both charge and discharge, a comparison which can be most readily observed by comparing the flat 1.5 V feature on the C/200 charge curve in figure 33 with that of the feature shifted to 200 mV higher potential with a positive slope. Further comparison with the 16<sup>th</sup> charge in figure 32 shows that it has migrated to even higher potentials at 1.8 V, with a far less pronounced plateau.

The rate dependence of the reversible cycling behavior suggests that there is a kinetically limited contribution to the low observed capacity in the Mo<sub>6</sub>Se<sub>8</sub> compound. Kinetic processes tend to improve at higher temperatures, as both reaction rates and ion transport properties tend to be higher with more thermal energy in the environment. The effect of temperature will be explored in the next section to confirm the capacity is indeed kinetically limited.

### **5.3.2 Temperature effects on the performance of Mo<sub>6</sub>Se<sub>8</sub>**

Measurements were carried out on several different electrodes cycled at the same current rate although operated at different temperatures using a silicone heat bath. Representative results for C/10 cycling for the first and third cycles at three different temperatures are shown below in figure 34. Capacity dramatically increased with temperature, and more than doubled as the temperature was increased from ambient temperatures to 75 degrees C. Further increases in temperature were not possible due to the low boiling point of acetonitrile (82 degrees C). Both the discharge and charge curves became less steep with increasing temperature. The characteristic charging plateau which was non-existent at the C/10 rate at room temperature developed at higher temperatures and lowered in potential from 1.8 V back towards 1.5 V on the first cycle. High capacity fade rate is still observed between the cycles and the columbic efficiency of the high temperature cells was somewhat lower than that of room temperature cells in general. The plateau features observed on the first cycle at higher temperatures became less pronounced on subsequent cycles, gradually steepening in slope and shifting to higher potentials. The observed features and behavior at higher temperature and higher cycling rates are similar to those at lower temperature and slower cycling rates, which suggests that the increased temperature improves the kinetics of the cycling process, resulting in improved electrode performance.



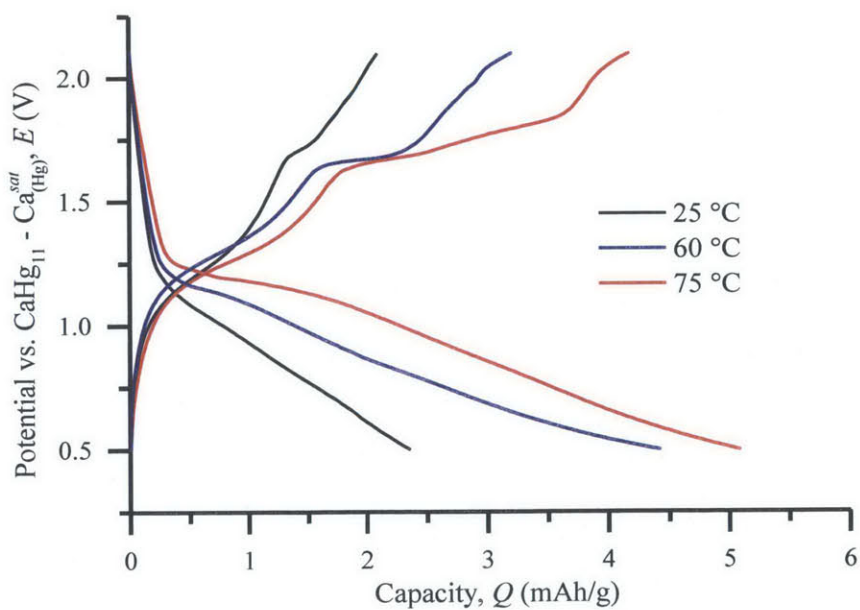
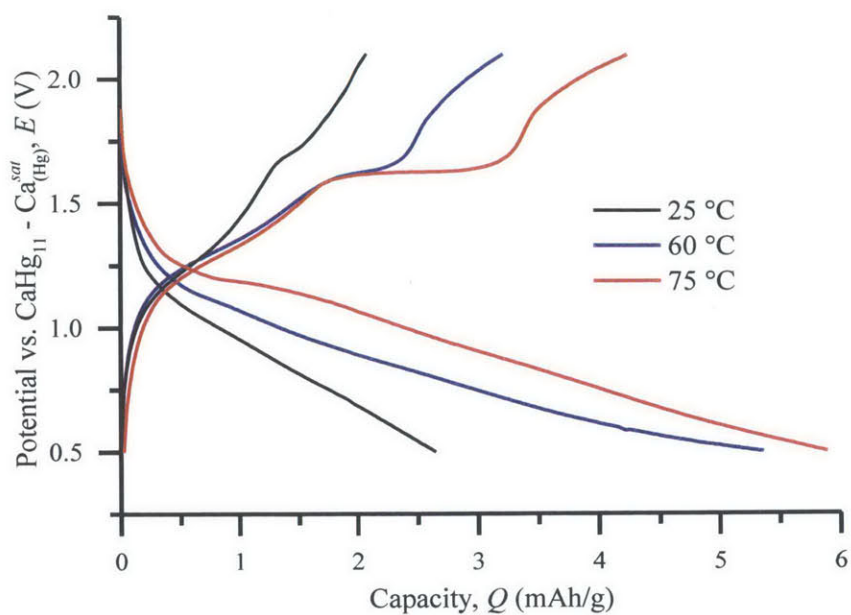


Figure 34. **Galvanic cycling temperature series.** First (top) and third (bottom) cycles are shown for C/10 rate cells tested at different temperatures.

Even though the comparison of the first and third cycles of the electrodes shows an improvement in capacity, as well as distinct features that develop with increased temperature, single electrode studies



were carried out to show that the improved capacity is indeed due to improved kinetics at higher temperature, rather than other differences between each of the electrodes. A single electrode was assembled by standard procedures and cycled for 50 cycles at room temperature. The cycling was halted, and the cell was heated to 60 degrees C and cycled for an additional 50 cycles at the same rate. The results of the cycling are shown in figure 35 below.

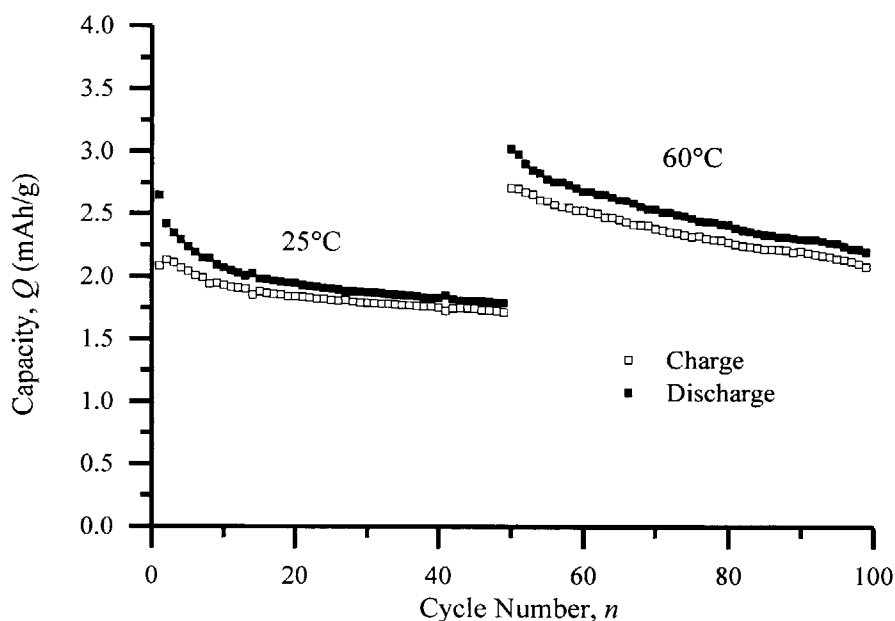


Figure 35. **Variation of capacity with temperature.** Capacity data is presented for a single cell operated at C/10 rate at room temperature for 50 cycles, and then operated at elevated temperature for another 50 cycles.

The electrode capacity fades with cycle number as would be expected. However, upon heating, the capacity of the cell spikes to above the initial cell capacity. This discontinuous increase in capacity can be attributed to improved kinetics within the electrode, allowing for greater insertion of calcium at the same cycling rate. The observed capacity fade rate is higher at the higher temperature.

If the effect observed in figure 35 above is indeed due to the change in kinetics as a result of temperature, and not due to some irreversible alteration of the material, one would expect that various changes in temperature would affect the capacity discontinuously between these shifts. Another cell was

assembled and subjected to cycling at the C/10 rate at a variety of temperatures, the results of which are shown in figure 36 below.

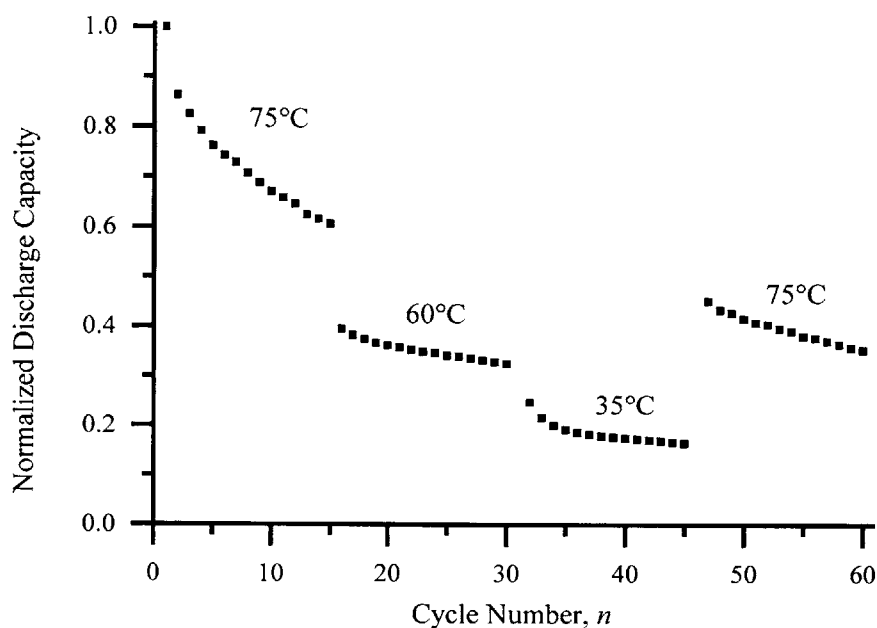


Figure 36. **Temperature dependence of normalized discharge capacity.** Data presented are normalized to first cycle discharge capacity. Temperature was adjusted during several hours of OCV measurement.

The initial capacity of the cell is highest at high temperatures, and fades at a rapid rate. Upon discontinuous cooling between the 15<sup>th</sup> and 16<sup>th</sup> cycle, the observed capacity drops to approximately two-thirds of the previous cycle. A discontinuous drop is observed again between the 30<sup>th</sup> and 31<sup>st</sup> cycles, after another change in cell temperature. Finally, the temperature of the system is increased to the original high temperature and the capacity of the cell recovers. Furthermore, the recovery in capacity appears to line up well with where one would expect the capacity to be from an extrapolation of the fade rate of the first high temperature cycling segment. These observations strongly support that the changes in cycling performance are a direct result of improved kinetics due to temperature change.

Figure 37 below provides a visual comparison of the first cycling behavior for individual cells cycles at both low and high rates and at low and high temperatures. The most striking feature of the plot is

the improved performance observed with both rate and temperature. The greatest improvement in capacity with temperature is observed at faster cycling rates, which makes sense as faster cycling rates tend to limit electrode capacity more extremely in the case of the lithium ion literature.<sup>70,77</sup>

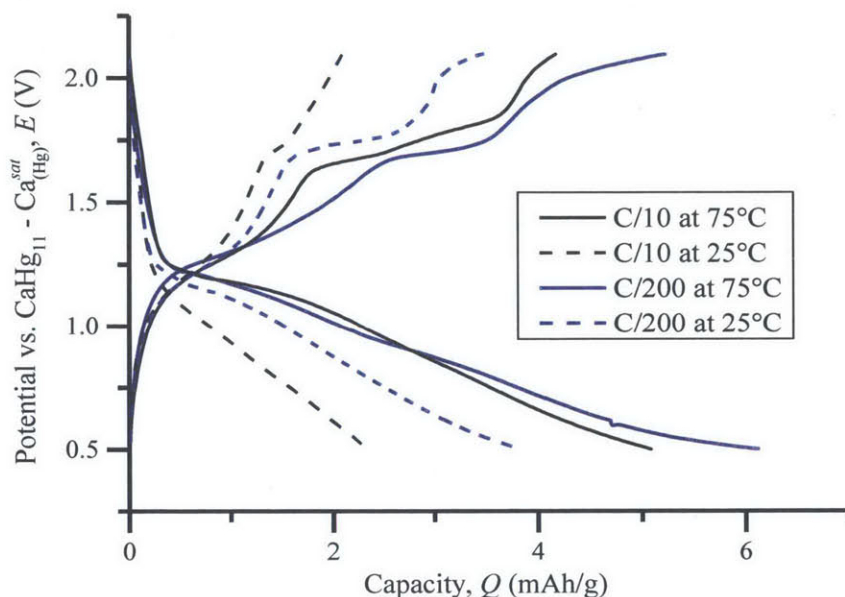


Figure 37. **Comparison of cycling rate and temperature effects.** First cycle is shown for four independent electrodes charged and discharged at different rates and temperatures. All electrodes utilized the same test vessel, electrolyte, and reference and counter electrodes for consistency.

The results presented in this subsection are all consistent with the hypothesis that the  $\text{Mo}_6\text{Se}_8$  electrode exhibits severe kinetic limitations. Distinct plateaus begin to evolve on calcium insertion and removal as the temperature of the system is increased. The observed improvement in capacity performance is due to improved kinetics at the electrode due to increased temperature and not due to differences in the electrodes or cell assembly procedures, as evidenced by the discontinuities in capacity at temperature transitions within particular cells, and the reversible nature of shift in capacity as temperature is increased and decreased. Higher temperature cycling can be combined with slower cycling rates to further improve electrode performance, suggesting that a maximum capacity threshold for the material has not been reached, and that further modifications to address electrode kinetics might be effective at further increasing obtainable electrode capacity.

### 5.3.3 Particle size effects on the performance of $\text{Mo}_6\text{Se}_8$

Particle size reduction is a common technique by which kinetically sluggish electrodes are improved. Smaller particles have shorter diffusion distances, which results in improved solid-state transport of ions during a given time, and improves electrode performance in diffusion limited cases. Furthermore, smaller particles have a higher surface area to volume ratio, and thus have higher true surface areas, which will improve cases where electrode performance is limited by interfacial processes. The primary particle size of the  $\text{Mo}_6\text{Se}_8$  powders studied in the preceding sections was found to be on the micron-scale  $2.25 \pm 2.17$  microns with a wide distribution by SEM/TEM analysis, with some particles found to be as large as 10 microns in diameter (see appendix C for a more detailed discussion of particle size determination). A typical SEM image of the micron-scale particles is shown in figure 38 below.

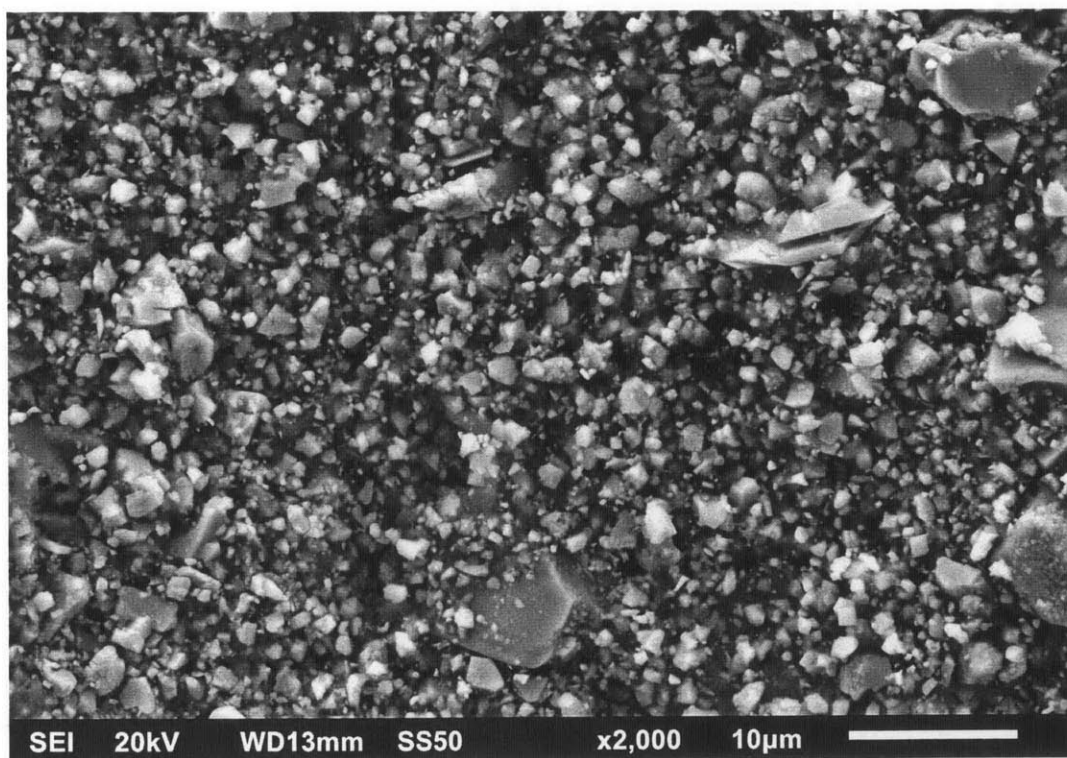


Figure 38. **SEM image of typical “microscale”  $\text{Mo}_6\text{Se}_8$  particles.** A heterogeneous distribution of particle sizes is observed, under standard backscattered SEM imaging under low magnification.

Such a large average particle size, with an inhomogeneous particle size distribution, could explain the poor capacity of the electrode. Furthermore, if indeed only the smallest of the particles were

electrochemically active, most of the active material mass would actually be contained within the larger particles, a fact which is not captured in the simple particle size average. Reduction of average particle size and homogenization of the particle size distribution should improve electrode performance in the case of kinetic limitations.

A common method of particle size reduction is high energy ball milling, in which larger powders can be ground to sub-micron scales by high energy agitation in the presence of milling media (typically steel or refractory oxide balls). High energy milling is a promising technique to decrease the size of such large particles, however such treatments have been shown in the literature to damage the Chevrel phase and degrade electrochemical performance as it is metastable and undergoes a gradual phase transformation upon milling.<sup>78</sup> Rather than traditional ball milling, powders were cryomilled using a McCrone micronizing mill and liquid nitrogen. The logic of the choice was that by milling powders at lower temperatures, for very short times, the undesirable phase transformations within the Chevrel phase could be avoided. Powders were synthesized by standard procedure (described in Chapter 3), placed in the milling media, and liquid nitrogen was poured into the chamber. Milling was carried out for three 5-minute periods, with additional liquid nitrogen added between each period. The primary particle size distribution was found to be  $1 \pm 0.5$  microns, representing an effective reduction and homogenization of the particle size distribution.

An alternative synthesis procedure was used to directly synthesize more mono-disperse particles with a smaller particle size without the need for post-synthesis milling. The procedure utilized pre-milled precursor materials as well as lower temperature and shorter synthesis time to produce smaller, fully reacted Chevrel phase particles without allowing for enough time for particle coarsening to occur (see Chapter 3 for a full description of the procedure). The new synthesis technique was successful in producing sub-micron scale particles with an average particle size of  $343 \pm 133$  nm and a fairly uniform particle distribution. A typical SEM micrograph of the as-synthesized “nanoscale” particles is shown in figure 39 below.

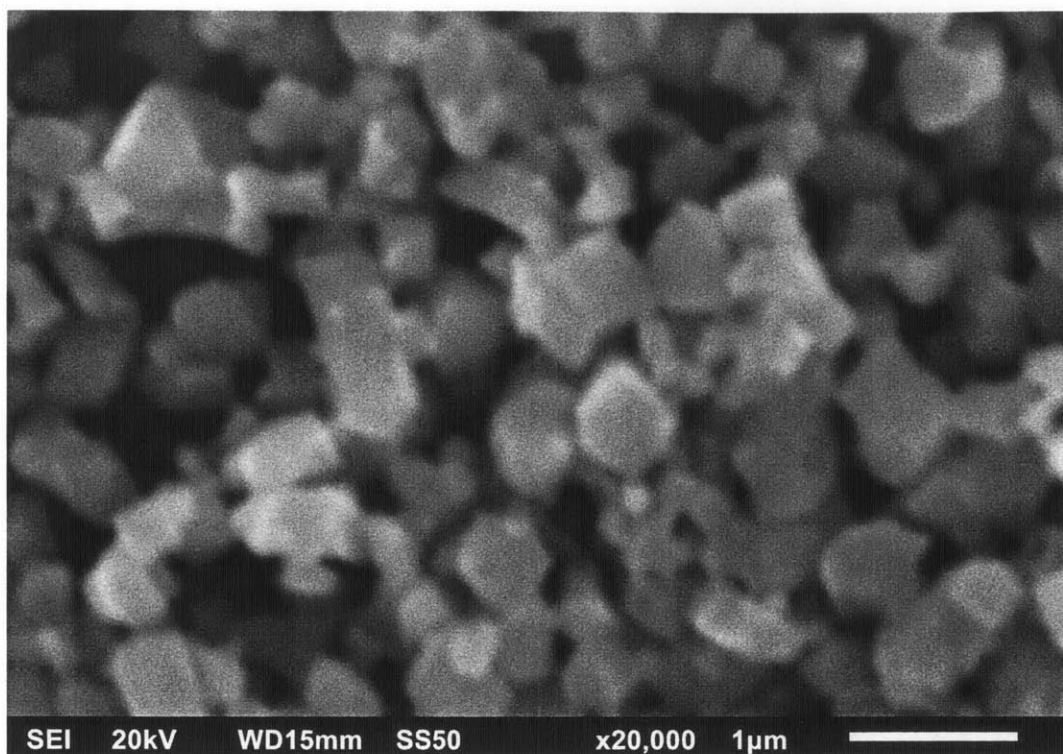


Figure 39. SEM image of typical “nanoscale”  $\text{Mo}_6\text{Se}_8$  particles. Uniform particle size distribution is observed under high magnification, with typical particle sizes on the order of a third of a micron.

Individual electrodes of all three different  $\text{Mo}_6\text{Se}_8$  preparation techniques (microscale, cryomilled, and nanoscale) were assembled by standard techniques and cycled at slow rates ( $C/200$ ). Both the cryomilled and the nanoscale particles exhibited improved performance over their microscale counterparts, as can be seen in figure 40, with the nanoscale material showing the greatest improvement. The most notable difference between the nanoscale profile and the other profiles is the presence of a distinct plateau at 1.2 V upon discharge. This flat region is indicative of intercalation in the Chevrel phase, and is similar to those plateaus observed with other divalent ions such as magnesium, zinc, and cadmium.<sup>50,51,79</sup> The plateau does not extend until the theoretical capacity, and begins to trail off into a sloping feature as the discharge continues. This behavior is very similar to behavior observed during cadmium intercalation into the  $\text{Mo}_6\text{Se}_8$  phase during the first cycle, and is indicative of limited transport properties in the material due to its large size.<sup>50</sup>



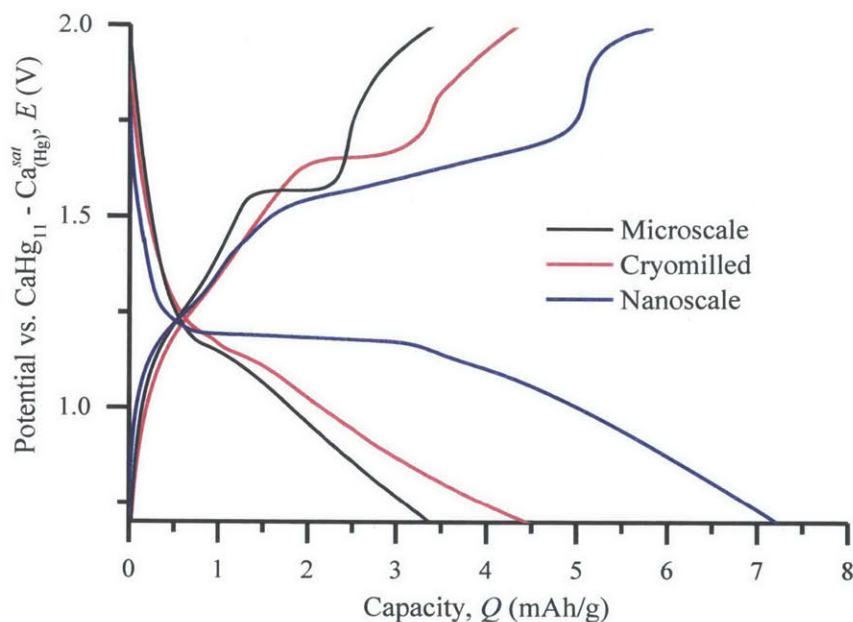


Figure 40. Effect of particle size on first cycle behavior of  $\text{Mo}_6\text{Se}_8$ . Cells were cycled at C/200 rate at room temperature.

The nanoscale  $\text{Mo}_6\text{Se}_8$  material was chosen for further study as it exhibited the best performance with respect to achievable capacity. Further electrodes were prepared and cycled at both room temperature and elevated temperature, as well as subjected to various chemical and structural characterization techniques (see Chapter 6). Figure 41 below compares the first cycle behavior for the nanoscale material at room temperature and at elevated temperature to the previously studied microscale material at room temperature. At elevated temperatures, the plateau feature becomes more pronounced and continues for a larger capacity on discharge. Similarly, a more flat sloping plateau-like feature is observed on charge. The increasing length of the plateau features (both absolute and relative to the total observed capacity) and the higher first cycle columbic efficiency both support the theory of a kinetically limited capacity within the  $\text{Mo}_6\text{Se}_8$  Chevrel phase.

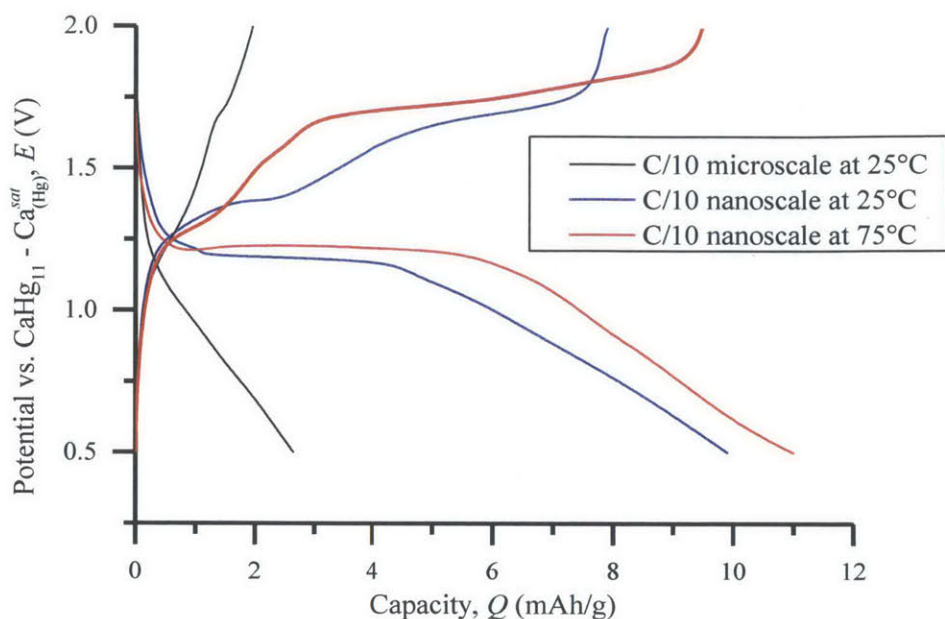


Figure 41. **Nanoscale first cycle performance.** Curves presented were collected on independently prepared electrodes utilizing the same experimental cell (electrolyte, counter, and reference electrodes).

Further cycling was carried out for the various cells described above, with the capacity data summarized in figure 42 below. The nanoscale material is observed to show a four-fold increase in capacity at room temperature and a five-fold increase in capacity at elevated temperatures on early cycles. The capacity fade rate of the nanoscale material was much higher than that of microscale material, although the capacity continued to exceed double that observed in the microscale system for prolonged cycling (over 100 cycles). The increased capacity fade rate could be due to increased mechanical degradation of the electrode brought about by volume changes resulting from greater electrode utilization, and would be consistent with prevailing theories on electrochemical fracture mechanics as a mechanism for capacity fade.<sup>80</sup>



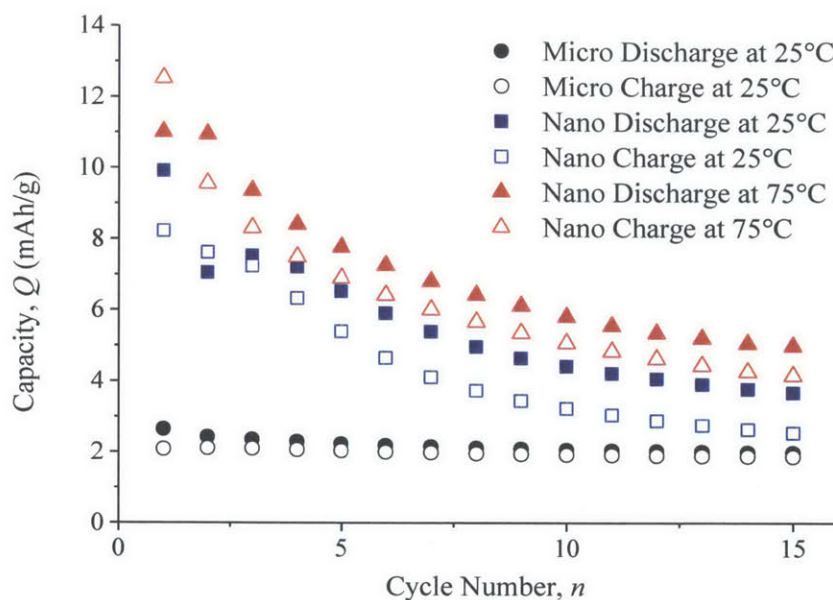


Figure 42. **Cycling performance of nanoscale  $\text{Mo}_6\text{Se}_8$  electrodes.** Three different electrodes were tested in the same electrochemical cell utilizing the same electrolyte, counter, and reference electrodes.

Particle size reduction results support the hypothesis that the limited capacity is indeed due to kinetic limitations, likely due to the poor mobility of calcium within the material due to its relatively large size and divalency. Cation size and charge correlate to mobility within the Chevrel phase structure, as they affect the sites which can be occupied within the material by the ions as well as the relative magnitudes of energetic gaps between sites required for mobility.<sup>57,81,82,83</sup> Namely, large cations tend to be localized at a central site within the calcogen cube within the structure, rather than being delocalized towards the cube's periphery.<sup>57,81</sup> The next section will seek to validate this hypothesis of transport-limited capacity and further improve cell performance through permutations of the Chevrel phase chemistry in order to locally disrupt the location of calcium occupancy within the unit cell.

### 5.3.4 Compositional effects on the performance of $\text{Mo}_6\text{Se}_8$

The  $\text{Mo}_6\text{Se}_8$  Chevrel phase is a metastable phase, and its preparation calls for the creation of a ternary  $\text{Cu}_2\text{Mo}_6\text{Se}_8$  phase from which copper ions are de-intercalated, typically by chemical means. The removal of copper ions does little to perturb the overall Chevrel structure due to their small size, allowing

it to maintain its open cavities suited to intercalation of other ions. It has been suggested the presence of residual copper within the structure could improve the mobility of other ions by already occupying some of the deepest energetic “traps” within the structure and helping “push” other ions along their way.<sup>57,81</sup> Other studies have examined the effects of co-intercalation of lithium and magnesium ions and found that co-intercalation of multiple ions is indeed a possibility.<sup>81</sup> The use of residual copper to displace sites for calcium intercalation from cavity center – hence improving ion mobility – may also work in the case of calcium, although there could also be negative contributions due to steric effects as calcium is larger than other ions studied within the literature.

Microscale  $\text{Cu}_2\text{Mo}_6\text{Se}_8$  Chevrel phase particles were synthesized and lightly acid leached at pH 3 for several hours to partially remove copper from the sample. SEM EDS confirmed a residual copper concentration on the order 3 to 5 atomic percent (but less than the 12 percent that would be expected from the as-synthesized material). The open circuit voltage of this material is observed to be lower than that of its non-copper containing cousin, registering 1.75 V as opposed to the typical 1.90 V, which would be expected from the already partially intercalated phase. Figure 43 below shows a cyclic voltammogram of the  $\text{Cu}_x\text{Mo}_6\text{Se}_8$  material. The first sweep is observed to be substantially different from subsequent sweeps, with an intercalation peak observed in the region of 1.5 V as compared to the 1.2 V characteristic of the pure  $\text{Mo}_6\text{Se}_8$ , and a second pronounced intercalation peak in the region of 0.8 V which is not present in the pure phase. Similarly, there appears to be a wave in the region of 1.2 V as well, similar to that in magnitude of subsequent sweeps. The first sweep de-intercalation behavior was also different, with the lowest peak at around 1.4 V and a larger peak occurring above 1.7 V. The behavior was not reproduced on subsequent scans, and the large deintercalation peak in the region of 1.7 to 2.0 V continued to shrink in magnitude with time.

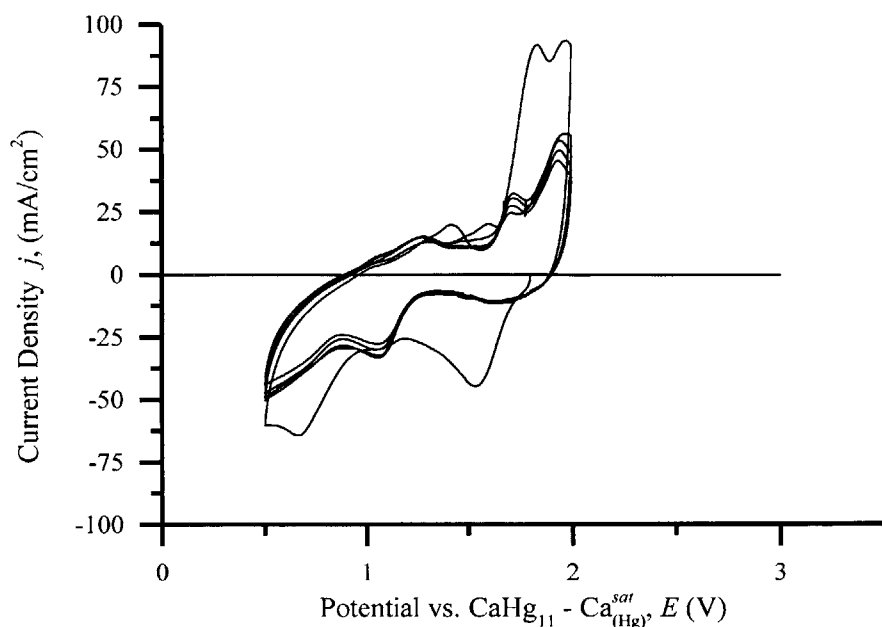


Figure 43. **Cyclic voltammogram of  $\text{Cu}_x\text{Mo}_6\text{Se}_8$ .** Additional waves observed in the copper-containing material can be seen, however beyond the first sweep the signal associated with these waves gradually vanishes, a result of the electrochemical removal of copper from the system.

Galvanic cycling of the copper-containing material showed no appreciable improvement over its pure counterpart beyond the first cycle. Copper de-intercalation occurred at a lower potential than calcium deintercalation from the structure, and was not recoverable. The cycling behavior was poor. Post mortem SEM-EDS showed comparable calcium content to previous microscale samples. Attempts to cycle the material below 1.6 V to prevent copper removal showed no appreciable capacity benefit as well. As such, the presence of copper within the structure did not yield significantly different results beyond the first cycle, and any transport benefit due to the presence of copper is lost once it is de-intercalated from the structure.

Thus far calcium has been shown to be electrochemically inactive in the  $\text{Mo}_6\text{S}_8$  Chevrel phase, and to exhibit kinetically inhibited performance in the  $\text{Mo}_6\text{Se}_8$  Chevrel phase. Given the improvement in performance with increasing calcogen atom size, and the fact that the telluride derivative Chevrel phase structure has been reported in the literature, one would assume the  $\text{Mo}_6\text{Te}_8$  phase would show improved

electrochemical performance. Unfortunately, due to the band structure of  $\text{Mo}_6\text{Te}_8$ , previous authors have shown that electrochemical intercalation into the  $\text{Mo}_6\text{Te}_8$  phase is impossible.<sup>64</sup> However, work in the magnesium literature has demonstrated that mixed calcogen Chevrel phase structures, such as  $\text{Mo}_6\text{S}_7\text{Se}_1$  are of benefit to cation mobility within the structure.<sup>76</sup> The benefit is likely due to the increasing polarizability of the larger calcogen atoms as well as some asymmetry introduced to the intercalant ion cavity by the presence of different sized neighboring atoms. A mixed calcogen Chevrel phase,  $\text{Mo}_6\text{S}_{0.5}\text{Se}_{6.5}\text{Te}_1$  was explored with the hope that the presence of some tellurium would benefit the calcium insertion process. As a large atom, tellurium should help to increase the size of internal cavities within the material, as well as be more polarizable and as such allow for easier transport of calcium between sites. Furthermore, a small amount of sulfur was added to the structure as well under the assumption that the structure could be distorted somewhat asymmetrically to create sites where calcium could sit off-center within the intercalation cavity, which should serve to improve its mobility.

$\text{Cu}_2\text{Mo}_6\text{S}_{0.5}\text{Se}_{6.5}\text{Te}_1$  was synthesized via a high temperature solid-state route from elemental precursors, and then chemically leached to produce  $\text{Mo}_6\text{S}_{0.5}\text{Se}_{6.5}\text{Te}_1$ , in the exact same furnace alongside  $\text{Mo}_6\text{Se}_8$  samples. The thermal treatment profile and leaching conditions were identical. The particle size distribution was found to be similar to that of the  $\text{Mo}_6\text{Se}_8$  samples, with an average particle diameter of  $2.5 \pm 1.5$  microns. Sample morphology of the  $\text{Mo}_6\text{S}_{0.5}\text{Se}_{6.5}\text{Te}_1$  phase was somewhat unique in that the as-synthesized crystallites exhibited more pronounced faceting than the selenide and sulfide Chevrel structures, as can be seen in figure 44. SEM/EDX was used to check the composition of over a dozen particles, which were found to all have similar composition of the expected stoichiometry. The mixed-composition Chevrel structure exhibited a similar morphology to its sulfide and selenide cousins upon further processing (acid leaching, grinding, electrode preparation, etc...) The theoretical capacity of the  $\text{Mo}_6\text{S}_{0.5}\text{Se}_{6.5}\text{Te}_1$  phase is 87 mAh/g, which is similar to the theoretical capacity of 88.8 mAh/g for the  $\text{Mo}_6\text{Se}_8$  phase.

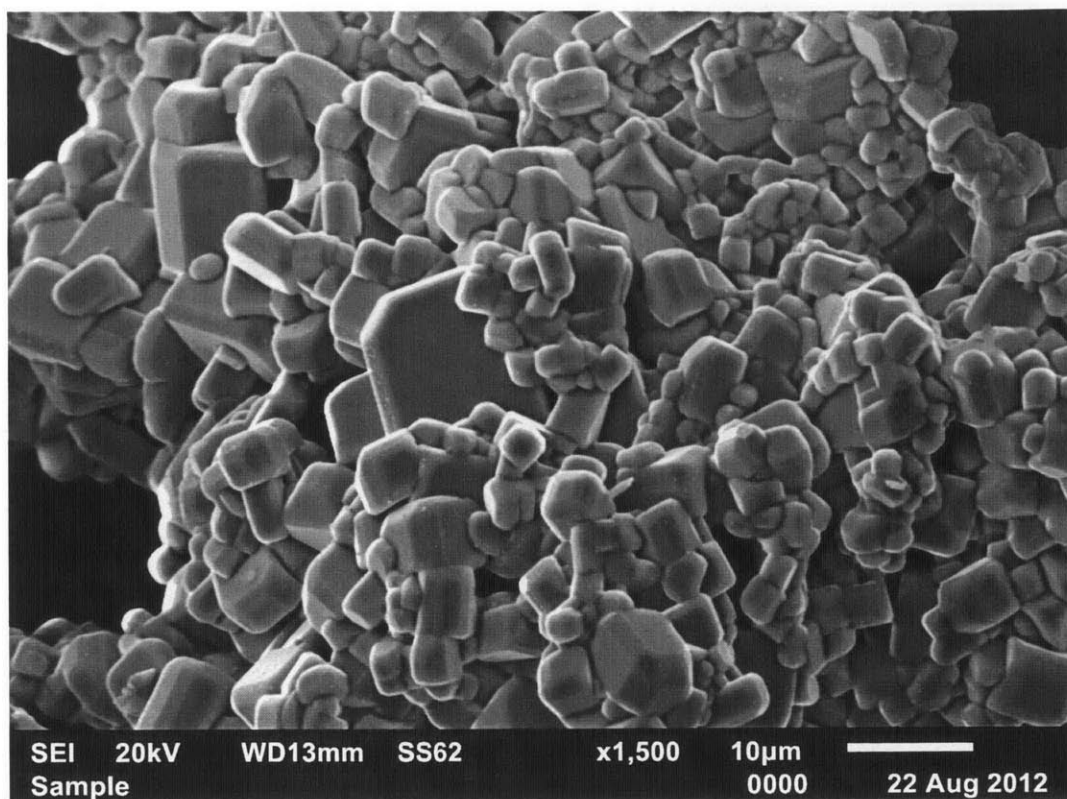


Figure 44. SEM image of as-synthesized  $\text{Cu}_2\text{Mo}_6\text{S}_{0.5}\text{Se}_{6.5}\text{Te}_1$ . Faceted mixed-chevrel phase crystallites are observed over a wide particle size distribution range.

Cyclic voltammetry was performed on the  $\text{Mo}_6\text{S}_{0.5}\text{Se}_{6.5}\text{Te}_1$  material, which was observed to be electrochemically active in a similar potential region to the pure selenide phase. Galvanic cycling tests were performed to quantify the performance of the new material. The first and third cycles of a typical  $\text{Mo}_6\text{S}_{0.5}\text{Se}_{6.5}\text{Te}_1$  sample and a typical  $\text{Mo}_6\text{Se}_8$  sample are shown in figure 45. Both samples consisted of a similar micro-scale particle size distribution, however the mixed Chevrel phase electrode exhibited more than double the capacity of its pure counterpart. On the discharge profile, the mixed phase exhibited greater “plateauing” in the region of 1.2 V, in addition to having an overall gentler discharge slope than observed in  $\text{Mo}_6\text{Se}_8$  at the C/10 rate. The plateau feature on charge is much more pronounced in the  $\text{Mo}_6\text{S}_{0.5}\text{Se}_{6.5}\text{Te}_1$  sample as well. The differences between the electrochemical behavior of the  $\text{Mo}_6\text{S}_{0.5}\text{Se}_{6.5}\text{Te}_1$  phase and the  $\text{Mo}_6\text{Se}_8$  phase are consistent with the hypothesis that the telluride-containing mixed calcogen Chevrel phase allows for greater calcium mobility within the structure, resulting in improved electrode performance. Most importantly the improvement in performance is

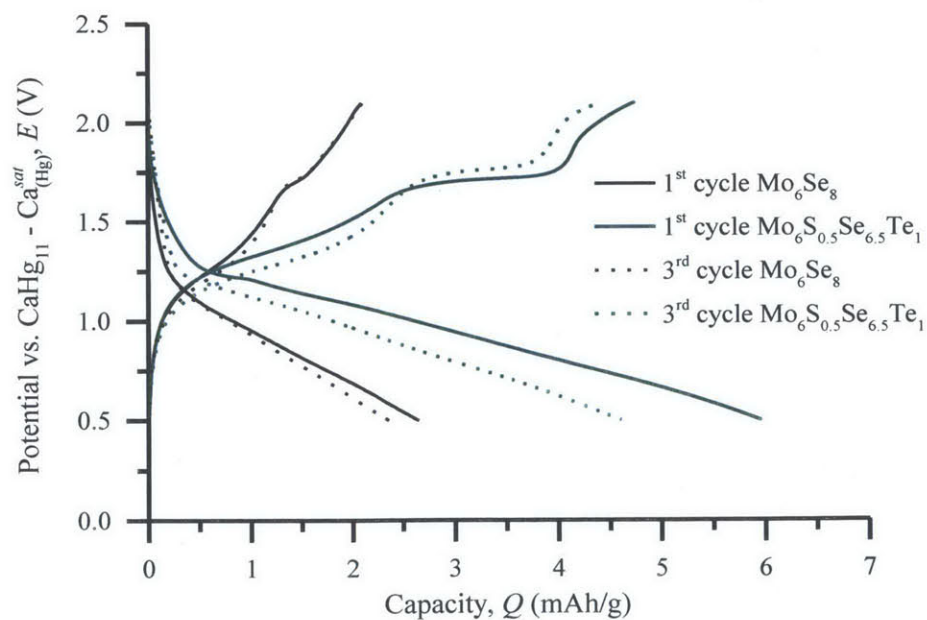
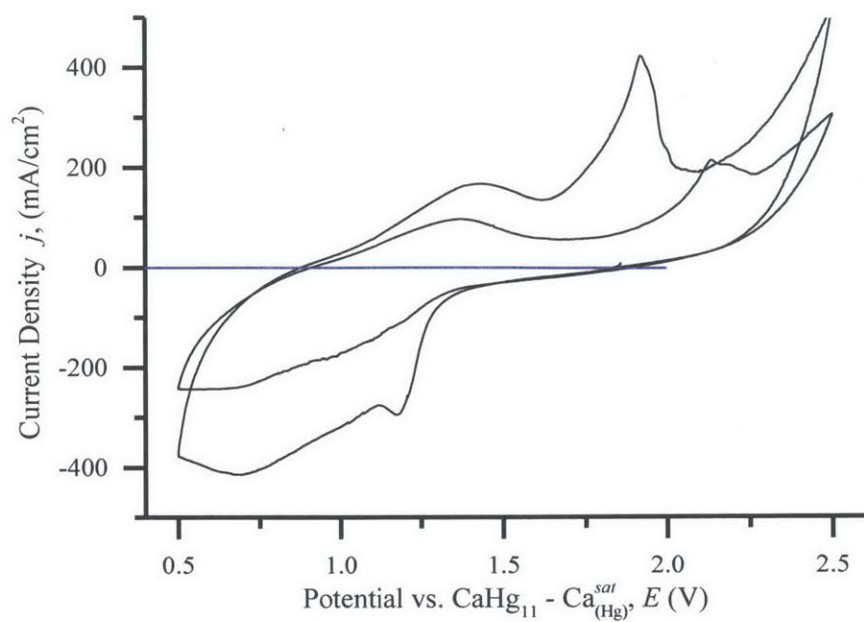


Figure 45. **Electrochemical behavior of  $\text{Mo}_6\text{S}_{0.5}\text{Se}_{6.5}\text{Te}_1$ .** Cyclic voltammogram (top) and galvanic cycling behavior (bottom) shown for  $\text{Mo}_6\text{S}_{0.5}\text{Se}_{6.5}\text{Te}_1$  in calcium electrolyte. All data collected at room temperature.

observed in a case where the particle size distribution (and hence surface area) is the same between the two samples, suggesting that bulk calcium transport is indeed the kinetically limiting factor of interest, rather than some surface mediated or other non-transport kinetically limited process which would show improvements in the cases of rate reduction, particle size reduction, and temperature increase.

## 5.4 Chapter Summary

This chapter has spanned a wide range of electrochemical behaviors associated with calcium. The journey began with the validation of the  $\text{CaHg}_{11}\text{-Ca}_{(\text{Hg})}^{\text{sat}}$  electrode and calcium perchlorate in acetonitrile via study of the behavior of  $\text{V}_2\text{O}_5$ , a known calcium intercalation compound. It continued with a broad survey of potential calcium electroactive materials candidates identified from the literature. From this survey, the  $\text{Mo}_6\text{Se}_8$  Chevrel phase material was identified as a promising candidate for further study as a calcium intercalation material. Limited electrochemical capacity was observed in the  $\text{Mo}_6\text{Se}_8$  material, owing to kinetic limitations of calcium mobility. Several techniques were employed to test the kinetically limited capacity hypothesis; (1) increase in cell operating temperature, (2) decrease in cycling rate, (3) decrease in particle size, and (4) permutation in electrode chemistry to improve calcium ion mobility. Capacity improvements from the baseline 3 percent reversible capacity for microscale  $\text{Mo}_6\text{Se}_8$  (room temperature, C/10 rate) were observed in all of these cases, however the maximum capacity obtained in the study was still less than 15 percent the theoretical capacity of the Chevrel phase material assuming a terminal stoichiometry of  $\text{Ca}_2\text{Mo}_6\text{Se}_8$ , or less than 25 percent assuming a terminal stoichiometry of  $\text{Ca}_1\text{Mo}_6\text{Se}_8$ , representing an improvement of 400 percent in electrode performance from the baseline. The combination of these factors suggests that the electrode capacity is indeed transport limited, and possibly also sterically limited by calcium's large ionic size.

# **Chapter 6:**

## **Materials Characterization in Support of Calcium Intercalation**

The preceding chapter explored the electrochemistry of the  $\text{Mo}_6\text{Se}_8$  Chevrel phase in a calcium-containing electrolyte solution. Presumably, the electrochemical signals measured were the result of a faradaic process involving the interaction of calcium from the electrolyte with the  $\text{Mo}_6\text{Se}_8$  material. Electrochemical measurements themselves however, directly measure electrons, and not chemical species. The presumption of a faradaic process involving calcium, namely that of calcium intercalation, requires the support of non-electrochemical materials characterization techniques – support which will be provided in this chapter in the form of chemical and structural analysis through SEM, EDS, TEM, and XPS (Chapter 3 provides brief technique descriptions).

### **6.1 SEM/EDS analysis of $\text{Mo}_6\text{Se}_8$**

Post-mortem SEM analysis of  $\text{Mo}_6\text{Se}_8$  electrodes was carried out to investigate the post-intercalation morphology of powders as well as search for the presence of calcium in the samples. EDS spectra obtained exhibited distinct calcium peaks, while control spectra obtained on as-synthesized samples exhibited none. A typical EDS spectra is shown below in figure 46. The quantification of dozens of such spectra revealed an average calcium content of 2.7 +/- 0.5 atomic percent. Given the low accuracy of SEM-EDS, this observation is consistent with the electrochemical history of samples, which



corresponded to approximately  $1/6^{\text{th}}$  of theoretical capacity of the electrodes and a discharged stoichiometry of approximately  $\text{Ca}_{0.33}\text{Mo}_6\text{Se}_8$ , from which an expected calcium content of  $\sim 2.3$  atomic percent would be predicted.

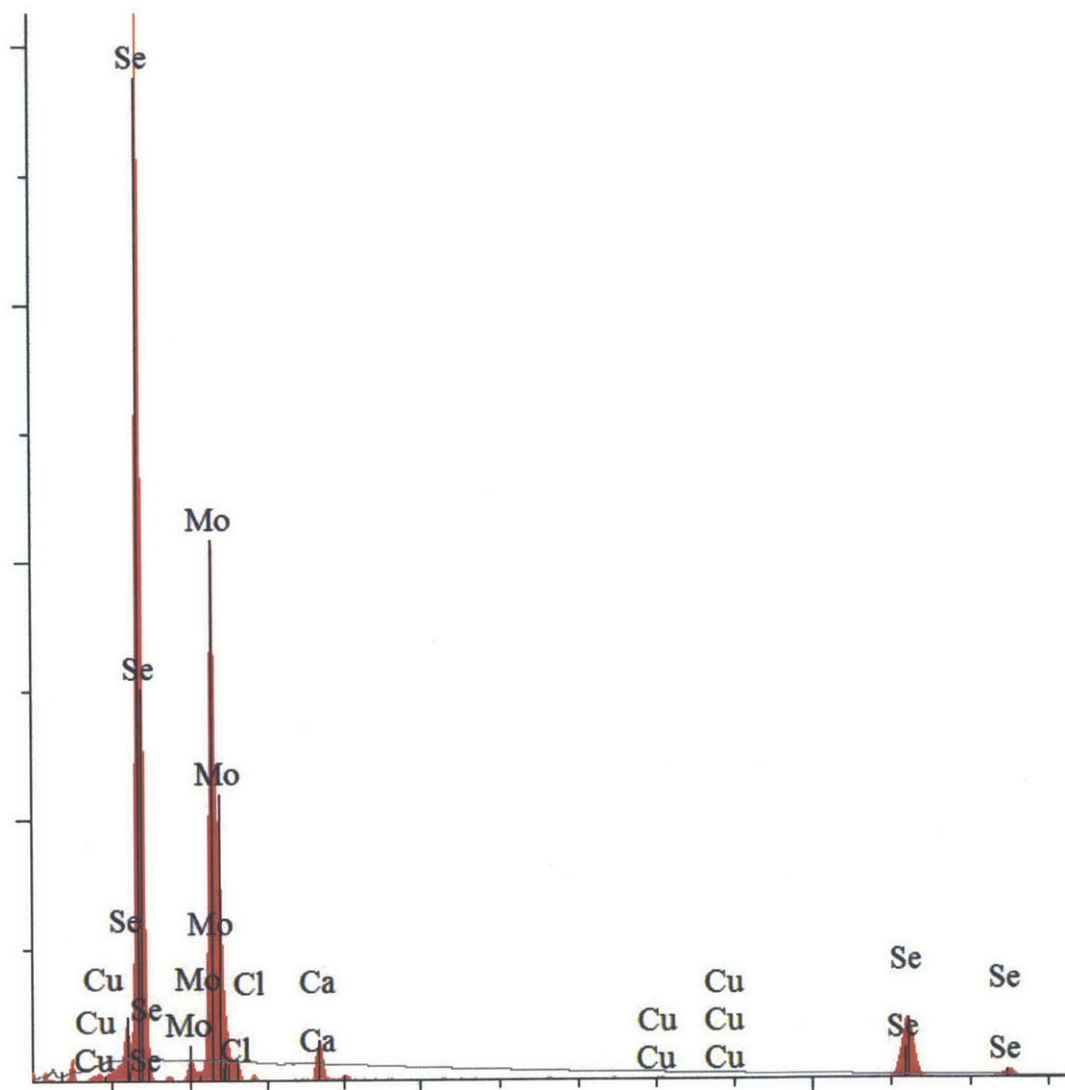


Figure 46. Typical SEM-EDS spectra obtained for  $\text{Ca}_x\text{Mo}_6\text{Se}_8$ . Calcium content is clearly observed. Copper has been essentially removed from the sample, and although chlorine is slightly convoluted with the molybdenum peak little chloride is present.

Although samples were rinsed in clean acetonitrile prior to post-mortem SEM analysis, the calcium to chlorine ratio was examined to ensure that the calcium signal was not due to physisorbed calcium perchlorate salts. In all cases, chlorine content was found to be less than that of calcium content, whereas

an adsorbed salt are expected to exhibit approximately twice as much chlorine as calcium. Although the chlorine peak lies within the shoulder of the molybdenum peak, rendering exact quantification of the chlorine signal difficult, un-rinsed control samples confirmed that calcium perchlorate adsorption onto the sample surface resulted in a larger chlorine signal than was obtained from the rinsed samples. The observed calcium content was somewhat higher than the  $\text{Ca}_{0.33}\text{Mo}_6\text{Se}_8$  composition that would be expected from the electrochemical signal, however the increased calcium presence is likely due to reaction of calcium with moisture or oxygen in the atmosphere, resulting in the formation of a surface calcium oxide layer, a fact supported by the enriched oxygen content of the experimental samples. Regardless, post-mortem chemical analysis confirms that calcium plays a role in the electrochemical signal observed, and is consistent with calcium intercalation, to within the error of the experimental technique.

Sample morphology of the post-mortem samples was found to be similar to that of the pre-electrochemistry samples, as evidenced by the comparison of a representative SEM micrograph shown in figure 47 below to the pre-intercalation SEM image presented previously in figure 39. No areas of salt chunks or contamination, and no new particle morphologies or byproducts were observed, either in physical appearance or by chemical analysis. Preliminary SEM-EDS results support the chemical presence of calcium as the electroactive species and rule out other contaminants as well. The lack of a distinct morphology change or distinct regions of new chemistry is supportive of an intercalation mechanism, although the SEM EDS spot size is quite large to state this conclusively, and TEM-EDS is undertaken to strengthen this observation in section 6.3

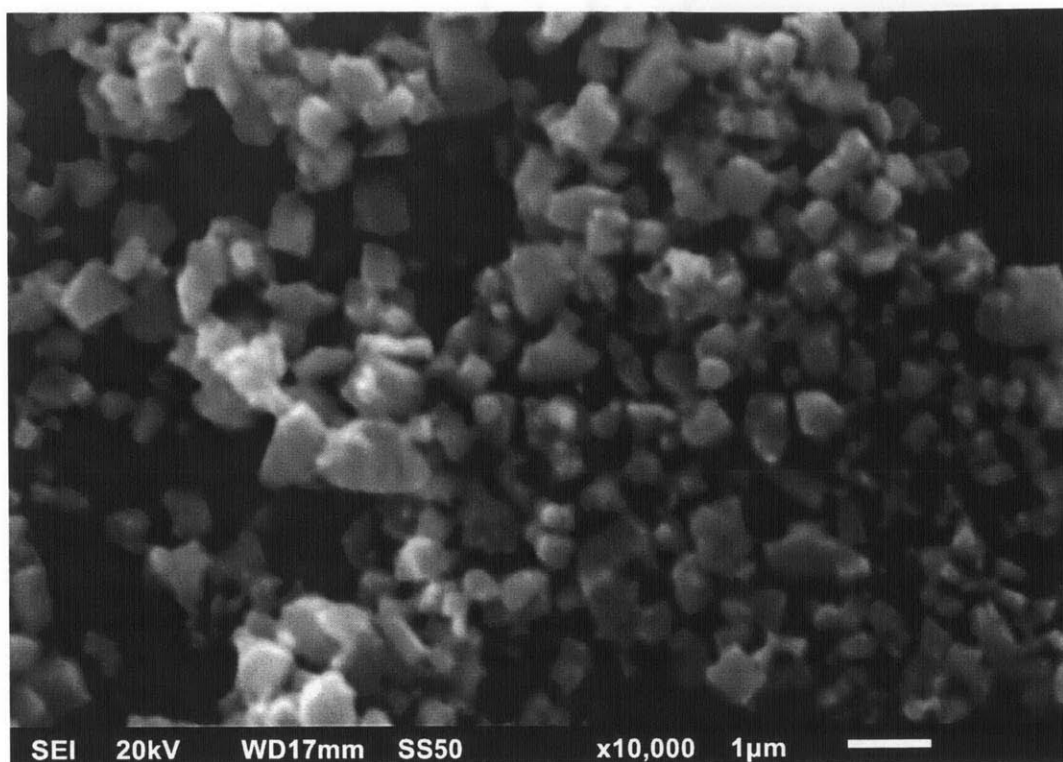


Figure 47. Typical post-mortem SEM image of  $\text{Ca}_x\text{Mo}_6\text{Se}_8$  powders. Electroactive powders broken off of the mesh electrode by mechanical agitation were dry mounted for SEM observation. Sample morphology, particle size, and homogeneity are similar to pre-electrochemical control samples.

## 6.2 XRD Analysis of $\text{Ca}_x\text{Mo}_6\text{Se}_8$

Intercalation materials, particularly Chevrel phase class compounds often show a pronounced structural change upon intercalation, owing to occupancy of previously unoccupied sites within the crystal structure. Chevrel phase compounds, in the case of large divalent ions, are observed to undergo a phase change associated with a distortion of lattice parameters and an increase of unit cell volume.<sup>50</sup> Although the electrochemical signal suggests only the partial calciation of  $\text{Mo}_6\text{Se}_8$  to a maximal extent of  $\text{Ca}_{0.30}\text{Mo}_6\text{Se}_8$ , one would still expect to observe some structural change associated with calcium insertion into the structure. Unfortunately, the potential of the electrode insertion reaction is so low, and the reactivity of calcium with oxygen and moisture so high, that reactivity with the atmosphere is of great concern as chemical oxidation of the electrode has the potential to remove calcium from the structure and form a surface layer, necessitating the use of air sensitive sample preparation techniques. Two such

techniques were applied in this thesis, a beryllium-windowed o-ring sealed sample holder and a glass capillary sample holder, both described in greater detail in Chapter 3.

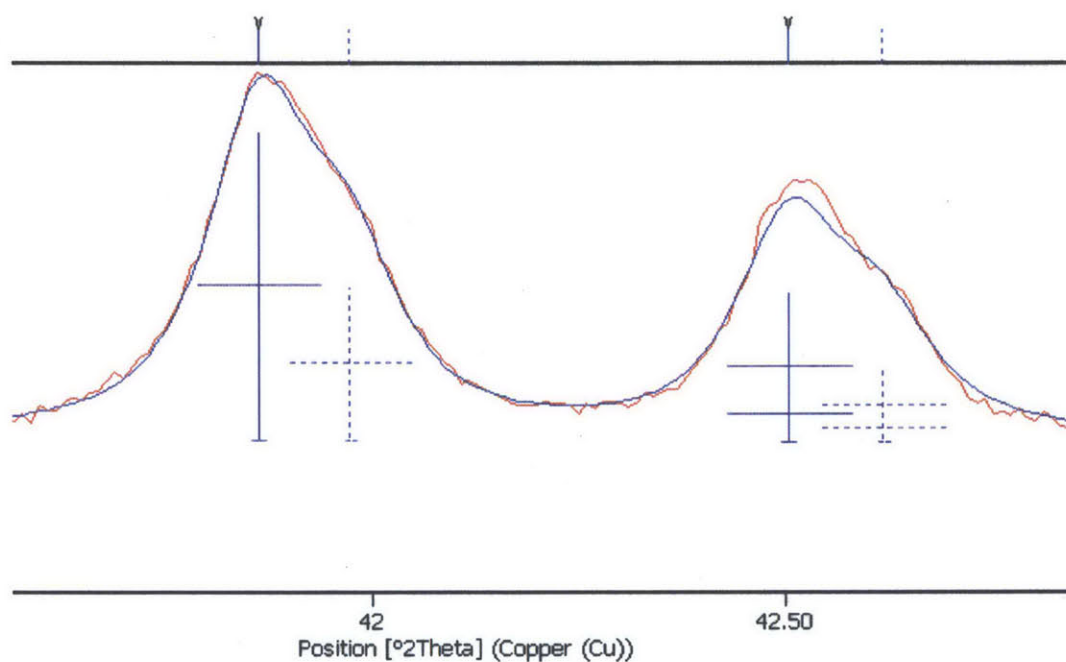
Capillary measurements were believed to provide the best sample seal, and thusly the best resistance to sample degradation due to oxygen and moisture contamination, and were used for data collected for phase analysis. Preliminary analysis of obtained XRD data for  $\text{Ca}_x\text{Mo}_6\text{Se}_8$  nominally matched phase-pure  $\text{Mo}_6\text{Se}_8$  indexed spectra based on simple background determination and peak search and match methods. No impurity or additional phase peaks were observed in the sample. Rietveld refinement was performed to search for subtle differences in the lattice parameters and peak structures between the electrochemically calciated and star indexed reference pattern for phase-pure  $\text{Mo}_6\text{Se}_8$ . Full discussion of the Rietveld refinement as well as tables of the refined parameters as well as agreement indices can be found in Appendix D. In brief summary, refinement of the  $\text{Ca}_x\text{Mo}_6\text{Se}_8$  yielded minor lattice distortions as compared to the indexed sample. The refined  $a$  and  $c$  lattice parameters were found to be 9.5579 Å and 11.1539 Å while the reference pattern parameters were 9.5448 Å and 11.2095 Å, representing a difference of +0.14% and -0.50% respectively. A partially occupied calcium site was found at coordinates  $x = 0.55$ ,  $y = 0.52$ ,  $z = 0.33$  with an occupancy fraction of 0.06. Numerous perturbations on the calcium site parameters were performed, with each refinement converging to the above stated values.

Although promising, the above-stated comparison would be incomplete without appropriate XRD and Rietveld analysis of in-house synthesis  $\text{Mo}_6\text{Se}_8$  to provide a more robust control spectrum. Such analysis yielded lattice parameter values that also differed from the indexed  $\text{Mo}_6\text{Se}_8$  reference pattern which were very close to the measured  $\text{Ca}_x\text{Mo}_6\text{Se}_8$  parameters (deviation of less than 0.005% was observed). The difference between the in-house control and reference patterns can be accounted for by differences in synthesis technique as the reference pattern is for a true phase pure sample synthesized at 1400°C from elemental precursors, while in-house samples were synthesized with a ternary copper component and then acid leached to remove copper. The differences in lattice parameters can either be attributed to small variation in lattice distortions due to the presence and transport of copper during the

Mo<sub>6</sub>Se<sub>8</sub> synthesis process. Alternatively, they could be explained by small residual amounts in the as-leached control sample. SEM EDS analysis supports a very small fraction of residual copper, so either theory is plausible. Thus, the more rigorously correct comparison between the Rietveld analyses of the Ca<sub>x</sub>Mo<sub>6</sub>Se<sub>8</sub> and in-house Mo<sub>6</sub>Se<sub>8</sub> samples shows little variation in lattice parameter. Possible explanations for this include that little lattice distortion occurs for small degrees of calcination within the structure. This is plausible by comparison, as the insertion of a full sodium ion into Mo<sub>6</sub>Se<sub>8</sub> results in minimal changes in the a lattice parameter, and insertion of a full cadmium ion into Mo<sub>6</sub>Se<sub>8</sub> results in minimal changes in the c lattice parameter.<sup>50</sup> Another potential explanation for the similarity of the Ca<sub>x</sub>Mo<sub>6</sub>Se<sub>8</sub> and Mo<sub>6</sub>Se<sub>8</sub> patterns involves sample contamination and degradation of the former due to exposure to oxygen or moisture, even though utmost care was taken during sample preparation and data collection. A final possible reason for the similarity in lattice parameters between the experimental and control samples can be attributed to the formation of a small surface layer of new calcium rich material. Depending on sample dimensions, such a core-shell structure could potentially not provide as strong a diffraction signal of the core phase as would a two-phase mixture of phase pure particles, as powder XRD is a bulk technique involving x-ray penetration within samples to provide for diffraction of interior lattice planes.

Although appreciable differences in lattice parameter were not observed in the Ca<sub>x</sub>Mo<sub>6</sub>Se<sub>8</sub> and Mo<sub>6</sub>Se<sub>8</sub> samples, peak intensities and ratios of peak intensities were observed to differ between the samples. Perturbation analysis of the Rietveld model for Ca<sub>x</sub>Mo<sub>6</sub>Se<sub>8</sub> was used to demonstrate that these intensities could be accounted for by variation of the calcium occupancy within the structure, an example of which is illustrated in figure 48 below. The experimentally observed Ca<sub>x</sub>Mo<sub>6</sub>Se<sub>8</sub> peak at 42.5 degrees displays somewhat higher intensity than predicted by Rietveld refinement of the pure Mo<sub>6</sub>Se<sub>8</sub> phase (Ca occupancy = 0), even though the peak at 42 degrees matches quite well. Increasing the calcium occupancy fraction (Ca occupancy = 0.3) results in a shift in the relative magnitudes of the peaks: the refined 42 degree peak shrinks intensity while the 42.5 degree peak grows. Allowing the calcium occupancy to vary as a refinement parameter offered the best fit of the peaks at Ca occupancy = 0.06.

Chevrel phase compounds have numerous peaks with intensities that correlate to intercalant ion occupancy, particularly in the fractional intercalation regimes. For example, as magnesium is deintercalated from the  $\text{MgMo}_6\text{S}_8$  compound, several peaks are observed to shrink in intensity as others grow.<sup>60</sup> The observed variation in peak intensities in spectra obtained for  $\text{Ca}_x\text{Mo}_6\text{Se}_8$  are consistent with some degree of electrode calcination.



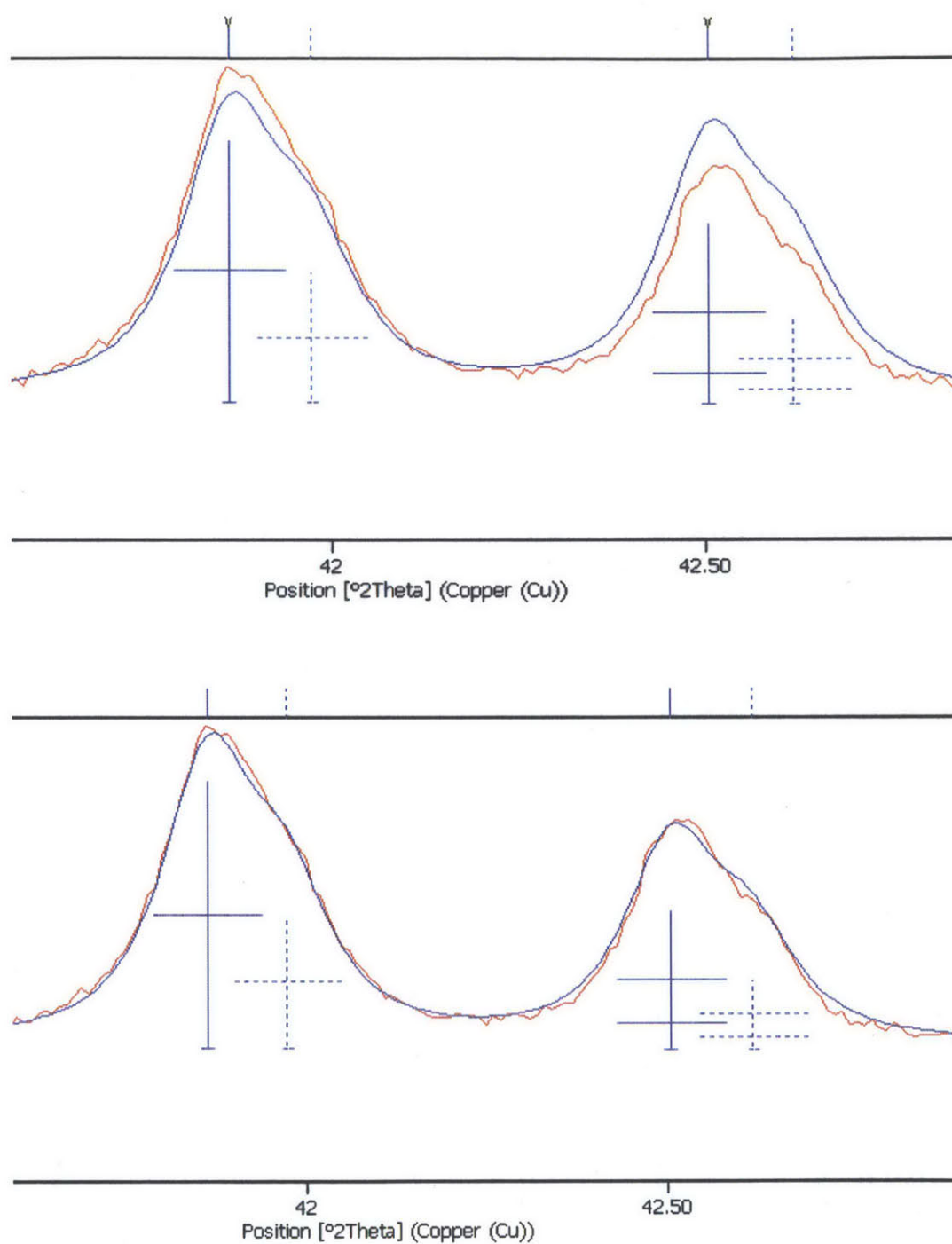


Figure 48. **Intensity comparison of experimental and Rietveld XRD spectra.** Rietveld parameters were fixed while calcium occupancy was varied from 0 (top) to 0.3 (middle). The best fit is obtained at the refinement convergence value of 0.06 (bottom).

Further examples are presented in Appendix D. Consistently, best visual agreement between measured and calculated peak intensities occurs at occupancy = 0.06, the refined value.

Partial electrode amorphization presents another possibility for the observed electrochemical signal, and absence of appreciable crystallographic lattice parameter change. One would expect bulk amorphization of particles to be accompanied by a broad amorphous hump, which would be difficult to detect in capillary measurements as the glass vessel adds its own amorphous scatters. Beryllium windowed chamber measurements on zero background sample holders were undertaken to test for sample amorphization and no distinctive background patterning associated with amorphization was observed. While in theory, it could be possible that a small surface layer of amorphized regions of particles with an appreciable amount of crystalline phases left at their core could result in a mostly crystalline signal, TEM results further contradict the likelihood of amorphization.

### **6.3 TEM Analysis of $\text{Ca}_x\text{Mo}_6\text{Se}_8$**

TEM analysis (utilizing a JOEL 2010F Transmission Electron Microscope) of post-mortem electrodes was used as a complementary particle-level technique to the bulk analysis XRD and SEM techniques. Unfortunately, available facilities did not include air-sensitive sample loading and transport vessels, such that meaningful single particle diffraction data could not be extracted for intercalated phases. Exposure to air would potentially degrade any calcium-rich phases through calcium depletion, reverting any structural change due to intercalation. However, compositional analysis at the particle scale was possible even with exposed samples, as was general structural analysis.

A representative close-up TEM micrograph is shown in figure 49 below, demonstrating the pronounced crystallinity of the post-mortem samples.

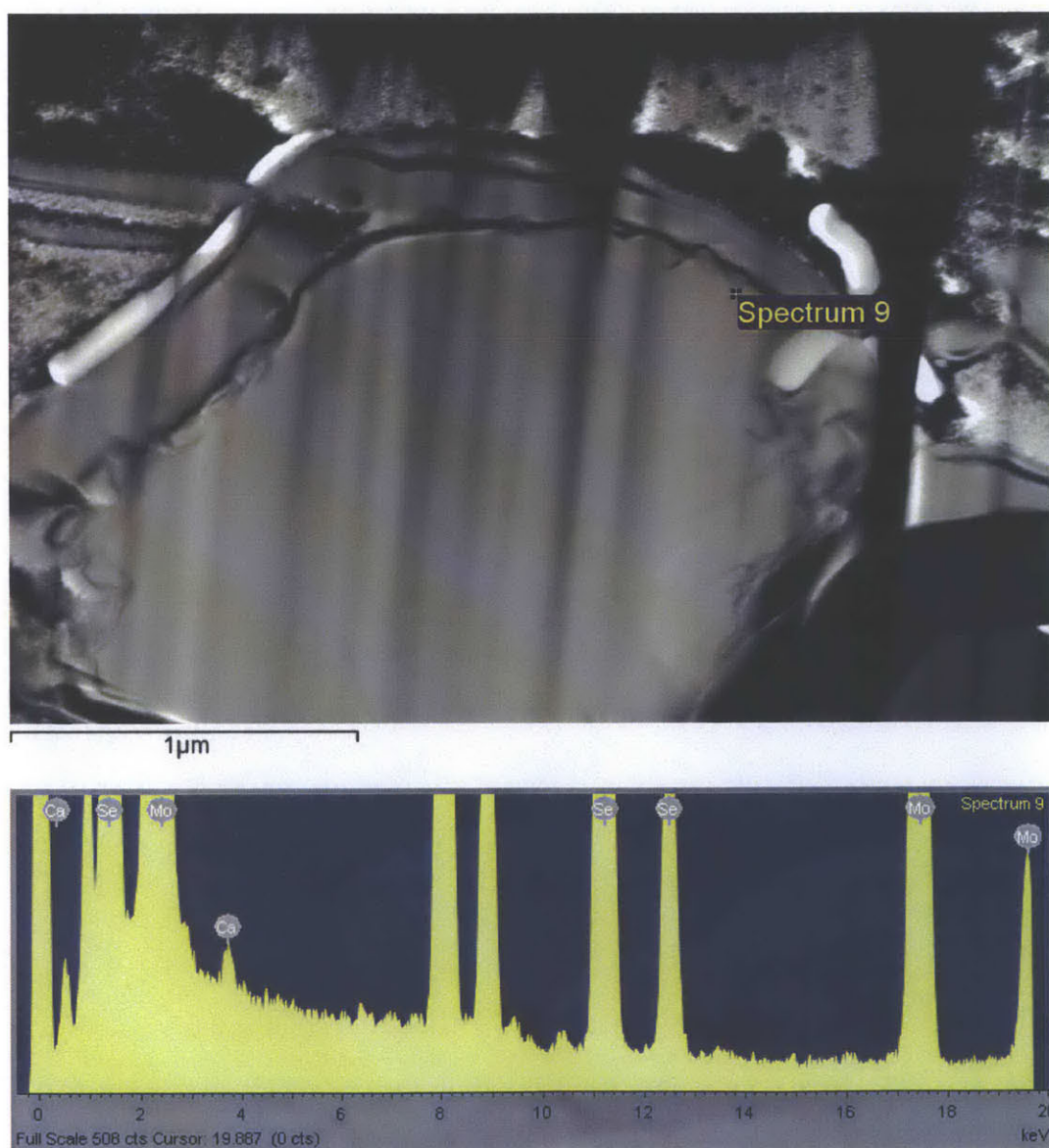




Figure 49. **Typical TEM image of  $\text{Ca}_x\text{Mo}_6\text{Se}_8$  particle.** Crystalline planes are visible throughout the sample, all the way to the edge of the particle, as well as across the particle interior.

With the exception of a couple of minor small regions near some particle surfaces (on the order of 5 nm or less across), individual particles were observed to be entirely crystalline. Interestingly, some particles were observed to be single crystalline in nature while others were observed to be polycrystalline, as can be seen by the Moiré fringes (lines indicative of overlapping grains at different orientations in a particle) observable in some images. Dozens of particles were imaged, and all distinctly lacked locally amorphized regions of the appropriate scale to account for the electrochemical signal observed to be the result of an amorphization process, when making reasonable assumptions for the charge transfers that would be involved in this system.

An EDX study was carried out in dark field scanning TEM (DF-STEM) mode on both microscale and nano-scale  $\text{Mo}_6\text{Se}_8$  post-mortem samples. Focused ion beam milling (FIB) was used to thin microscale powders until they were thin enough to be electron transparent. Examination of the microscale powders consistently showed that larger particles had lower fractional calcium content than smaller particles. Furthermore, the exterior of cross-sectioned larger particles displayed a higher calcium signal than their interior. Typical EDS spectra obtained are shown in 50 below, along with corresponding TEM micrographs of sectioned particles.



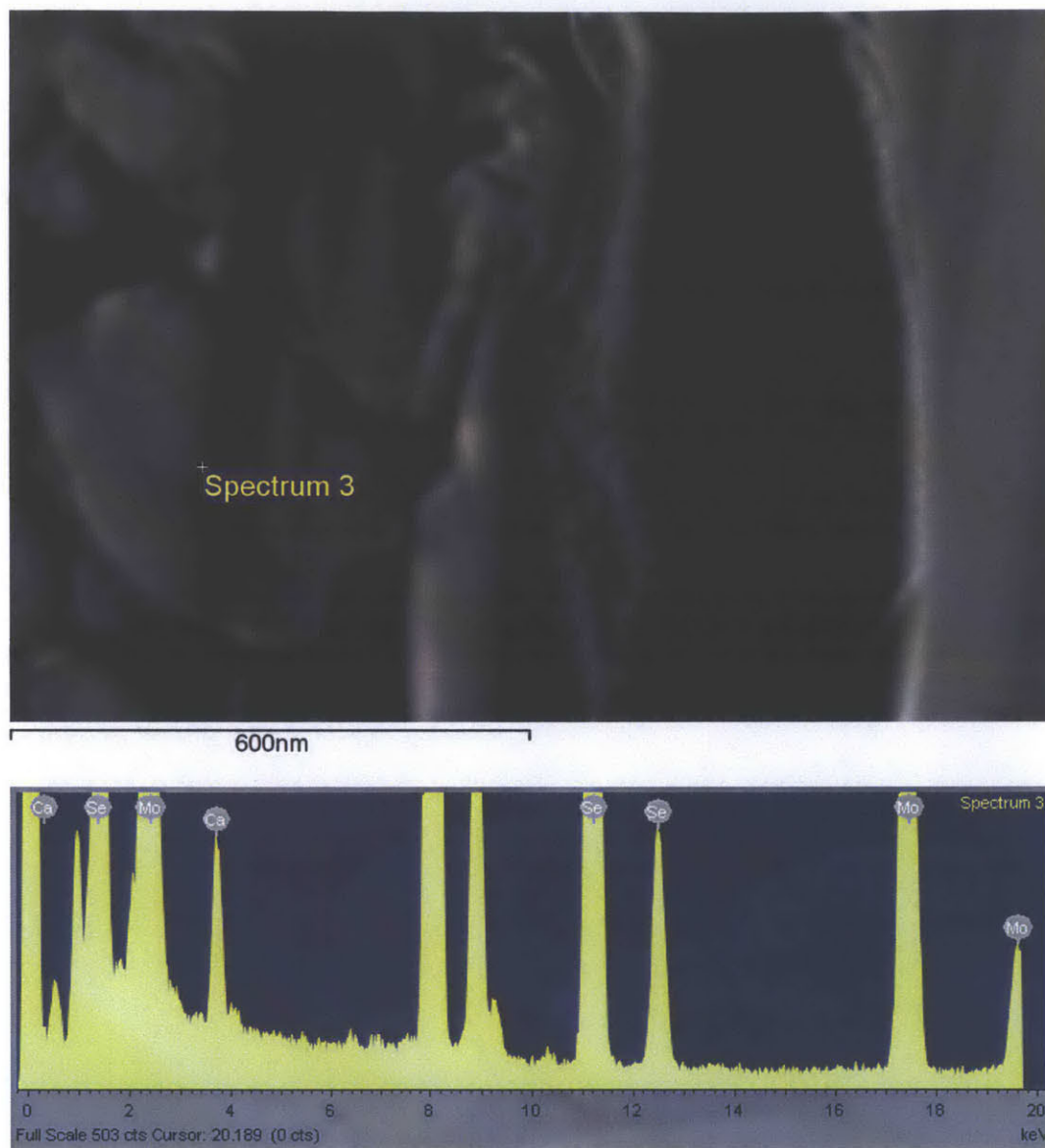


Figure 50. Typical TEM images of  $\text{Ca}_x\text{Mo}_6\text{Se}_8$  particle cross-sections and corresponding EDS spectra. Both a 2 micron and half micron grain are shown. EDS spectra locations are denoted on the TEM images. Higher calcium signal is observed in the smaller particle.

Much higher calcium signal was observed in smaller particles than in larger particles in “microscale” electrochemical samples, as classified in Chapter 5. A more in depth study was carried out with “nanoscale” particles to quantitatively characterize the calcium distribution. Nanoscale samples were



characterized without additional FIB preparation, as they were sufficiently small to be electron transparent. TEM images and EDS spectra were obtained for approximately two dozen particles, representative images of which are shown in figure 51 below.



Figure 51. **Typical dark-field TEM image of “nanoscale” particles.** Several un-sectioned particles are shown. A dozen such images were used for particle sizing studies.

The particle size distribution of nanoscale samples was found to have an average diameter of  $315 \pm 157$  nm, which is consistent with the value of  $343 \pm 133$  nm obtained through SEM analysis (see Appendix C for further discussion). EDS point scans were carried out to determine calcium content at the individual particle scale. All of the particles appeared similar under the microscope, and none of them had drastically different overall composition or calcium content from any other, suggesting that all particles underwent a similar electrochemical process involving some degree of calciation, rather than calciation of only a fraction of particles within the entire electrode.

EDS line scans were carried out across several particles to examine the distribution of calcium within the particles (a typical line scan is shown below in figure 52).

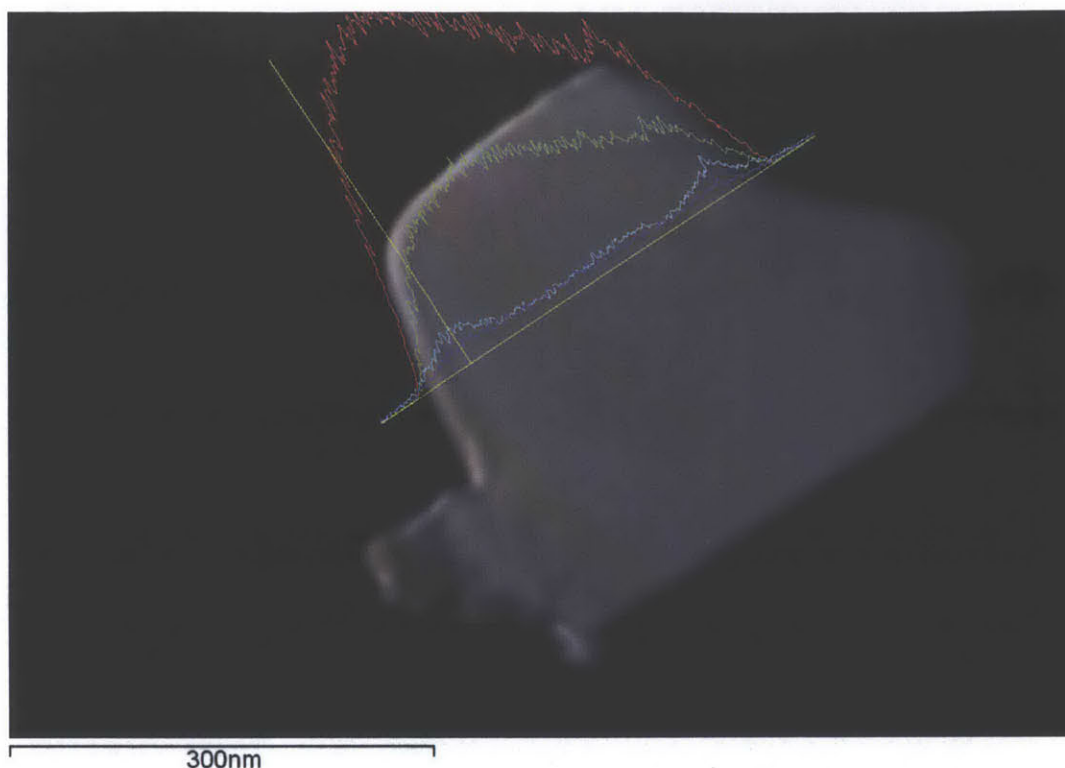


Figure 52. **Typical TEM-EDS line scan of  $\text{Ca}_x\text{Mo}_6\text{Se}_8$ .** Molybdenum (red), selenium (green), calcium (blue), and oxygen (purple) spectra are shown. Calcium concentration is observed to track with oxygen concentration.

Calcium signal was found to be greatest at the surface of the particles, and coupled strongly with an oxygen signal. This observation supports the conclusion that exposure of the calcinated  $\text{Mo}_6\text{Se}_8$  material to air results in extraction of calcium from the material and the formation of calcium oxide. A distinct calcium oxide phase could not be resolved on the surface of the particles to within the resolution of the TEM EDS measurement, and was always coupled with some molybdenum and selenium signal. Chlorine was not found on the particle surface, and supports earlier conclusions from the SEM EDS data that the presence of calcium is not simply due to an adsorption of calcium perchlorate salt from the electrolyte. EDS point scans were carried out on a dozen particles at both surface and interior locations. Fractional calcium content was determined utilizing molybdenum and selenium constituents. The average “interior” calcium concentration was found to be  $6.4 \pm 3$  atomic percent, while the “exterior” local calcium

concentration was observed to be 17 +/- 8.2 atomic percent. The exterior numbers are substantially larger, supporting the line scans in the assessment of local enrichment of calcium at the particle surface.

## 6.4 XPS Analysis of $\text{Ca}_x\text{Mo}_6\text{Se}_8$

SEM and TEM analytical methods showed strong support for calcium as the active electrochemical species in the behavior of  $\text{Mo}_6\text{Se}_8$  electrodes, however conclusive XRD evidence of a distinct calciated phase was not observed. The presence of calcium in intercalation cavities within the  $\text{Mo}_6\text{Se}_8$  structure should have an effect on the local binding energies of the host atoms given the valence shift on the molybdenum atoms and the interaction of the selenium with calcium as an additional nearest neighbor cation. XPS was used to search for these local binding energy shifts by comparing pre- and post-intercalation samples. Although a surface sensitive technique, the penetration depth of XPS (up to 10 nm) was enough to examine chemical signal from several unit cells deep.

Control and electrochemical samples were prepared on copper substrates in glovebox and loaded into an XPS air sensitive sample transport vessel. Samples were triply rinsed in clean acetonitrile to ensure minimal surface adsorption of electrolyte salts. Preliminary XPS spectra were collected on a Physical Electronics Versaprobe II X-ray Photoelectron Spectrometer, over a wide range of energies to determine which peaks would offer the best comparative signal. The  $\text{Ca}2p$ ,  $\text{O}1s$ ,  $\text{Se}3d$ , and  $\text{Mo}3d$  peaks were chosen for a more detailed study, as they were isolated and distinct from interference with other chemical peaks in the sample. Spot size was 50 microns in diameter, such that approximately 1,000 distinct particles were interrogated at any given time. The carbon  $1s$  peak, associated with environmental carbon, was used to adjust for peak shift due to charging. The remaining peaks of interest associated with calcium, molybdenum, selenium, and oxygen are shown in figured 53-56 below for both a control sample and three electrochemical sample regions.

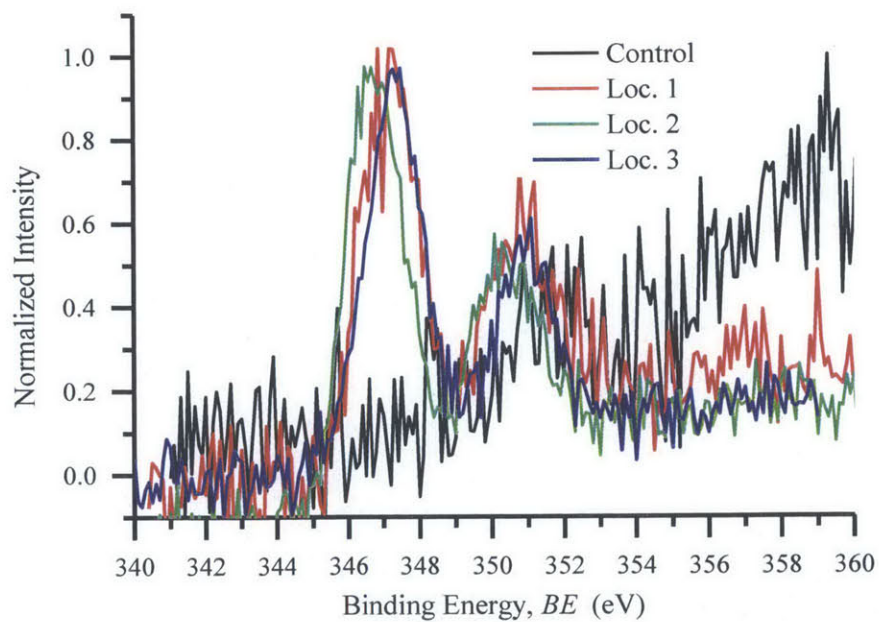
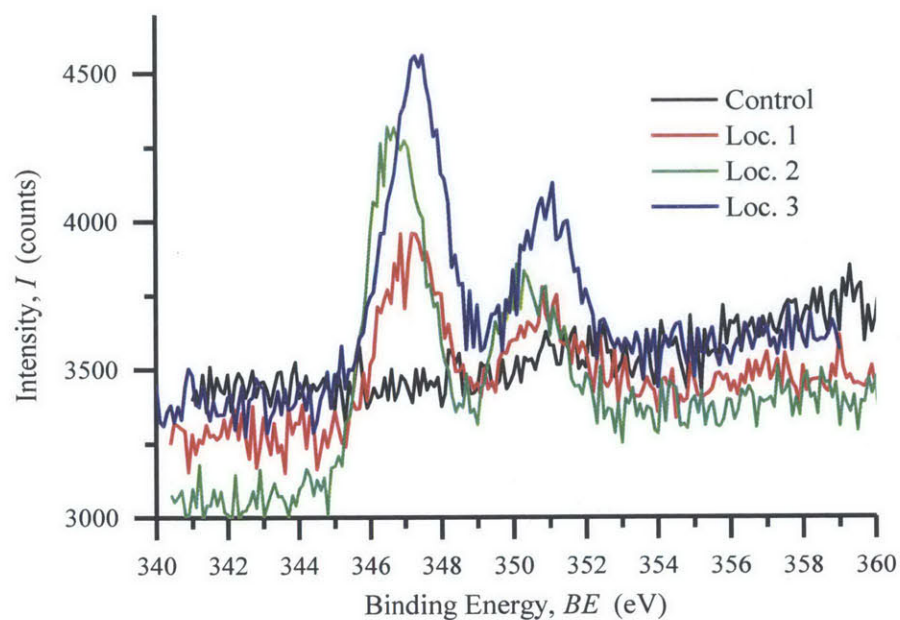


Figure 53. XPS spectra for Ca2p. As collected (top) and normalized (bottom) intensities are shown. Calcium is clearly present in the three  $\text{Ca}_x\text{Mo}_6\text{Se}_8$  samples, however none is present in the virgin  $\text{Mo}_6\text{Se}_8$ .

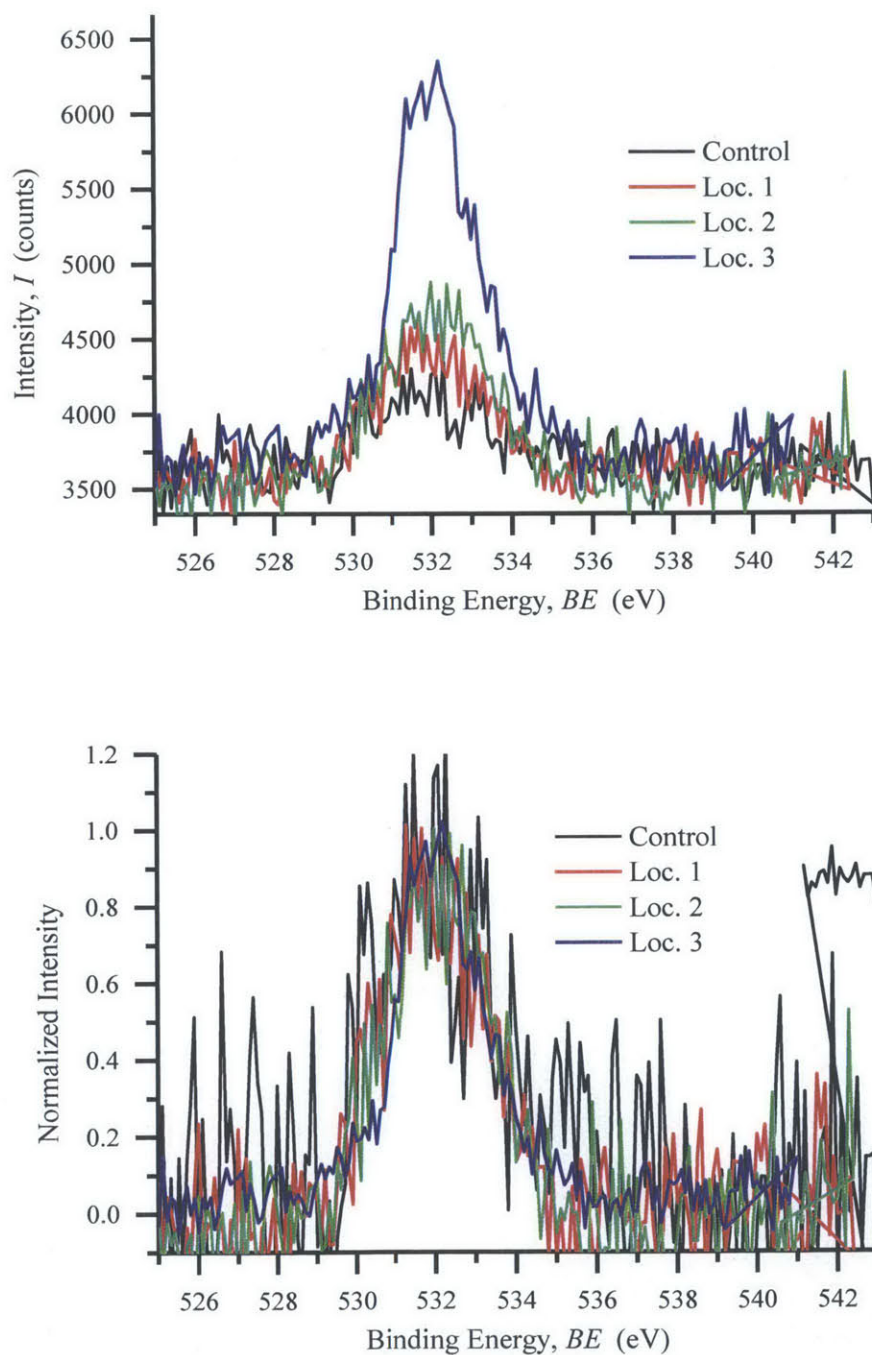


Figure 54. **XPS spectrum for O1s.** As collected (top) and normalized (bottom) intensities are shown. Surface oxygen is found in all samples. Good agreement is observed between oxygen binding energies amongst the samples.  $\text{Ca}_x\text{Mo}_6\text{Se}_8$  samples show higher oxygen content than virgin  $\text{Mo}_6\text{Se}_8$ .



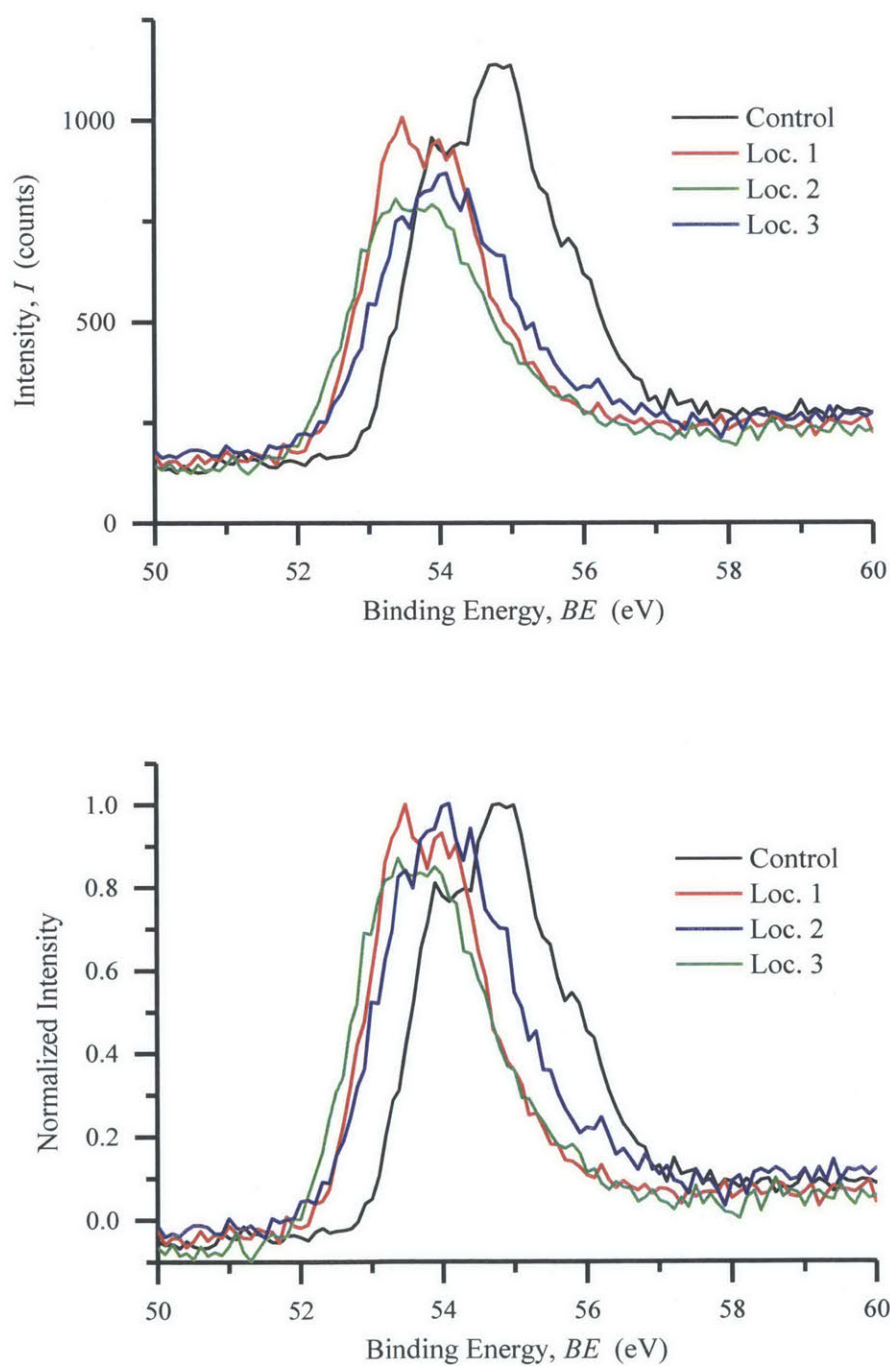


Figure 55. XPS spectrum for Se3d. As collected (top) and normalized (bottom) intensities are shown. Differences in binding energy and binding energy distribution can be seen for the  $\text{Ca}_x\text{Mo}_6\text{Se}_8$  samples as compared to  $\text{Mo}_6\text{Se}_8$ .

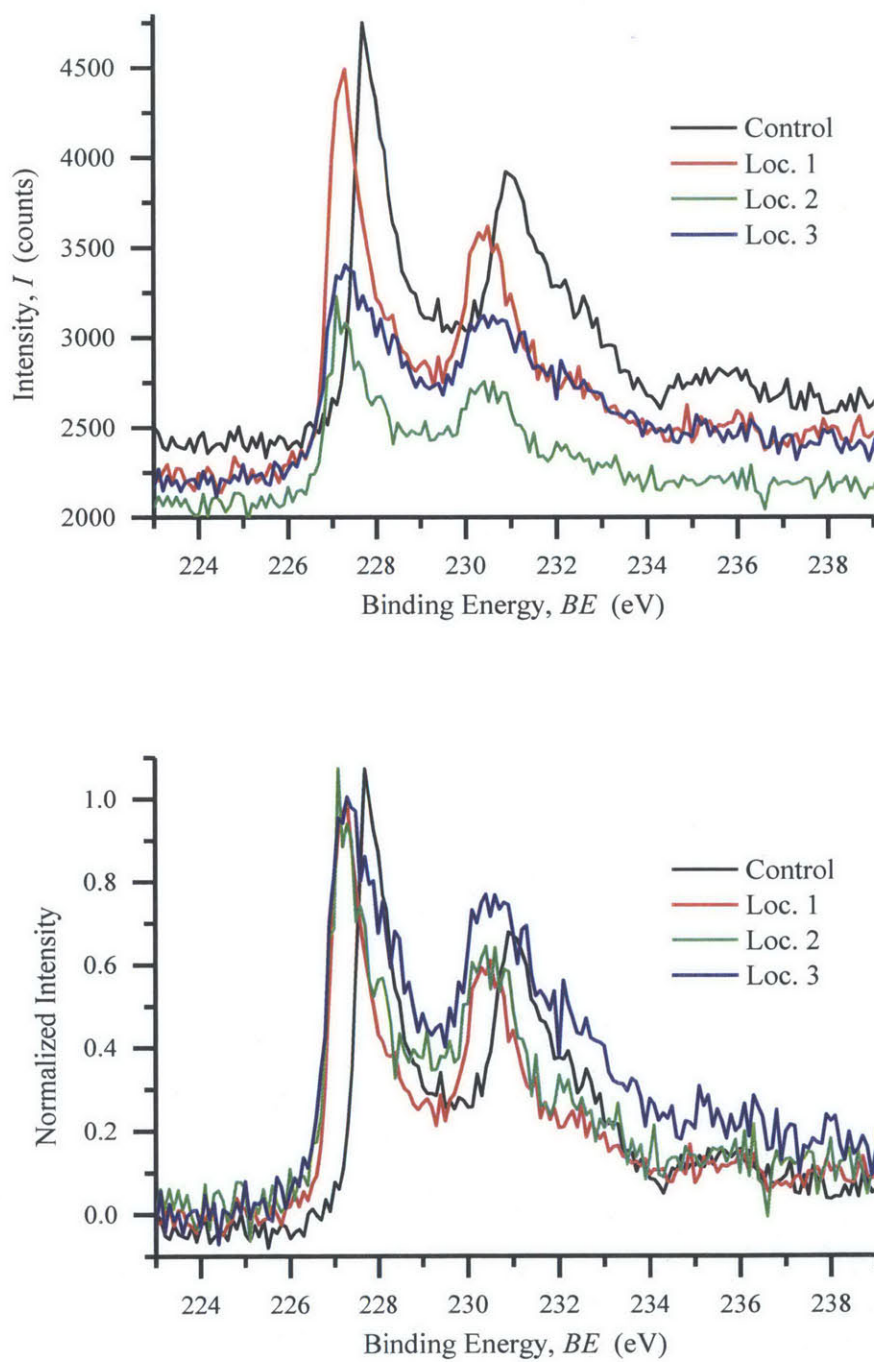


Figure 56. **XPS spectra for Mo3d.** As collected (top) and normalized (bottom) intensities are shown. Differences in binding energy and binding energy distribution can be seen for the  $\text{Ca}_x\text{Mo}_6\text{Se}_8$  samples as compared to  $\text{Mo}_6\text{Se}_8$ .

Calcium presence was confirmed in all three experimental samples, while no calcium was observed in the control sample, as evidenced by distinct pair of Ca2p peaks within the as-collected experimental XPS spectra and the lack of pronounced calcium peaks within the control sample. Quantification showed a very high surface concentration of calcium relative to molybdenum and selenium, much higher than would be expected based off of the nominal electrochemical stoichiometry of  $\text{Ca}_{0.33}\text{Mo}_6\text{Se}_8$ . Calciated samples also showed much higher oxygen content when compared to the control sample. Chlorine was not present, suggesting that the oxygen is not due to perchlorate anions on the sample surface. These observations are consistent with the formation of some amount of calcium oxide at the surface of the powders, possibly due to reaction of the calciate material with oxygen or moisture, in spite of the fact that air sensitive sample preparation techniques were used. Furthermore, the enriched calcium surface layer could indicate that the calciation process of the  $\text{Mo}_6\text{Se}_8$  particles results in a core-shell structure, where calcium preferentially resides in the surface region of the material and is unable to penetrate more deeply, as the presence of this calciated layer inhibits further calcium penetration. This would result in a higher shell concentration of calcium and a mostly phase-pure core structure, rather than a uniform single bulk  $\text{Ca}_{0.33}\text{Mo}_6\text{Se}_8$  phase. Both of these possibilities serve as reasonable explanations as to why obtaining quantifiably different XRD spectra presented extreme difficulty, as in both instances the bulk composition of the  $\text{Mo}_6\text{Se}_8$  particles would be pure single phase during the course of ex-situ XRD measurements.

In spite of the calcium-rich surface layer phenomenon and the presence of additional oxygen in the electrochemical samples, strong signal was obtained for both the molybdenum and selenium peaks in both sets of samples. The molybdenum to selenium ratio from sample quantification was approximately 3:4, which is consistent with the expected stoichiometry. The selenium and molybdenum peak positions and shapes varied substantially between the control and electrochemical samples. Such shifts are indicative of differing local environment of near-surface molybdenum and selenium atoms. Unfortunately, indexed XPS spectra are not documented for selenide derivative Chevrel phase

compounds, particularly with calcium, and as such direct comparison of the peaks to known spectra is impossible. However, energy shifts in selenium and molybdenum tend to follow general trends based on their local environment, and as such a qualitative analysis of the behaviors is possible, and will be the point of further discussion.

The selenium control sample appears to be composed of several peak features in the range of 54-56 eV, with one large peak centered just under 55 eV and subsequent smaller shoulders. These energies are consistent with those of selenium and transition metal selenides found in the NIST database.<sup>84</sup> For example, the phase  $\text{Nb}_3\text{Se}_4$  is reported to have a selenium peak at a binding energy of 54.90 eV. The electrochemical samples display a distinct shift to lower binding energies, with the central feature now consisting of convoluted twin peaks in the range of 53-54 eV. The shoulder peaks creating the feature at 56 eV have essentially vanished, while the intensity at 55 eV is markedly reduced. Furthermore, the sample appears to exhibit a distribution of binding energy states of selenium, suggesting that different local environments are observed, as would be expected from some unit cells being calcinated with a valence shift having occurred on the molybdenum metal center, while others are not. Several compounds containing divalent ions such as  $\text{Cd}^{2+}$  and  $\text{Zn}^{2+}$  as selenium nearest neighbors exhibit a shift in the selenium peak to lower binding energies. The a shift to lower binding energies cannot be explained by the presence of oxygen or the binding of organic ligands formed as some sort of electrolyte decomposition product, as both of those tend to raise the binding energy of the selenide peak to the 56-59 eV range.<sup>84</sup> Thus, the shift in the magnitude of the selenium peaks is consistent with interaction with a divalent, closed-shell ion, for which calcium is a candidate.

Molybdenum atoms in the electrochemically treated  $\text{Mo}_6\text{Se}_8$  samples are expected to exhibit a lower fractional formal oxidation state than those in virgin  $\text{Mo}_6\text{Se}_8$ , as it has received electrons to charge compensate for the intercalant ion within the structure. The lower oxidation state species is expected to exhibit a shift to lower binding energy through XPS analysis, a change reflected when comparing the data. Although no molybdenum selenide Chevrel phase spectra were available for comparison, there are

spectra available for the sulfide structure.  $\text{HoMo}_6\text{S}_8$  and  $\text{PbMo}_6\text{S}_8$  are both Chevrel phase compounds, both of which show a reduced binding energy of the molybdenum 3d5/2 electron than in the case of the pure molybdenum sulfide phase, again consistent with observations in the selenide data.<sup>84</sup>

## 6.5 Chapter Summary

The goal of this chapter was to support the claim of calcium intercalation as the phenomenon behind the electrochemical behavior of the  $\text{Mo}_6\text{Se}_8$  Chevrel phase. Evidence was presented from a number of chemical and structural characterization techniques including SEM, TEM, EDS, XPS, and XRD, and was found to be fairly reproducible and consistent across multiple post-mortem electrodes. Calcium was found in all electrochemical samples in the case of each characterization technique, and was found in quantities consistent with calcium intercalation on the bulk electrode scale. Calcium was observed to localize to the surface of individual particles, by both TEM-EDS and XPS techniques, in quantities that would exceed the expected concentration of even a fully calciated  $\text{Ca}_2\text{Mo}_6\text{Se}_8$  phase. The presence of increased oxygen signal in electrochemically treated samples, particularly those with exposure to atmosphere post-mortem, suggests calcium leaching from the material via a chemical means involving a reaction with oxygen is the likely culprit for this excess calcium. Calcium perchlorate salt adsorption was ruled out as an explanation of this phenomenon due to inconsistent chloride ion to calcium ion ratio, which should be 2:1 for the formation of  $\text{Ca}(\text{ClO}_4)_2$ , but was instead found to be less than 1 in all cases.

No distinct particles of new phases were identified based on chemical means, and the particle morphology of pre- and post- intercalation compounds was found to be similar. This suggests that the electrons indeed participate in a reaction involving the  $\text{Mo}_6\text{Se}_8$  phase rather than the formation of an additional distinct phase such as the nucleation of some alternative calcium-containing species. Furthermore TEM studies eliminated the possibility that the formation of an amorphous product could account for the electrochemical signal observed. Bulk structural analysis via XRD did not show conclusive signs of the formation of  $\text{Ca}_1\text{Mo}_6\text{Se}_8$  or  $\text{Ca}_2\text{Mo}_6\text{Se}_8$  phases, as would be expected by analogy

to other Chevrel structures (such as with the case of magnesium derivatives). Some differences were observed between control and experimental XRD spectra, and are consistent with some small degree of calcium intercalation across the entire particle, or a small surface region of calcination at the individual particle level which would weaken the influence on the XRD pattern. Experimental lattice parameters for  $\text{Ca}_x\text{Mo}_6\text{Se}_8$  differed from those expected from indexed reference patterns, however they were similar to those obtained from in house control samples. Experimental intensity values, however, could not be reproduced utilizing phase pure  $\text{Mo}_6\text{Se}_8$  and better agreement between modeled and experimental data was obtained with the addition of a low-occupancy fraction calcium site. These subtle XRD variations, combined with the XPS data, suggest that the local environment of atoms within the  $\text{Mo}_6\text{Se}_8$  unit cells has changed post-electrochemistry. When taken together, all of these observations paint a compelling picture of calcium intercalation as the likely phenomenon at play in the observed  $\text{Mo}_6\text{Se}_8$  electrochemistry.

## **Chapter 7**

# **Concluding Remarks and Future Directions**

Today is an exciting time for electrochemists: batteries are poised to make their biggest impact on society since their invention. Batteries, in the past, presented the dominant means of electricity generation (utilizing primary cells), and springboarded engineering and science through the 19<sup>th</sup> century. With the advent of other means of electricity generation, as well as the internal combustion engine, the world has exploded into the modern technological age thriving on petrochemical products. Batteries in this new age have found their niche as the dominant power source for consumer and mobile applications. However, in addition to constant pressures to improve performance metrics for mobile applications, batteries are now expected to help carry the weight of a greening society as this petrochemical world begins the movement towards a more sustainably-minded future. The scale of energy generation and consumption on the earth is enormous, and requires that battery researchers approach the development of novel technologies with new performance metrics in mind. Energy density and specific energy are now joined by cost, scalability, and environmental impact as crucial factors in battery design for various applications. Scientists, engineers, and designers will be driven to address an ever-expanding demand for energy storage markets as this shift is made: an exciting array of scientific questions will be asked and answered as a result of society's broadening energy storage portfolio.

Multivalent ion batteries are likely to play a key role in that portfolio, as they offer improvements in energy density over current state of the art lithium ion technologies. Furthermore, given the scale of automotive transportation needs and cost as a key driver, novel chemistries comprised of earth abundant elements will play a role in this industry, if not in the immediate future then eventually as electric vehicle markets continue to grow. This thesis serves to address the question of whether calcium makes sense to explore as one of these novel chemistries. Calcium batteries, although drastically underrepresented in the literature, make sense from a theoretical standpoint, as calcium is an abundant divalent ion and offers a low plating potential. Furthermore, the charge density of calcium is lower than that of magnesium, offering promise that it might be possible to avoid some of the charge density related transport issues encountered by magnesium ion batteries. The development of practical calcium batteries requires several key innovations; (1) a suitable calcium intercalation compound must be identified, (2) an electrolyte capable of plating and stripping metallic calcium must be developed, (3) the electrode/electrolyte system must be compatible with each other as well as with cell components, and (4) conditions of market cost and scalability must be met by all cell components. This thesis primarily concerns itself with investigation of the first necessary innovation, that of a calcium intercalation compound.

The first major contribution of this thesis is the decoupling of the study of calcium intercalation compounds from the problem of reversible calcium electro-deposition by the development of a novel reference electrode, counter electrode, and electrolyte system. The  $\text{CaHg}_{11}\text{-Ca}_{(\text{Hg})}^{\text{sat}}$  electrode offers a potential stable to within  $\pm 2$  mV for many weeks, which allows for more precise electrochemical studies than could be performed with previously used fritted and pseudo-reference electrodes commonly used in the literature. The  $\text{CaHg}_{11}\text{-Ca}_{(\text{Hg})}^{\text{sat}}$  faradaic counter electrode is able to act as both a calcium ion source and sink, which reduces the need for complex cell geometries and frits or electrolyte depletion associated with non-faradaic counter electrodes. Acetonitrile and calcium perchlorate are commonly available shelf reagents, and require no complex organometallic syntheses to be carried out to create an



electrolyte. This system provides a simple avenue for rapid and accurate testing of calcium intercalation materials candidates, a tool that is sorely lacking from the literature.

One caveat to the system presented is that it does not necessarily address all issues of compatibility between the electrolyte and the positive electrode material of interest. Compatibility between electrode materials and electrolyte happens on a case by case basis, and although there are cross-cutting classes of electrolytes that work with a broad selection of lithium-ion materials, such as  $\text{LiPF}_6$  in ethylene carbonate : dimethyl carbonate (EC:DMC), there are instances where electrolyte selection is an issue. Magnesium perchlorate salts have been shown to elicit different behavior from identical  $\text{Mo}_6\text{S}_8$  electrodes depending on if they were dissolved in propylene carbonate or acetonitrile solvents, due to the difference in the solvation shells of calcium ions in the electrolyte solution.<sup>60</sup> Screening of candidates in this particular electrolyte and system should aim to be inclusive, and not exclusive in nature, such that possible electrode materials are revisited in different electrolyte compounds as they become known.

Although not a commercially viable system, due to its low theoretical capacity, low voltage, and high costs, the Chevrel phase is a good model compound for the study of multivalent ion intercalation, and was identified as such from a survey of potential candidates based on prior art. This work is the first to demonstrate successful calcium intercalation into the Chevrel phase, even though calcium is not quite a good “fit” for the Chevrel structure and exhibits extreme kinetic limitations. Several classical materials science “knobs” – rate, temperature, particle size, and chemistry – were used to explore the kinetics of the system, and found to support this hypothesis. Chemical and structural data strongly support calcium as the active species involved in the electrochemical process, and preclude other phenomena such as electrode amorphization or another electrodeposition, decomposition, or corrosion process. Conclusive XRD structural data of the bulk  $\text{Ca}_1\text{Mo}_6\text{Se}_8$  or  $\text{Ca}_2\text{Mo}_6\text{Se}_8$  phases was not obtained partly due to the inability to fully electrochemically intercalate calcium into the Chevrel structure, and partly due to calcium’s propensity to react with oxygen.

Calcium's extreme reactivity is one of the continuing challenges of calcium-ion research, and is even exacerbated over the difficulties associated with the magnesium-ion field. Given the opportunity, metallic calcium reacts with essentially everything to remove oxygen, and poses a significant challenge to the development of a system that can operate with a stable calcium anode. However, even in the case of a positive electrode where calcium exists at a higher potential and is thus lower in its reactivity, the formation of calcium oxide still poses a problem, particularly in the exploration of low-voltage materials such as Chevrel phase compounds. This is a problem shared by a number of other possible multivalent-ion intercalation chemistries such as magnesium, beryllium, and even aluminum. In this sense, lithium and sodium are much easier to work with as a number of positive electrode materials lie at sufficiently high potential to offer greater resistance to electrode oxidation. The low voltage of the  $\text{Mo}_6\text{Se}_8$  compound, combined with calcium's nature, greatly multiplies the need for oxygen and moisture control at all steps of electrochemical study and characterization. Standard glovebox procedures, which for the case of lithium and sodium may be acceptable, may not be sufficient in the case of ions such as magnesium or calcium. Scientists seeking to work in this area should pay particular attention to protocols used for sample preparation, and take all possible steps to reduce oxygen partial pressure in the environment such as the inclusion of additional getters and extra care to ensure robust seals. Oxygen contamination can have a disastrous effect on both electrochemical performance, as well as in-situ or post-mortem materials characterization techniques.

In addition to improving cell preparation and analytical protocols to further reduce oxygen contamination, there are several possible directions, both experimental and computational, that future work on the study of the behavior of calcium in the Chevrel phase. Although literature evidence of the  $\text{Ca}_1\text{Mo}_6\text{S}_8$  phase along with a partial phase diagram of the Ca-Mo-S ternary system, no such data are available for the its selenide derivative structure.<sup>46,47,85</sup> Experimental work could be taken to characterize the calcium-molybdenum-selenium ternary phase space over a wide temperature range to look for potential intercalation product phases. Calcium-containing Chevrel-type selenide structures could be

synthesized and characterized. Direct synthesis of the  $\text{Ca}_1\text{Mo}_6\text{Se}_8$  phase is reported in the literature at a temperature of 1800 C, and would make a good starting point for such work, however operating in this temperature regime poses its own set of challenges.<sup>46</sup> The work could expand to synthesize a suite of compounds of varying calcium content. Once suitable  $\text{Ca}_x\text{Mo}_6\text{Se}_8$  samples were prepared, they could be used to provide a more accurate comparison base line for the electrochemically treated  $\text{Mo}_6\text{Se}_8$  samples for both XRD and XPS studies.

As an alternative to the experimental route, a computational approach could be taken to the same problem to give some indication of the expected phases by developing a computational phase diagram. Another possible computational avenue relies not on predicting phases and phase boundaries for the ternary system, but instead to assume an appropriate Chevrel structure for one of the  $\text{Ca}_x\text{Mo}_6\text{Se}_8$  phases, and then to allow the unit cell parameters to relax to look for local energy minima in such a structure. Very preliminary work in this area was carried out for  $\text{Ca}_1\text{Mo}_6\text{Se}_8$  by collaborators<sup>i</sup>, and served as the starting point for reitveld analysis of XRD patterns, however a more in depth study was not undertaken. Such work, when performed in detail, could also provide for rough material capacities and intercalation potentials which could be compared to experimental results.

In-situ XRD experiments would probably be the most useful means by which to improve the characterization of the electrochemical behavior of an individual  $\text{Mo}_6\text{Se}_8$  electrode during the discharge process. The most precise way to obtain very clean XRD data on the system would be to utilize a diffractometer enclosed entirely in a glovebox atmosphere. Furthermore, a substantial redesign of current in-situ XRD cells would be needed to accommodate such an experiment with the system of interest. Such double protection from atmosphere, combined with the immediate data collection (rather than an inherent time delay involved in post-mortem analysis), would provide additional safeguards against oxygen contamination and sample degradation. In addition to XRD data, solid state nuclear magnetic resonance (NMR) studies provide another means of probing bulk chemical/structural data, and could be carried out

---

<sup>i</sup> Miao Liu, Electrochemical Technologies Group, Lawrence Berkeley National Laboratory

as a means to explore the binding state of subsurface atoms within the structure to complement the surface-sensitive analysis provided for by XPS.

Ultimately, there easily exists work for several more doctoral candidates in the study and characterization of Chevrel phase electrochemistry involving calcium. More broadly however, the future of multivalent and calcium-ion batteries does not lie with the Chevrel phase. The structure is too low voltage, and offers too low a capacity to be useful for most applications. New cathode compounds must be higher voltage, offer higher ion mobility, and be capable of achieving higher capacities. Such new cathodes require having a single transition metal able to undergo a multiple redox shift within a compound, as opposed to the two thirds valence shift per molybdenum atom in the Chevrel phase. Work in this area exists in the lithium-ion field, where authors have begun to explore transition metal oxide ions, such as nickel, are capable of multiple electron shifts per formula unit. It is also likely that vanadium undergoes a similar multi-redox shift in vanadium pentoxide intercalation of trivalent ions such as yttrium.<sup>11</sup> Several materials design principles for future calcium-intercalation compounds can be gleaned from the work presented in this thesis. Intercalation hosts should generally consist of metal oxides, as the high electronegativity of the species provides for a high free energy of formation, and hence a high potential. However, such hosts should also contain some polarizable anionic species to improve anion mobility. Such species tend to be lower in electronegativity, and typically involve sulfides, selenides, or tellurides, and as a result they tend to offer a lower theoretical operating voltage. A successful future cathode for calcium-ion batteries will likely combine anions to achieve these two competing effects, voltage and mobility, in such a way that the transition metal center of the material is allowed to undergo multiple redox shifts. Such is necessary for multivalent ion intercalation cathodes to see their full potential, although constituent atoms need not be limited to group 16 of the periodic table, and may evolve to include select group 17 elements such as fluorine or chlorine, and even potentially nitrogen in this careful tradeoff. The author is confident that a new generation of intercalation cathodes, particularly designed for multivalent ions, will be discovered in the coming years. The means of such a discovery,

whether it will be experimental intuition and ingenuity, modern calculation and theory, or mere coincidence and chance, is what remains to be seen. It is the author's sincere hope that this work has presented a step in that direction towards a future where multivalent batteries have come of age.

# Appendices

## A. Aluminum and the Chevrel Phase

As an intercalation compound, the  $\text{Mo}_6\text{X}_8$  ( $\text{X} = \text{S}, \text{Se}, \text{Te}$ ) Chevrel phases are unique in that they are found to provide up to four electrons per formula unit, distributed amongst the six molybdenum atoms in the structure. This “fractional” distribution of electrons on each molybdenum atom is postulated to be the reason why the structure is able to undergo redox shifts of multiple electrons per formula unit without the severe kinetic limitations typical observed in transition metal oxide structures.<sup>10,11</sup> In the case of monovalent ions such as lithium and sodium, the Chevrel structure is observed to uptake a single ion first, corresponding to a single electron transfer step per formula unit. Upon further intercalation, two additional ions are incorporated into the structure simultaneously, corresponding to a double redox transfer step on the six molybdenum cluster. At even lower potentials a final ion is taken up by the structure in a final single electron redox shift. This behavior is associated only with monovalent ions, divalent ions tend to behave quite differently within the structure. In the cases of magnesium, cadmium, and zinc studied in the literature (see Chapter 2 for discussion), it is observed that the structure undergoes two double redox shifts. The de-intercalated structure accommodates a single divalent ion upon intercalation, followed by an additional divalent ion. In both the monovalent and the divalent intercalation cases, the terminal stoichiometry is observed to occur after four electrons accommodated by the molybdenum cluster, as would be expected from the theoretical literature.<sup>64</sup> Given the flexibility of the structure with regards to the manner in which these four electrons are lodged, a natural question arises as

to whether the Chevrel phase compounds would be able to accommodate trivalent ions with the same ease that they appear to be able to accommodate their small monovalent and divalent cousins.

In order to probe the possibility of trivalent ion intercalation into the Chevrel structure, a suitable trivalent ion must be identified. Such an ion should have a single redox state as to avoid problems associated with multiple valences in the electrolyte, as well as be small enough to comfortably fit within the chevrel cavities, which appear to have a critical radius for intercalation on the order of 100 pm.<sup>50</sup> Both yttrium and aluminum stood out as potential candidates, with some precedent of intercalation reported within the literature. Yttrium was found to intercalate into a vanadium pentoxide structure,<sup>11</sup> although a hybrid counter electrode system and quasi-reference electrode were used, making it a less ideal system for study. Aluminium shuttling has been reported in symmetric cells of vanadium oxide.<sup>91,92,93</sup> Additionally, Oak-Ridge National Laboratory (ORNL) has recently reported on the intercalation of aluminum ions into a manganese oxide compound.<sup>94</sup> The work was carried out using aluminum metal half cells enabled by an ionic liquid electrolyte. Given that a true half-cell has been devised for the study of aluminum intercalation compounds, and the fact that yttrium's ionic radius is on the order of 100 pm while aluminum's ionic radius is reported to be under 70 pm, aluminum was chosen as a candidate ion to explore trivalent intercalation into the Chevrel structure.

Before delving directly into experimental trials, let us take a moment to consider what the expected behavior of the aluminum ion would be in the Chevrel phase. Assuming that the limiting factor in intercalation is the four electrons able to be accommodated by the six molybdenum cluster, one would expect a terminal phase stoichiometry of  $\text{Al}_{1.33}\text{Mo}_6\text{Se}_8$ . However, obtaining such a terminal stoichiometry would necessitate that an aluminum ion, in proximity to a particular unit cell of  $\text{Mo}_6\text{Se}_8$ , be compensated for by the presence of one additional electron in each two neighboring unit cells in addition to the extra electron within the host cell. This condition would seem to violate the condition of local charge neutrality within the crystal at the unit cell level, and unless the “additional” aluminum ion were to be positioned in such a way that it could easily interact with multiple unit cells and occupy alternating cavities within the

structure. Assuming a single aluminum ion per cavity, the terminal phase could be imagined to consist of stoichiometric  $\text{Al}_1\text{Mo}_6\text{Se}_8$ . For this terminal composition, one is lead to imagine that a single intercalation event occurs within the structure. One would expect to observe the following equilibrium  $\text{Mo}_6\text{Se}_8 + \text{Al}^{3+} + 3\text{e}^- \leftrightarrow \text{Al}_1\text{Mo}_6\text{Se}_8$  at a singular value of thermodynamic potential. Such an intercalation reaction would require the simultaneous accommodation of 3 electrons per formula unit of  $\text{Mo}_6\text{Se}_8$ , a process which, although plausible, may not be possible within the material itself.

In order to probe the intercalation properties of aluminum into the Chevrel phase experimentally, the work on the unique aluminum electrolyte developed by ORNL was reproduced. The ORNL investigators used a binary solution of aluminum chloride ( $\text{AlCl}_3$ ) with ethyl-methyl-imidazolium chloride (EMIMCl). The study found that the chloride ion complexes with the  $\text{AlCl}_3$  structure to form an  $\text{AlCl}_4^-$  anion in solution. Furthermore, it was found that depending upon the acidity or basicity of the solution (controlled by the ratio of EMIMCl to  $\text{AlCl}_3$ ), the ability for the solution to reversibly plate and strip aluminum was directly affected. It was observed that a ratio of 2:1 of  $\text{AlCl}_3$  to EMIMCl was preferred as an electrolyte for aluminum half-cells.<sup>94,95</sup>



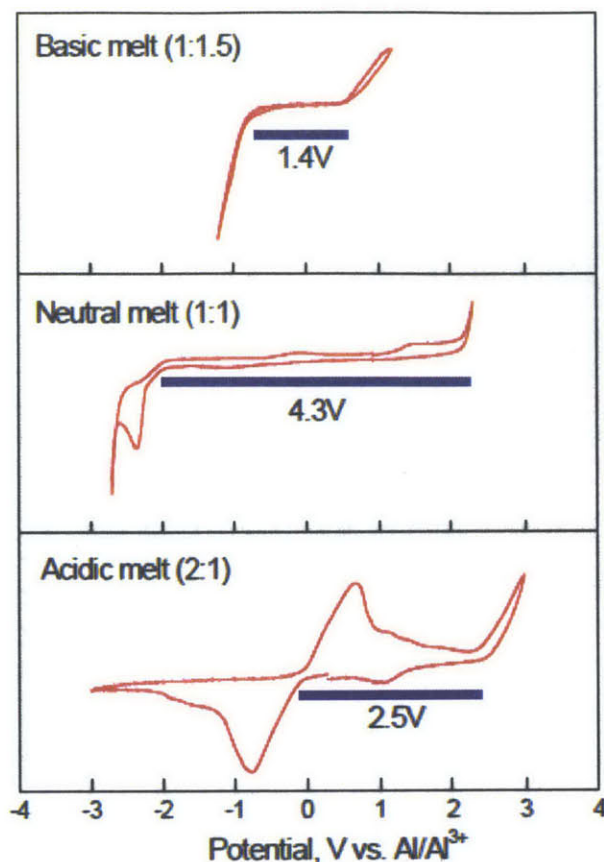


Figure 57. Cyclic voltammograms of various  $\text{AlCl}_3$ -EMIMCl ionic liquids. Electrodeposition and stripping is observed in the acidic melt, however the basic and neutral melts are not appropriate for aluminum anode operation.

An ionic liquid in the same family as EMIMCl, Butyl-Methyl-Imidazolium Chloride (BMIMCl) was synthesized in house. This ionic liquid was prepared in a 2:1 ratio directly and allowed to equilibrate. The two components, initially solids, formed a single liquid phase after several days. This electrolyte was stored in an argon filled glovebox, and found to be stable for several months.

Electrochemical characterization of the BMIMCl- $\text{AlCl}_3$  electrolyte was carried out prior to studies involving the chevrel phase active material. High purity aluminum wire (99.999% purity, 1 mm diameter, Sigma Aldrich) was obtained for use as both a reference electrode and a counter electrode. Wires were lightly sanded in an argon-filled glovebox prior to testing to remove some of the surface oxide film. The potential between two pieces of aluminum wire was measured to be under ten millivolts, suggesting that a somewhat stable, although not ideal equilibrium potential was established. Vitreous carbon was identified as a candidate current collector material for use as both a substrate for intercalation

material powders and as an inert electrode for electrolyte studies, as it would not be expected to form various compounds with aluminum. ORNL reports having used platinum as a current collector for their voltammetric deposition/stripping and intercalation experiments; however from a cursory inspection of the aluminum-platinum phase diagram it appears that numerous intermetallic compounds and reasonable solubility of aluminum in platinum exist, opening the door to potential alloying reactions.

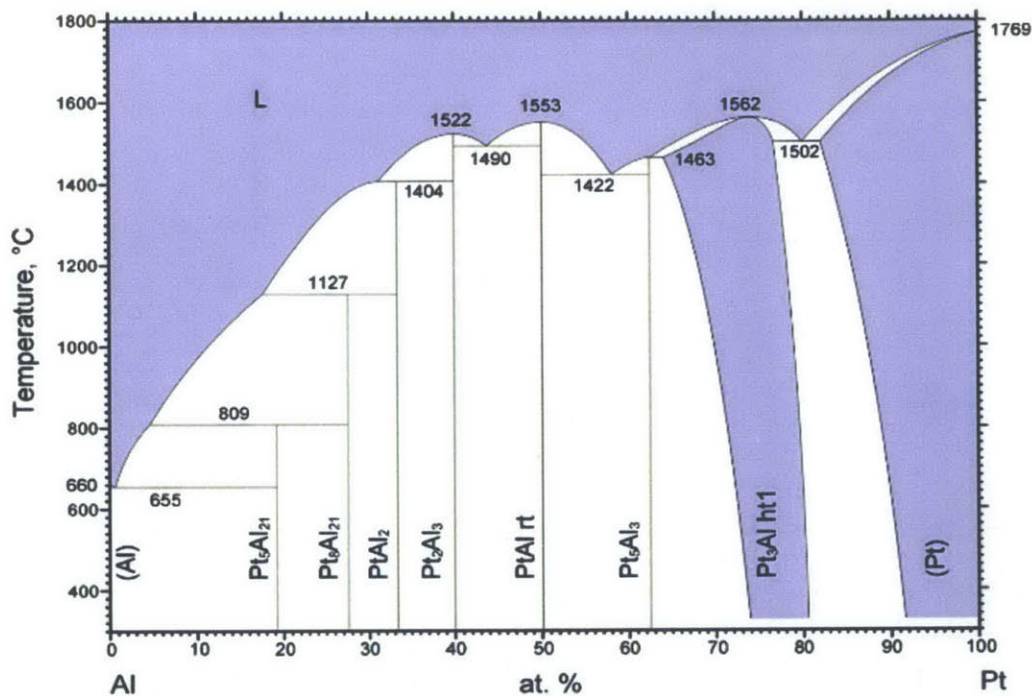


Figure 58. **Calcium-platinum phase diagram.** Image of the calcium-platinum phase diagram<sup>96</sup> displaying high solubility of aluminum in platinum over a wide temperature range.

One would expect these alloys to present themselves before aluminum deposition, particularly given the large solubility of aluminum in the platinum phase. It seems plausible that the ORNL work demonstrates alloying and de-alloying with platinum, rather than pure aluminum deposition. This assertion seems founded based on the overall form of the cyclic voltammetry presented by the ORNL investigators. In-house voltammetry was performed on the BMIMCl-AlCl<sub>3</sub> system on a vitreous carbon electrode encased in glass, with an exposed active area of 1 mm diameter. The voltammograms obtained are somewhat distinct from the work presented by ORNL.

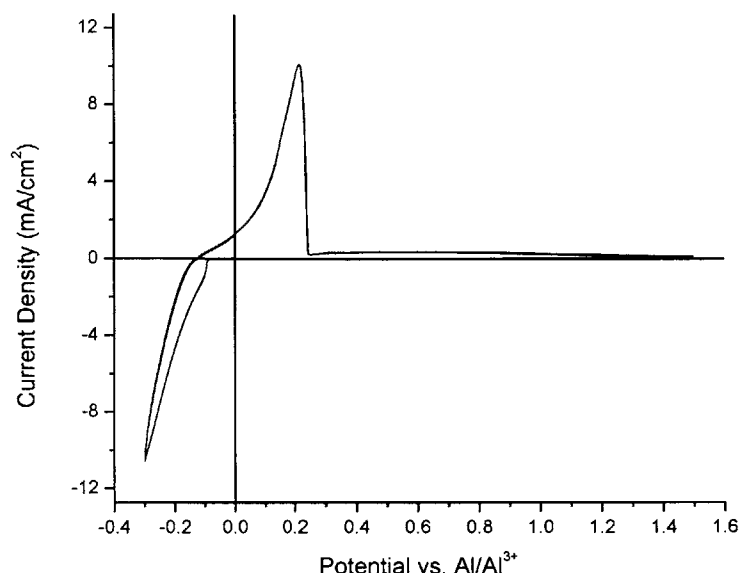


Figure 59. **Cyclic voltammogram of Al deposition/dissolution on carbon WE.** Sweep rate of 1 mV/s on glassy carbon rod electrode showing distinct plating and stripping peaks.

An aluminum deposition wave was observed after about -100 mV overpotential, and a corresponding stripping peak was observed upon the reverse sweep. Unlike the data from ORNL, the stripping peak appears characteristically sharp, suggesting the process we observe is indeed aluminum plating. The current drops off sharply once the last bit of aluminum is removed from the surface of inert substrate. This is in contrast to a gradual de-alloying process, where the current signal tends to slowly wander off to zero.

The determination was made that the BMIMCl-AlCl<sub>3</sub> electrolyte, when paired directly with aluminum metal counter and reference electrodes, had demonstrated adequate performance as an aluminum ion shuttling electrolyte. Voltammetric studies were undertaken to interrogate the performance of Chevrel phase compounds in this system. Mo<sub>6</sub>Se<sub>8</sub> composite electrode powders were prepared in a ratio of 60% Mo<sub>6</sub>Se<sub>8</sub>, 10% amorphous carbon, and 30% PTFE binder particles. The powders were manually pressed onto a 1 mm diameter vitreous carbon electrode using a gentle rubbing motion. Cyclic voltammetry was performed on the electrode. A typical result is shown below in figure 60.

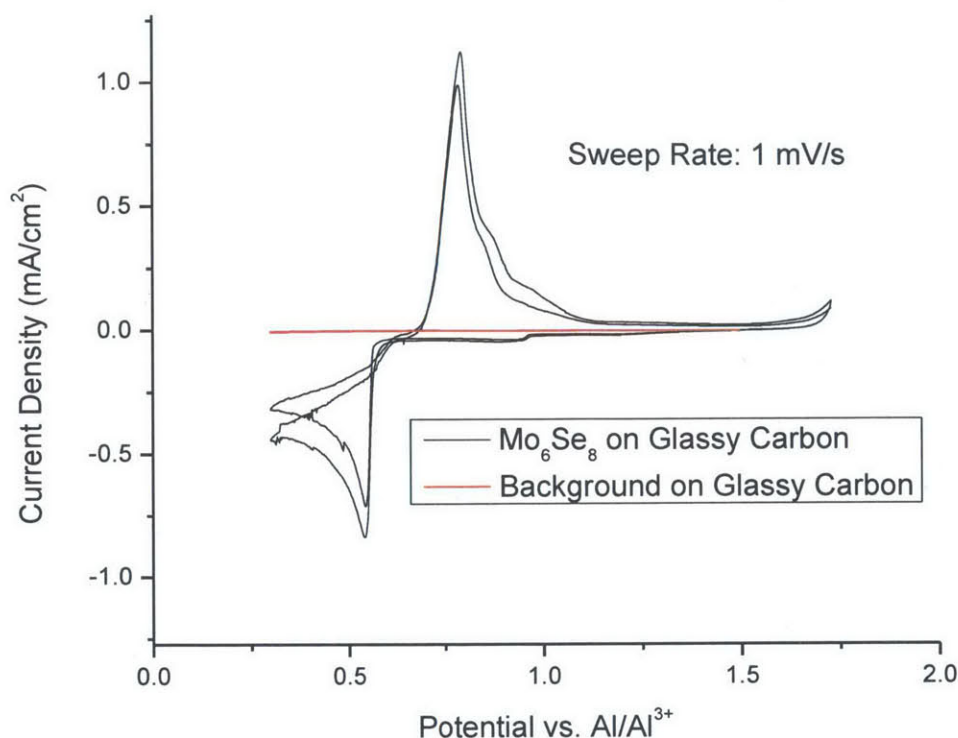


Figure 60. Cyclic voltammogram of  $\text{Mo}_6\text{Se}_8$  on carbon WE. Sweep rate of 1 mV/s. Electrode diameter of 1 mm.

One can clearly identify a single large peak on both the cathodic and anodic sweeps. These two peaks are at substantially higher current densities than background, suggesting the peak is due to an interaction between the electrolyte and the  $\text{Mo}_6\text{Se}_8$  phase. The potential of the main “insertion” peak occurs at about 0.5 V vs.  $\text{Al}/\text{Al}^{3+}$ . This potential for insertion of aluminum into the structure makes sense by a rough comparison with the literature concerning magnesium insertion into the  $\text{Mo}_6\text{Se}_8$  phase. The onset of  $\text{Mg}^{2+}$  insertion is found to be about 1.1 V vs.  $\text{Mg}/\text{Mg}^{2+}$ . The conversion factor between the Al and Mg reference electrodes is roughly 0.7 V, thus one would expect intercalation in the region of 0.6 V vs.  $\text{Al}/\text{Al}^{3+}$ . Of course this analysis is hardly conclusive, but the presence of aluminum insertion peaks at roughly this potential is hardly surprising.

Closer analysis of the cyclic voltammogram reveals a small wave occurring prior to the main insertion peak, at about 1.0 V vs.  $\text{Al}/\text{Al}^{3+}$ , consisting of a slight signal above background at a very minor

current density. Additionally, although the primary intercalation wave appears to have the form of a single peak, the deintercalation wave in fact appears as though it is comprised of three distinct components. The onset of the primary deintercalation wave occurs at roughly 750 mV, while a second wave appears in its wake at around 900 mV and a third around 1 V. It is evident from the voltammetric results that whatever is occurring when the  $\text{Mo}_6\text{Se}_8$  Chevrel compound is cycled in the presence of an aluminium conducting electrolyte is not a single ion intercalation/deintercalation event accompanied by a simultaneous 3-electron transfer process.

In order to further probe the nature of the  $\text{Mo}_6\text{Se}_8$  electrode in the aluminum-containing ionic liquid, galvanic cycling tests were performed. The pressed disk electrode was too small to cycle at an appreciable rate given equipment restrictions, thus galvanic tests needed to be carried out on a larger volume of active material. The brittle nature of glassy carbon is a consideration for use as a current collector, and limits both the form factor in which it can be obtained and the mechanical loads which it is capable of sustaining. Duocel Reticulated Vitreous Carbon (100 PPI) was obtained as a foam block and was carefully trimmed to appropriate dimensions (2 mm x 5 mm x 10 cm). The carbonaceous network was extremely porous, resulting in a high current collector resistance (approximately 85 ohms over 5 linear cm), and was also extremely fragile. Steel disks were used as backing at the top of electrode to distribute the stress of the electrical connectors from crumbling the foam.  $\text{Mo}_6\text{Se}_8$ /Carbon/PTFE composite electrode powders were *lightly* pressed into the foam using a small spatula. Unfortunately, given the fragility of the current collector, it was difficult to press sufficiently to prevent some powders from losing electrical contact, thus quantitative capacity data was not collected from these trials. Qualitative galvanic discharge/charge behavior is demonstrated in figure 61 below.



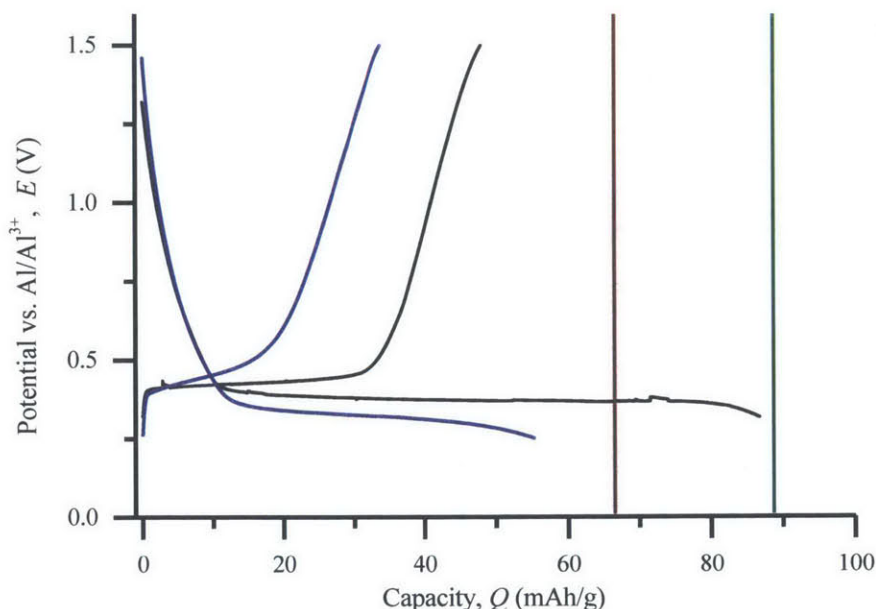


Figure 61. **Galvanic cycling behavior of  $\text{Mo}_6\text{Se}_8$ .** First discharge and charge cycles shown for C/8.5 (blue) and C/85 (black) cycling rates. Red line corresponds to  $\text{Al}_1\text{Mo}_6\text{Se}_8$  and the green line corresponds to  $\text{Al}_{1.33}\text{Mo}_6\text{Se}_8$  theoretical capacities respectively.

Qualitatively, the curves look exactly as one would expect based on the voltammetry results. The bulk of the discharge appears to occur in a single step, with a small amount of capacity becoming available at a higher potential. On charging we observe a somewhat flat plateau, followed by an steep increase in charging potential.

Although interesting results were obtained, and it is quite possible that an operational aluminum-ion battery was cycled, the above system will prove to be of little practical use as a commercial battery. The potential of the  $\text{AlMo}_6\text{Se}_8$  phase is too low to make a useful positive electrode material, but too high to be used as a negative electrode intercalation compound. Still, as a model system for aluminum ion intercalation, the Chevrel phase is particularly interesting. Unfortunately, further electrochemical measurements on the  $\text{AlMo}_6\text{Se}_8$  system were not undertaken given that this work was not the primary focus of this thesis, which devotes itself to the consideration of calcium ion systems. One could easily lay out a course for further study of the behavior of the aluminum system interrogated here by comparison to

the studies discussed with regards to calcium in this thesis. Namely, the following future experiments would prove instrumental:

1. Chemical analysis to confirm that the electrochemical behavior observed is indeed that of aluminum ion intercalation. Potentiostatic discharging of  $\text{Mo}_6\text{Se}_8$  to various potentials could be used in conjunction with chemical analysis to obtain a theoretical OCV discharge curve.
2. XRD analysis to confirm and characterize the structural change upon aluminum intercalation, as well as the various phases present at stages of discharge.
3. Quantitative capacity data, as well as rate performance studies of the system.

Aluminum itself is a particularly interesting anode for electrochemical storage. As a material it is inherently safe, cheap, and abundant. Should aluminum-ion intercalation batteries be successfully developed and commercialized, they would certainly occupy their fair share of the energy storage market. Unfortunately, in addition to difficulties associated with multivalent ion intercalation, aluminum ion batteries will need to overcome hurdles associated with low system operating voltage given the relatively high deposition potential of aluminum. There is cause for hope however, and the author firmly believes that aluminum, alongside calcium, magnesium, and sodium, is a strong candidate for battery development.

## **B. Beryllium and the Chevrel Phase**

Beryllium is a very high charge density divalent ion that is somewhat less metallic in behavior than other alkali and alkali earth metals. Beryllium electrochemistry is rarely investigated as it is both toxic and difficult to work with, however similarities between beryllium and aluminum make it reasonable to assume that beryllium electrodeposition and stripping can be carried out in electrolytes similar to that of aluminum. Following the literature precedent for aluminum electrodeposition, a beryllium electrolyte was developed through the eutectic formation of a beryllium chloride –

butylmethylimidazolium chloride ionic liquid. A viscous liquid gradually formed upon exothermic reaction. Figure 62 below captures the formation of a binary liquid phase at room temperature.



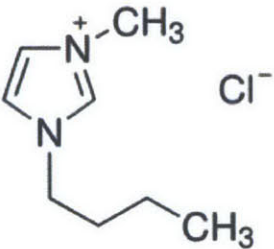

<p><b>Beryllium Chloride</b> T<sub>m</sub> ~ 400 °C  BeCl<sub>2</sub></p> 	<p><b>BeCl<sub>2</sub> – BMIMCl (2:1 molar ratio)</b> T<sub>m</sub> &lt; R.T.</p> <p><b>Viscous liquid forms upon mixing.</b></p> <p><b>Fluidity and conductivity improve at elevated temperature.</b></p> 
<p><b>Butylmethylimidazolium Chloride</b> T<sub>m</sub> ~ 70 °C</p>  	

Figure 62. Comparison of beryllium chloride and ionic liquid properties.

Beryllium metal disk counter and reference electrodes were immersed in the electrolyte and found to maintain an open circuit voltage between them ranging between 0 and 40 mV. The reference offered poor precision and reproducibility, however the potential likely resides close to that of beryllium plating potential. A silver wire working electrode was selected for initial study, and cyclic voltammetry was performed. The formation of a surface plating product could be observed, and the wire darkened substantially in color upon electrochemical cycling. SEM/EDS confirmed beryllium content of the deposited sample, however precise quantification is generally poor with low atomic weight elements, particularly with thin coatings. A typical cyclic voltammogram as well as SEM micrograph are shown in 63 below.



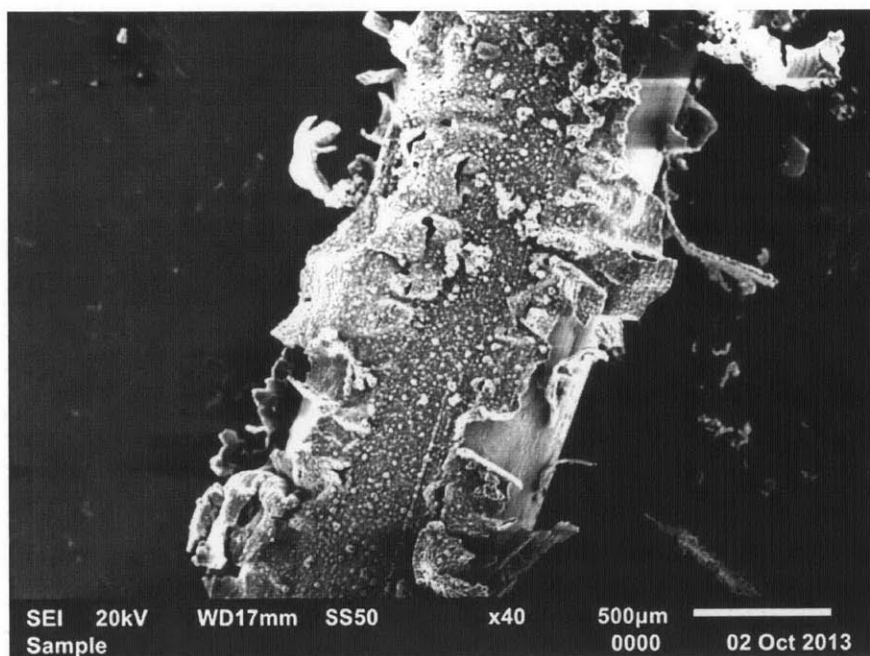
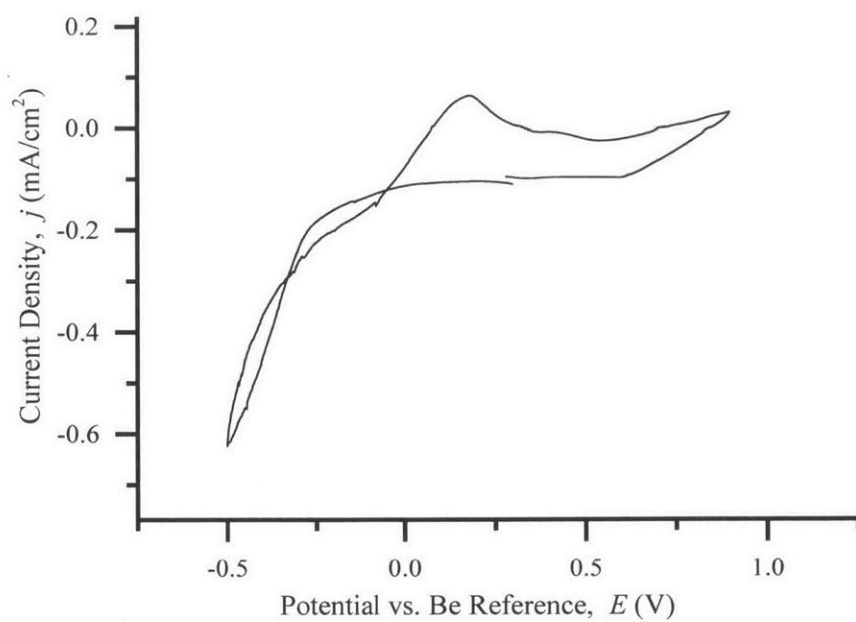


Figure 63. Cyclic voltammogram of  $\text{BeCl}_2\text{-BMIMCl}$  electrolyte and SEM micrograph of deposit. Cyclic voltammogram (top) collected at a sweep rate of 1 mV/s on submerged silver wire. Deposition product produced by potentiostatic hold at -0.5 V vs. reference.

Divalent ions are typically observed to insert into the Chevrel phase in a two-step process involving the insertion of a singular ion at two different potentials. In the case of beryllium, one would expect the insertion process to be governed by the formation of the  $\text{Be}_1\text{Mo}_6\text{Se}_8$  and  $\text{Be}_2\text{Mo}_6\text{Se}_8$  phases. Given beryllium's small size, no steric issues would be expected to inhibit the insertion process. Standard  $\text{Mo}_6\text{Se}_8$  cathode powders were slurry cast onto a silver wire current collector. Cyclic voltammograms performed on the electrodes displayed reversible electrochemical activity, a typical example of which is shown in figure 64 below.

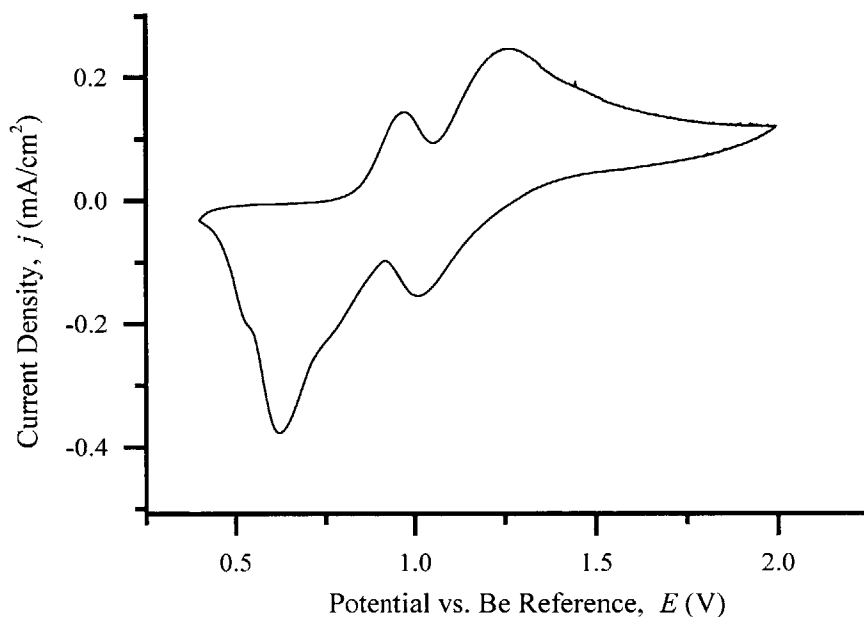


Figure 64. **Cyclic voltammogram of  $\text{Mo}_6\text{Se}_8$  in beryllium electrolyte.** Sweep rate of 1 mV/s. Double wave structure is observed as would be expected from divalent ion intercalation and deintercalation.

Two insertion and deinsertion peaks are observed in the voltammogram, in the potential region that would be expected for Chevrel phase electrochemistry. Further voltammetric studies of different sweep ranges showed that the observed peaks are coupled, and that positive current cannot be drawn unless preceded by an earlier negative current. The qualitative form and potential are consistent with the two-step insertion of beryllium into  $\text{Mo}_6\text{Se}_8$ . Further studies would need to be undertaken to confirm the behavior is indeed due to beryllium intercalation. Given its extremely high charge density, beryllium is a

particularly interesting scientific intercalation candidate, however caution should be taken by future investigators in working with beryllium compounds.

### **C. Particle Size Determination**

Several different particle size distributions are reported throughout this thesis, all of which were reported based on primary particle size determination via averaging of SEM or TEM images. Although it should be obvious to the reader that particles, particularly those that have been milled or pressed, will be composed of complex morphologies rather than simple spheres, an assumption of spherical geometry was made for this thesis. Each of the reported particle size distributions consists of an average particle diameter and corresponding standard deviation taken as the breadth of the distribution. Such a method allows for a single variable to capture the relative sizing effects in the system, and on average, should represent a good approximation of the actual diffusion length required to reach the interior of some particles.

TEM particle sizing was conducted by averaging particle diameters in images of dozens of particles. Each particle was measured in two dimensions approximately orthogonal to each other, in order to account for particles with elongated profiles in a particular direction. Figure 66 below shows a typical image with associated annotations along the measured directions. Representative particles for TEM were chosen by selection of a particular area at low magnification, and then precisely measuring all particles in an associated “cluster” or grouping in that section of the image. Particles were dilute enough on the TEM grid to distinctly measure each particle individually without worry about convolution with neighboring particles. The particle size reported does not take into account whether samples are single crystal or polycrystalline, rather it looks at the entire particle as the unit of interest.

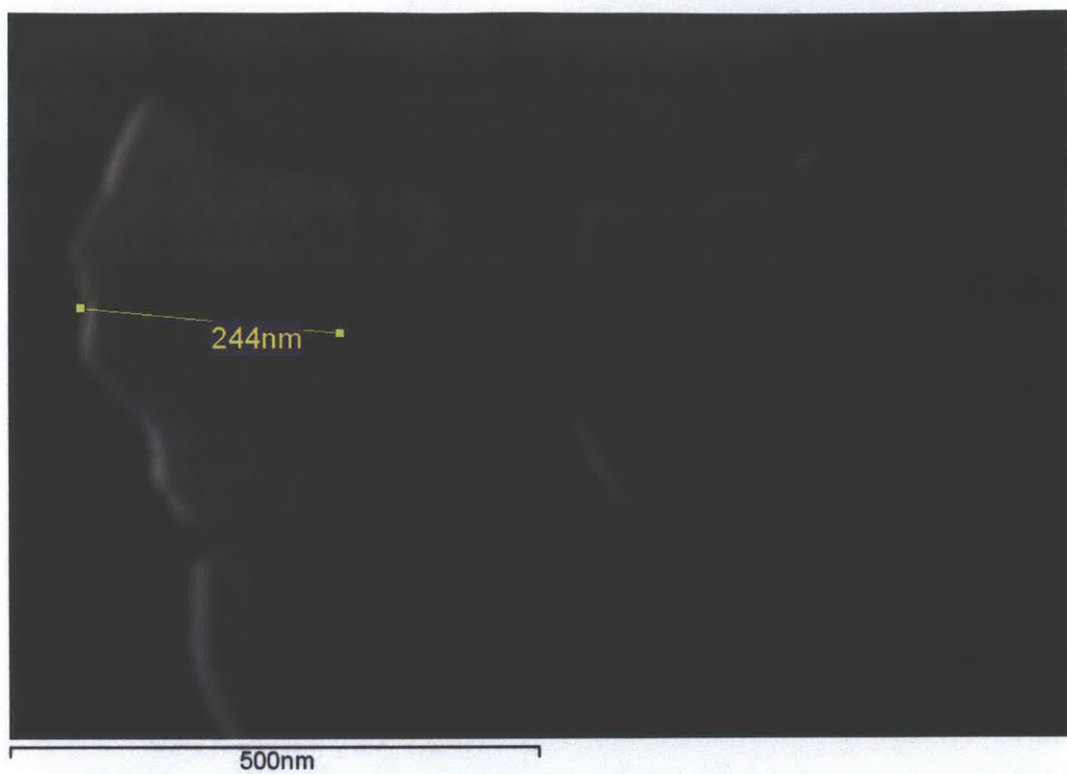
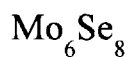


Figure 65. TEM micrographs of typical Mo<sub>6</sub>Se<sub>8</sub> particles.

Particle size distributions derived from SEM images posed some more interesting challenges than those from TEM, namely selection bias and edge effects. Given that SEM samples tended to be more densely packed with particles than TEM grids, simple visual selection of picking particles at random from the SEM image could result in a bias in favor of larger particles. Imagine picking at random a large particle whose area covers one tenth of an image when the entire image contains one hundred particles. The probability of selecting such a particle would be 10 percent via random selection of a point on the image, while it would be only 1 percent if each particle was indexed and one would be chosen at random. Technically, the latter method provides for a more accurate measure of particle size distribution. However, suppose in the same case that all of the remaining particles were so much smaller that exclusion of this one large particle would skew the average to far lower values than physically true. Its inclusion however, with a small fraction of smaller particles, would skew it in the other direction. In order to avoid this conundrum, a biased selection process was chosen such that numerous random points were selected within the image and a single diameter was taken in an arbitrary direction for each particle. Large particles that were “doubly” selected in a particular image were not measured a second time. By selecting a large number of particles per image, enough small particles were chosen in addition to large particles to provide a balanced average particle size that did not change appreciably with the inclusion of additional particles into the average. Typically on the order of 50 to 100 particles were averaged per distribution.

#### **D. XRD Analysis and Discussion**

All x-ray diffraction data presented in this thesis were collected on a Rigaku SmartLab Multipurpose Diffractometer with a 9 kW rotating anode generator and high flux beam. Data were analyzed using HighScore Plus software. Reitveld refinement parameters are given in table 5 below.



<b>a</b>	<b>b</b>	<b>c</b>	<b>Re</b>	<b>Rwp</b>	<b>GOF</b>
9.558175	9.558175	11.15346	1.747	5.134	8.642
<b>Site</b>	<b>x</b>	<b>y</b>	<b>z</b>	<b>occ.</b>	
Mo	0.17008	0.15003	0.10626	0.983599	
Se1	0.03426	0.32368	0.0833	0.943215	
Se2	0	0	0.28242	0.9546	



<b>a</b>	<b>b</b>	<b>c</b>	<b>Re</b>	<b>Rwp</b>	<b>GOF</b>
9.557907	9.557907	11.15396	1.897	3.044	2.575
<b>Site</b>	<b>x</b>	<b>y</b>	<b>z</b>	<b>occ.</b>	
Mo	0.17107	0.151314	0.107191	0.993423	
Se1	0.036312	0.326198	0.082792	1	
Se2	0	0	0.285162	0.998956	
Ca	0.55355	0.51979	0.333542	0.063	

Table 5. **Reitveld refinement parameters.** Typical rietveld refinement parameters for fitting calciated and uncalciated experimental spectra.

Unit cell parameters were not observed to vary between the calciated and decalciated samples. A slight shift in the lattice positions of selenium atoms was observed however. Calcium site positions were initially set at the center of the cavity and allowed to relax to preferred locations. Calcium occupancy was determined by fitting peak intensities of particular peaks by manually varying the occupancy number and allowing for convergence of the model. Figures 66 and 67 below show typical intensity fitting behavior.

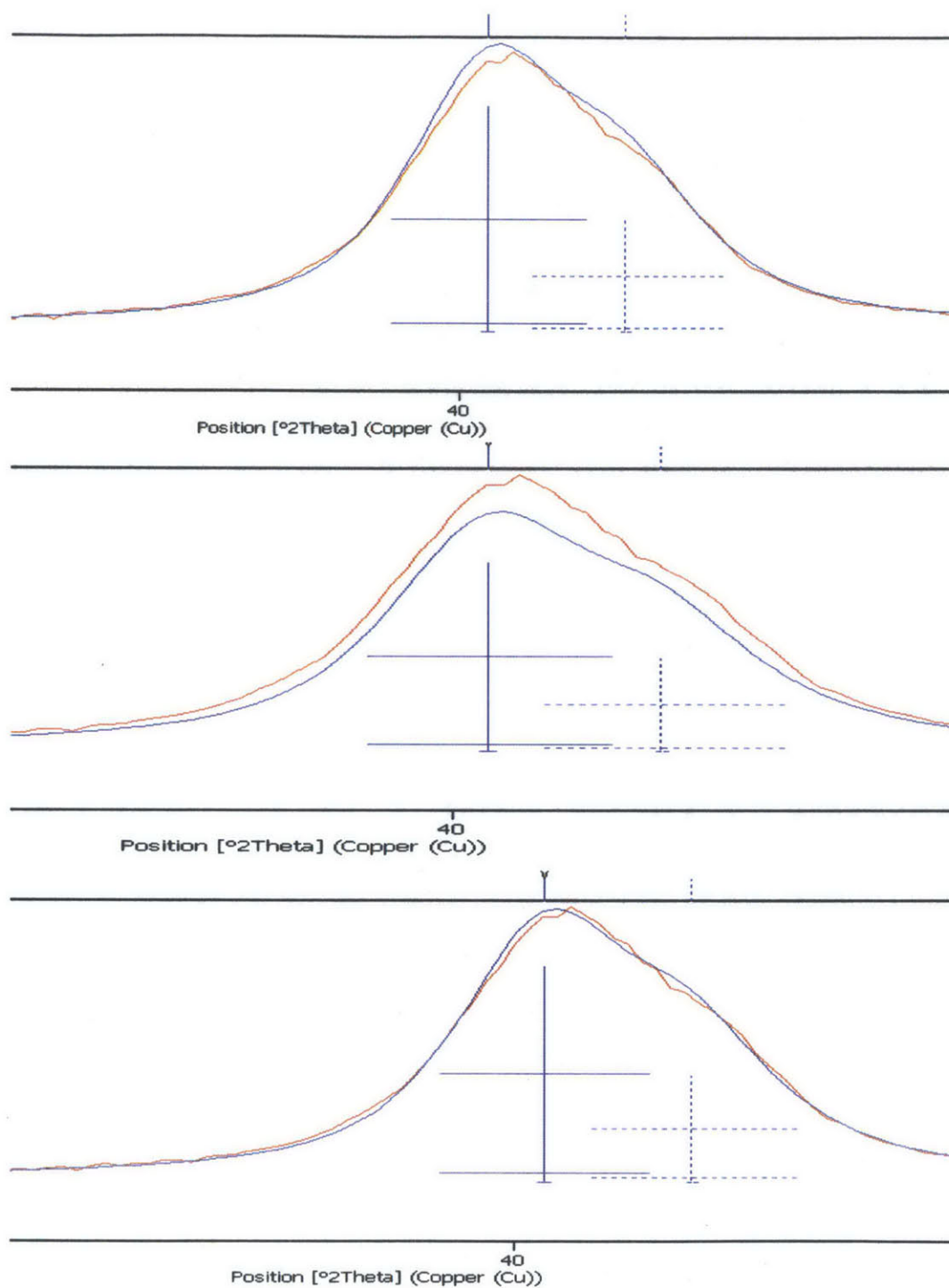


Figure 66. **Intensity comparison of experimental and Rietveld XRD spectra.** Rietveld parameters were fixed while calcium occupancy was varied from 0 (top) to 0.3 (middle). The best fit is obtained at the refinement convergence value of 0.06 (bottom).

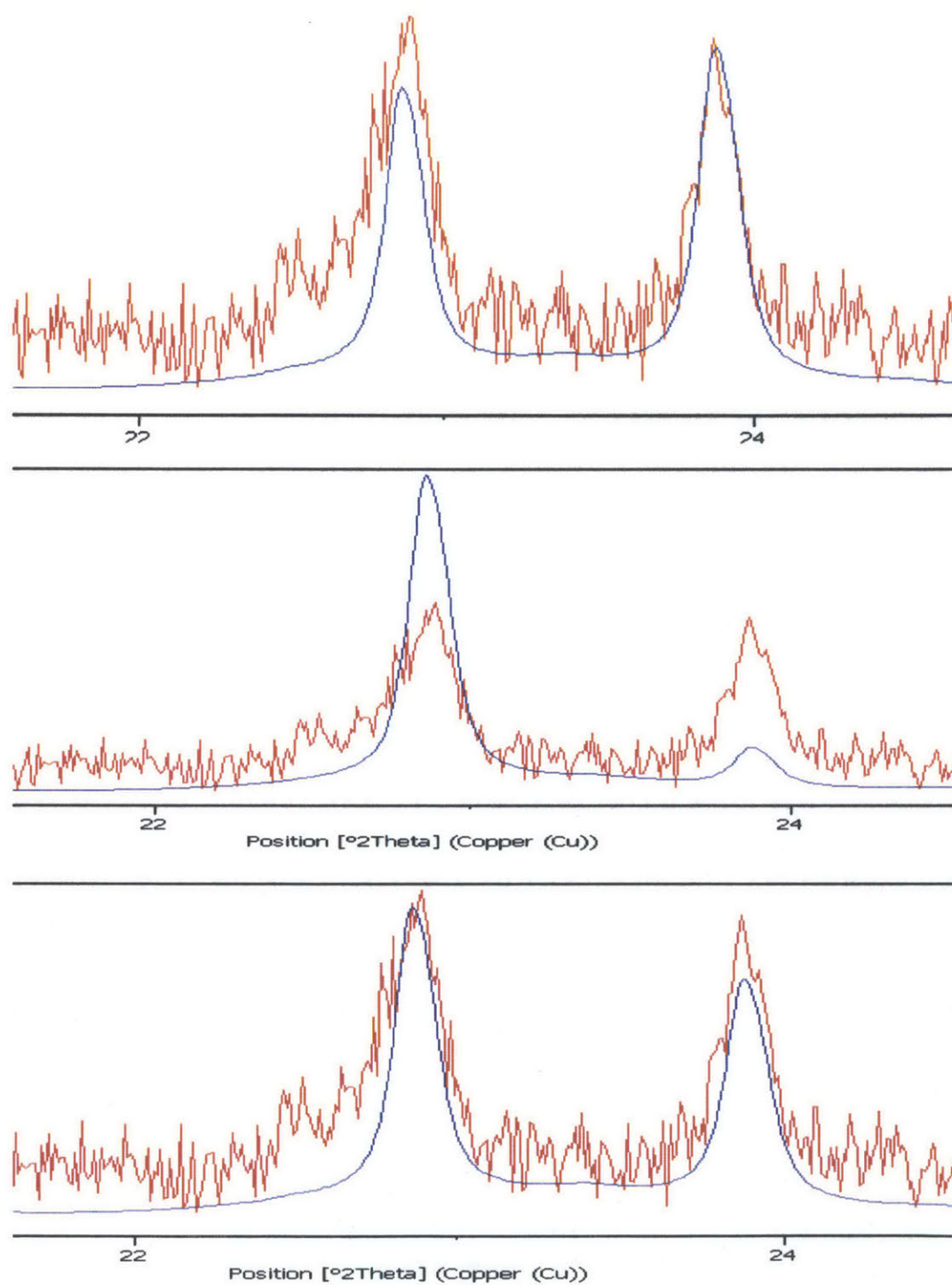


Figure 67. **Intensity comparison of experimental and Rietveld XRD spectra.** Rietveld parameters were fixed while calcium occupancy was varied from 0 (top) to 0.3 (middle). The best fit is obtained at the refinement convergence value of 0.06 (bottom).



Generally, a strong correlation was observed between the intensity of certain peaks within the XRD pattern and the calcium occupancy level, as illustrated in figures 48, 66, and 67. The ratio of intensities of particular peaks varied with calcium content in such a way that the best fit was found to occur at 0.063 calcium occupancy fraction. Through the symmetry operations of the unit cell performed based on the location of calcium sites within the structure, a calcium fraction of 0.063 was correlated with the stoichiometry of  $\text{Ca}_{0.367}\text{Mo}_6\text{Se}_8$  as the degree of calcination of the phase present. Electrochemical results predict an experimental stoichiometry of  $\text{Ca}_{0.3}\text{Mo}_6\text{Se}_8$ , which is reasonably close to the stoichiometry predicted by the rietveld model.

Interestingly, minimal unit cell volume change was observed in the sample, however this is consistent with observations in several other Chevrel phase intercalant compounds where volume change is negligible at low degrees of intercalation.<sup>57</sup> Ultimately, further XRD data should be collected to validate the level of calcination observed within the electrode and correlate it more directly with chemical analysis techniques, as well as to establish statistically significant results.

# Bibliography

- [1] Bradwell, D. J.. *Liquid Metal Batteries: Ambipolar Electrolysis and Alkaline Earth Electroalloying Cells*. Dissertation, Massachusetts Institute of Technology, 2011.
- [2] Bard, A.J. and Faulkner, L.R.. *Electrochemical Methods: Fundamentals and Applications, Second Edition*. John Wiley and Sons, Inc., 2001.
- [3] R.D. Shannon, and C.T. Prewitt. Effective Ionic Radii in Oxides and Fluorides. *Acta Cryst.*, B25:925-946, 1969.
- [4] L.H. Ahrens. The use of ionization potentials. Part 1. Ionic radii of the elements. *Geochimica et Cosmochimica Acta*, 2:155-169, 1952.
- [5] David R. Lide (ed.), *CRC Handbook of Chemistry and Physics, 85th Edition*. CRC Press. Boca Raton, Florida, 2005.
- [6] R.S. Carmichael (ed.), *CRC Practical Handbook of Physical Properties of Rocks and Minerals*, CRC Press, Boca Raton, FL, 1989.
- [7] K.K. Turekian *McGraw-Hill Encyclopedia of Science and Technology*, 4, 627, 1970.
- [8] A. Eftekhari. Potassium secondary cell based on Prussian blue cathode. *Journal of Power Sources*, 126:221-228, 2004.
- [9] K. Itaya et al. Spectroelectrochemistry and Electrochemical Preparation Method of Prussian Blue Modified Electrodes. *J. Am. Chem. Soc.*, 104:4767-4772, 1982.
- [10] M. Bervas, L.C. Klein, and G.G. Amatucci. Vanadium oxide-propylene carbonate composite as a host for the intercalation of polyvalent cations. *Solid State Ionics*, 176:2735-2747, 2005.
- [11] G. G. Amatucci et al. Investigation of Yttrium and Polyvalent Ion Intercalation into Nanocrystalline Vanadium Oxide. *Journal of the Electrochemical Society*, 148:A940-A950, 2001.
- [12] S. Nordlinder, J. Lindgren, and T. Gustafsson. The Structure and Performance of  $\text{Na}^+$ ,  $\text{K}^+$ , and  $\text{Ca}^{2+}$  - Vanadium Oxide Nanotubes. *Journal of the Electrochemical Society*, 150:280-E284, 2003.

- [13] M. Hayashi et al. Electrochemical characteristics of calcium in organic electrolyte solutions and vanadium oxides as calcium hosts. *Journal of Power Sources*, 119-121:617-620.
- [14] Vanýsek, P.. “Electrochemical Series”, in *Handbook of Chemistry and Physics: 92nd Edition*, 2011.
- [15] H. Kim, et al. Liquid Metal Batteries: Past, Present, and Future. *Chem. Rev*, 113:2075-2099, 2013.
- [16] H. Kim, et al. Thermodynamic Properties of Calcium-Bismuth Alloys Determined by Emf Measurements. *Electrochim. Acta*, 60:154-162, 2012.
- [17] K. A. See et al. A High Capacity Calcium Primary Cell based on the Ca-S System. *Advanced Energy Materials*, 3:1056-1061, 2013.
- [18] G.G. Amatucci et al. An Asymmetric Hybrid Nonaqueous Energy Storage Cell. *J. Electrochem. Soc.*, 148:A911, 2001.
- [19] J. N. Butler. The Standard Potential of the Calcium Amalgam Electrode. *J. Electroanal. Chem.*, 17:309-317, 1968.
- [20] Whitacre, J.F. et al. An aqueous electrolyte, sodium ion functional, large format energy storage device for stationary applications. *Journal of Power Sources*, 213:255-264, 2012.
- [21] Guminiski, C. Ca-Hg Phase Diagram, ASM Alloy Phase Diagrams Center, P. Villars, editor-in-chief; H. Okamoto and K. Cenual, section editors; <http://www1.asmiinternational.org/AsmEnterprise/APD>, ASM International, Materials Park, OH, 2006.
- [22] Davy H.. Electro-chemical researches on the decomposition of the earths; with observations on the metals obtained from the alkaline earths, and on the amalgam procured from ammonia. *Philosophical Transactions of the Royal Society of London* **98**: 333–370, 1808.
- [23] T. Mussini, P. Longhi, and S. Rondinini. Standard Potentials of Amalgam Electrodes in Aqueous Solutions, Temperature Coefficients and Activity Coefficients of Metals in Mercury. *Pure and Appl. Chem.*, 57:169-179, 1985.
- [24] H.J. Mueller, E.H. Greener, and D.S. Crimmins. The Electrochemical Properties of Dental Amalgam. *J. Biomed. Mater. Res.*, 2:95-119, 1968.
- [25] T. Mussini and A. Pagella. Standard Potentials of the Calcium Amalgam Electrode at Various Temperatures, with Related Thermodynamic Functions. *Journal of Chemical and Engineering Data*, 16:49-52, 1971.
- [26] M. Tamele. The Electrolytic Potential of Calcium. *J. Phys. Chem.*, 28:502-505, 1924.
- [27] J. Chlistunoff and Z. Galus. Kinetics and thermodynamics of the Ca(II)/Ca(Hg) system in water. *J. Electroanal. Chem.*, 267:105-116, 1989.
- [28] M. Lan et al. Determination of the Diffusion Coefficients of Lithium and Calcium in Mercury. *Chinese Journal of Analytical Chemistry*, 1999-02.

- [29] C. Gurninski. The Ca-Hg (Calcium-Mercury) System. *Journal of Phase Equilibria.*, 14:90-96, 1993.
- [30] P.G. Bruce et al. Multivalent cation intercalation. *Solid State Ionics*, 53-56:351-355, 1992.
- [31] R.A. Guidotti and P. Masset. Thermally activated (“thermal”) battery technology Part I: an overview. *Journal of Power Sources*, 161:1443-1449, 2006.
- [32] D. Linden and T.B. Reddy, eds. *Handbook of Batteries*. New York, McGraw-Hill, 2002.
- [33] P.C. Butler, R. A. Guidotti, and P.J. Masset. Primary batteries – reserve systems: Thermally Activated Batteries: Calcium. *Encyclopedia of Electrochemical Power Sources*, 137-140, 2009.
- [34] S. M. Selis et al. A High-Rate, High-Energy Thermal Battery System. *Journal of the Electrochemical Society*, 111:6-13, 1964.
- [35] Y. Wang, K. Takahashi, and K. H. Lee. Nanostructured Vanadium Oxide Electrodes for Enhanced Lithium-Ion Intercalation. *Advanced Functional Materials*, 16:1133-1144, 2006.
- [36] S. Licht, Y. Wang, and G. Gourdin. Enhancement of Reversible Nonaqueous Fe(III/VI) Cathodic Charge Transfer. *J. Phys. Chem.*, 113:9884-9891, 2009.
- [37] K.A. Walz et al. Characterization and performance of high power iron (VI) ferrate batteries. *Journal of Power Sources*, 134:318-323, 2004.
- [38] S. Licht et al. Chemical synthesis of battery grade super-iron barium and potassium Fe(VI) ferrate compounds. *Journal of Power Sources*, 99:7-14, 2001.
- [39] M. Koltypin et al. The study of  $K_2FeO_4$  ( $Fe^{6+}$ -super iron compound) as a cathode material for rechargeable lithium batteries. *Journal of Power Sources*, 146:723-726, 2005.
- [40] S. Licht et al. Silver Mediation of Fe(VI) Charge Transfer: Activation of the  $K_2FeO_4$  Super-iron Cathode. *J. Phys. Chem.*, 106:5947-5955, 2002.
- [41] L. E. Ross et al. *Calcium/Iron Disulfide Secondary Cells*. New York, American Institute of Aeronautics and Astronautics, Inc., 1980, p. 581-585.
- [42] T. Oshima, M. Kajita, and A. Okuno. Development of Sodium-Sulfur Batteries. *Applied Ceramic Technology*, 1:3, 269-276, 2004.
- [43] R. Chevrel. Un Nouveau Sulfure de Molybdene:  $Mo_3S_4$  Preparation, Proprietes et Structure Cristalline. *Mat. Res. Bull.* 9:1487-1498, 1974.
- [44] R. Chevrel, C. Rossel, and M. Sergent. The Structure of  $SnMo_6S_8$  and the Superconducting Properties of the Series  $Sn_xMo_6S_8$  and  $M_ySn_xMo_6S_8$  ( $M = La, Ce, Pr, Eu, Gd, Ho, Lu, Y, In, U$ ). *Journal of the Less-Common Metals*, 72:31-43, 1980.
- [45] O. Pena, P. Gougeon, and M. Sergent. Growth of Single Crystals of the  $YbMo_6S_8$  Phase and Refinement of its Crystal Structures. *Journal of the Less-Common Metals*, 99:225-232, 1984.

- [46] C. Geantet et al. Superconducting State of  $\text{Ca}_x\text{Mo}_6\text{S}_8$  at Ambient Pressure. *Physica C*, 153-155:481-482, 1988.
- [47] C. Geantet et al. Evidence of Superconductivity in  $\text{Ca}_x\text{Mo}_6\text{S}_8$  Single Crystals at Normal Pressure. *Solid State Communications*, Vol. 64, No. 11:1363-1368, 1987.
- [48] O. Pena et al. Crystal Structure and Normal State Physical Properties of  $\text{Ho}_x\text{Mo}_6\text{S}_8$  ( $0.88 < x < 1.0$ ) Single Crystals. *Journal of the Less-Common Metals*, 105:105-117, 1985.
- [49] E. Gocke et al. Molybdenum Cluster Chalcogenides  $\text{Mo}_6\text{X}_8$ : Intercalation of Lithium via Electron/Ion Transfer. *Inorganic Chemistry*, 26:1805-1812, 1987.
- [50] E. Gocke et al. Molybdenum Cluster Chalcogenides  $\text{Mo}_6\text{X}_8$ : Electrochemical Intercalation of Closed Shell Ions  $\text{Zn}^{2+}$ ,  $\text{Cd}^{2+}$ , and  $\text{Na}^+$ . *Journal of Solid State Chemistry*, 70:71-81, 1987.
- [51] M.D. Levi, et al. Kinetic and Thermodynamic Studies of  $\text{Mg}^{2+}$  and  $\text{Li}^+$  Ion Insertion into the  $\text{Mo}_6\text{S}_8$  Chevrel Phase. *Journal of the Electrochemical Society*, 151:A1044-A1051, 2004.
- [52] E. Levi, Y. Gofer, and D. Aurbach. On the Way to Rechargeable Mg Batteries: The Challenge of New Cathode Materials. *Chem. Mater.*, 22:860-868, 2010.
- [53] E. Lancry et al. Leaching Chemistry and the Performance of the  $\text{Mo}_6\text{S}_8$  Cathodes in Rechargeable Mg Batteries. *Chem. Mater.*, 16:2832-2838, 2004.
- [54] E. Levi et al. A review of the problems of the solid state ions diffusion in cathodes for rechargeable Mg batteries. *J. Electroceram.*, 22:13-19, 2009.
- [55] P.G. Bruce et al. Chemical Intercalation of Magnesium into Solid Hosts. *J. Mater. Chem.*, 1:705-706, 1991.
- [56] E. Levi et al. Phase Diagram of Mg insertion into Chevrel Phases,  $\text{Mg}_x\text{Mo}_6\text{T}_8$  (T=S, Se). 2. The Crystal Structure of Triclinic  $\text{MgMo}_6\text{Se}_8$ . *Chem. Mater.*, 18:3705-3714, 2006.
- [57] E. Levi et al. New Insight on the Unusually High Ionic Mobility in Chevrel Phases. *Chem. Mater.* 21:1390-1399, 2009.
- [58] E. Levi et al. The crystal structure of the inorganic surface films formed on Mg and Li intercalation compounds and the electrode performance. *J. Solid State Electrochem.*, 10:176-186, 2006.
- [59] M.D. Levi et al. The effect of the anionic framework of  $\text{Mo}_6\text{X}_8$  Chevrel Phase (X = S, Se) on the thermodynamics and kinetics of the electrochemical insertion of  $\text{Mg}^{2+}$  ions. *Solid State Ionics*, 176:1695-1699, 2005.
- [60] E. Levi et al. Phase Diagram of Mg insertion into Chevrel Phases,  $\text{Mg}_x\text{Mo}_6\text{T}_8$  (T=S, Se). 2. The Crystal Structure of the Sulfides. *Chem. Mater.*, 18:3705-3714, 2006.
- [61] D. Aurbach et al. Prototype systems for rechargeable magnesium batteries. *Nature*, 407:724-727, 2000.

- [62] E. Levi et al. Cu<sub>2</sub>Mo<sub>6</sub>S<sub>8</sub> Chevrel Phase, A Promising Cathode Material for New Rechargeable Mg batteries: A Mechanically Induced Chemical Reaction. *Chem. Mater.*, 14:2767-2773, 2002.
- [63] Y. Gofer et al. Improved Electrolyte Solutions for Rechargeable Magnesium Batteries. *Electrochemical and Solid-State Letters.*, 9:A257-A260, 2006.
- [64] K. Yvon. *Current Topics in Materials Science* (E. Kaldis) Vol. 3, North-Holland Amsterdam, 1979.
- [65] M.D. Levi et al. The effect of the anionic framework of Mo<sub>6</sub>X<sub>8</sub> Chevrel Phase (X = S, Se) on the thermodynamics and the kinetics of the electrochemical insertion of Mg<sup>2+</sup> ions. *Solid State Ionics*, 176:1695-1699, 2005.
- [66] Ortiz, L.A.. *A Spectroscopic and Electrochemical Study of Chlorotitanates in Molten Salt Media*. Dissertation, Massachusetts Institute of Technology, 1996.
- [67] W. Weppner and R. A. Huggins. Determination of the Kinetic Parameters of Mixed-Conducting Electrodes and Application to the System Li<sub>3</sub>Sb. *J. Electrochem. Soc.*, 124:10 1569-1578, 1977.
- [68] Avery, K. C.. *The Role of Phase Transformation in the Rate Performance Limited LixV<sub>2</sub>O<sub>5</sub> Battery Cathode*. Dissertation, Massachusetts Institute of Technology, 2008.
- [69] S. A. Barriga. *An Electrochemical Investigation of the Chemical Diffusivity in Liquid Metal Alloys*. Dissertation, Massachusetts Institute of Technology, 2013.
- [70] R. Malik. *First-Principles Investigation of Li Intercalation Kinetics in Phospho-Olivines*. Dissertation, Massachusetts Institute of Technology, 2013.
- [71] T. Jiang et al. Electrodeposition of aluminium from ionic liquids: Part II - studies on the electrodeposition of aluminum from aluminum chloride (AlCl<sub>3</sub>) - trimethylphenylammonium chloride (TMPAC) ionic liquids. *Surface and Coatings Technology*, 201:10-18, 2006.
- [72] H. Liu et al. Aluminum-ion Batteries: a New Solution for Energy Storage beyond Li-ion Batteries. *Poster Abstract, 4<sup>th</sup> Symposium on Energy Storage Beyond Lithium, PNNL*, 2011.
- [73] H.H. Willard and G. F. Smith. The Perchlorates of the Alkali and Alkaline Earth Metals and Ammonium. Their Solubility in Water and Other Solvents. *J. Am. Chem. Soc.*, 45:286-297, 1923.
- [74] J. Panzer. Nature of Calcium Acetate. *Journal of Chemical and Engineering Data*, 7:140-142, 1962.
- [75] E. Lancry et al. Molten salt synthesis (MSS) of Cu<sub>2</sub>Mo<sub>6</sub>S<sub>8</sub> – New way for large-scale production of Chevrel phases. *Journal of Solid State Chemistry*, 179:1879-1882, 2006.
- [76] D. Aurbach et al. Progress in Rechargeable Magnesium Battery Technology. *Adv. Mater.*, 19:4260-4267, 2007.
- [77] A. Singhal et al. Nanostructured electrodes for next generation rechargeable electrochemical devices. *Journal of Power Sources*, 129:38-44, 2004.

- [78] E. Lancry et al. The effect of milling on the performance of a Mo<sub>6</sub>S<sub>8</sub> Chevrel phase as a cathode material for rechargeable Mg batteries. *J. Solid State Electrochem.*, 9:259-266, 2005.
- [79] M. D. Levi et al. A comparative study of Mg<sup>2+</sup> and Li<sup>+</sup> ion insertions into the Mo<sub>6</sub>S<sub>8</sub> Chevrel phase using electrochemical impedance spectroscopy. *Journal of Electroanalytical Chemistry*, 568:211-223, 2004.
- [80] W. H. Woodford. *Electrochemical shock : mechanical degradation of ion-intercalation materials*. Massachusetts: Massachusetts Institute of Technology, 2013.
- [81] E. Levi et al. Crystallography of Chevrel Phases, MMo<sub>6</sub>T<sub>8</sub>(M = Cd, Na, Mn, and Zn, T = S, Se) and Their Cation Mobility. *Inorg. Chem.*, 48:8751-8758, 2009.
- [82] A. Mitelman et al. New cathode materials for rechargeable Mg batteries: fast Mg ion transport and reversible copper extrusion in Cu<sub>y</sub>Mo<sub>6</sub>S<sub>8</sub> compounds. *Chem. Commun.*, 41:4212-4214, 2007.
- [83] A. Mitelman et al. On the Mg trapping mechanism in electrodes comprising Chevrel phases. *ECS Transactions, Meet. Abstr.* 2006 MA2006-02(5): 308, 2007.
- [84] NIST X-ray Photoelectron Spectroscopy Database, Version 4.1 (National Institute of Standards and Technology, Gaithersburg, 2012); <http://srdata.nist.gov/xps/>.
- [85] Andruszkiewicz, R. Ca-Mo-S Phase Diagram, ASM Alloy Phase Diagrams Center, P. Villars, editor-in-chief; H. Okamoto and K. Cenzual, section editors; <http://www1.asminternational.org/AsmEnterprise/APD>, ASM International, Materials Park, OH, 2006.
- [86] R. Y. Wang et al. Highly Reversible Open Framework Nanoscale Electrodes for Divalent Ion Batteries. *Nano Lett.*, 13:5748-5752, 2013.
- [87] E. Levi and D. Aurbach. Chevrel Phases, M<sub>x</sub>Mo<sub>6</sub>T<sub>8</sub>(M = Metals, T = S, Se, Te) as a Structural Chameleon: Changes in the Rhombohedral Framework and Triclinic Distortion. *Chem. Mater.*, 22:3678-3692, 2010.
- [88] R. Schollhorn and M. Kumpers. Topotactic Redox Reactions of the Channel Type Chalcogenides Mo<sub>3</sub>S<sub>4</sub> and Mo<sub>3</sub>Se<sub>4</sub>. *Mat. Res. Bull.*, 12:171-788, 1977.
- [89] J. Lee et al. Todorokite-type MnO<sub>2</sub> as a zinc-ion intercalating material. *Electrochimica Acta*, 112:138-143, 2013.
- [90] G. Gershinsky et al. Electrochemical and Spectroscopic Analysis of Mg<sup>2+</sup> Intercalation into Thin Film Electrodes of Layered Oxides: V<sub>2</sub>O<sub>5</sub> and MoO<sub>3</sub>. *Journal of the American Chemical Society*, 29:10964-10972, 2013.
- [91] Q. Li and N. J. Bjerrum. Aluminum as anode for energy storage and conversion: a review. *Journal of Power Sources*, 110:1-10, 2002.
- [92] Jayaprakash N., Das S. K. & Archer L. A. The rechargeable aluminum-ion battery. *Chem. Commun.* 47, 12610–12612, 2011.

- [93] Reed L. D. & Menke E. The roles of V<sub>2</sub>O<sub>5</sub> and stainless steel in rechargeable Al-ion batteries. *J. Electrochem. Soc.* 160, A915–A917, 2013.
- [94] G.M. Brown et al. A High Energy Density Aluminum Battery, U.S. Patent Application 12/895, 487, 2010.
- [95] G. Levitin, C. Yarnitzky, and S. Licht. Fluorinated Graphites as Energetic Cathodes for Nonaqueous Al Batteries. *Electrochemical and Solid-State Letters*, 5:A160-A163, 2002.
- [96] Subramanian, P.R.. Ca-Pt Phase Diagram, ASM Alloy Phase Diagrams Center, P. Villars, editor-in-chief; H. Okamoto and K. Cenzual, section editors;  
<http://www1.asminternational.org/AsmEnterprise/APD>, ASM International, Materials Park, OH, 2006.



# Epilogue

I personally consider the work contained within this thesis to be only a small, relatively unimportant part of my graduate school career. I have spent the better part of the last decade at MIT, first as an undergraduate and later as a graduate student. The MIT community is truly one of a kind; rich in remarkable individuals and unrivaled social interactions. Spending time as a part of this community has shaped me as a person in innumerable ways, and given me opportunities for which I am truly grateful.

Among the many passions and past times that I have discovered in my time at the institute, teaching stands out as one of the most rewarding. I think teaching and learning are the most important aspects of university life, and ironically also the most undervalued and misunderstood. Teaching and learning go beyond the classroom, into every laboratory, student group, and open space on campus. Academia is an environment of communal learning, where colleagues teach each other through their questions and challenges of each other's work. The common understanding of the standard model of education is that "professors teach and students learn." This one-sided approach misses the fact we learn together – students teach through their questions and interactions with each other. I can recall numerous times where professors have been inspired in their own research while discussing material related to undergraduate lectures – in common vernacular the professors have learned. Personally, my teaching has taught me so much more than I could have ever learned on my own. That's what I find special about academia, and what I hope shines through from these ramblings: a university is a place we all come when striving to better ourselves – a betterment which we achieve through each other. Often times though, students first arriving to a college campus don't realize this is the true face of education. They assume they're here to learn some information from someone who knows what they're talking about. They miss the point. In my time at MIT I have literally taught hundreds of students innumerable facts, some of which some of these students may have even remembered. However, it is my true hope, that in some

small sense, I have helped at least a few of these students grasp the bigger picture of the world and their role in it. Those of us that are lucky enough to be at MIT are special. We are the creators of information and the interpreters of fact, and we have a responsibility to approach the future in a malleable manner. Successive generations of students are the future, and whatever small effect I have on the world will pale in comparison to the ripple effect of those who will come after me. I consider it my greatest success to have inspired or helped just a few of these future souls, in whatever way I was able to contribute.

To continue this grandiose epilogue, I thought it would be suitable to share one of my favorite quotes. Einstein once said of education, “Education is not the learning of facts, but the training of the mind to think.” This quote has always resonated with me personally. We progress through life and learn things, building experience and a framework with which to approach the world. The same is true of education. We learn facts, practice problems, and analyze data, all the while developing some intangible sense of understanding out the world and a framework for tackling the unknown. Everything we learn, in a sense, is a metaphor, and applicable to something else. Educators must help their students develop these frameworks, and both motivate and inspire them to do so. The goal of a true teacher is not the conveyance of content, but to assist in the creation of a frame of mind.

And so we go through life, building a catalogue of experiences that develop our personal frameworks and ultimately inform our decisions, only to die at the end of it. Philosophers have pondered for centuries for some greater meaning to it all, and many have come to different conclusions. One quote in particular, by Emerson, has stuck with me ever since a friend in high school gave me a mug with it written on it as a thank you for tutoring her in math. The mug sits on my desk as I write this. It reads:

*“To laugh often and much, to win the respect of intelligent people and the affection of children, to earn the appreciation of honest critics and endure the betrayal of false friends, to appreciate beauty, to find the best in others, to leave the world a bit better... to know even one life has breathed easier because you have lived. This is to have succeeded.”*

Through my teaching, I have found my success, and for this I am truly grateful.